Author:
Scholey, K. D

Title:
Developments in vertebrate flight : Climbing and gliding of mammals and reptiles, and the flapping flight of birds

DEVELOPMENTS IN VERTEBRATE FLIGHT: CLIMBING AND GLIDING OF MAMMALS AND REPTILES, AND THE FLAPPING FLIGHT OF BIRDS

by

KEITH D. SCHOLEY

A dissertation submitted to the University of Bristol in part fulfillment of the requirements for the degree of Ph.D.

PAGE
NUMBERS
CUT OFF
IN
ORIGINAL

DAMAGED TEXT IN ORIGINAL

M E M O R A N D U M

This thesis and the data presented herein are the results of my own original work except where due acknowledgement and reference are given. Neither the whole nor any part has previously been submitted to this or any other university towards any degree.

Signed

K D Scholey

10th November 1982

Keith D. Scholey

TABLE OF CONTENTS

	Page No.
Synopsis	1
CHAPTER 1	
General Introduction	3
CHAPTER 2	
The climbing and gliding locomotion of the flying squirrel Petaurista petaurista (Scuiridae) and the flying lizard Draco spilopterus (Agamidae)	
2.1 Introduction	7
2.2 Locations, materials and methods	8
2.3 Petaurista petaurista	
2.3.1 General behaviour	14
2.3.2 Results	16
(i) Climbing and gliding locomotion	16
(ii) Wing area, aspect ratio and lift coefficient of Petaurista petaurista	21
2.3.3 The energy cost of Petaurista petaurista when climbing and gliding, compared with that of quadrupedal arboreal locomotion	23
2.3.4 Discussion	28
2.4 Draco spilopterus	
2.4.1 General behaviour	35
2.4.2 Results	
(i) Climbing and gliding locomotion	37

2.4.3 Discussion 39
2.5 Conclusion 44
CHAPTER 3
The Evolution of Flight in Bats
3.1 Introduction 45
3.2 The fundamental problems and advantages of powered flight 47
3.3 The mechanism for bat evolution by first developing gliding 48
3.4 The disadvantages of gliding and their consequences in bat evolution 54
3.5 The evolution of nocturnal motion detection in bats 55
3.6 Conclusion 58
3.7 Selection pressure for the evolution of flight in birds 59
CHAPTER 4
An introduction to bird flight kinematics and aerodynamics
4.1 The history of the study of bird flight kinematics 61
4.1.1 Initial studies 61
4.1.2 Hovering and slow forward flight 61
4.1.3 Fast forward flight 63
4.2 Relating wing beat kinematics to morphology 66
CHAPTER 5
Materials, Locations, and Methods
5.1 Photography 72

5.1.1 Photographic materials 72
(i) Cameras 72
(ii) Film 73
(iii) Lenses 74
(iv) Camera mounts 74
5.1.2 Field locations 75
5.1.3 Filming techniques 77
(i) Framing rate and shutter speed slection 77
(ii) The limits of maximum f number 78
(iii) Field filming 78
(iv) Laboratory filming 78
5.2 Analysis 81
5.2.1 Analysis apparatus 81
5.2.2 Analysis technique 82
(i) Temporal analysis 82
(iia) Direct angle analysis 83
(iib) Indirect estimate of amplitude 86
(iii) Scaling of birds in flight in field conditions 86
(iv) Flight speed estimation 88
(v) Frame by frame analysis technique 89
(va) Head-on or tail-on 89
(vb) Side-on 91
(vi) Repeatability and errors of frame by frame analysis 92
5.2.3 Statistical analysis 95

CHAPTER 6

Wing beat kinematics in cruise flight

6.1 Introduction 100

6.2 Description of wing strokes and distribution of speed in the downstroke

6.2.1 Group A

(i) Birds larger than 1kg 104

(ii) Birds smaller than 1kg 106

6.2.2 Group C 107

6.2.3 Group B 109

6.3 Zebra finch cruise flight: wing stroke description 111

6.4 Kinematic variation with morphology: An analysis by correlation 113

6.4.1 Wing beat frequency 113

6.4.2 Downstroke ratio 114

6.4.3 Stroke amplitude 115

6.4.4 Stroke plane angle 115

6.4.5 Wing tip downstroke velocity 116

6.5 The variation of kinematic parameter with morphology, flying speed and remaining kinematics. An aerodynamic approach 117

6.5.1 The Pennycuick prediction 117

6.5.2 A modification including amplitude and downstroke ratio 120

6.6 Discussion

6.6.1 The allometric analysis 125

6.6.2 The aerodynamic analysis 128

6.6.3 Distribution of speed of the wing tip in the downstroke 134

6.6.4 Downstroke wrist extension 138

CHAPTER 7

Hovering and slow forward flight

7.1 Introduction 140

7.2 Hovering 142

7.2.1 Hummingbird (Chlorostilbon melanorhyncus) 142

7.2.2 Birds using the "feathered" upstroke 142

7.2.3 Birds using the tip reversal upstroke 144

7.2.4 Discussion 146

7.3 Take-off requiring running 150

7.3.1 Introduction 150

7.3.2 Ruppell's griffon vulture (Gyps ruppellii) 150

7.3.3 White pelican (Pelecanus onocrotalus) 152

7.3.4 Comparison of the take-off of the white pelican and the Ruppell's griffon vulture 154

7.3.5 Other running take-off techniques 155

7.4 Landing in the wandering albatross 157

7.5 Clap and fling 159

7.6 Steady flight at speeds between hovering and cruise 161

7.6.1 Introduction 161

7.6.2 Kinematics of the kestrel Falco tinnunculus in steady slow forward flight 161

7.6.3 Discussion 163
7.7 The scaling of maximum power kinematics 166
7.8 General discussion of hovering and slow forward flight 168

CHAPTER 8
General discussion of flapping flight in birds 171
8.1 A comparison of the kinematics of cruise and slowest speed flight 171
8.2 Conditions for using the upstroke in flapping flight to generate lift 176
8.3 An importance of rapid wing accelleration 178
8.4 Lift coefficient and steady state aerodynamics in cruise flight 179

CHAPTER 9
Conclusions 180

References 189

Appendix 1A

Acknowledgements

SYNOPSIS

The behaviour of the flying squirrel Petaurista petaurista and of the flying lizard Draco spilopterus was recorded, and climbing speeds, glide angles and speeds measured and lift coefficients calculated. The energy cost of the climbing and gliding locomotion of P.petaurista was estimated and shown to be less than that for running through a forest canopy.

The energy saving theory for gliding mammals was developed into a theory for the evolution of flight and of sensory systems in bats. This was then applied to birds.

Birds, which use mainly continuous flapping flight, were filmed in fast forward and/or slow forward or hovering flight using a high speed cine camera. Detailed observations of the various wing strokes were made and the kinematic parameters of wing beat frequency, downstroke ratio, stroke amplitude, stroke plane angle and wing tip velocity were recorded at either or both flight speeds.

Allometric relationships were found for the variation of each kinematic parameter with body mass and the dependence of each on body mass, wing span and area determined by using multiple regression analysis.

Aerodynamic and mechanical predictions for flapping flight were tested. It was found that:

1) For fast forward flight:

a) wing beat kinematics scale similarly to those predicted if the aerodynamic requirements for horizontal flight are limited, and if it is assumed that lift coefficient is constant with mass and that steady state aerodynamics apply.

b) the upstroke is increasingly used for weight support, the higher the aspect ratio of the wing.

2) For hovering and slow flight:

a) wing stroke patterns and use of the upstroke vary with aspect ratio and slow flying speed.

b) clap and fling (or near clap and fling) is used by many species.

c) slowest flight kinematics (for limited data) scale similarly to those predicted if the wing angular velocity is limited by material strength.

CHAPTER 1

GENERAL INTRODUCTION

Vertebrate flight has evolved separately on several occasions and to varying levels of sophistication. In order to fly, these vertebrates must increase their body surface area so that their body weight is supported by forces of lift or drag. If drag forces predominate, the angle of descent of the animal is greater than 45^{o} and the animal is said to be parachuting. If this angle is less than 45^{o}, aerodynamic lift forces are dominant and the animal is said to be gliding (Rayner, 1981) Species capable only of parachuting include the flying frog Phrynohyas venulosa and the flying gecko Ptychozoon sp. True gliders are represented amongst the extant reptiles by the flying lizards of the genus Draco, and gliders have evolved separately amongst extant mammals at least four times. Powered flight has developed in two extant vertebrate groups, the birds and the bats, and the extinct pterosaurs were almost certainly capable of this sophisticated form of flight.

Powered flight, once fully developed, has many clear uses, but an explanation for the evolution of this form of locomotion is not necessarily so obvious. It is the energetic advantages of flight which are of paramount importance in its development. The comparison of the cost of various forms of transport

was first discussed by Gabrielli and Von Karman (1950) for man-made machines. They did this by finding the power required to move unit weight of a machine at its transport speed, which is equivalent to the energy required to move unit weight through unit distance. This "cost of transport" is, in this form, dimensionless. Schmidt-Nielsen (1972) expressed the cost of transport for a variety of animals as the energy required to transport unit body mass through unit distance and showed that, in terms of energy cost for a given body mass, flying is a far cheaper form of locomotion than running. This is because flying is fast. Although for similar sized animals the power required for an animal to fly level is far greater than that required to run, the time taken to fly a given distance, and consequently the period of energy expenditure, are far less than if the animal were to run that distance. Norberg (in press), emphasising this point, says that a 15g passerine on migration can fly 1000km non-stop in about 24h, a distance and speed which could never be achieved by a similar sized mouse!

The aerodynamic principles governing animal flight are summarised by Pennycuick (1972a, 1975) and Lighthill (1974, 1977). The generation of aerodynamic lift to support the body weight must involve some induced drag. The power required to fly must overcome induced drag and that associated with the frictional forces produced when the air comes into contact with the body and the wing surface areas. This frictional

drag is termed parasite drag for the body and profile drag for the wings. In gliding flight the rate of loss of potential energy, which is directly proportional to the rate of sink of the animal, must be sufficient to overcome these three components of drag. If this rate of sink is to be reduced without altering the aerodynamic shape of the animal, it must flap the wings to generate extra thrust. This can enable the animal to fly horizontally and climb, and also to remain airborne over a wide range of flight speeds. The components of drag vary in their magnitude depending on the flying speed of the animal. Power models to estimate aerodynamic power in flapping flight over a range of flying speeds have been developed by Pennycuick (1968, 1975), Tucker (1973) and Rayner (1979a, b, c). Figure 1.1 shows, for a bird, a typical power curve (power against flying speed), which is produced by the sum of the calculated curves for induced power, profile power and parasite power by the Rayner model. The total power curve shows that there is a flight speed of minimum power V_{mp}, given by the lowest point of the curve, and a flight speed of maximum range V_{mr} for a given fuel supply. V_{mr} is defined by the point of contact with the curve of a tangent from the origin where the ratio of power to speed is a minimum, and hence too the energy expended per distance travelled. If any of the three components of drag are altered, V_{mp} and V_{mr} can be changed. Classic aerodynamic theory

Figure 1.1

Power curve, (aerodynamic power required for a range of flight speeds) for the pigeon Columba livia calculated by the Rayner power model (Rayner, 1979a and b). The total power curve P(V) is produced by the sum of the curves for induced power P_i, profile power P_{pro} and the parasite power P_{par}. The minimum power speed V_{mp} and the maximum range speed V_{mr} are indicated.

Figure 1.1

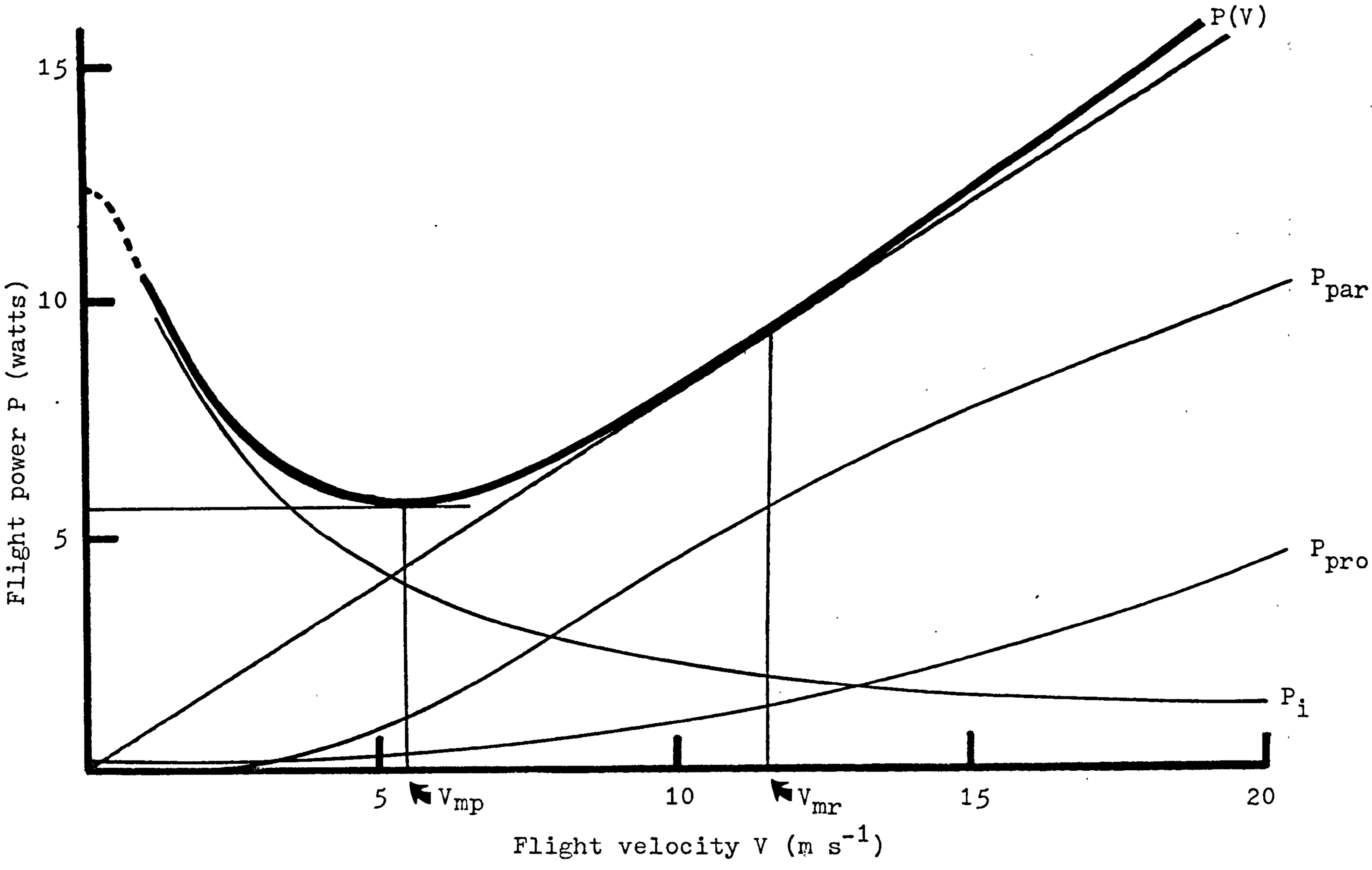
P(V)
P_{par}
P_{pro}
P_i
15
10
5
Flight power P (watts)
5
V_{mp}
10
V_{mr}
15
20
Flight velocity V (m s^{-1})

shows that induced power is largely dependent on the span of the wings, and that profile power is dependent on their area, and so, by altering the wing shape, the power curve and the positions of V_{mp} and V_{mr} can be varied to suit the ecological requirements of the particular animal. In gliding and flapping flight wing shapes probably also have physical and environmental limiting factors, which again depend on the way of life of the particular animal.

This thesis broadly follows the development of flapping flight, with firstly a study of two climbing and gliding vertebrates, the flying squirrel Petaurista petaurista and the flying lizard Draco spilopterus. The selection pressure to reduce the cost of transport by gliding is investigated for the flying squirrel, and this is then developed into a theory of the powered flight evolution of bats, which is then related to that of birds. The remaining chapters consider the flapping flight of birds in order to find relationships between bird morphology and wing beat kinematics, in slow forward flight or hovering, and fast forward flight. In the conclusion the information of these various studies is used to produce general ideas about the conditions, mechanisms and nature of selection of flight evolution in vertebrates, and the limits of flight design and adaptive radiation of this specialised form of locomotion.

CHAPTER 2

THE CLIMBING AND GLIDING LOCOMOTION OF THE FLYING SQUIRREL PETAURISTA PETAURISTA (SCUIRIDAE) AND THE FLYING LIZARD DRACO SPILOPTERUS (AGAMIDAE)

2.1 Introduction

The adaptation for gliding from tree to tree has evolved separately on numerous occasions amongst arboreal vertebrates, especially in the Old World (Rayner, 1981). There are recordings of the glide performance of many of these species, but in the vast majority of cases these are single estimates with the measuring technique rarely described. Many recordings for gliding mammals are reviewed by Thorington and Lawrence (1981), and they have found that the glide ratios for gliding mammals are generally between 1:2 and 1:3. The gliding marsupial Petaurus breviceps has been recorded gliding at angles between 11° and 27° (Nachtigall, Grosch and Schultze-Westrum, 1974). Nachtigall (1979a) also reports glide angles of between 20° and 30° taken from film of Petaurus breviceps, but it is not clear whether the mammal is gliding from tree to tree or simply parachuting to lose height. Klingel (1965) carried out a detailed study of the glide performance of three species of flying lizard of the genus Draco and found glide angles varying from 9° to 18°.

Single measurements of glides are insufficient for determining the glide performance of such vertebrates because the overall glide consists of an initial steep dive followed by a steady glide. A single measurement gives a combination of both, and so gives no indication of the actual glide angle. It is found in this work that the flying squirrel Petaurista petaurista and the flying lizard Draco spilopterus can alter their glide angle depending on the conditions, from a shallow glide to steep parachuting. A single measurement can therefore be misleading. In this study a large number of glides, over various distances, have been recorded in natural conditions for P.petaurista and D.spilopterus. These give good estimations of glide angles and glide speeds usually used by them.

MacKinnon (1978) suggests that flying squirrels must make large energy savings on travel costs compared with their non-gliding competitors, and so have correspondingly larger foraging ranges. Here the energy cost of the climbing and gliding locomotion of P.petaurista is estimated, and the benefits, in energy saving, of this form of locomotion are discussed.

2.2 Locations, materials and methods

The observations and measurements of the climbing and gliding locomotion of the giant red flying squirrel Petaurista petaurista (Sciuridae) and of the flying

lizard Draco spilopterus (Agamidae) were made in Brunei, a state on the island of Borneo in South East Asia (3° North, 115° East). P.petaurista was found near Lamunin, a town 25km south west of Brunei's capital Bandar Seri Begawan. The observation site was a water tank clearing on the top of a ridge overlooking valleys on either side. Forest covers the ridges and valleys and, although this forest has been selectively logged, many primary forest trees remain and there is secondary forest of great variety. The height of the majority of primary forest trees is in excess of 20m. Views of about 500m are possible to the south of this site, and of 300m to the north. Three nest site trees of P.petaurista have been identified between 20m and 100m from the perimeter of the water tank clearing, and up to eight individuals have been seen from this site at one time. Draco spilopterus was observed in a garden in Bandar Seri Begawan where it is common on the tree trunks and branches. Trees in this garden were generally about 10 ± 3m high.

All the views from the Lamunin water tank site were systematically photographed in black and white using a 35mm Pentax MX camera with a 28mm focal length lens. The flying squirrels were generally observed between 18.00 and 19.30 hours, and their take-off and landing sites were recorded on prints of the site view photographs. When possible, times of the glides and continuous climbing were measured with a stop watch,

Figure 2.1

Distances and angles measured and calculated for the glide of Petaurista petaurista are shown. r_1 and r_2 are the distances measured to the take-off and landing positions respectively, and the angles α_h and β_h are the angles between these points and the horizontal with respect to the observer. The calculated heights above the observer of the take-off and landing points are h_1 and h_2 respectively, and the angle between the points, relative to the observer, is θ_r. The horizontal glide distance is D, and the direct glide distance is G; the direct glide angle is θ_{dg}. H represents the height between the take-off and landing points.

Figure 2.2

The difference between the direct glide angle and the actual glide angle. G, D, H and θ_{dg} are the same as in Figure 2.1. d is the initial distance fallen by the squirrel and θ_g is its actual glide angle.

Figure 2.1

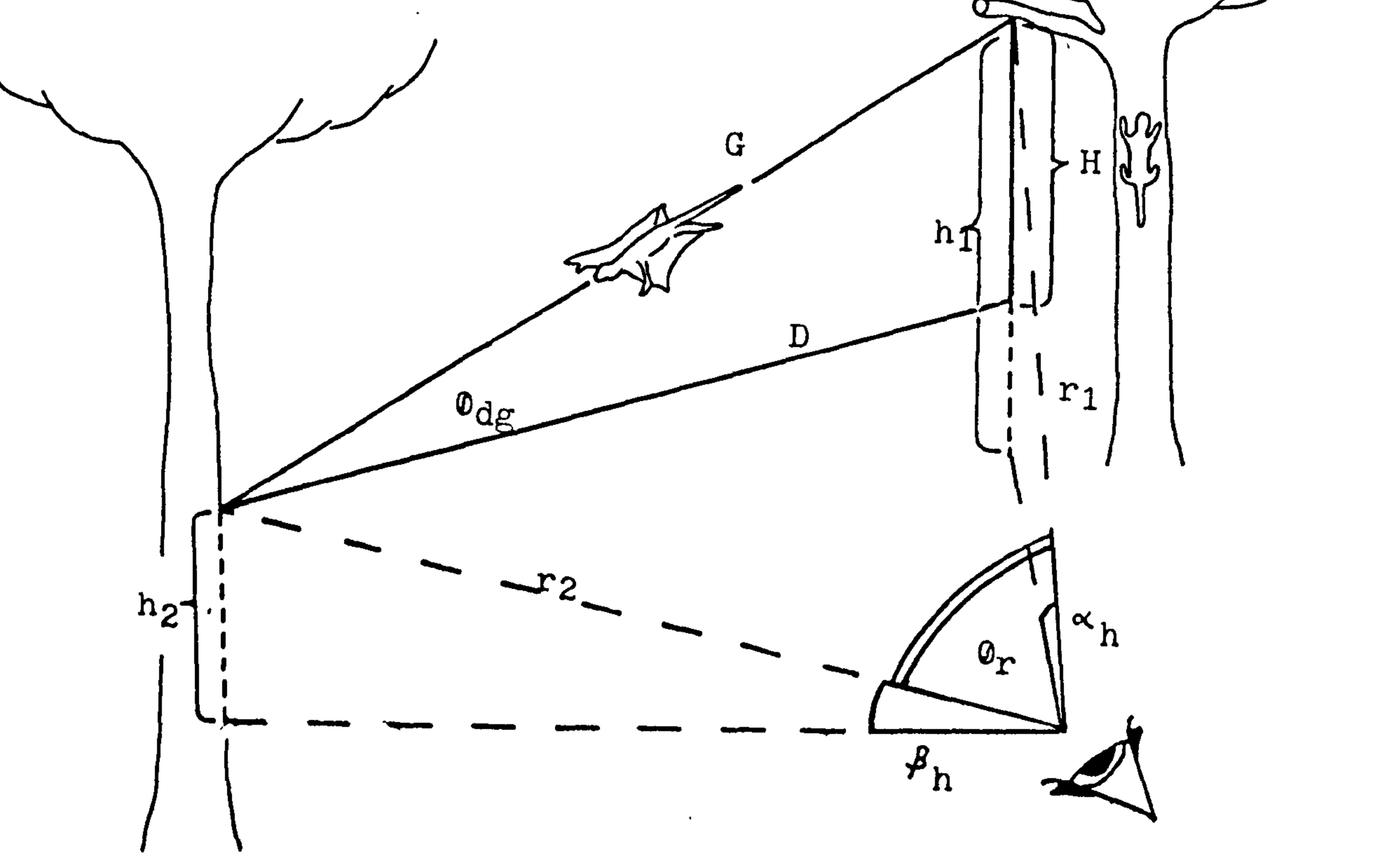

Figure 2.2

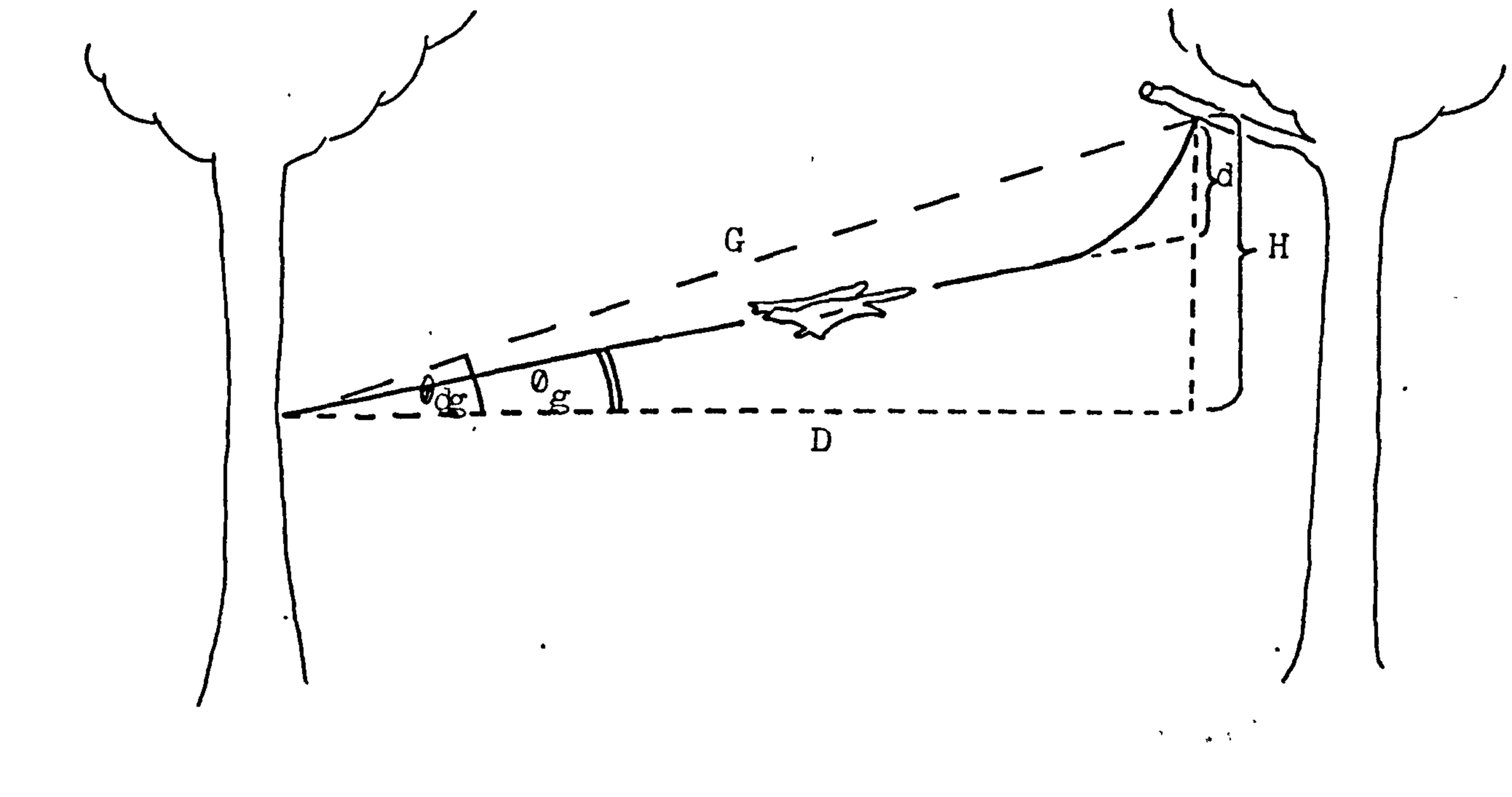

accurate nominally to 0.1 sec. As P.petaurista is active in poor illumination, surveying the positions of take-offs and landings is both difficult and inaccurate if done immediately after they have occurred. By recording these positions on the prints they could be surveyed on the following day in good illumination. The recording technique also considerably reduces the observer's work load during the squirrels' active period.

The dense secondary growth around the tree bases prohibited direct measurements between trees with tape measures, and instead the following survey technique was used, whereby the surveyor could remain on the clearing. The data recorded for a glide by P.petaurista are illustrated in Figure 2:1. The distance to the take-off position r_1 and the landing position r_2 were measured with a Rangematic optical range finder, which has a base of 0.25m and was considered accurate to $\pm$2.5m at the maximum range of 120m for which it was used. The angle between these two positions θ_r was measured with a pocket sextant, accurate nominally to the nearest arc minute, but in the case of this work, where exact sites in the tree foliage are difficult to pinpoint, the accuracy was taken to the nearest 10 minutes.

The direct glide distance G can be found, given that

$$G = \left(r_1^2 + r_2^2 - 2 r_1 r_2 \cos \theta_r\right)^{1/2} \qquad (2.1)$$

The direct glide distance G is an approximation to the actual glide distance, the latter consisting of an initial dive and then a shallow glide, as illustrated in Figure 2.2 . The heights, relative to the surveyor's eye, of the take-off position h_1 and the landing position h_2 are found by measuring the angles α_h and β_h with a clinometer, and from these

$$h_1 = r_1 \sin \alpha_h \qquad (2.2)$$

$$h_2 = r_2 \sin \beta_h \qquad (2.3)$$

The clinometer is accurate to 10 minutes of arc. The difference in the two heights gives the glide 'drop distance' H, and the direct glide angle $\emptyset_{dg}$ can be found by

$$\emptyset_{dg} = \text{arc} \sin \frac{H}{G} \qquad (2.4)$$

and the horizontal glide distance D by

$$D = G \cos \emptyset_{dg} \qquad (2.5)$$

The glide ratio can then be found as H/D. If a glide time T_g was recorded, then an estimate of the overall glide speed V_{dg} could be made from

$$V_{dg} = \frac{G}{T_g} \qquad (2.6)$$

but this is an approximation to the actual glide speed as explained later in this chapter (2.3.2(i)). Climbing speeds could be estimated by recording the positions of the start and end of a continuous climb and timing it. The distance climbed could be found by using the survey technique described above.

The glides of Draco spilopterus were measured in a similar way to those of P.petaurista, but in this case the bases of the trees were easily accessible and so horizontal glide distances could be measured directly with a tape measure. The clinometer was used to determine heights.

The dimensions of D.spilopterus were found by catching individuals in the study area. This can be done by chasing the animal down the tree trunk with a wide broom; once on the ground it will generally 'freeze' and can be picked up.

It was not practicable to trap and measure P.petaurista. Its relative dimensions in flight were estimated from 16mm cine film, taken by the BBC Natural History Unit in Sabah, of P.petaurista gliding overhead. It is not possible to know if the animal is completely level with the camera film plane, and so these results are only estimates. A series of 20 suitable frames were traced and body length, membrane span and membrane area were recorded in arbitrary units (Figure 2.3). The ratios between these parameters were found for 20 frames, and a mean calculated. A

Figure 2.3

Dorsal view of Petaurista petaurista in flight. The wing span b is the distance between the tips of the two cartilaginous spines and the body length l is that between the tip of the nose and the base of the tail. The 'wing' area is given by the area of membrane and that of the body limbs and tail between parts of the membrane.

Figure 2.3

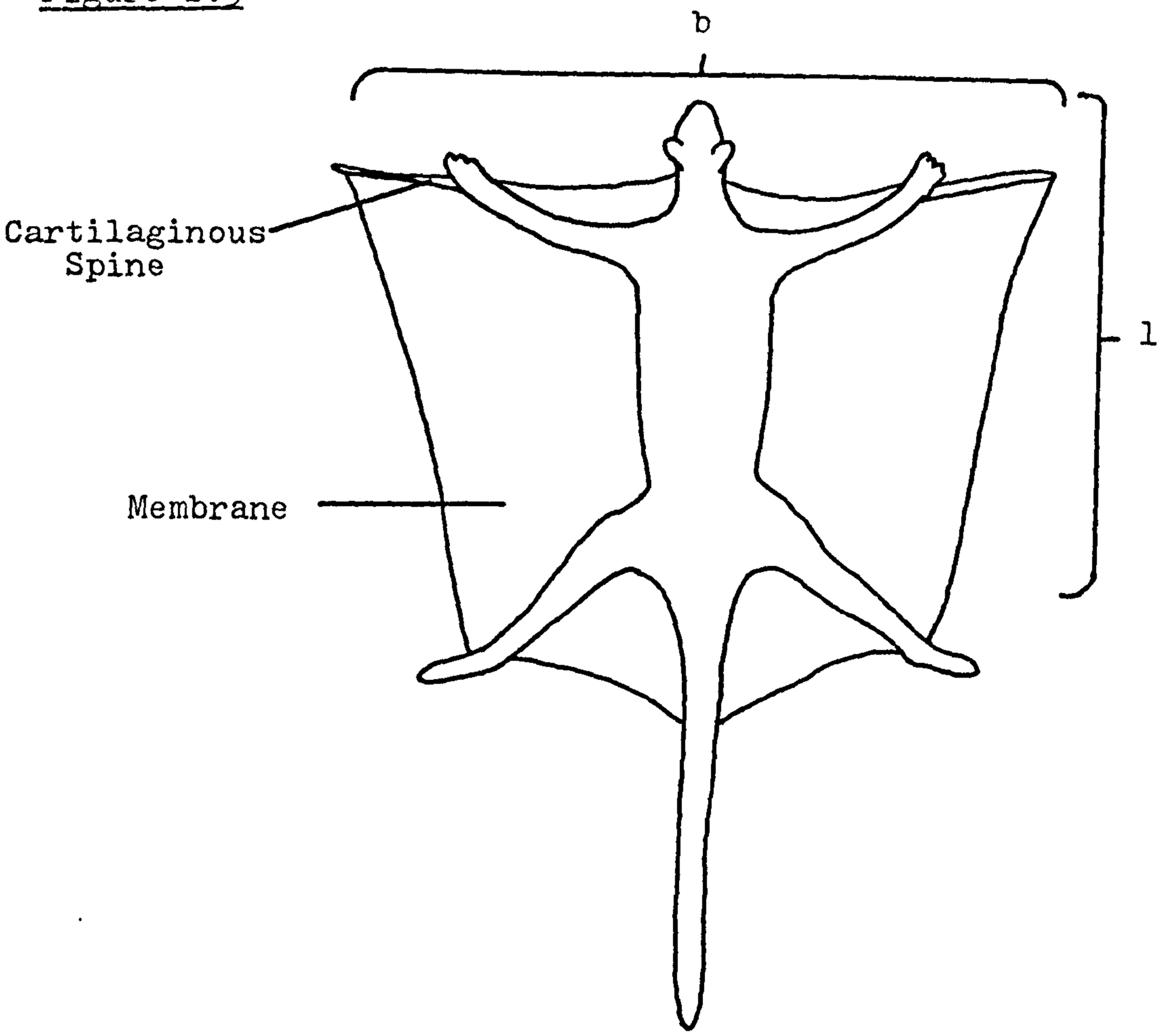

measurement of body length and mass of P.petaurista is given by Davis (1962) and the above ratios can be used to estimate the span and membrane area (Table 2.1).

Table 2.1

(A) Ratios of body dimensions of Petaurista petaurista

RATIO	MEAN	S.D.
BODY LENGTH : 'WING' SPAN	0.98	0.10
('WING' SPAN)^2: 'WING' AREA	1.52	0.15

(B) Estimated dimensions of Petaurista petaurista using the above ratios and the body mass and length measurements of Davis (1966)

BODY MASS (Kg)	BODY LENGTH (m)	WING SPAN (m)	WING AREA (m^2)	ASPECT RATIO	WING LOADING (N m^{-2})
1.33	0.4	0.41	0.110	1.52	120

2.3 Petaurista petaurista

2.3.1 General behaviour

Petaurista petaurista, like all other gliding mammals, is nocturnal (Walker, 1964) and remains within its nest during the day. At the Lamunin site three nest trees were known; two nests were in holes in dead trees, but the third appeared to be amongst the leaves of an epiphyte in a living tree. This is surprising, as flying squirrels are generally believed to nest only in hollows of dead trees (MacKinnon, 1978; Walker, 1964). The large size of P.petaurista (approximately 1.3kg) may make it less vulnerable to predators, and so allow it to have more flexibility in its nest site selection.

P.petaurista usually becomes active in the evening between 30 and 15 minutes before complete darkness. The time of emergence from the nest was noted for an individual over a period of three weeks and it varied by only five minutes. Having left the nest, the squirrel generally climbs to the top of its nest tree, and then grooms itself for up to 10 minutes. The extensive membrane of P.petaurista is likely to be very susceptible to parasites and so to require considerable grooming. When this has been completed, it will start gliding from tree to tree, the height lost by each glide being gained by tree climbing between glides. The details of the gliding and climbing are given in

Section 2.3.2 and are illustrated in Figure 2.2 . By this time the ambient light intensity was very low, with silhouette photography of the animal against the sky being just possible with 400ASA film. The climbing and gliding locomotion usually continued until the animal was out of sight, or until it was too dark to observe it. Occasionally, after only a few glides, the animal would remain amongst a tree's foliage, feeding on leaves. Presumably the squirrel climbs and glides until it reaches a suitable feeding tree.

P.petaurista moves out of its nocturnal niche during courtship and mating. On two occasions, during August 1976 and June 1979, up to eight individuals were seen to be active from 15.00 hours onwards. Generally they were in pairs, chasing each other using their climbing and gliding locomotion. The squirrels did not move throught the forest in one direction, as they generally do in the evening, but instead went round in large circles. The gliding sometimes involved spectacular displays of control such as, in one instance, a 180^{o} turn, so that the squirrel took off and landed on the same tree. This diurnal behaviour, on both occasions, lasted for only three days, and on the final day during 1979 a pair were seen copulating on an horizontal branch. A third squirrel, presumably a male, approached the mating couple and a fight ensued, resulting in the challenger being pushed from the branch.

As it fell it opened its membranes and glided to a nearby tree. After this day, all the squirrels returned to the usual nocturnal behaviour patterns. The diurnal behaviour is interpreted as being a period of partner selection, where gliding displays are of great importance. Once pairs are formed mating occurs, after which the squirrels return immediately to their normal nocturnal behaviour. P.petaurista is apparently solitary except during this brief mating period.

During the courtship behaviour P.petaurista was observed gliding during a rainstorm. This did not seem to impair its performance; any water collected on the membranes was periodically shaken off between glides.

2.3.2 Results

2.3.2(i) Climbing and gliding locomotion

The glide of Petaurista petaurista is illustrated in Figure 2.2. It consists of an initial steep dive, which becomes progressively shallower until the squirrel is in a steady shallow glide. At the end of the glide it increases its angle of incidence, presumably to reduce speed, but the glide angle appears to remain constant.

The horizontal distance covered and the vertical distances fallen, for all the recorded glides, are plotted on Graph 2.1 . The slope of the straight line between each point and the origin gives the direct glide

angle $\emptyset_{dg}$ for each particular glide. If the squirrel is assumed to be gliding each time at a minimum glide angle, then the line of 'best fit' through all the points should approximate to the actual glide angle $\emptyset_g$, and the intercept with the y-axis to the initial drop distance d of the dive. Linear regression is unsuitable for the calculation of the line of 'best fit', as its calculation implies that one variable in the bivariate plot is independent and can be measured with negligible error, while the other is dependent and subject to measurement error. Here, there is error in the measurement of both variables, and in such a case the reduced major axis (R.M.A.) is suitable for calculating the line of best fit. The use and calculation of the reduced major axis is discussed in detail in Chapter 5.2.3. The R,M.A. for all the data is shown by the solid line on Graph 2.1; it gives a glide angle of 11.9 ± 1.8^{o} and an initial drop of 7.5 ± 2.1m (see Table 2.2). The wide confidence limits result from the considerable scatter of the data, which is in turn due to the limits of the survey technique and because P.petaurista is unlikely to minimise its overall glide angle during every glide. For reasons which may include restricted landing sites, or the need to turn during a glide, the overall glide angle for a single glide is not always minimised. This is especially true for short glides, when the squirrel may have to glide at a steeper angle to land on the preferred clear

Graph 2.1

Vertical distance H against Horizontal distance D for glides of Petaurista petaurista. The solid line is the RMA for all the points and the broken line is the RMA for the 'best glide' data given by the circles enclosing clear stars. The equations for these RMA lines are given in Table 2.2

Graph 2.2

Direct glide distance G against glide time for Petaurista petaurista. (See Table 2.2 for equations). The RMA is represented by a solid line.

Graph 2.1

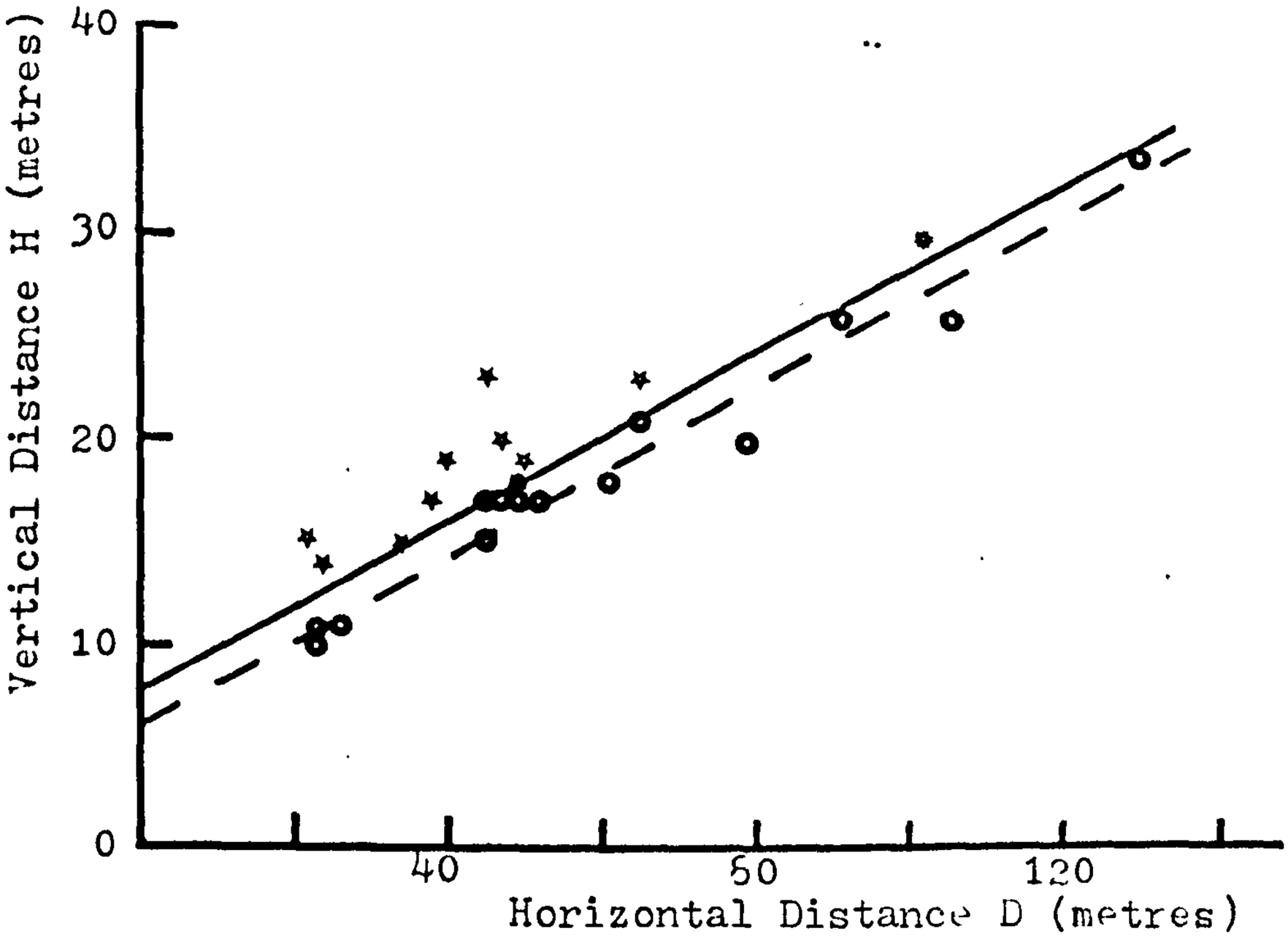

Graph 2.2

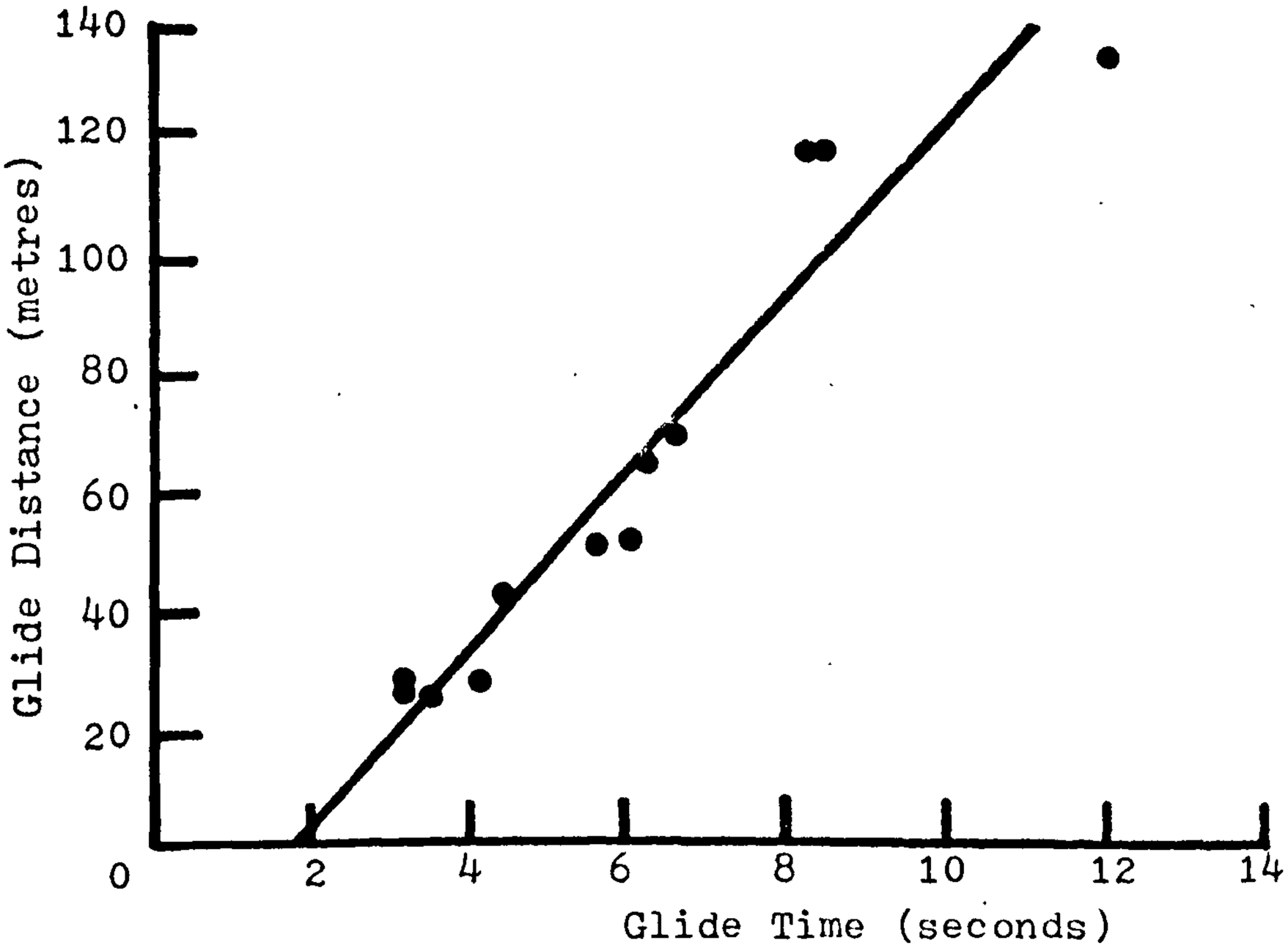

TABLE 2.2 Correlation of vertical and horizontal glide distances of Petaurista petaurista (see Graph 2.1)

		N	r	F	α	β (θg^{o})	α Range		β Range	
							$\alpha-$	$\alpha+$	$\beta-$ (θg^{o})	$\beta+$ (θg^{o})
ALL DATA	Y(X)	26	0.933	161	8.25	0.196(11.1)	6.24	10.3	0.165(9.37)	0.228(12.8)
	RMA		***		7.45	0.210(11.9)	5.44	9.47	0.178(10.1)	0.242(13.6)
BEST GLIDE DATA	Y(X)	15	0.982	834	6.23	0.206(11.6)	4.58	7.88	0.181(10.3)	0.230(13.0)
	RMA		***		6.10	0.209(11.8)	4.35	7.66	0.185(10.5)	0.234(13.2)

Correlation of glide distance and glide time of Petaurista petaurista (see Graph 2.2)

		N	r	F	α	β	α Range		β Range	
							$\alpha-$	$\alpha+$	$\beta-$	$\beta+$
ALL DATA	Y(X)	12	0.955	104	-23.0	14.4	-43.4	-2.7	11.3	17.6
			***		-27.1	15.1	-47.5	-6.7	11.9	18.3

portion of the tree trunk rather than into the foliage. On a long glide it can minimise its glide angle and still land on the exposed tree trunk. Having some of the shorter recorded glides at a steeper angle tends to make the R.M.A. line artificially shallower, with a higher intercept on the y-axis. To avoid this bias in the data, a 'best glide' R.M.A. line, given by the broken line on Graph 2.1, has been calculated. This takes into account only the data points below the first 'all points' R.M.A. line, and gives a glide angle θ_g of 11.8 $\pm$ 1.4^o and an initial drop distance of the dive of 61 $\pm$ 1.7 m. This line gives a similar glide angle to that of the 'all points' line, but the intercept gives a lower drop distance. For the reasons given above, this is considered to be a more realistic measurement of P.petaurista's glide performance.

The initial dive is required to convert the squirrel's potential energy into the required kinetic energy for the glide. P.petaurista must have a minimum glide speed for its minimum glide angle, below which it stalls, and this speed must be achieved by the dive. The dive is initially very steep, estimated visually to be between 50^o and 70^o to the horizontal. As its speed and kinetic energy increase, the glide is rounded out into the shallower 12^o glide.

The glide is apparently steady, and generally P.petaurista will hold a straight glide path of presumably constant glide speed. Control is good,

and it can turn very sharply by rolling the body about its axis. The glide speed can be found by determining the slope of the R.M.A.line of the glide distance G against time T_g for all the recordings (Graph 2.2). This gives a glide speed of 15.1 ± 3.2m s^{-1} , and the intercept of the time axis at 1.9s indicates the time required for accelerating in the dive and decelerating when landing.

During the glide the angle of incidence of the squirrel appears to be slightly below the horizontal, and so its angle of attack is likely to be between 5^{o} and 10^{o}. About 5 to 10m before reaching the landing site the squirrel dramatically increases its angle of incidence, as illustrated in Figure 2.4, but its glide angle does not appear to alter. This is different from smaller flying squirrels (Borodulina and Blagosklonov, 1951) and the flying lizard Draco (Klingel, 1965; Scholey, Chapter 2.4.2) which gain height during landing. The combination of maintaining the same glide angle but increasing the angle of incidence implies that P.petaurista is dramatically increasing its angle of attack. This increases induced drag and causes deceleration, as well as bringing the body into a suitable attitude for landing on a vertical tree trunk. As the incidence increases, it appears that the hind limbs are brought forward, slackening the membrane and increasing its camber. The high camber, together with the low aspect ratio of the wing

Figure 2.4

The increase in the angle of incidence of Petaurista petaurista during landing (angles a - d). The glide angle appears to remain constant, and so the squirrel is greatly increasing the angle of attack during landing.

Figure 2.4

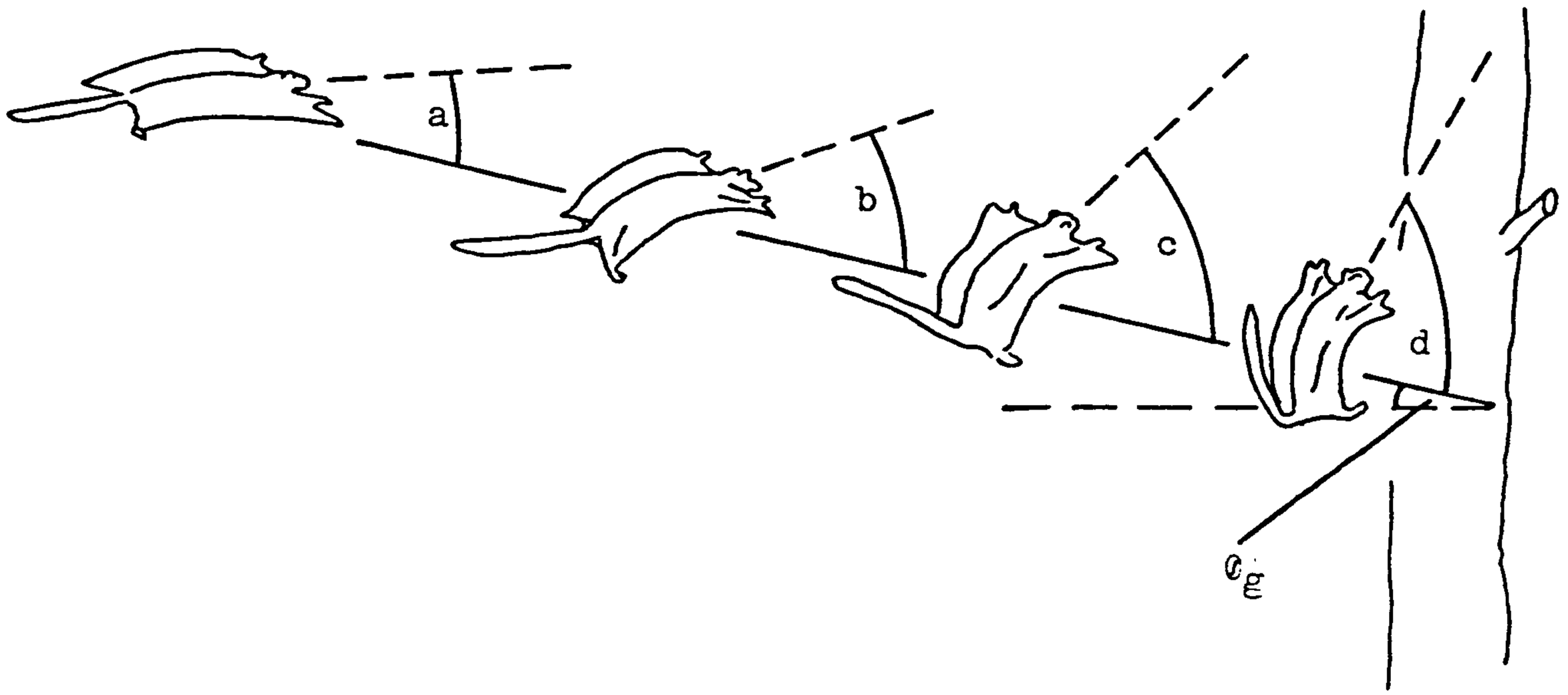

and fur on the top surface, are probably of importance in keeping the air flow attached at high angles of attack, so preventing stalling. Nachtigall (1979b) has shown that a skin of the marsupial glider Petaurus is capable of sustaining lift at very high angles of attack. By the time Petaurista petaurista reaches its landing site its forward velocity has been greatly reduced, and the limbs are brought forward to absorb the remaining kinetic energy on landing. Generally P.petaurista lands on exposed tree trunks, but on two occasions it was seen to land amongst leafy branches, and it was once observed landing on a 20cm diameter vine.

After landing, the squirrel will usually pause for a few seconds before beginning to climb. The climbing action is illustrated in Figure 2.5; it is a bounding gait, with the pairs of fore and hind limbs being moved together. The fore limbs extend to grasp the surface of the tree trunk with the long claws of the manus, and the hind limbs are then brought up beneath the body. The fore limbs are released and stretched forward as the hind limbs are extended, and once again the claws of the fore limbs grip the trunk while the hind limbs are again moved forward. The mean climbing speed of P.petaurista on vertical or near vertical tree trunks is $0.7 \pm 0.2 m\ s^{-1}$. The tree is not usually scaled in one continuous climb, although this may occur; usually the squirrel pauses at intervals up the tree and carefully surveys the area

Figure 2.5

The climbing gait of Petaurista petaurista while scaling a vertical tree trunk (a - e). f is a dorsal view of c showing how the forelimbs are spread sideways to grip the trunk while the hind limbs are moved forwards and backwards, close to or beneath the body. There is not an equal time difference between each illustrated position, and there is no accurate time record for this sequence.

Figure 2.5

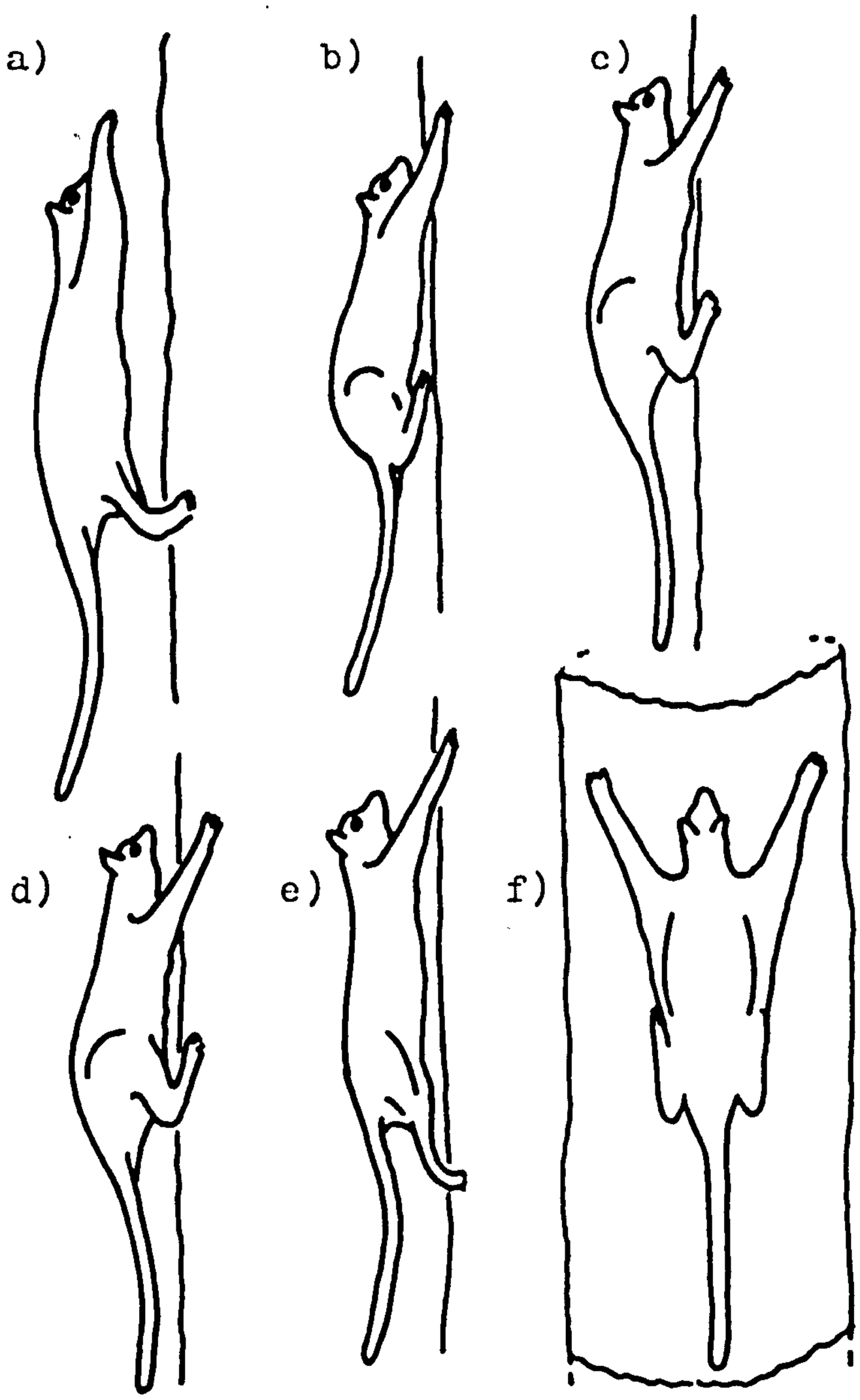

around it. These pauses are probably not caused by exhaustion, since long climbing periods were observed, but are more likely to allow the animal to check for possible dangers while it is on the exposed tree trunk.

When moving within the branches of large trees, P.petaurista often makes large jumps, and extends the membranes to retard its fall. In these cases the body attitude remains approximately horizontal and the squirrel has little forward speed. It is supported predominantly by drag forces, not by lift as in gliding, and so can be considered to be parachuting (Figure 2.6B) as its glide angle is less than 45^{o} (Rayner, 1981). When parachuting the membrane is slackened to trap air and so increase drag.

2.3.2(ii) Wing area, aspect ratio and lift coefficient of Petaurista petaurista

The wing area of P.petaurista can be estimated from the dimensions of the specimen recorded by Davis (1962) and the ratios obtained from the 16mm cine film. In flight, the ratio of body length to total span of the fore limbs is 0.98 ± 0.10, and it is interesting to note that 35% of the span is produced by the extended cartilaginous spines of the wrists (Figure 2.3). The aspect ratio ($span^2/area$) is 1.52 ± 0.15. Aspect ratio is dimensionless and can be found directly from the cine film. Again, the cartilaginous spines are important in improving the aspect ratio.

Figure 2.6A

Petaurista petaurista gliding. The glide angle θ_g is less than 45^o and so the resultant force R required to balance the weight mg is produced predominantly by the lift force L and not that of drag D which retards the forward motion of the squirrel.

Figure 2.6B

Petaurista petaurista parachuting. The glide angle is greater than 45^o, and so the resultant force R required to balance the weight mg is produced predominantly by the drag force D and not that of lift L.

Figure 2.6A

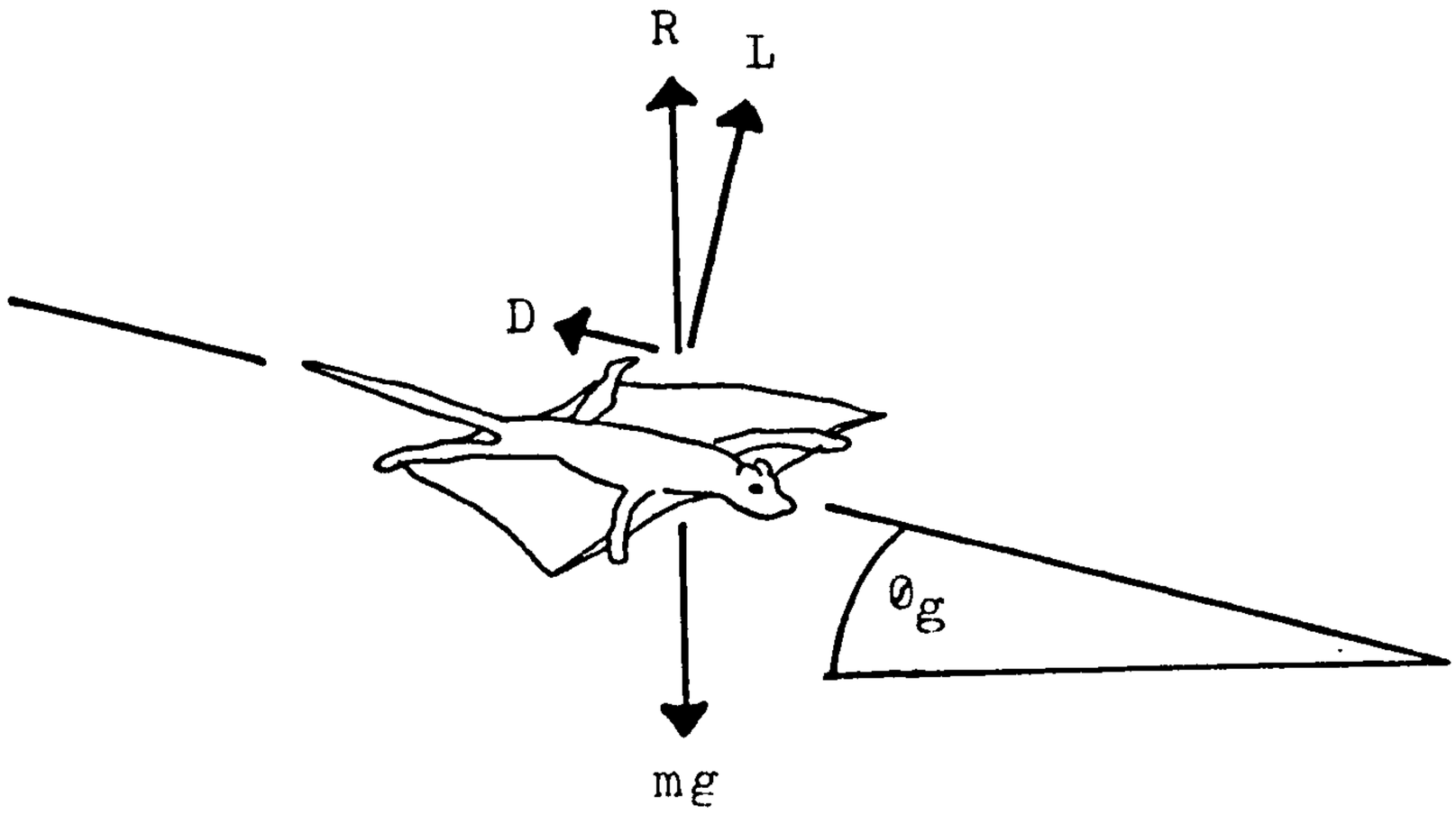

Figure 2.6B

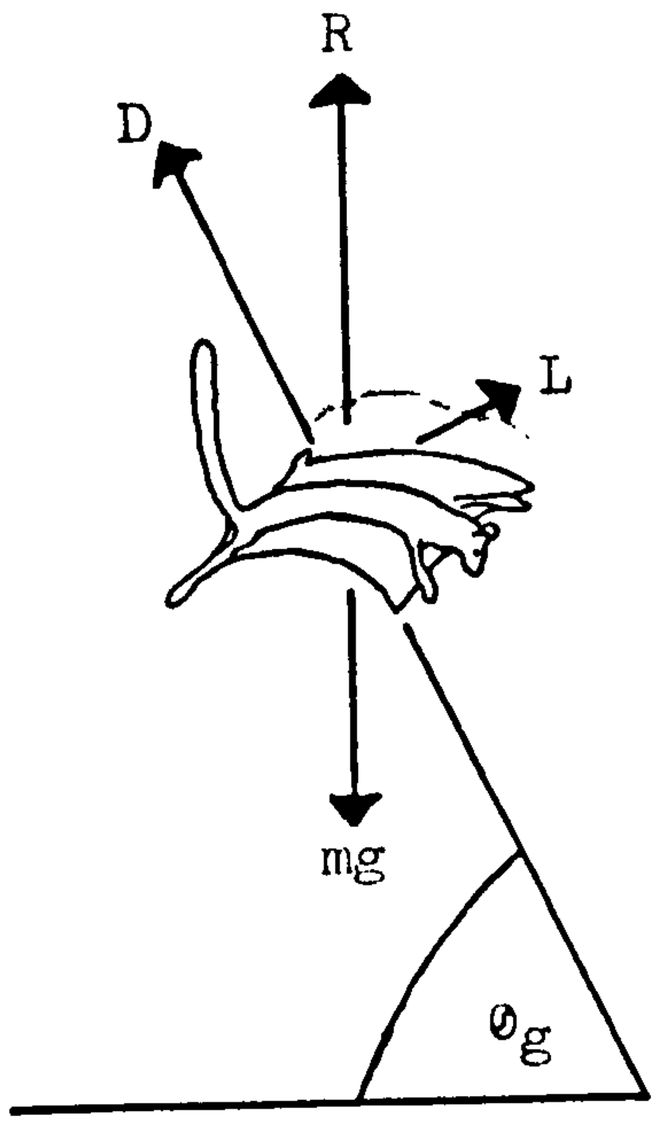

Given that the body length of the specimen measured by Davis (1962) was 0.4m, and its mass 1.33kg, then its span would be 0.408 ± 0.05 and, given an aspect ratio of 1.52, its area would be approximately $0.110m^2$. This means that the wing loading of P.petaurista is about 120N m^{-2}, which is equivalent to very high wing loading of birds such as ducks with similar mass.

If P.petaurista is in a steady glide, with constant glide angle θ_g and speed V_g, then the forces acting are as illustrated in Figure 2.6A. The lift L is given by

$$L = \tfrac{1}{2} \rho S V_g^2 C_L , \qquad (2.7)$$

where ρ is the air density of 1.22kg m^{-3}, S is the wing area, and C_L is the lift coefficient. The lift must support the weight, so that

$$L = mg \cos \theta_g , \qquad (2.8)$$

where m is the body mass and g is the acceleration due to gravity (9.81m s^{-2}). The lift coefficient can then be written as

$$C_L = \frac{2 m g \cos \theta_g}{\rho V_g^2 S} \qquad (2.9)$$

or, with mg/S expressed as wing loading N

$$C_L = \frac{2N \cos \theta}{\rho V^2} g \quad . \qquad (2.10)$$

P.petaurista, with a wing loading of 120N m^{-2}, a glide angle of 12^o, and a glide speed of 15.1m s^{-1}, has a lift coefficient of 0.84.

2.3.3 The energy cost of Petaurista petaurista when climbing and gliding, compared with that of quadrupedal arboreal locomotion

Gliding in rainforest is a means of locomotion, and might result in energy saving over conventional quadrupedal locomotion. The work of Taylor (1977) makes it possible to estimate the metabolic power consumption of a mammal when running P_r by

$$P_r = f V_r + \alpha P_b \quad , \qquad (2.11)$$

where $f = 10.7m^{0.6}$, m is the body mass, V_r is the running speed, α is a constant given by Taylor as 1.7 and P_b is the basal metabolism which he expresses as

$$P_b = 3.5\ m^{0.75} \quad . \qquad (2.12)$$

The power required for vertical climbing P_c can be

found from Equation (2.11) if the extra rate at which work must be done against gravity is accounted for. This is dependent upon the climbing efficiency y of the squirrel and its body weight, and is expressed by Rayner (personal communication) as

$$P_c = \left(g + \frac{mg}{y}\right) V_c + \propto P_b \quad , \qquad (2.13)$$

where g is the acceleration due to gravity of 9.81m s^{-2} and V_c is the climbing speed. Taylor et al (1972) found climbing efficiencies for a number of mammals running up an incline of 15^o. Of these, the chimpanzee (Pan troglodytes) gave the highest efficiency of 0.66, and man gave the lowest, 0.34 . The efficiency of vertical climbing is likely to be less, and in this study two values - 0.2 and 0.4 - are used, the efficiency of the squirrel probably having an intermediate value.

There are no measurements of the power required to glide P_g for gliding mammals. It has been recorded for a herring gull (Larus argentatus) by Baudinette and Schmidt-Nielsen (1974) as being

$$P_g \simeq 2 P_b \quad , \qquad (2.14)$$

while Pennycuick (1972b) calculated it to be approximately $1.5P_b$. The Baudinette - Schmidt-Nielsen value is

used here as an estimate, although any close similarity in this respect between birds and flying squirrels is doubtful. However, since P_g is very small compared to P_c, errors in the estimation of P_g will have little effect on the total power estimate of climbing and gliding.

For a given journey, the total cost will depend on the proportion of vertical climbing to gliding which is given by the direct glide angle θ_{dg} (Figure 2.2). θ_{dg} varies with horizontal glide distance D because the initial drop d is constant. The variation of θ_{dg} with D is shown in Graph 2.3, given that d is 6m and the actual glide angle θ_g is 12^o. For similar reasons the overall glide speed V_{dg} will vary with D as the time to accelerate to and decelerate from V_g is constant at about 1.9s.

Given the above relationships, for any value of horizontal glide distance D_1, the height H_1 required can be found, and if the climbing speed is known, then the time spent climbing T_{c_1} to height H_1 can be calculated. The energy E_{c_1} required to climb to height H_1 is given by

$$E_{c_1} = \left[\left(\delta + \frac{mg}{y}\right) V_c + \propto P_o\right] T_{c_1} . \qquad (2.15)$$

Similarly; the time T_g required to glide distance D_1

can be found, and so the energy spent gliding E_{g_1} for that distance is

$$E_{g_1} = 2 P_b T_{g_1} \quad . \tag{2.16}$$

The total energy expended E_t to travel the horizontal distance D_1 is given by the sum of E_{c_1} and E_{g_1}. The metabolic cost of transport C_g, defined here as the energy required to move unit weight through unit distance, for any value of D, is given as

$$C_g = \frac{E_t}{mgD} \quad . \tag{2.17}$$

This cost of transport is dimensionless. It can now be seen how the cost of transport is dependent upon the distance travelled by each glide or similarly the overall glide angle $\emptyset_{dg}$. Graph 2.4 is a plot of cost of transport against glide distance D for two values of y (0.2 and 0.4), and it can be seen that this cost is dramatically reduced for glides up to 60m, above which it only declines slightly. Clearly it pays P.petaurista to climb high trees and extend its glide to 60m or more.

From Equation (2.11), the metabolic cost of transport of a mammal running horizontally is

$$C_r = \frac{P_r}{mg V_r} \quad . \tag{2.18}$$

Graph 2.3

The variation of direct glide angle θ_{d_g} with horizontal glide distance.

Graph 2.4

Cost of transport against the horizontal distance travelled. The two solid curves are for the climbing and gliding locomotion of Petaurista petaurista, assuming a body mass of 1.33kg, a climbing speed of 0.7m s^{-1}, a direct glide angle as given in Graph 2.3, a glide speed of 15m s^{-1} and an acceleration and deceleration period of 1.9s during which the mean speed is assumed to be 7.5m s^{-1}. The higher curve is for a climbing efficiency of 0.2 and the lower for one of 0.4. The horizontal broken line gives the cost of horizontal unimpeded running at 1.0m s^{-1} of a similar sized non-gliding squirrel.

Graph 2.3

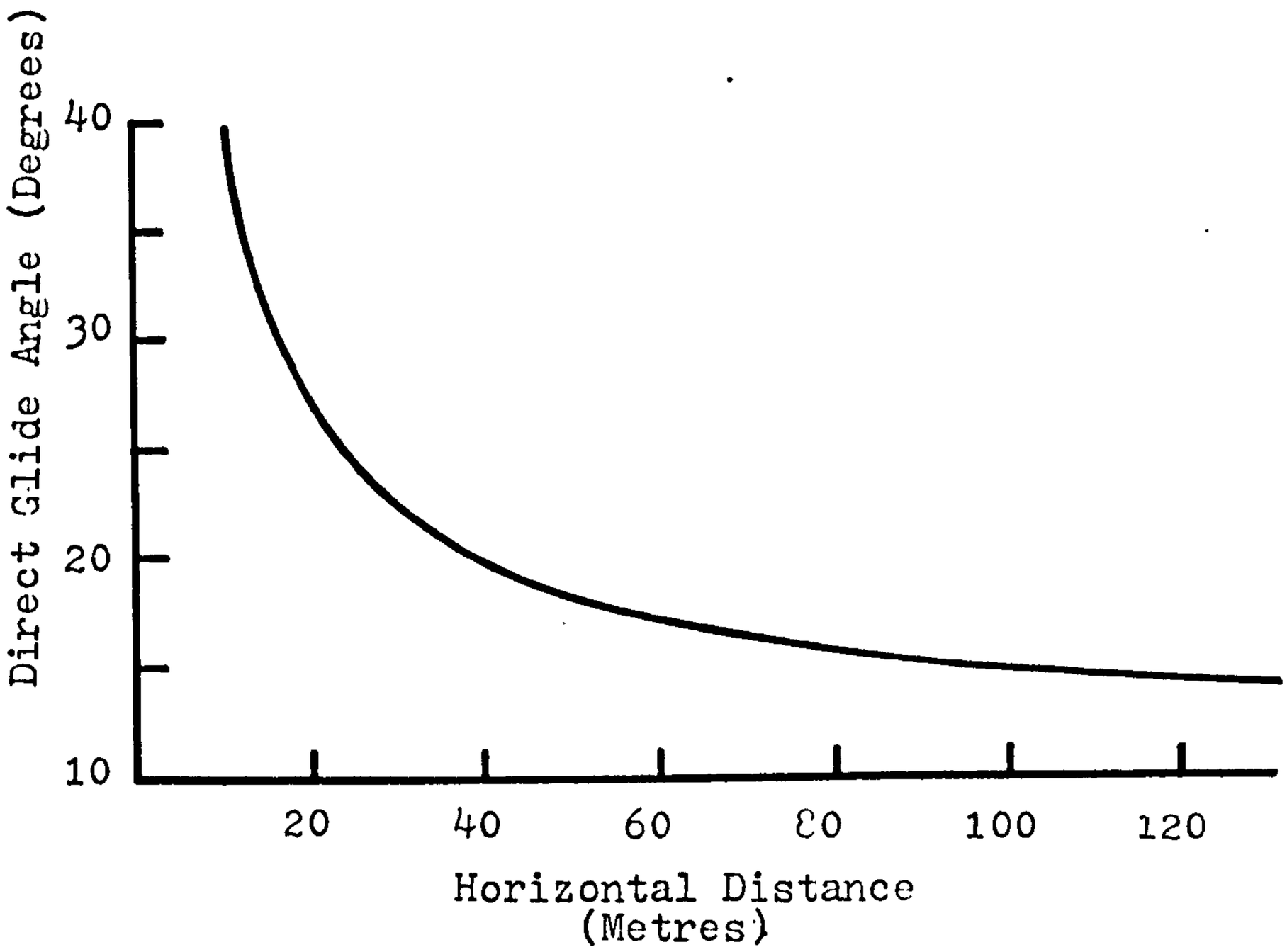

Graph 2.4

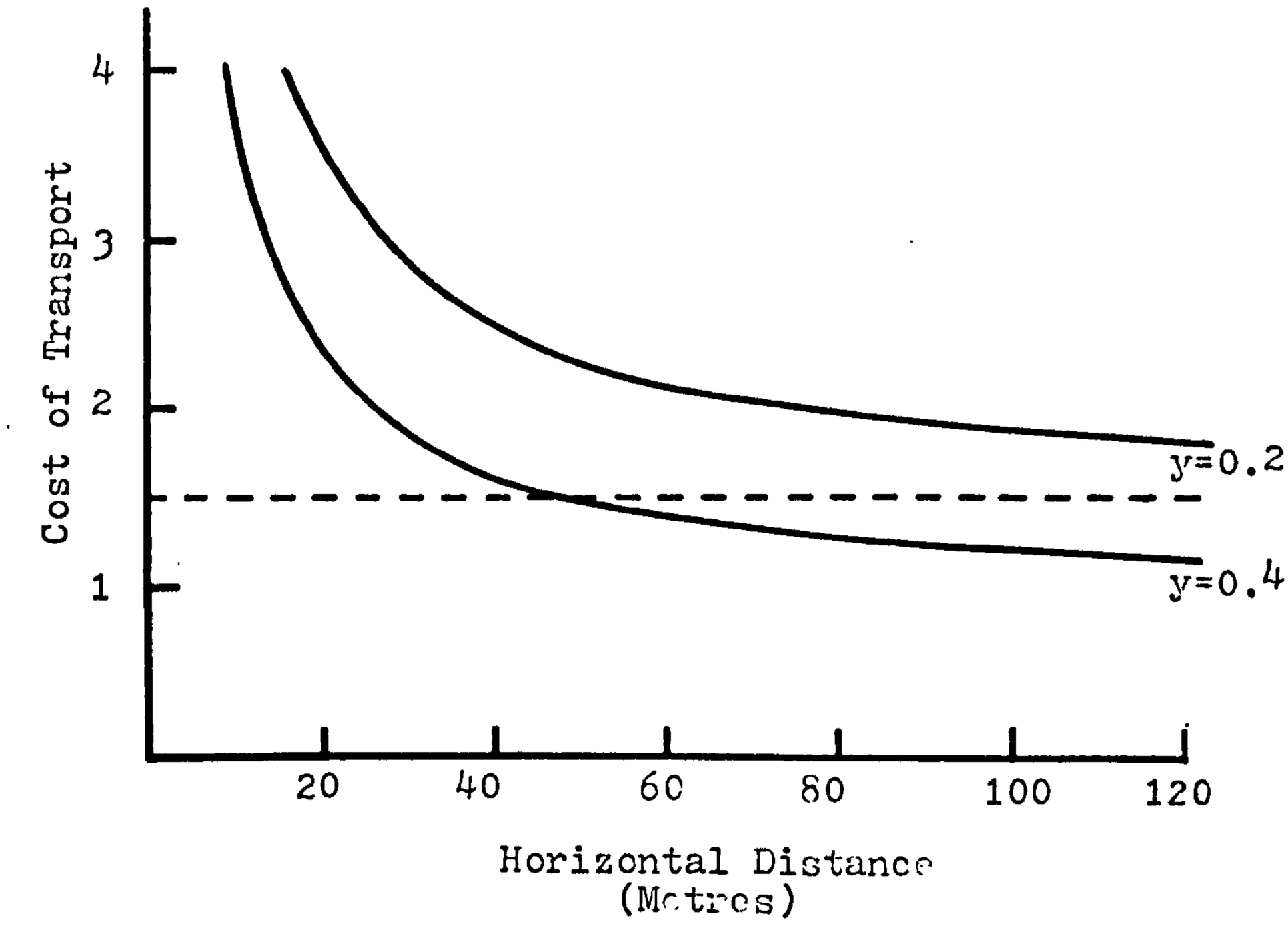

This is again dimensionless. To compare the costs of P.petaurista's climbing and gliding locomotion with conventional quadrupedal arboreal locomotion, a diurnal squirrel equivalent, such as Ratufa (1.0 to 1.5kg) must be found, and its running speed through the forest canopy determined. Unfortunately Ratufa is relatively rare and elusive. A smaller common squirrel, Callosciurus notates was trapped, found to have a body mass of 0.235kg, and released to run through a straight line of closely positioned Casurina trees. Its average speed was 2.2m s^{-1}, and this was almost certainly acheived by sprinting anaerobically. Crude estimates of normal commuting speeds by C.notates were made using the usual survey technique and gave speeds of 1.0 ± 0.5m s^{-1}.

Maximum running speeds of quadrupeds theoretically remain constant with body mass (Hill, 1950) and have been found to do so with large bovine quadrupeds (Alexander et al 1977). With arboreal squirrels it is likely that larger ones must commute more slowly and "cautiously" than smaller individuals, due to the effect of their mass on bending or breaking branches. It is therefore assumed here that the commuting speed of Ratufa would not greatly exceed that of Callosciurus. The metabolic cost of transport for a non-gliding squirrel of body mass 1.33kg, running horizontally at 1.0 m s^{-1} is 1.5, and is given in Graph 2.4 for comparison with the gliding costs. It must be.

stressed that this is the cost expected for an animal running on a treadmill, and not through a forest canopy. As such, it is probably a minimum cost and the actual cost of forest commuting, with all the required changes in speed, height and direction, must be far higher. Furthermore, the gliding locomotion is direct whereas quadrupedal locomotion often requires large detours to reach a destination.

2.3.4 Discussion

The results suggest that Petaurista petaurista must glide 60m or more to minimise its cost of transport, in which case its environment must contain trees higher than 20m. This form of locomotion, by an animal of its size, is probably restricted to environments with mature primary forest trees. P.petaurista cannot always glide 60m or more, as the recordings on Graph 2.1 show. Graph 2.1 does however give a biased indication of the distribution of glide distances in favour of short glides. This is because only about a third of the glides observed could be recorded, and those omitted were generally longer glides in excess of 60m where the squirrel's landing was obscured by foliage.

Given the interpretation of the results section, that the cost of running through a forest canopy is much higher than 1.5 for a normal quadruped of

similar size to Petaurista petaurista, then it appears that climbing and gliding in rain forest is energetically cheaper than running. The high gliding speed also makes P.petaurista's commuting faster than a non-gliding competitor, and this may be important in allowing more time at a feeding site. Gliding in mammals has evolved as a means of locomotion and not as an escape mechanism as is sometimes suggested.

The low cost of transport is of importance to P.petaurista as, for a given fuel load, this cost is inversely proportional to its foraging range. This range is termed the 'foraging radius' by Pennycuick (1979). A large foraging radius is important in tropical rain forest for animals with a fixed nest site, as at certain times of the year suitable food can be well scattered through the forest. This is because rain forest is composed of numerous species of tree with, for example, some 3000 species in North Borneo (Brown, 1955) and members of the same tree species are usually well scattered. The majority of trees produce fruit and fresh leaves in seasons, but some have irregular cycles, whilst others can continuously produce new leaves (Medway, 1972). Hence, out of the 'fruiting seasons' herbivores must survive on the well scattered, non-seasonal plants. Mature leaves are generally not a suitable food source (Wolda, 1978).

The reasons why all other rain forest herbivorous

mammals have not developed this advantageous form of locomotion are as follows: firstly, animals such as higher primates do not require nest sites, mainly because they can carry their young from birth, so large daily foraging radius is of no importance. Secondly, the power required to climb, given in Equation (2.13) is proportional to (body mass)$^{1.1}$ and so climbing requires more specific energy the larger the animal is. Climbing and gliding becomes correspondingly less favourable with increase in size and P.petaurista, being one of the largest gliding mammals, is probably close to the body mass limit above which significant energy savings can no longer be achieved. Two disadvantages of being a gliding mammal are that the membranes make the animal more cumbersome when running (MacKinnon, 1978; Sollberger, 1943), and the gliding action exposes the animal from the protection of the foliage and is predictable in its direction and eventual landing site. Both factors must make gliding mammals very susceptible to predators, especially birds. Monkey eating eagles (Pithecophaga jefferyi) in the Philippines regularly prey on colugos (Cynocephalus spp.).

The combination of these two disadvantages probably results in gliding mammals having to be nocturnal. Their nocturnal habit is curious, as gliding through a forest in daylight would be far less demanding on the animal's sensory systems. Squirrels are

predominantly visual animals and vision becomes less effective for detecting speeds as the ambient light intensity is reduced (Lythgoe, 1979). The selection pressure causing nocturnalism in P.petaurista is unlikely to be food availability, as leaves are equally available in the day and at night. There may be thermoregulatory advantages in climbing and gliding at night, but this is unlikely as normal quadrupeds and gliding mammals require similar maximum metabolic rates; also P.petaurista showed no indication of 'over-heating' during its diurnal courtship behaviour. As MacKinnon (1978) suggests, possible predation by diurnal carnivorous birds probably forces gliding mammals to be nocturnal. Although gliding mammals are preyed upon at night by owls (Walker, 1964; Fleay, 1954; Grzimek, 1967), the incidence of predation is likely to be less at night than during the day , due simply to the greater number and diversity of diurnal avian predators compared to nocturnal ones.

It is surprising that P.petaurista should abandon the protection of nocturnalism during its courtship. Its vision must be adequate for judging its own glides at night, but may not be suitable for scrutinising other squirrels' glide performances some distance away. Such scrutiny is probably of great importance in the sexual selection of P.petaurista, and this must outweigh the risks of being diurnal. These risks are minimised by having a short courtship period. It is also

intersting to note that the courtship period did not occur at the same time in both years and this is probably a deliberate irregularity to prevent potential predators from predicting when the squirrels will be vulnerable.

The gliding squirrels and their non-gliding counterparts must occupy slightly different niches in order to remain sympatric. The difference must be subtle, as the two counterparts occupy approximately the same vertical level in the forest (MacKinnon, 1978). If so, it is suggested that the diurnal squirrels, being less cumbersome and probably more efficient feeders than the gliding squirrels, specialise in feeding on the more abundant food sources, while gliding squirrels, utilising their larger foraging radii, specialise in feeding on more scattered food, which would be out of range of the diurnal squirrels at certain times of the year.

The cost of transport of <u>P.petaurista</u> is directly dependent upon its direct glide angle θ_{dg}, which is in turn determined by the actual glide angle θ_g and the initial drop distance d. This squirrel could improve its direct glide angle by firstly increasing its membrane area, so reducing its wing loading and consequently its glide speed. The lower the glide speed, the less the kinetic energy which has to be gained during the initial dive; any reductions made to this initial height loss would cause dramatic

reductions in the direct glide angle, particularly for short glides. Lower glide speeds would increase the energy costs for gliding, but these would be far outweighed by the reductions in climbing costs, resulting from reducing the direct glide angle. The actual glide angle $\emptyset_g$ could in turn be improved by increasing the aspect ratio of the 'wings'. To effect these two improvements, P.petaurista would probably have to increase the length of its fore limbs, and possibly use the digits of the manus to support the membrane, as has been done by bats. This would probably greatly reduce its performance as a quadruped. P.petaurista has compromised in a manner that has allowed it to develop its gliding structure as far as possible without altering its basic quadruped form while keeping the manus free for effective food manipulation and climbing. The cartilaginous spines of the fore limbs, hingeing at the wrist, are an important adaptation of the flying squirrels (Petauristidae) as they greatly improve the wing area and aspect ratio while requiring no changes in the size of the fore limbs or the structure of the manus. The scaly tailed squirrels (Anomaluridae) have a convergent structure which hinges between the humerus and the radius and ulna. The length of the spine is probably limited by its mechanical properties.

Further development of the gliding structures would bring the squirrels into competition with.

fruit bats (Megachiroptera) and this has probably restrained any such developments in extant gliding mammals. Chapter 3 discusses the possible developments of gliding mammals when no such restraints existed, during the evolution of the bats themselves.

2.4 Draco spilopterus

The specimens studied were identified as Draco cornutus according to the key of Boulenger (1885). D.cornutus has since been classified as a subspecies of D.spilopterus by Hennig (1936).

2.4.1 General behaviour

Members of the genus Draco are diurnal, being active through most of the day (Hairston, 1957; Alcala, 1967). Draco spilopterus cornutus forages by landing usually between 1m and 3m from the base of a tree trunk, then climbing up the tree trunk and periodically stopping tofeed on ants. This is a typical foraging technique of the genus, and ants make up the bulk of the diet (Hairston, 1957; Reyes, 1968; Mertens, 1960). During the climb D.spilopterus may also stop, raise its head and flick out its gular appendage several times. This is probably a territorial display, and it is described and discussed in detail by Hairston (1957) and Alcala (1967). Occasionally two individuals land on the same tree, and invariably they chase each other until one glides to a fresh tree. This chasing may involve running down the tree trunk, an action which very rarely happens during foraging. The foraging climb, up a typical 10m tree, can take between 10 and 30 minutes. Once near the top of the tree, D.spilopterus usually climbs along a branch to the edge of the tree's foliage,

and then, with no prior indication, takes off and glides to a new tree or, in a few cases, glides down to the base of the same tree. The trunk foraging climb is then repeated. D.spilopterus is not selective in its choice of tree species on which it forages, and the tagging experiments of Alcala (1967) on D.volans show that they have fairly small home ranges that do not usually exceed 150m from the centre of the territory.

Draco does not tend to use gliding as an escape mechanism but, when threatened, it will first remain stationary and then run up the tree (Hairston, 1957). If D.spilopterus is pursued and prevented from climbing higher, it will usually run to the base of the tree, and only occasionally will it glide from the trunk. Its major predators are probably birds. A chestnut breasted malcoa (Phaenicophaeus javanicus) was observed eating a bright green lizard, which was almost certainly Draco. Malcoas generally feed on large insects, but are reported to eat lizards occasionally (Smythies, 1960). Birds of prey were sometimes seen in the study area, particularly the serpent eagle (Spilornis cheela) and these are also likely to be predators of Draco.

The wing colour of D.spilopterus cornutus varies from olive green similar to the body colour, to bright orange and red. A specimen of D.volans found in the study area would spread its wings when threatened revealing its bright orange coloration. This response was not observed in D.spilopterus cornutus.

2.4.2 Results

2.4.2(i) Climbing and gliding locomotion

The glide of Draco spilopterus cornutus differs from that of Petaurista petaurista in that D.spilopterus gains height during landing (Figure 2.7). This is also reported for other species of Draco (Klingel, 1965). The actual glide angle θ_g can still be calculated by the method used for P.petaurista, by taking the reduced major axis (RMA) of vertical distance fallen against horizontal glide distance travelled. . The only difference is that in the case of Draco the initial height loss of the dive will be underestimated, as the intercept with the vertical distance axis is the difference between this height loss and the height gained on landing. All the glide recordings are plotted on Graph 2.5 and given in Table 2.3, and the R.M.A. line gives a glide angle of 22.1 $\pm$ 2.8^{o} and an initial height loss of 0.67 $\pm$ 0.55m. For similar reasons to those for P.petaurista a 'best glide' R.M.A. line is fitted for all the points below the 'all points' R.M.A. line, and this gives a glide angle of 18.6 $\pm$ 2.3^{o} and an initial height loss of 0.87 $\pm$ 0.39m. Glide speed is again found by the R.M.A. of glide distance on glide time, plotted on Graph 2.6 . Only a few glide times were recorded for D.spilopterus due to its very unpredicatable take-off behaviour, and these results give a glide speed of 5.5 $\pm$ 1.9m s^{-1}. Klingel's (1965) glide time

Figure 2.7

The glide path of Draco spilopterus. Some of the initial height loss in the dive d is regained during landing when the lizard climbs through a height c. θ_{dg} and θ_{g} are the direct glide angle and the actual glide angle respectively.

Figure 2.7

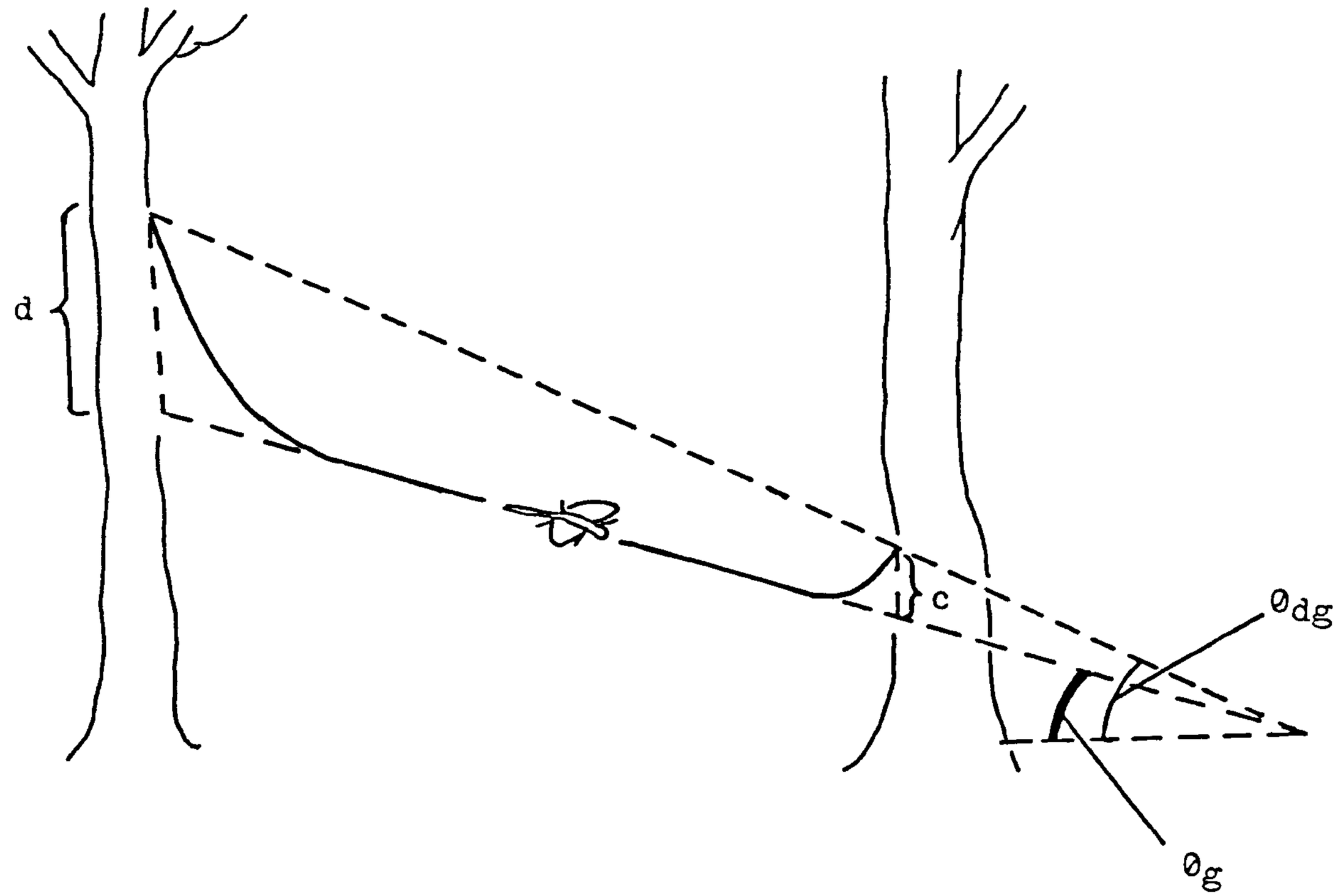

Graph 2.5

The vertical distance fallen (metres) against the horizontal distance travelled (metres) for glides of Draco spilopterus. The solid line is the R.M.A. line for all the points, whereas the broken line is the R.M.A. line for only the points denoted by a black circle surrounding a white star. These points all lie below the solid R.M.A. line and are the 'best glide' records. The equations of the lines and the correlation coefficients are given in Table 2.3.

Graph 2.6

The glide distance (metres) against the glide time (seconds) for Draco. The solid circles are for records of Draco spilopterus, and the open circles are those made by Klingel (1965). The R.M.A. is given for all the points. The R.M.A. equations and correlation coefficients are given in Table 2.3.

Graph 2.5

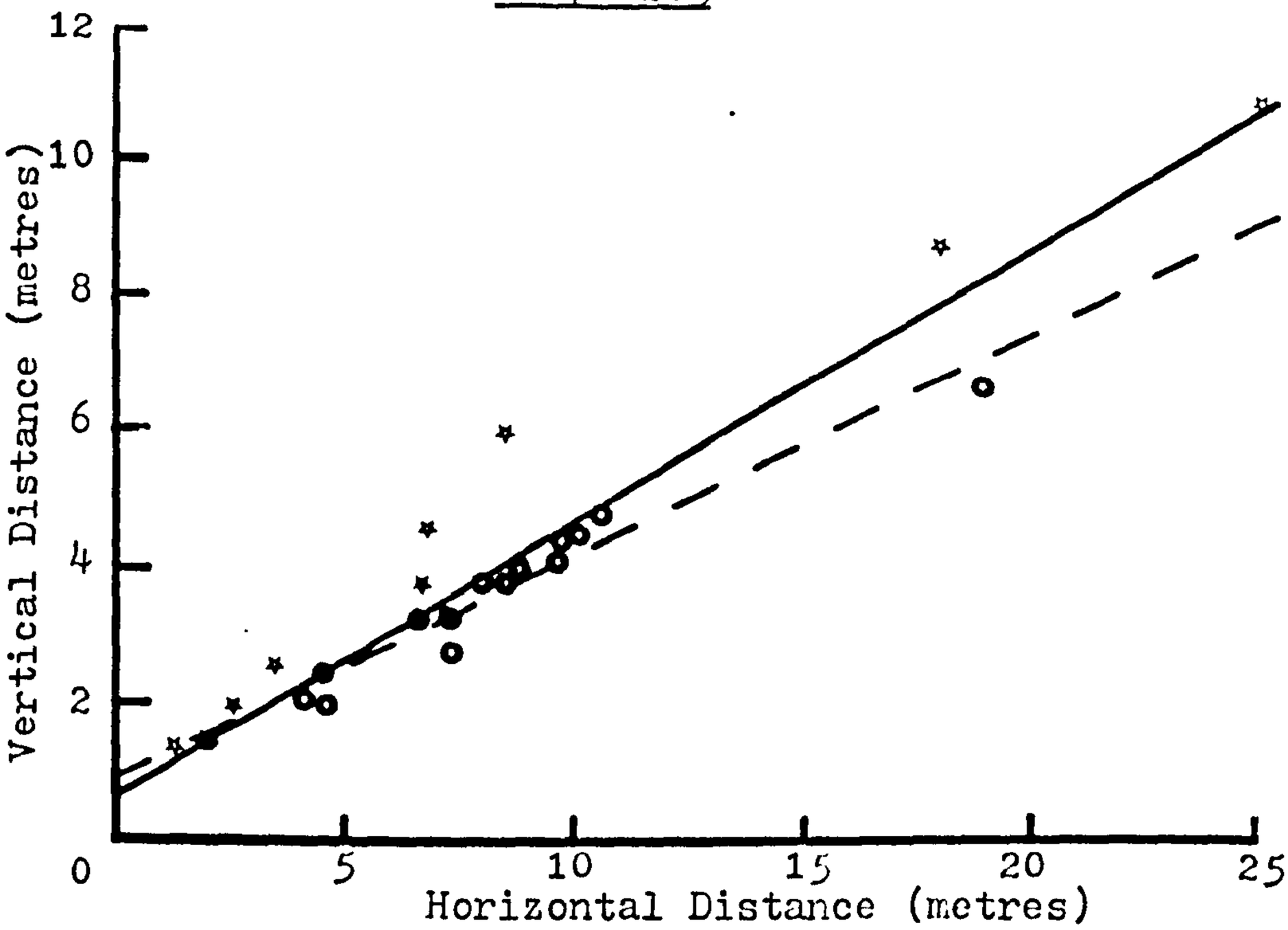

Graph 2.6

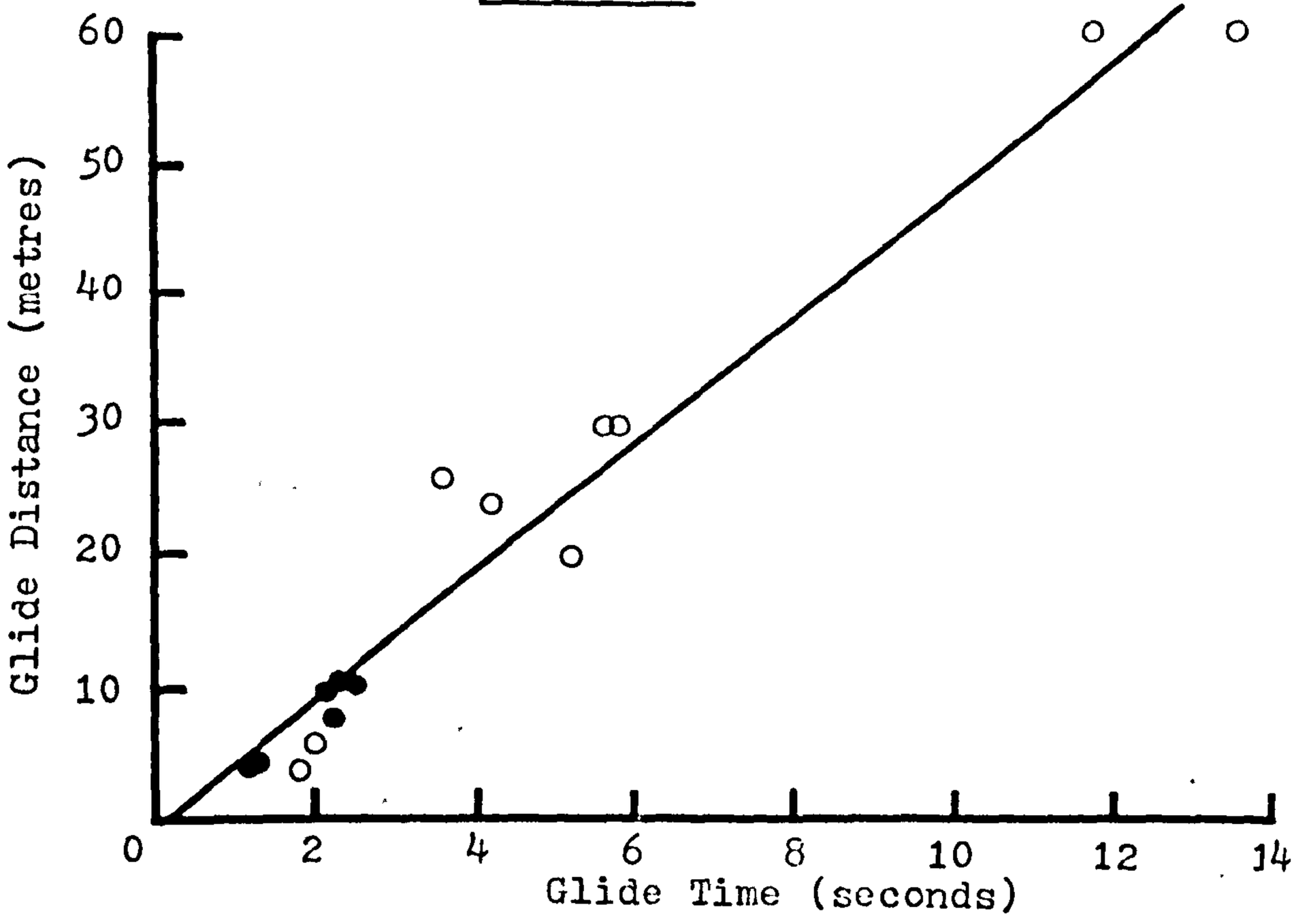

Table 2.3

a) Correlation of vertical and horizontal glide distances of Draco spilopterus (see Graph 2.5)

		N	r	F	α	β (0_g^o)	α RANGES		β RANGES	
							α -	α +	β - (0_g^o)	β + (0_g^o)
ALL DATA	Y(X)	23	0.954 ***	214	0.828	0.387(21.2)	0.227	1.38	0.332(18.4)	0.442(23.8)
	RMA				0.672	0.405(22.1)	0.119	1.23	0.351(19.3)	0.460(24.7)
BEST GLIDE DATA	Y(X)	15	0.976 ***	262	0.934	0.328(18.2)	0.548	1.32	0.285(15.9)	0.327(20.4)
	RMA				0.870	0.336(18.6)	0.483	1.26	0.293(16.3)	0.380(20.8)

b) Correlation of glide distance and glide time of Draco (see Graph 2.6)

		N	r	F	α	β	α RANGES		β RANGES	
							α -	α +	β -	β +
Draco Spilopterus DATA ONLY	Y(X)	7	0.957 ***	54.4	-2.03	5.23	-5.76	1.69	3.41	7.06
	RMA				-2.50	5.47	-6.23	1.23	3.64	7.29
Draco Spilopterus & Klingel Draco sp. DATA	Y(X)	16	0.978 ***	308	-8.710	4.90	-3.99	2.57	4.30	5.50
	RMA				-1.17	5.01	-4.46	2.11	4.41	5.61

(See Chapter 5.3 for further details)

data has been included on the graph, and when this is taken into account the glide speed is given as 5.0 ± 0.6m s^{-1}. Klingel only quotes horizontal glide distance for these times, but as these distances are generally large they approximate to the glide distance.

The dimensions of two specimens of Draco spilopterus are given in Table 2.4 . The lift coefficients C_L for these individuals are also given, having been calculated assuming a glide angle of 19^o and a glide speed of 5m s^{-1}.

The initial dive of Draco volans was estimated by Klingel (1965) to be at an angle of 45^o to the horizontal, with the body held at the same angle. This angle was not measured for D.spilopterus, but was estimated to be between 40^o and 60^o. Once in the steady glide D.spilopterus has a slightly positive angle of incidence, and so its angle of attack is probably greater than 20^o. During landing the angle of incidence increases greatly, but the lizard gains height (Klingel, 1965) and so the angle of attack may not be significantly altered.

Klingel (1965) investigated the control of Draco in flight, and showed it to be very good. He believes that tail flexure and curvature of the back (so altering the wing camber) are the most important control mechanisms. Observations on D.spilopterus are in agreement with Klingel as far as precision gliding is concerned. D.spilopterus can turn sharply

Table 2.4

Dimensions of Draco spilopterus and calculated lift coefficients assuming a glide angle of 19^{o} and a glide speed of 5m s^{-1}.

BODY MASS (Kg)	WING SPAN (m)	WING AREA (m^2)	ASPECT RATIO	WING LOADING (N m^{-2})	LIFT COEFFICIENT
$4.5x10^{-3}$	$8.8x10^{-2}$	$2.8x10^{-3}$	2.8	15.8	0.98
$4.0x10^{-3}$	$7.5x10^{-2}$	$2.3x10^{-3}$	2.5	17.1	1.06

in flight, and it does so occasionally soon after take-off, so that it can glide to a lower position on the same tree. It can land on small targets, such as 2cm diameter bamboo poles, and one individual was seen to glide through a wire fence, the holes in which were square with wire sides at 45^{o} to the horizontal, and the maximum distance between diagonally opposite corners of each hole was only 10cm! Generally the air was still when D.spilopterus was observed, but when gusts of wind did occur the lizard appeared to compensate. One individual was seen to glide about 1m above a 2m high ridge which was perpendicular to a prolonged gust of wind. As it traversed the ridge it did not appear to lose height and its measured overall glide angle (data not included on Graph 2.5) was 16.3^{o} over a horizontal distance of 14.1m. Clearly, whether by intention or not, this lizard was slope soaring! Captured specimens when released from heights below 2m, and with no close 'target' trees, would often simply parachute to the ground when disturbed.

The climbing gait does not differ from normal lizards, Draco's wings having no attachments to the limbs, and D.spilopterus has a climbing speed of $0.6 \pm 0.2 m\ s^{-1}$.

2.4.3 Discussion

The relatively high lift coefficient used by Draco

spilopterus is probably only achieved by gliding at a high angle of attack and this in turn is only possible due to the specialised design of its wings. A low aspect ratio wing is beneficial as it will stall at high angles of attack and the wing tip design of Draco may be of importance in this respect, as semicircular tips are superior to rectangular ones (Zimmerman, 1932). If the wing chord of D.spilopterus is taken as 35mm, then Reynold's number is approximately 1.2×10^4, and so it will have a laminar flow in the boundary layer. The cambered flat plate wing design is a consequence of this Reynold's number. A laminar flow boundary layer would separate from the wing at relatively low angles of attack and it is possible that the ribs supporting the wings, running approximately parallel to the wing's leading edge, may act as spoiler wires. The subsequent turbulent boundary layer would separate at far higher angles of attack and result in very substantial increases in lift coefficient as has been suggested for dragonfly wings by Hertel (1966). For such a mechanism to be feasible the ridges of the ribs should be roughly the same height as the boundary layer. If the boundary layer δ_β for a flat plate is given as

$$\delta_\beta = 5.0\sqrt{\frac{\mu l}{\rho V_g}}$$ (Schlichting, 1968)

where μ is the viscosity of air (1.8×10^{-5}poise). If the wing chord is 3.5×10^{-2}m and the glide speed V_g is 5m s^{-1}, then the boundary layer is 1.6mm thick. The ribs were estimated crudely to be 0.5mm above the membrane, and so could be of importance in causing turbulence.

The overall glide angles measured here agree with that of Hairston (1957), but Klingel (1965) records far lower overall glide angles for D.volans, D.melanopogon, and D.taeniopterus. I have tabulated Klingel's data in Table 2.5 , calculated the respective overall glide angles and estimated the actual glide angles, assuming that the initial height loss of the dive is 0.5m. Generally, the actual glide angles are considerably shallower than those I have measured. The best glide angles of between 8^{o} and 9^{o} which Klingel's data suggests for D.melanopogon and D.taeniopterus seem very unrealistic for an animal with the dimensions of Draco.

It is possible that these species are more proficient gliders than D.spilopterus, but not to the extent of the above anomalies. As Klingel's measurements must have been made in a large clearing, at least 60m square, air currents could have affected his specimen's glide performance. A second cause for the anomalies could be that all of Klingel's measurements are of captive specimens released up poles, whereas the majority made in this study are of free

Table 2.5

Glide data of Klingel (1965) for three species of Draco (actual glide angles are estimated assuming a height loss of 0.5m in the dive).

SPECIES	VERTICAL GLIDE DISTANCE		HORIZONTAL GLIDE DISTANCE	DIRECT GLIDE ANGLE		ESTIMATED ACTUAL GLIDE ANGLE	
	Mean (m)	Range (m)	(m)	Mean (Degrees)	+ − (Degrees)	Mean (Degree	+ − (Degree
D.volans	2.65	2.5-3	10	14.8	14-17	12.1	11.3-14
D.volans	2.8	2.5-3.1	12	13.0	11.8-14.5	10.9	9.5-12.2
D.volans		3.25	11.1 11.8		16.3 15.4		13.9 13.1
D.Melanopogon & D.taeniopterus	8.5	7.8-9.7	30	15.8	14.6-17.9	14.9	13.7-17.0
D.Melanopogon & D.taeniopterus	9.65	9.1-9.8	60	9.1	8.6-9.3	8.7	8.1-8.8

lizards gliding naturally. However, the few recordings I made using Klingel's technique gave glide angles similar to the natural glides.

The behaviour of Draco is totally different from that described for Petaurista, and so too is the explanation for its gliding adaptation. Petaurista feeds on leaves in the forest canopy and must climb solely to gain potential energy for its means of horizontal transport, gliding. Draco climbs tree trunks to forage for food, and so the gain in potential energy for gliding is a by-product of its foraging. Draco rarely climbs down the trunk to reforage an area (if it does reforage a trunk it first climbs to the top and then glides to the trunk's base) but carries out a continuous foraging climb which may have the advantage of surprising the prey.

Presumably, a non-gliding Draco competitor would have to expend energy climbing the trunk and then expend further energy transporting itself by quadrupedal locomotion to a fresh trunk and descending that trunk to enable it to forage its surface. So for Draco's very specialised form of trunk foraging the energetic advantages of gliding are obvious, and the energy cost estimations which were required to explain the locomotion of Petaurista are unnecessary.

It was argued that gliding mammals must be nocturnal to avoid excessive avian predation, and these arguments should apply to Draco. Draco

probably has to be diurnal because it is a poikilotherm, its food source may be only diurnal, and its relatively small reptilian eyes are probably not suitable for judging glides in poor illumination (Chapter 3.5; Lythgoe, 1979). The reasons for it being able to remain diurnal may be that it is protected on the tree trunks by good camouflage and, if pursued by a predator, it is an agile climber; its flight apparatus does not impair the movements of the limbs. Vulnerability during the glide may be reduced by individuals in some cases having brightly coloured wings which possibly mimic those of poisonous Lepidoptera. This could be very effective in preventing predation by birds such as malkoas which are predominantly insectivorous. It is possible that Draco is itself distasteful and has genuine warning coloration. As Draco does not have to maximise its glide distance to minimise its overall glide angle, it can have short glides which give any potential predator less time to react to this vulnerable behaviour. The combination of the above factors enable Draco to exist as the only extant genus of regularly gliding diurnal vertebrates.

2.5 Conclusion

These two studies illustrate how climbing and gliding can be used in two types of foraging behaviour to reduce the animal's energy expenditure. The gliding technique is similar for both, but the application is very different. Draco gains its potential energy from gliding as a by-product of its foraging, and uses the glide to transport itself over short distances to fresh foraging sites. Its overall glide angle must be sufficiently small to enable it to travel the horizontal distance between tree trunks but otherwise this angle has little consequence. Petaurista, on the other hand, must climb purely to gain potential energy for its glide and so glides over long distances to reduce its overall glide angle and consequently its amount of climbing. The energy saving strategy of Petaurista is suitable for numerous types of vertebrates and hence its form of gliding has evolved separately several times (Height et al., 1974; Kirsch, 1968; Fleay, 1947; Rayner, 1981).

CHAPTER 3

THE EVOLUTION OF FLIGHT IN BATS

3.1 Introduction

Evidence for how bats evolved is largely lacking, and so their evolution is generally left to supposition. The earliest bat known in the fossil record is Icaronycteris index of the Eocene. This mammal is remarkably similar in structure to the present day Microchiroptera (Jepson, 1970). There is a complete lack of fossil evidence indicating the ancestry of I.index or suggesting how it may have evolved its specialised structure adapted for powered flight; moreover, I.index cannot be directly linked to any of the present day groups of bats (Jepson, 1970). Indeed, it is by no means clear whether the order Chiroptera is mono- or polyphyletic, as there is no direct evidence linking the Microchiroptera and the Megachiroptera to a common bat ancestor (Smith, 1977).

The theories of flight evolution in mammals at present fall into two categories. The first, that bats evolved through a gliding stage, has been suggested by various workers including Pennycuick (1972a) and Smith (1977). Smith describes how a small arboreal mammal might first have evolved gliding, in a similar way to extant gliding mammals, and then by extending the digits of the manus could have

increased the wing surface and so provided a structure suitable for powered flight. The second theory proposes that bat flight evolved by small mammals leaping into the air to catch prey and extending the jump by flapping rudimentary wings (Jepson, 1970; Pirlot, 1977). Pirlot emphasises that hovering flight was selected for first, and that bats then radiated into their present aerial niches. Clark (1977) has strongly criticised Jepson and Pirlot on the basis of the physiological and energetic inadequacies of this explanation. Jepson gives equally strong criticism to theories involving a gliding stage in flight evolution. When referring to the changes from gliding to powered flight he states that "no-one has successfully proposed any kind of selection pressure that would be effective in the change from one niche to another" (Jepson, 1970).

This account supports the hypothesis that a gliding stage was required for the evolution of flight in bats. On energetic grounds it is easier to explain flight evolution in such a 'top down' manner because the energy required is already available in the form of potential energy. With the exception of flying fish, there has not been a satisfactory energetic explanation of flight evolving from the 'bottom up'. This chapter gives a feasible theoretic description of the mechanism by which flight may have evolved in bats, and of the selection pressure required, which

Jepson claims is absent. This mechanism also suggests why the sensory systems of the Megachiroptera and the Microchiroptera differ, and how they may have evolved.

3.2 The fundamental problems and advantages of powered flight

The aerodynamic power required for flying at different speeds can be estimated for birds and bats using the theoretical work of Pennycuick (1968, 1975) and the more recent work of Rayner (1979c). Both show that flying at low speeds (speeds below or close to the gliding stalling speed) and especially hovering, requires far more power than flying forwards at the minimum power speed (Figure 1.1). Vertebrates which can hover aerobically are small (below 100g) and are morphologically and physiologically adapted for this strenuous form of powered flight. For these reasons it is inconceivable that flight evolved by first developing hovering, as suggested by Pirlot (1977) and Jepsen (1970). Bat flight evolution is most likely to have occurred by the ancestor first gaining the forward speed required for minimum powered flight. This is easily achieved by initially evolving gliding; the transition thence to powered flight from a glider is a relatively simple one, the glider already possessing wings.

The overall advantage of flight to a mammal, compared with the ability to run, is that flight enables

it to have a very low cost of transport (Schmidt-Nielsen, 1972). The selection pressure for low transport cost has caused gliding flight evolution in mammals (Chapter 2) and probably also evolution of powered flight.

3.3 The mechanism for bat evolution by first developing gliding

Gliding in mammals has evolved in a convergent manner at least six times in extant mammals (Height et al., 1974; Kirsch,1968; Fleay, 1954) and it seems very likely that an ancestral gliding 'proto-bat' would also have developed in the same manner. In the absence of any fully developed flying mammal competitors, this proto-bat would not have been restricted from developing its gliding apparatus further, to reduce the transport costs, as are extant gliding mammals (Chapter 2).

Lowering the cost of transport would have involved structural changes to reduce the overall glide angle θ_{dg} by a) increasing the wing area and so reducing the wing loading and consequently the glide speed and the initial drop distance of the glide, and b) increasing the aspect ratio of the wing. ($span^2$/area) and so reducing the induced drag and consequently the actual glide angle θ_g. These modifications could have arisen gradually, by supporting the extra membrane with the digits of the manus and

continually increasing the length of these digits (Figure 3.1) as Smith (1977) suggests. As the gliding proto-bat's overall glide angle was reduced it would become less dependent upon climbing, and so adaptations for efficient quadruped climbing could be sacrificed, and substituted with gliding adaptations. These developments would eventually become limited by the strength of the elongated digits, and by the impracticability of having a very high area and high aspect ratio wing in a rain forest canopy.

This highly developed gliding mammal would have had to develop its thoracic musculature and to a lesser extent that of the pelvis, to support the enlarged wings and also to instigate control movements. These movements could be modified into very low amplitude flapping and so increase the velocity of the air passing over the wings and hence also the lift from the wings. This extra lift could be used to further reduce the direct glide angle. It is interesting to note that the glide speed of the fruit bat Rousettus aegyntiacus, at its minimum glide angle of 8-10^{o}, is 7-8m s^{-1} (Pennycuick, 1971) and its minimum power speed is about 6-7m s^{-1}. The gliding proto-bat would therefore have been able to achieve the flying speed for developing minimum powered flight.

Low amplitude flapping would only have been of benefit to the proto-bat if the energy required for flapping was less than that saved by reducing the

Figure 3.1

Suggested stages of evolution of a bat from a quadruped (a-e). The length of the forelimbs and digits are progressively lengthened and the tail reduced. The wing area and aspect ratio is increased at each stage.

Graph 3.1

Cost of transport against glide angle for a proto-bat during its flight evolution.
An example of the reduction in cost of transport as the overall glide angle of a proto-bat, weighing 1.16N, is progressively reduced. It is assumed to glide at 6m s^{-1} and climb at 0.7m s^{-1}. The constants used to calculate climbing power are as in Chapter 2.3 and its climbing efficiency assumed to be 0.2. The reductions in 'glide angle' from 7^{o} to horizontal have been calculated by assuming the evolution of flapping flight.

Figure 3.1

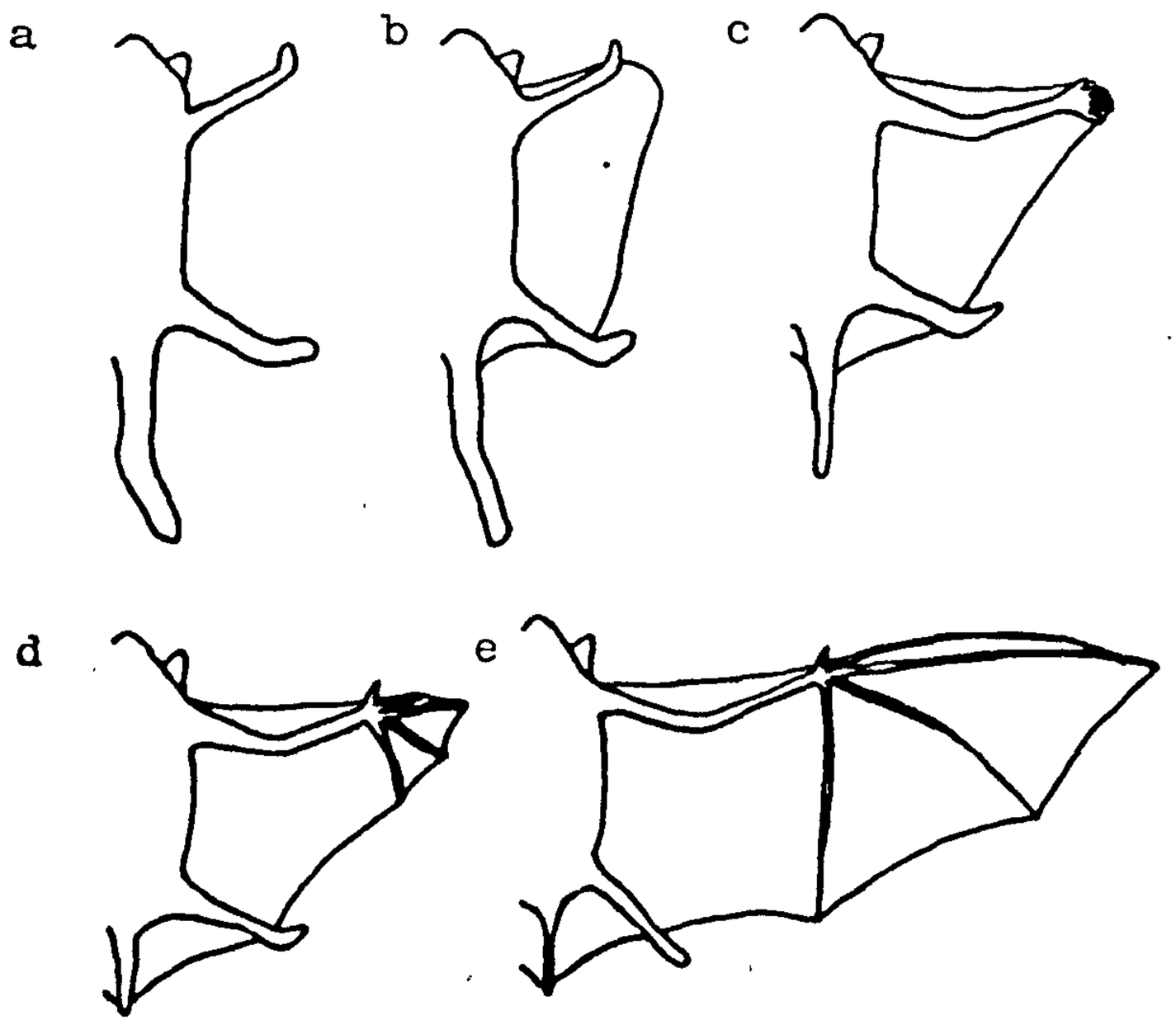

Graph 3.1

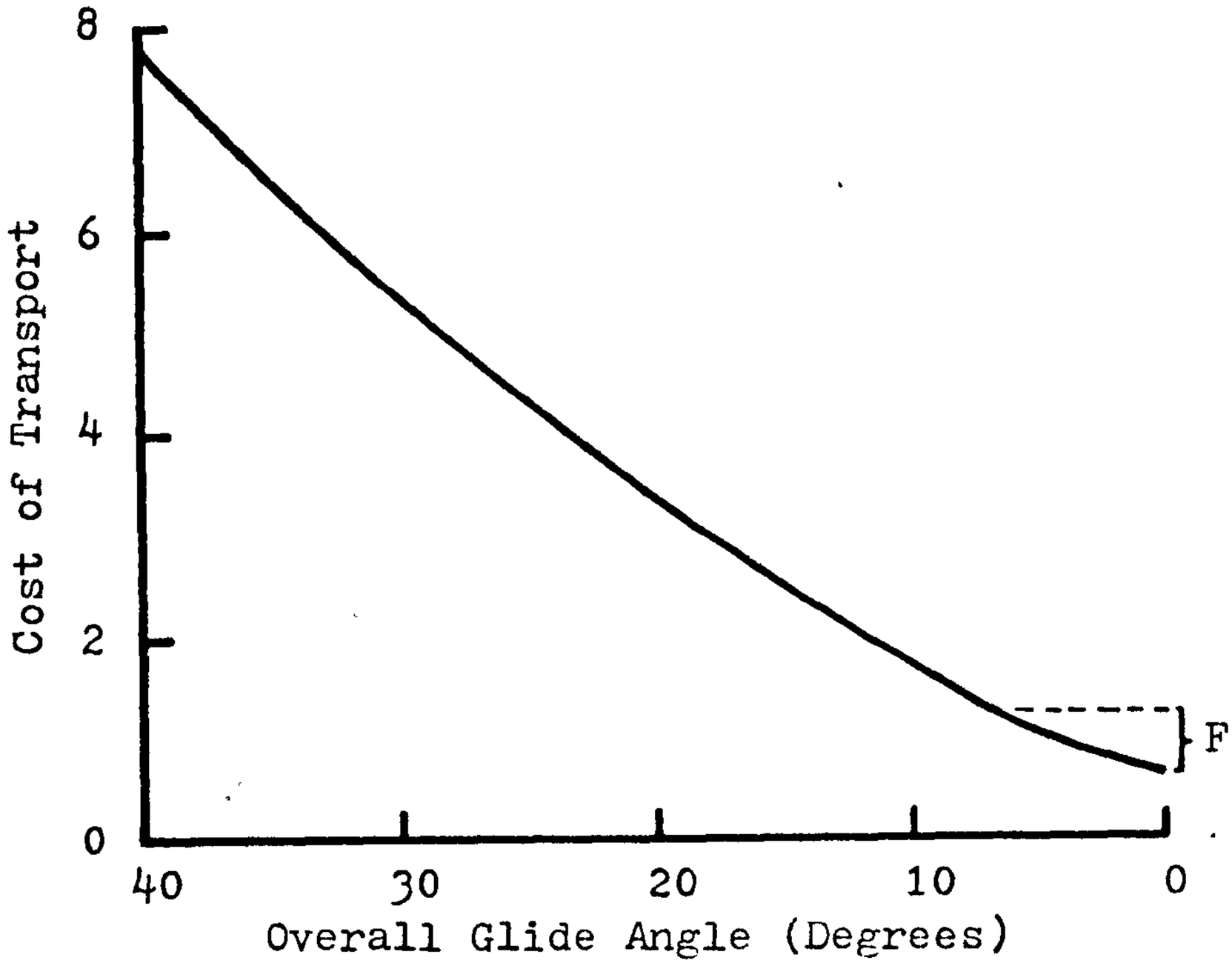

amount of climbing. The power required to fly P can be estimated from the lift to drag ratio (Pennycuick, 1975) with

$$P = W\left(\frac{D}{L}\right)V \qquad (3.1)$$

given that W is the body weight, V is the flying speed, L is the lift and D is the drag. In gliding, the power P_g is equivalent to the rate of loss of potential energy. If the glide angle is lessened by improving the lift to drag ratio by gentle flapping, then the rate of loss of potential energy is reduced to P_{gf}. The induced power required from this flapping P_f is given by the difference between P_g and P_{gf}. Flapping also causes a slight increase in profile power due to the increased air speed of the wings, but for this argument it is assumed to be negligible. To test if cost of transport reductions can be made by flapping, consider a hypothtical proto-bat having the dimensions of Rousettus aegyptiacus as given by Pennycuick (1971), with a body weight of 1.16N, a wing area of $0.057m^2$ and an aspect ratio of 5.42 . It is assumed to have a glide speed V_g of 6m s^{-1} at a lift coefficient of 0.92 . If this is so, then the lift produced during gliding, calculated from Equation (2.7), will be 1.152N and, given Equation (2.8), then the glide angle will be 6.73^{o}. If the drag during gliding D_g is given by

$$D_g = W\sin\theta_g \qquad (3.2)$$

then D_g will be 0.136N, and the rate of loss of potential energy will be 0.82W. If the proto-bat reduces its glide angle by 2^o by flapping, then its lift must be 1.156N, its drag 0.096N and its rate of loss of potential energy 0.58W. The extra aerodynamic power from flapping must be 0.24W. If the mechanical efficiency of the proto-bat is considered to be similar to other flying vertebrates, then it can be assumed to be about 0.23 (Pennycuick, 1975) and so the extra metabolic power required to reduce its glide angle by 2^o will be 1.04W.

If the metabolic power required for climbing is given by Equation (2.13) and the proto-bat is assumed to climb at 0.7m s^{-1}, then its metabolic climbing power will be 7.3W. Over a journey of 100m the proto-bat, gliding at 6.73^o, must expend 36J in climbing to regain lost height, whereas if the gliding angle is reduced by 2^o by flapping, the climbing energy cost will be only 18J. Assuming that the proto-bat continues to fly at 6m s^{-1} when flapping, then the overall cost of transport is reduced from 1.25 when just gliding at 6.73^o to 1.1 when the angle of descent is reduced to 4.73^o by flapping. If all the climbing is replace by flapping, then the cost of transport is further reduced to 0.72 as illustrated in Graph 3.1 . This is in agreement with the results of Thomas (1975) who found that the metabolic cost of transport of the flying fox Pteropus gouldi (0.78kg) is between 0.6 and

0.7 in cruise flight.

Since flapping further reduces the cost of transport of a gliding mammal, it is quite feasible that a fully developed gliding proto-bat could first have developed very small amplitude wing beats, causing correspondingly small reductions in glide angle, and could then have slowly increased this amplitude until horizontal flight was finally achieved at the minimum power speed. The mechanical and physiological adaptations for powered flight could have occurred gradually, developing at each stage to suit the animal's requirements. Having achieved minimum power horizontal flight, further adaptation could occur to enable the proto-bat to fly at faster and slower speeds. For gliding, flight stability is important and so gliding mammals have long tails. Manoeuvrability would become increasingly important to the proto-bat as it developed powered flight, and so the tail would be continually reduced.

If the Chiroptera are polyphyletic, is this method of flight evolution suitable for explaining the evolution of flight in the Megachiroptera and in the Microchiroptera? For the Megachiroptera, the evolutionary process described above is easy to envisage. That a fruit eating gliding mammal should simply extend its foraging radius by evolving powered flight is logical, since extant fruit bats still behave in this foraging manner. A Pteropus vampyrus colony in Brunei Bay has a foraging radius in excess of 30km,

giving a foraging area of at least 3000km^2. This is an ultimate strategy to cope with the irregular fruiting system of rain forest.

The explanation for the evolution of flight in the Microchiroptera is not as straightforward, but again extant gliding mammals offer some useful clues. Large gliding mammals (above 100g) tend to be fruit and leaf eaters, while smaller ones tend to be omnivorous (Walker, 1964). Small gliding mammals have evolved this form of locomotion to extend their foraging radii, as with the herbivores, because a) the plant part of their diet fluctuates in abundance and distribution seasonally and b) Wolda (1978) has shown that rain forest insect populations fluctuate with plant productivity. A small rain forest arboreal omnivorous mammal therefore benefits in a similar way to a larger herbivore if it can extend its foraging radius. An omnivorous gliding proto-Microchiropteran could have developed horizontal flight simply to extend its foraging radius, while still feeding on plant products and insects once it had landed. Although the majority of the extant Microchiroptera feed on flying insects, some including the Glossophaginae and the Phylloncycterinae still forage on plant material (Wilson, 1973), while other insect eating bats such as Plecotus can prey on insects on foliage. It seems that even now there are no shortages of niches for fully developed, non-flying bats to obtain food. It

is likely that the proto-Microchiropteran stock were omnivorous and evolved horizontal flight to extend the foraging radius, then developing flying techniques to allow radiation into the numerous niches which the group now occupies. This would include the catching of insects in flight, which clearly requires a sophisticated flying vertebrate.

3.4 The disadvantages of gliding and their consequences in bat evolution

Birds had evolved before bats (Jepsen, 1970) and so avian predation would have caused a proto-bat, in its gliding stage, to be nocturnal; this is the case for all extant gliding mammals (Chapter 2). As the proto-bat evolved powered flight, especially at flying speeds below and above the minimum power speed, the high muscular power output required would have caused a cooling problem. This has been largely solved by the loss of hair from the wing membranes and the use of the wings as 'radiators'; vasodilatation of the blood vessels in the thin membranes causes cooling (Bartholomew et al., 1964). This adaptation is suitable for a nocturnal flying animal but unsuitable in daylight, as the ultraviolet radiation would destroy the unprotected membranes (Pennycuick, 1972a). This has probably hindered bats from occupying diurnal niches, although some have overcome this problem. Lasiurus, for example, can withstand daylight due

to the fur on its membranes (Novick and Leen, 1969). However, as Novick (1977) suggests, the aerodynamic demands for a naked wing membrane are in conflict with the protection from insolation.

3.5 The evolution of nocturnal motion detection in bats

Bats have had to develop sensory systems that can detect the relative motions involved in flight in very low illuminations. The Microchiroptera use echolocation, whereas the Megachiroptera rely on vision to navigate (with the exception of Rousettus which has a crude echolocation system unrelated to that of the Microchiroptera (Novick, 1958)). The difference is curious, as the Megachiroptera are unlikely to have lost the echolocating adaptation. If the Chiroptera are polyphyletic, then the theory of flight evolution via a gliding stage offers an explanation of why the difference has arisen.

Large gliding mammals such as Petaurista petaurista appear to rely on vision to judge their nocturnal glides. P.petaurista is a relatively large mammal whose head size can 'house' large eyes. As eyes become smaller they become less effective because a) image sharpness is reduced by diffraction at the pupil aperture, and the diffraction gets worse as the absolute size of the pupil decreases and b) visual receptors are limited to a minimum size, and so the

relative 'grain size' of the retina increases as the size of the eye decreases (see Lythgoe (1979) for review).

Small insectivores such as shrews cease to use vision, probably because their eye size has had to become too small to provide an adequate image. For a mammal wishing to detect motion at night, the inadequacies of a small eye are accentuated. The glide speed of gliding mammals will be approximately proportional to body mass$^{\frac{1}{6}}$, whereas the volume of the head is approximately proportional to body mass. Hence, the visual task of motion detection is only slightly reduced for smaller gliding mammals, whereas the head volume and consequently the maximum eye size are reduced at a far greater rate. For a gliding mammal there must be a critical mass, below which it can no longer rely on vision for its navigation. The gliding marsupial Acrobates (12-14g) and the "scaly tail" Idiurus (25-35g) could well be below this mass; they appear to have relatively small eyes, and Acrobates has extensive fibrillae on the head and tail (Walker, 1964), a feature of poor sighted animals.

A proto-Megachiropteran, at its gliding stage, would have been predominantly a herbivore, and as such would probably have been larger than 100g. It would have been large enough to support an eye of adequate size for nocturnal gliding, and so flight evolution would have progressed relying on vision.

An omnivorous proto-Microchiropteran could have been very small, and consequently below the critical mass where vision can be relied upon for nocturnal gliding. It may have possessed a crude echolocation system similar to that found in extant insectivores (Gould et al., 1964; Buchler, 1976). The shrew Sorex vagrans produces low intensity ultrasounds of poor 'definition', and Buchler (1976) believes that these are used to gain a general 'acoustic image' of the environment, and that the system is not suitable for 'target location' as is the Microchiropteran system. The transition to the target location system could have occurred during gliding and powered flight evolution. The proto-bat could have first used its poor resolution echolocation system to detect very large targets such as tree trunks,during early gliding evolution; as it became more proficient at gliding and later powered flight, the echolocation system could be gradually modified to suit the mammal's navigational requirements, becoming increasingly accurate in determining relative speeds and positions of obstacles and landing sites. Many extant Microchiroptera still use their echolocation system for navigation only, as with the flower feeding bats of the Phyllostomatidae. This developed, high resolution echolocation system would now also be capable of detecting small moving objects and so the proto-bat, now fully evolved for powered flight, would be preadapted for occupying nocturnal aerial insect-catching niches.

3.6 Conclusion

The consequences of bat evolution, via a gliding stage, are that bats are structurally and physiologically adapted only for nocturnalism, and hence largely excluded from colonising diurnal niches. Birds, which evolved before bats (Jepsen, 1970) from an ancestral reptilian stock, were dependent upon vision and so evolved flight diurnally, successfully occupying all the diurnal vertebrate aerial niches. They have since also occupied some nocturnal insect-catching niches, but these have been limited to birds having a body mass above 30g (Fenton, 1974), presumably because below this weight they cannot house large enough eyes for the visual task. The Microchiroptera, evolving a complex echolocation system, have been able to dispense with the scale dependent visual system and fill all the nocturnal insect-catching niches for vertrebrates with a body mass of less than 30g. As neither birds nor the Megachiroptera have ever developed a complex echolocation system, it is possible that such development must occur simultaneously with flight evolution, as has been suggested above. If so, then it is highly unlikely that the Megachiroptera radiated from a common Chiropteran ancestor which had already evolved flight. This, coupled with the lack of evidence linking the two suborders (Smith, 1977) suggests that the Chiroptera are polyphyletic. As the selective pressure and the mechanism of

flight evolution were probably very similar in both cases, it is not surprising that the two groups show such a high degree of convergence in their flight morphology. Therefore, it should not be assumed that similarities in flight morphology are indicative of a common ancestry.

3.7 Selection pressure for the evolution of flight in birds

There are two proposals for the evolution of flight in birds, and both are based upon the fossils of Archaeopteryx. The generally accepted proposal is that birds had an arboreal ancestor and developed flight through gliding stages, in a similar manner to that described for bats in this chapter. This theory was first postulated by Hurst (1895), and more recently by de Beer (1954) and Bock (1965, 1979). In such theories Archaeopteryx is usually assumed to have been an intermediate stage, as a glider or weak powered flyer. The general benefits of flight are usually assumed to have caused this evolution, and specific selection pressures are not given.

The second proposal was put forward by Ostrom (1974, 1975, 1979). He believes Archaeopteryx to have been a cursorial biped representing a preflight stage in bird evolution, in which the fore limbs were used as nets to trap insects. Ostrom believes that the selection pressure for bird flight

evolution was to catch insects in flight by using extended jumps. Recently it has been suggested that there is evidence from the flight feathers (Feduccia and Tordoff, 1979) and the pectoral girdle (Olson and Feduccia, 1979) of Archaeopteryx to show that it was at least capable of gliding, and probably also of powered flight. It is therefore possible that Archaeopteryx does not represent an intermediate stage in bird flight evolution.

If the preflight bird ancestor was arboreal, the selection pressure and the mechanism of flight evolution may have been the same as that described in this chapter for bats. The ancestral bird may have first become a homeotherm and commenced egg incubation and associated nest building. An increase in parental care would mean that, if only for the breeding season, the foraging radius would become of importance. As with 'fixed home' arboreal mammals, low cost of transport would have been selected for to increase this radius. Cost of transport reductions could have been made by evolving gliding and then flapping flight, in a similar manner to that proposed for bats. This selection pressure can adequately explain bird flight evolution to the stage of horizontal powered flight, and this is possibly the stage reached by Archaeopteryx.

CHAPTER 4

AN INTRODUCTION TO BIRD FLIGHT KINEMATICS AND AERODYNAMICS

4.1 The history of the study of bird flight kinematics

4.1.1 Initial studies

The study of the kinematics of bird flight is essential in the investigation of powered flight, and the subsequent estimation of the energy cost of this sophisticated form of locomotion. The movements of the flapping wings, of even large birds, are too rapid to be accurately resolved by the human eye. Hence the investigation of bird flapping flight could only begin after the advent of photography in the last century. Photography enabled an image to be recorded of a very short period of the wing beat cycle, so that the wing appeared stationary. A series of such photographs could be used to show the change in wing position through the wing stroke and reveal the often complex wing movements. Pioneers of the photography of bird flight were Marey (1890) and Muybridge (1899). Marey developed a series of ingenious methods which enabled him to obtain sequences of photographs of birds in slow and fast forward flight. Sequences of Marey and Muybridge show the clap and fling of the pigeon.

4.1.2 Hovering and slow forward flight

As photographic equipment became more advanced,

motion or cine cameras were developed which were capable of very high image framing rates and so were suitable for investigating the flight of small birds with rapid wing beats. Such cameras were cumbersome and required the subject to be brightly illuminated, and were best suited for filming hovering and slow forward flight.

Stolpe and Zimmer (1939), using such apparatus, first discovered the hovering wing stroke of humming birds, whereby the wing remains fully extended throughout the cycle and lift is generated on the down and up stroke. During the downstroke the wing is swept through an almost horizontal stroke plane, with the dorsal surface of the wing uppermost. At the end of the downstroke the wing is rotated at the shoulder, so that the dorsal surface of the wing points downwards, and it is then swept backwards again through a near horizontal plane. This humming bird wing stroke has more recently been filmed and illustrated by Ruppell (1972a). Zimmer (1943) showed that the hovering wing stroke of an African sunbird differed from that of humming birds. He found the downstroke to have a steep angle of stroke plane, and that in the upstroke the wing was well flexed at the wrist and moved upwards close to the body.

Apparently this upstroke produces little or no useful aerodynamic work and in this thesis will be referred to as a 'feathered' upstroke (Norberg, 1975). The stroke has since been found to be typical of many small birds, especially passerines (Brown, 1963). A third hovering wing stroke is typified by the pigeon and was

described as early as 1890 by Marey and investigated in detail by Guidi (1938) and Brown (1948). In this wing cycle the primary feathers were found to be extended horizontally in a vertical slotted stack and flicked rapidly backwards through a near horizontal stroke plane. Brown (1963) called this a "tip reversal" upstroke, the primary feathers being inverted during the upstroke flick. He believed that the upward bending of the primary feathers during the flick suggested that they were generating an aerodynamic force. Dathe and Oehme (1978) obtained film of a number of species of birds, of various wing shapes and body sizes, hovering and review the three types of wing stroke. They showed that the path of the wing tip, in the tip reversal upstroke, is always higher than that of the downstroke, while the path of the feathered upstroke is always lower than its corresponding downstroke. Dathe and Oehme could find no anatomical reason why particular birds, apart from humming birds, should use either the feathered or the tip reversal upstroke.

4.1.3 Fast forward flight

The investigation of fast forward flight in birds has been limited by the difficulties of high speed cinematography of such flight. These include tracking and focusing on the rapidly moving bird and illuminating the large area through which it is flying. Generally such film has been taken in the field using natural light and has been limited to large birds. Storer (1948)

discussed the fast forward flight of large birds. He believed that the inner section of the wing, composed of secondary feathers, largely provides weight support while the primary feathers provide thrust, and that the inner section does so for the upstroke and the downstroke while the outer section does so only for the downstroke. Shestakova (1956) filmed gulls and terns in fast forward flight and largely agreed with Storer's conclusions. Brown (1963) reviewed fast forward bird flight and described how the wing stroke of the pigeon goes through distinct pattern changes as the bird accelerates. Brown believed that when birds are flying fast the downstroke has a forward propulsive force, while during the upstroke most of the wing is probably providing some lift as it rises but no propulsive force. He claimed that the general lack of propulsive force of the upstroke could be established from cinematography of large birds, such as swans, where the forward velocity falls during the upstroke and rises in the downstroke. McGahan (1973) filmed the Andean condor Vultur gryphus in slow and fast forward flapping flight. He calculated for fast forward flight angles of attack for the wing at a series of stages in the wing cycle and concluded that the midwing section was at a suitable angle of attack to provide lift in the upstroke and the downstroke. McGahan pointed out that any lift produced on the upstroke must oppose the forward motion of the bird, and believed that this is why condors have significantly lower air speeds when

flapping than when gliding. Herzog (1968) gives a useful review of fast forward flight, and Oehme and Kitzler (1974) filmed a variety of species of birds and listed a number of kinematic parameters for each species, such as the periods of the downstroke and the upstroke, the amplitude of the wing beat and the distribution of angular velocity during the downstroke. Until now this survey of Oehme and Kitzler provided the most comprehensive and diverse survey of large bird fast forward flight kinematics. The kinematics of small birds in fast forward flight have been rarely investigated, probably due to the problems of the cinematography. Bilo (1971, 1972) gives a detailed study of the down and upstrokes of the house sparrow Passer domesticus and says that lift and thrust are provided during both halves of the wing cycle.

4.2 Relating wing beat kinematics to morphology

An important reason for studying bird flight is to enable the energy cost of this form of locomotion to be calculated and so predict foraging and migration ranges. In an attempt to do this a series of power models have been developed. Their formulation and use are dependent upon a knowledge of flight kinematics. Pennycuick (1968) produced the most widely used power model for birds and this was based on a kinematic study of the pigeon Columbia livia flying in a wind tunnel at various speeds. The theory used classical theory for aircraft wings (blade element) and propellers (momentum jet). Since blade element theory assumes steady state aerodynamics this must also be assumed for the Pennycuick model, and a knowledge of lift and drag coefficients is also required. This model was modified by Tucker (1973). Rayner (1979a, b, c) dispensed with blade element theory and calculated induced power of bird flapping flight by predicting the vorticity in the wake of the bird and calculating the energy of the wake. He postulated that the wake consists of distinct vortex rings which are produced by each downstroke, and assumed that the upstroke is passive. Kokshaysky (1979) showed wake patterns similar to vortex rings behind small passerines indicating that the assumption that the upstroke is passive in such birds is correct. However, the studies of high speed cine film of large birds, reviewed above, suggest that this may not be so for large birds.

The Rayner power model requires detailed information of wing beat kinematics, the lack of which has hampered his theoretical work. He states in his thesis that "It would be of inestimable value if a programme of observations of both kinematics and morphological parameters for a large number of species in a variety of flight conditions was carried out." (Rayner 1978) It would obviously be of great value to be able to find how wing beat kinematics relate to morphology so that, from a bird's dimensions, its kinematics could be estimated and its flight power consumption calculated. Greenewalt (1975), using a very limited amount of wing beat frequency data of birds and insects, used allometry to find the relationship between frequency and wing span in hovering. He claims that the two are proportional and that this is evidence for his theory (Greenewalt, 1960) that the beating wings of insects and birds follow the principles of damped driven oscillatory systems. This implies that birds must have an elastic wing beat system, as found in insects, but Weis-Fogh (1972) failed to find one. It is clear that to establish the allometric relationships between bird kinematics and morphology considerably more data is required, over a wider range, than Greenewalt's, for both fast forward and slow or hovering flight. Also the assumption that wing beat frequency alone is a suitable parameter for representing the wing motions is unsound. The angle through which the wing is swept (amplitude) must also be accounted for.

Theories have been developed to predict flight kinematics in fast forward flight from morphology. These assume that the movements of the wings must be just sufficient to provide the required lift and thrust. Using blade element theory, Pennycuick (1975) produced a formula for calculating the minimum angular velocity of the wing required in steady forward flight for a bird of known size. Assuming a constant lift coefficient for all sizes of birds in steady forward cruise flight, Pennycuick predicted that, for geometrically similar birds, the minimum angular velocity should be proportional to body mass $^{-1/6}$. Using a similar theory Weis-Fogh (1977) produced a similar prediction that if aerodynamic considerations limit angular velocity it should scale as above. In an attempt to provide a simple formula for calculating wing beat frequency and to test the constant lift coefficient hypothesis, Pennycuick (1978) modified his theory to predict wing beat frequency from a bird's dimensions and a limited number of constants. He assumes that angular velocity and frequency of the wing beat should be directly proportional which, as stated above, may not be true, and so in the testing of this prediction in this thesis other kinematic parameters are also incorporated.

For fast forward flight there are therefore two approaches by which one can relate morphology to flight kinematics; firstly by allometry, finding empirical relationships between different parameters of morphology and kinematics; and secondly by testing theoretical

formulae with actual data and then modifying those formulae where necessary. The theoretical and allometric approaches can also be combined.

For slow forward flight and hovering it is unlikely that steady state aerodynamics pertain for most birds. Weis-Fogh (1972), using blade element theory, calculated the mean lift coefficient of the humming bird Amazilia when hovering and found it to be 1.8, which is near to the maximum possible for steady state aerodynamics. Norberg (1975) calculated the mean lift coefficient of the pied flycatcher Ficedula hypoleuca and found it to be 5.3 in hovering. This is too high to be explained by steady state aerodynamic theory. It is therefore not possible, using simple theory, to predict the required kinematics for hovering and slow forward flight as one can with fast forward. Birds flying at their slowest forward speed presumably are moving the wings at their maximum angular velocity. This is more likely to be limited by the strength of their materials (muscles, bones and tendons) than aerodynamic considerations. Hill (1950) argued that if the strength of the materials limits the maximum angular velocity of a limb then, on a simple theoretical basis and assuming geometrical similarity, the maximum angular velocity should be inversely proportional to the limb length. On a similar basis Pennycuick (1975), Lighthill (1977) and Weis-Fogh (1977) have postulated that, if the strength of materials limits the maximum angular velocity of the wing, it should scale as body mass$^{-\frac{1}{3}}$. It is interesting that

this is similar to the relationship Greenewalt (1975) found for hovering, when frequency is related to body mass. Strictly, it cannot be assumed that all birds are geometrically similar since Greenewalt (1975) has shown significant departures from geometric scaling rules. For example, aspect ratio, which should remain constant, generally increases with size, and wing area increases at a greater rate than predicted by geometric scaling. However Greenewalt's division of the birds in his survey into arbitrary groups based on wing loading sometimes confuses the relationship expected for all birds. Also, departures from geometric scaling are generally small and sometimes insignificant. Hence, for the relatively crude testing of the above predictions of wing angular velocity geometric similarity is still assumed. In the case of the testing of Pennycuick's (1978) prediction of wing beat frequency the dimensions of each bird are accounted for, eliminating errors caused by this assumption.

Here kinematic data has been collected of a number of species hovering or taking off, and allometric relationships have been found to see how kinematics vary with body mass.

The wing strokes in fast forward flight and slow or hovering flight are also described in detail, and these observations are combined with the allometric and aerodynamic analysis to give an overall indication

of how morphology and kinematics interact and how variations in wing shape can alter the use of the wing in flapping flight.

CHAPTER 5

MATERIALS, LOCATIONS AND METHODS

5.1 Photography

5.1.1 Photographic materials

5.1.1(i) Cameras

Three 16mm cine cameras were used, two being electrically driven high speed cameras, the Photosonics Actionmaster 1PD and the Photosonics 1PL, and the third a clockwork driven Bolex H16. The majority of the birds surveyed were filmed with the 1PL which has a continuous speed range up to 500fps and a variable shutter. The camera is specified to run within 1% of the pre-set framing rate, and its speed can be calibrated using LED (Light Emitting Diode) timing lights. These mark the edge of the film between the film perforations, at a point where the film is continuously running. Pulses of known duration and frequency were generated using an RS555 timing circuit, and these pulses were used to illuminate the LEDs. The distance between the start of successive marks on the film could then be used to calculate the film framing rate. This technique was successful for filming rates up to 300fps. Above this it was found not to be possible to produce a bright enough and sufficiently short pulse to cause a distinct timing band on the film,

as the current required destroyed the LED. The system is designed for colour film, which is more sensitive to the longer wave-lengths of light produced by LEDs than the black and white film used in this work. Few birds were filmed at a framing rate of more than 300fps. When timing lights were not available, film calibration was achieved by filming a stop watch. Both Photosonics cameras were periodically serviced and their running speed calibrated stroboscopically by the manufacturers; they were found to be running to specification. The 1PL once ran below the nominal running framing rate, during the filming in the Masai Mara in Kenya, due to a battery fault, but the actual running speed can be found from the timing marks.

The Actionmaster 1PD is similar to the 1PL, but it does not have a timing light facility, and it has a maximum framing rate of 400fps. This, and the Bolex H16 were calibrated by filming a stop-watch. The 1PD was used for framing rates up to 200fps, and the Bolex H16 up to its maximum of nominally 64fps. The camera used to film each species and the framing rate are given in Table 5.1 .

5.1.1(ii) Film

Kodak Tri X black and white reversal film, with a rated ASA of 200, was used in all cases with the exception of films taken in South Georgia. It can be uprated by one stop to effectively 400ASA with

little loss in quality. Ilford FP4 black and white negative film, with an ASA of 125, was used in South Georgia.

5.1.1(iii) Lenses

An Angenieux zoom lens with a focal length range of 12mm to 120mm and a minimum f number of 2.8 was used except in South Georgia, where a Cooke Telekinic Anastigmat lens with a focal length of 95mm was used. The Angenieux lens has a maximum distortion of 1.2% over its complete image at either extreme of focal length. The majority of birds were filmed so that their image filled only the central area(inside a ¼ width from any edge) within which the lens distortion is negligible. The distortion of the Anastigmat lens is within 1.5% for the full field of view.

5.1.1(iv) Camera mounts

The high speed cameras were usually mounted on a Quick Set pan and spring-tilt tripod head which enables smooth vertical and horizontal camera movements. The tripod head was usually supported by a Quick Set aluminium tripod. In Kenyan game reserves, where the camera operator had to remain within a vehicle, the camera could be mounted on the tripod head which was then clamped to the top of the windscreen of an open top Suzuki jeep. When rapid operation was required, the camera was supported, with the aid of a shoulder pad,

on the operator's shoulder, and used through the open jeep roof. The latter technique, although less stable, allowed 360° panning and target location which were not possible when the camera was clamped to the vehicle.

A still camera tripod was used to support the Bolex H16 in South Georgia and Peru.

5.1.2 Field locations

Filming locations were in England, Kenya, Peru and South Georgia.

In England, sea birds (Charadriiformes and Procellariiformes) were filmed at Stack Rocks in Pembrokeshire, Blakeney in Norfolk, and Bristol City Centre. Wildfowl (Anseriformes) were found at the Wildfowl Trust at Slimbridge in Gloucestershire, and captive birds of prey (Falconiformes) were filmed at the Hawk Conservancy near Weyhill in Wiltshire. Kestrels owned by J.Kirkwood at Langford in Somerset were used for field filming. Pigeons (Columbiformes), corvids (Passeriformes) and swifts (Micropodiformes) were filmed in Bristol.

In Kenya, East African lake birds (Pelecaniformes, Ciconiiformes, Anseriformes, Gruiformes and Coraciiformes) were filmed at lakes Baringo, Bogoria, Nakuru and Naivasha. Savanna birds (Ciconiiformes and Falconiformes) were generally found in the Masai Mara game reserve, and urban species (Falconiformes and Passeriformes) were filmed in Nairobi. Captive birds of prey (Falconiformes) owned by P.Davey and S.Thompsett were filmed in Nairobi.

A selection of Pacific sea birds (Pelecaniformes and Charadriiformes), cathartid vultures and birds of prey (Falconiformes) were filmed at Paracus in Peru, and the brown pelican Pelecanus occidentalis was filmed

in Miami in the United States of America. The majority of Procellariiformes included in this work were filmed by C.J.Pennycuick on Bird Island in South Georgia. Table 5.1 gives the location of each species filmed.

Table 5.1

Bird species filmed in the field with the filming location, type of camera, film framing rate and lens focal length.

The 1PD and 1PL cameras are manufactured by Photosonics, and the H16 is made by Bolex. The country of each location is indicated by the bracketed letters with UK for United Kingdom, K for Kenya, P for Peru and SG for South Georgia. The bird scientific names are taken from Gruson (1976).

Bird Species	Location	Camera Type	Film Speed Frames s^{-1}	Lens Focal Length mm
PROCELLARIIFORMES				
Wandering Albatross DIOMEDEA EXULANS	Bird Island(SG)	H16	60	95
Black Browed Albatross DIOMEDEA MELANOPHRIS	Bird Island(SG)	H16	60	95
Grey Head Albatross DIOMEDEA CHRYSOSTOMA	Bird Island(SG)	H16	60	95
Sooty Albatross DIOMEDEA FUSCA	Bird Island(SG)	H16	60	95
Giant Petrel MACRONECTES GIGANTEUS	Bird Island(SG)	H16	60	95
White Chinned Petrel PROCELLARIA AEQUINOCTIALIS	Bird Island(SG)	H16	60	95
Fulmar FULMARUS GLACIALIS	Stack Rocks(UK)	1PL	200	120

TABLE 5.1 cont.

PELECANIFORMES				
White Pelecan PELECANUS ONOCROTALUS	Lake Nakuru(K)	1PL	100	120
Pink backed Pelican PELECANUS RUFESCENS	Lake Nakuru(K)	1PL	100	120
Brown Pelican PELECANUS OCCIDENTALIS	Miami Harbour(USA)	H16	40	120
Chilean Pelican PELECANUS THAGUS	Paracus(P)	H16	40	120
Cormorant White Necked PHALACROCORAX CARBO	Lake Nakuru(K)	1PL	100 & 200	120
Anhinga ANHINGA ANHINGA	Naro Moro(K)	1PL	100	120
Peruvian Booby SULA VARIEGATA	Paracus(K)	H16	40	120
CICONIIFORMES				
Marabou Stork LEPTOPTILOS CRUMENIFERUS	Lake Naivasha(K)	1PL	100	120
Yellow Billed Stork IBIS IBIS	Lake Naivasha(K)	1PL	100	120
Saddle Bill Stork EPHIPPIORHYNCHUS SENEGALENSIS	Masai Mara(K)	1PL		60-120
White Stork CICONIA CICONIA	Masai Mara(K)	1PL		120
Great Egret EGRETTA ALBA	Lake Nakuru(K)	1PL	100	120
Little Egret EGRETTA GARZETTA	Lake Nakuru(K)	1PL	100	120
Grey Heron ARDEA CINEREA	Lake Nakuru(K)	1PL	100	120
Goliath Heron ARDEA GOLIATH	Lake Naivasha(K)	1PL	100	120

TABLE 5.1 cont.

Sacred Ibis THRESKIORNIS AETHIOPICA	Lakes Nakuru and Naivasha(K)	1PL	200 100	120 120
Hadada Ibis BOSTRYCHIA HAGEDASH	Masai Mara(K)	1PL	84	120
African Spoonbill PLATALEA ALBA	Lake Nakuru(K)	1PL	100	120
Lesser Flamingo PHOENICNAIAS MINOR	Lake Bogoria(K)	1PL	200	120
Greater Flamingo (Chilean) PHOENICOPTERUS RUBER	Lake Nakuru(K) Paracus(Chilean)	1PL H16 (P)	100 40	120 120
ANSERIFORMES				
Bewick Swan CYGNUS COLUMBIANUS	Slimbridge(UK)	1PD	200/ 100	120
Whooper Swan CYGNUS CYGNUS	Calaveroch(UK)	1PL	100	120
Barnacle Goose BRANTA LEUCOPSIS	Slimbridge(UK)	1PL	100	120
Mallard ANAS PLATYRHYNCHOS	Slimbridge(UK) Blakeney(UK)	1PL 1PL	200 200	120 120
Pintail Duck ANAS ACUTA	Slimbridge(UK)	1PL	200	120
FALCONIFORMES				
Andean Condor VULTUR GRYPHUS	Paracus(P)	H16	39	120
Turkey Vulture CATHARTES AURA	Paracus(P)	H16	40	120
Lappet Faced Vulture AEGYPIUS TRACHELIOTUS	Masai Mara(K)	1PL	84	120
White Head Vulture TRIGONOCEPS OCCIPITALIS	Masai Mara(K)	1PL	87	120

TABLE 5.1 cont.

Ruppell's Griffon GYPS RUPPELLII	Masai Mara(K)	1PL	84	120
White Backed Vulture PSEUDOGYPS AFRICANUS	Masai Mara(K)	1PL	84	120
Hooded Vulture NEOPHRON MONACHUS	Masai Mara(K)	1PL	84	120
Steppe Eagle AQUILA NIPALENSIS	Weyhill(UK) (captive)	1PL 1PD	200 100	120 120
African Fish Eagle HALIAEETUS VOCIFER	Lake Baringo(K)	1PD	100	120
Common Buzzard BUTEO BUTEO	Weyhill(UK) (captive)	1PL	200	120
Crowned Eagle HARPYHALIAETUS CORONATUS	Nairobi(K) (captive)	1PL	84	40-60
Black Kite MILVUS MIGRANS	Nairobi(K)	1PL	100	120
Bateleur TERATHOPIUS ECAUDATUS	Masai Mara(K)	1PL	84	60
Secretary Bird SAGITTARIUS DERPENTARIUS	Naivasha(K)	1PL	100	120
Osprey PANDION HALIAETUS	Paracus(P)	H16	40	120
African Goshawk ACCIPITER TACHIRO	Nairobi(UK) (captive)	1PL	200	120
Lagger Falcon FALCO JUGGER	Pembrokeshire(UK) (captive)	1PL	200	12,40 120
Lanner Falcon FALCO BIARMICUS	Weyhill(UK) (captive)	1PL	200	120
Kestrel FALCO TINNUNCULUS	Bristol(UK)	1PL	200	120
GRUIFORMES				
Crowned Crane BALEARICA PAVONINA	Nakuru(K)	1PL	100	120

TABLE 5.1 cont.

CHARADRIIFORMES				
Curlew NUMENIUS ARQUATA	Malindi(K)	1PL	84	120
Oystercatcher HAEMATOPUS OSTRALEGUS	Blakeney(UK)	1PL	200	120
Black Headed Gull LARUS RIDIBUNDUS	Bristol Docks(UK) Blakeney(UK)	1PD 1PL	100 200	120 120
Common Gull LARUS CANUS	Bristol Docks(UK)	1PL	100	120
Kittiwake LARUS TRIDACTYLUS	Stack Rocks(UK)	1PL	200	120
Common Tern STERNA HIRUNDO	Blakeney(UK)	1PL	200	120
Little Tern STERNA ALBIFRONS	Blakeney(UK)	1PL	200	120
Guillimot URIA AALGE	Stack Rocks(UK)	1PL	300	120
COLUMBIFORMES				
Rock Dove COLUMBA LIVIA	Bristol Docks(UK) (take-off)	1PL	200	20
Collord Dove STREPTOPELIA DECAOCTO	Slimbridge(UK)	1PL	200	120
Wood Pigeon COLUMBA PALUMBUS	Bristol Downs(UK)	1PL	200	120
STRIGIFORMES				
Veareaux's Eagle Owl BUBO LACTEUS	Nairobi(K) (captive)	1PL	84	-
APODIFORMES				
Common Swift APUS APUS	Bristol(UK)	1PL	200	120

TABLE 5.1 cont.

CORACIIFORMES				
Pied Kingfisher CERYLE RUDIS	Naivasha(K)	1PL	300	120
PASSERIFORMES				
Rook CORVUS FRUGILEGUS	Bristol Downs(UK)	1PD 1PL	100	120
Jackdaw CORVUS MONEDULA	Bristol Downs(UK)	1PD	100	120
Magpie PICA PICA	Bristol Downs(UK)	1PL	200	120

Source for Latin names - Gruson, 1976.

5.1.3 Filming techniques

5.1.3(i) Framing rate and shutter speed selection

It is essential that a fast enough shutter speed is selected for a specific bird, so that each image of the wing cycle is 'frozen', and also that the film framing rate, whenever possible, gives at least 20 frames per wing beat. This ensures that the maximum error, when measuring the wing beat frequency (wing beats per second) of a particular wing beat cycle, is within 5%. Higher framing rates are desirable to give greater statistical accuracy, but they have two disadvantages. Firstly, the higher the framing rate, the greater the amount of film required and the greater the expense of the survey. Secondly, the higher the framing rate, the longer the 'run up' time of the camera before it reaches its steady pre-set speed. When the 'run up' period is long (2 to 3 seconds between 300fps and 500fps) it is difficult to record rapid and unpredictable flight behaviour such as, for example, take-off.

As the Bolex H16 cine camera was limited in practice to 60fps and sometimes less, it was only suitable for filming large birds with low wing beat frequencies, and even then 20 frames per wing beat cycle was rarely possible. A guide to the shutter speeds and framing rates suitable for different size ranges of birds is given in Table 5.2 .

Table 5.2

Preferable film framing rates and shutter speeds for ranges of bird wing beat frequency.

BIRD WING BEAT FREQ. Hz	FILM SPEED Frames/ sec	SHUTTER SPEED sec^{-1}	EXAMPLES FROM THIS SURVEY
1-4	100	1,000	Vultures Swans
4-8	200	2,000	Falcons Pigeons
8-12	300	3,000	Auks Kingfishers
12-16	400	4,000	Large Passerine
16-20	500	5,000	Small Passerine

5.1.3(ii) The limits of maximum f number

As the shutter speeds required are relatively high (Table 5.2) and the film speed limited to 400ASA, bright sunlight or artificial light is generally essential. Even so, low lens f numbers of between 2.8 and 5.6 have to be used, and these generally prohibit the use of long focal length lenses with high minimum f numbers.

5.1.3(iii) Field filming

Attempts were made to record film of all the birds observed, head on and side on in cruise flight, and also in maximum power flight;efforts were made to keep the bird as near to the camera level as possible. Generally the bird was close enough to fill at least a quarter of the field of view. Film of maximum power flight usually involved the bird either hovering or during take-off. Limitations of location and behaviour of the birds made it rarely possible to achieve all these desired sequences for each bird.

5.1.3(iv) Laboratory filming

Film of a kestrel Falco tinunculus hovering and climbing vertically was obtained in the following manner: an area of the laboratory approximately $2m^2$ was illuminated using 4kw of Quartz Halogen electric lights, and a kestrel was attracted to fly in front of

a non-reflecting white background within the illuminated area, towards bait held in the experimenter's hand. Short periods of hovering were induced by quickly rotating the hand just before the kestrel landed upon it. The running time of the camera was controlled by a remote switch operated by the experimenter. The framing rate was 200fps.

The hovering flight of the budgerigar Melopsittacus undulatus and the zebra finch Poephila guttata was filmed in the net cage illustrated in Figure 5.1 . A suspended net bottom prevented the bird from settling anywhere except on the single perch provided. Flight was induced by moving the perch. A squared background was used for scale and position reference, and to check that the glass front of the cage was not causing image distortion. The cage was illuminated by 4kw of Quartz Halogen light, and the hovering was filmed at 500fps. The çamera was positioned 8m away from the background so that the scale of the background grid was nearly the same as that of the bird. Prominent features of thebird were measured, and related to its analyser image to check the similarity.

Film of the zebra finch in fast forward flight was obtained by constructing an 8m net tunnel which was long enough to allow bounding fast forward flight (Figure 5.2). Again, a suspended net base largely prevented settlement other than on the two perches, situated at either end of the tunnel. These perches

Figure 5.1

Apparatus for filming hovering and slow forward flight of small birds.

Figure 5.1

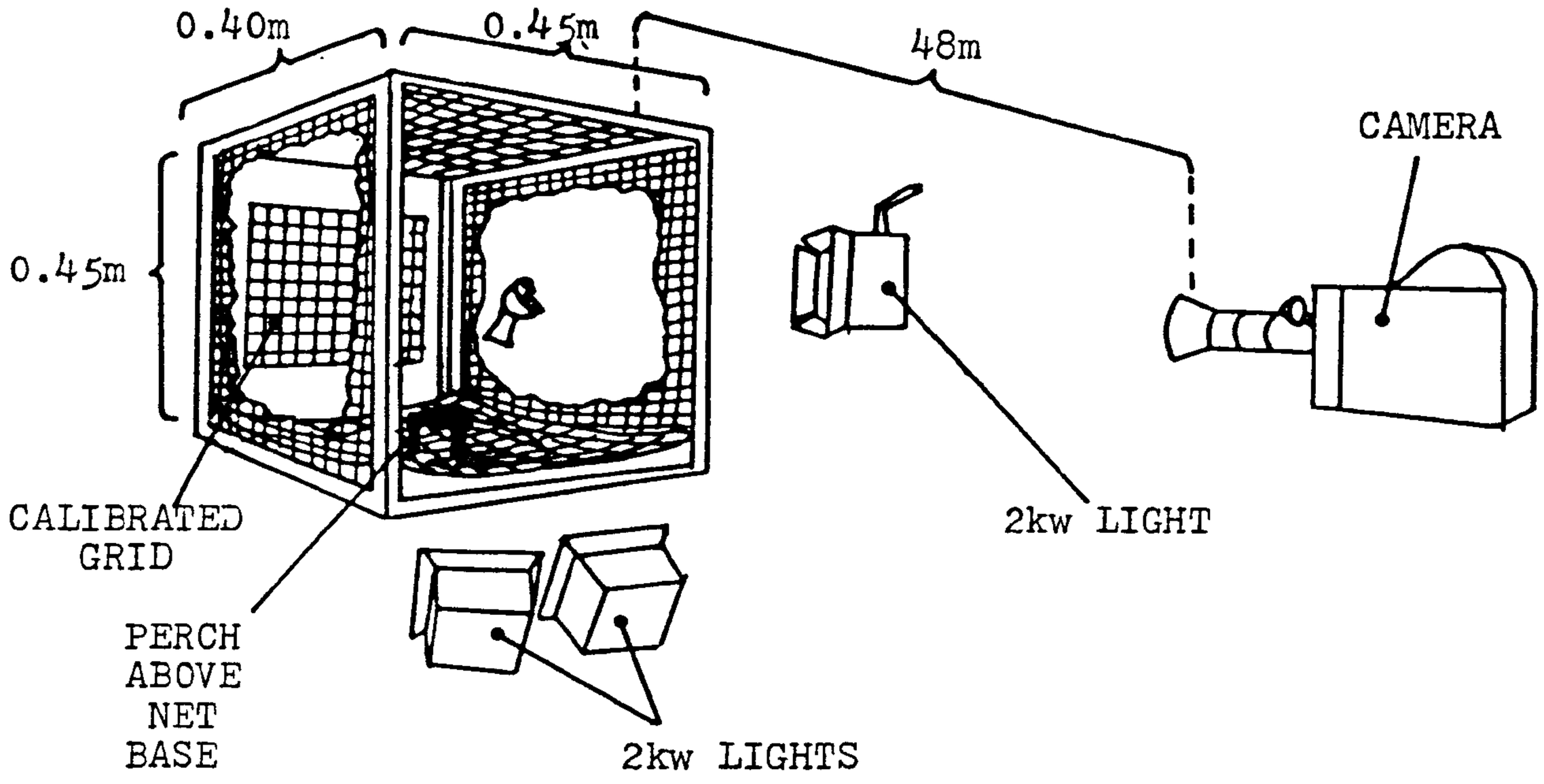
0.40m
0.45m
48m
CAMERA
0.45m
CALIBRATED GRID
2kw LIGHT
PERCH ABOVE NET BASE
2kw LIGHTS

Figure 5.2

Apparatus for filming fast forward flight of small birds. The flight of the zebra finch between the two illuminated perches was always direct, and so the front of the filming section of the 'tunnel' could be left open. This eliminated the problems of reflection and distortion caused by a glass front to the filming section.

Figure 5.2

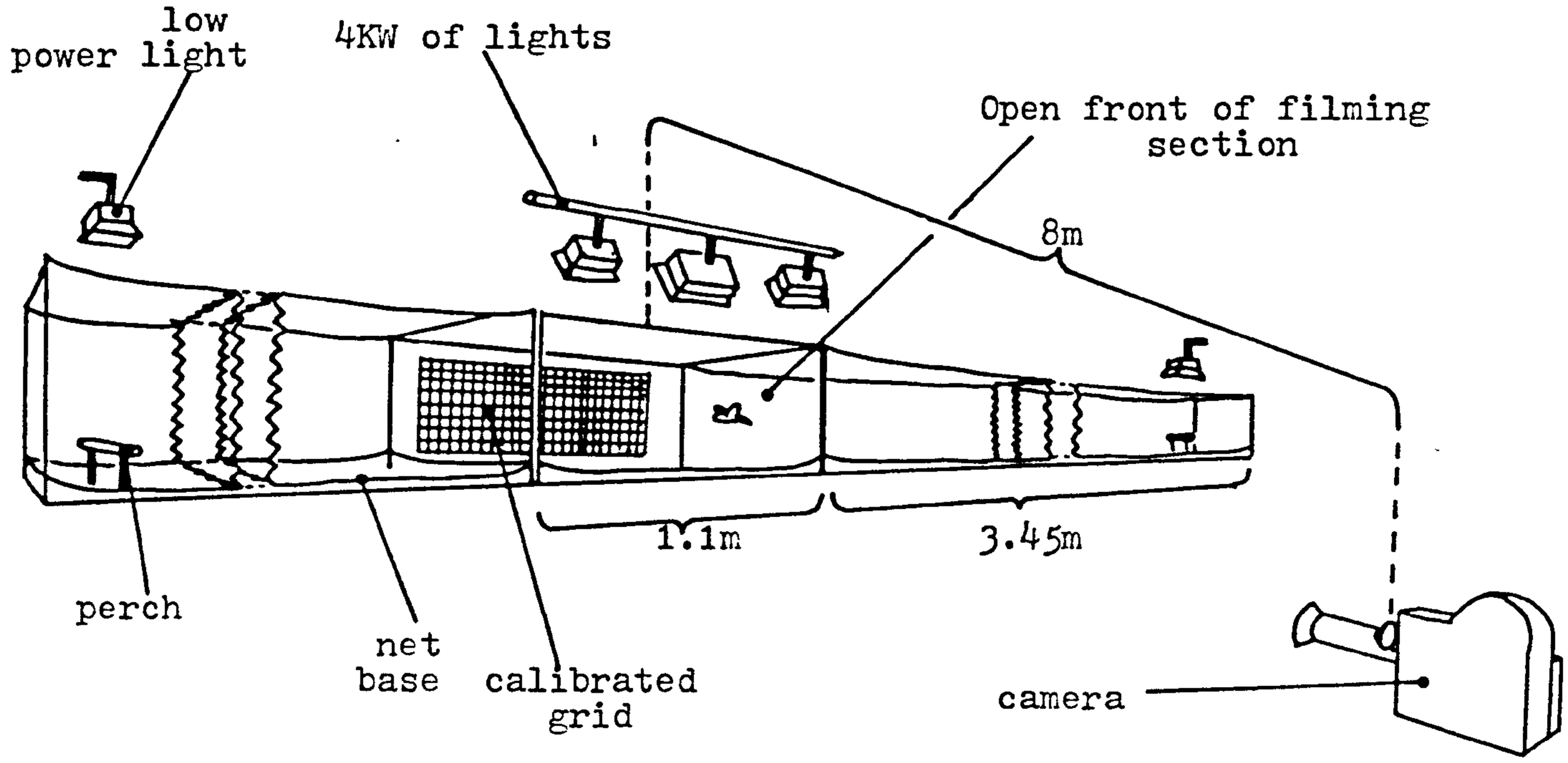
low
power light
4KW of lights
Open front of filming
section
8m
1.1m
3.45m
perch
net
base
calibrated
grid
camera

were illuminated. A central filming section 1.1m long, with a squared background for scale and position reference, was illuminated by 4kw of light. The camera was again placed 8m away to ensure similarity between the bird and the scale of the background. The filming section could have an open front, the finch always choosing to fly directly from perch to perch. Once started, the camera was allowed to reach its running framing rate of 200fps or 500fps before the bird was induced to fly along the tunnel by a sharp sound. The end of the camera 'run up' period can be judged audibly, as it reaches a constant note when its framing rate is at the pre-set speed.

5.2 Analysis

5.2.1 Analysis apparatus

Film analysis was done using an NAC MC-OB Film Motion Analyser; this records frame numbers and digitises, into absolute millimeters, the X and Y co-ordinates of movable cross wires on the analyser screen. Both frame number and X and Y co-ordinates can be zeroed at any point, and further values can be given relative to this zeroed position. Angles are found by aligning rotatable parallel lines on the screen with the image in question; the angle of this image line relative to the analyser horizontal can then be read from a vernier scale, accurate to 10 minutes of arc. If the camera was not horizontal during filming, this can be corrected for on the analyser by rotating the projector head of the analyser until the horizontal of the image is the same as that of the analyser.

Frame numbers and X and Y co-ordinates can be transferred via an IIMC interface system to a Research Machines 380Z micro computor, and then stored on floppy disc. The data can then be scaled to the actual distances moved by the analyser points in actual time (Section 2.2.3) and this data can then be treated by a series of programmes (Rayner, in preparation a) and plotted using a Hewlett Packard 7225A Graph Plotter.

5.2.2 Analysis technique

The film analysis can be divided into three levels. Firstly, there is temporal analysis of the various periods of the wing cycle. For this the film must be of a sufficient framing rate, but the view of the bird and its scale are of no importance.

Secondly,there is angle analysis, where the position of the bird relative to the camera is critical, but scale information is not required.

Thirdly, there is frame by frame analysis to give the change of position of points and the rate of these changes; scale, framing rate and the position of the bird relative to the camera are all important here.

5.2.2(i) Temporal analysis

Downstroke period and total period were found for each wing cycle by counting the number of frames for each and dividing it by the framing rate of the film. The beginning of the downstroke was taken as the frame in which wing tip bending was first observed, and hence when the primary feathers become loaded; the end of the downstroke was taken as the frame when bending and loading ceased. This system was chosen because it represents the period when the wing is loaded, and because the points of the beginning and end of the downstroke can be clearly seen. These wing tip

movements are not in phase with those of the proximal wing between the shoulder and the wrist. Recording downstroke period using the wrist would be unsuitable because the transition frames between upstroke and downstroke and vice versa are often unclear, and the movements do not necessarily coincide with the loaded and unloaded periods of the majority of the wing.

Total period was measured as the period between the beginning of consecutive downstrokes. The inverse of the total period (1/total period) gives the wing beat frequency f, and the downstroke ratio z is given by the downstroke period divided by the total period. The mean and standard deviation of the above values were found for a series of wing beat cycles for each individual in steady flight; if a group of birds of the same species had been filmed, then the overall mean and standard deviation were also found. This mean value has been used in the regression analysis of the results (Chapters 6 and 7).

5.2.2(iia) Direct angle analysis

The stroke amplitude ϕ is the angle through which the proximal wing is swept during the downstroke (Figure 5.3a). It can only be measured directly in cruise flight from film of a bird flying directly towards or away from the camera at approximately the same level as the camera. Stroke amplitude is divided

Figure 5.3a

Stroke amplitude analysis in cruise flight of a bird flying directly away from the camera. The stroke amplitude ϕ is the combination of the positive elevation ϕ_u and the negative elevation ϕ_d.

Figure 5.3b

The difference of the greatest negative elevation of the proximal and distal wing sections at the base of the downstroke. The proximal wing ϕ_d is used to measure negative elevation throughout this survey.

Figure 5.3a

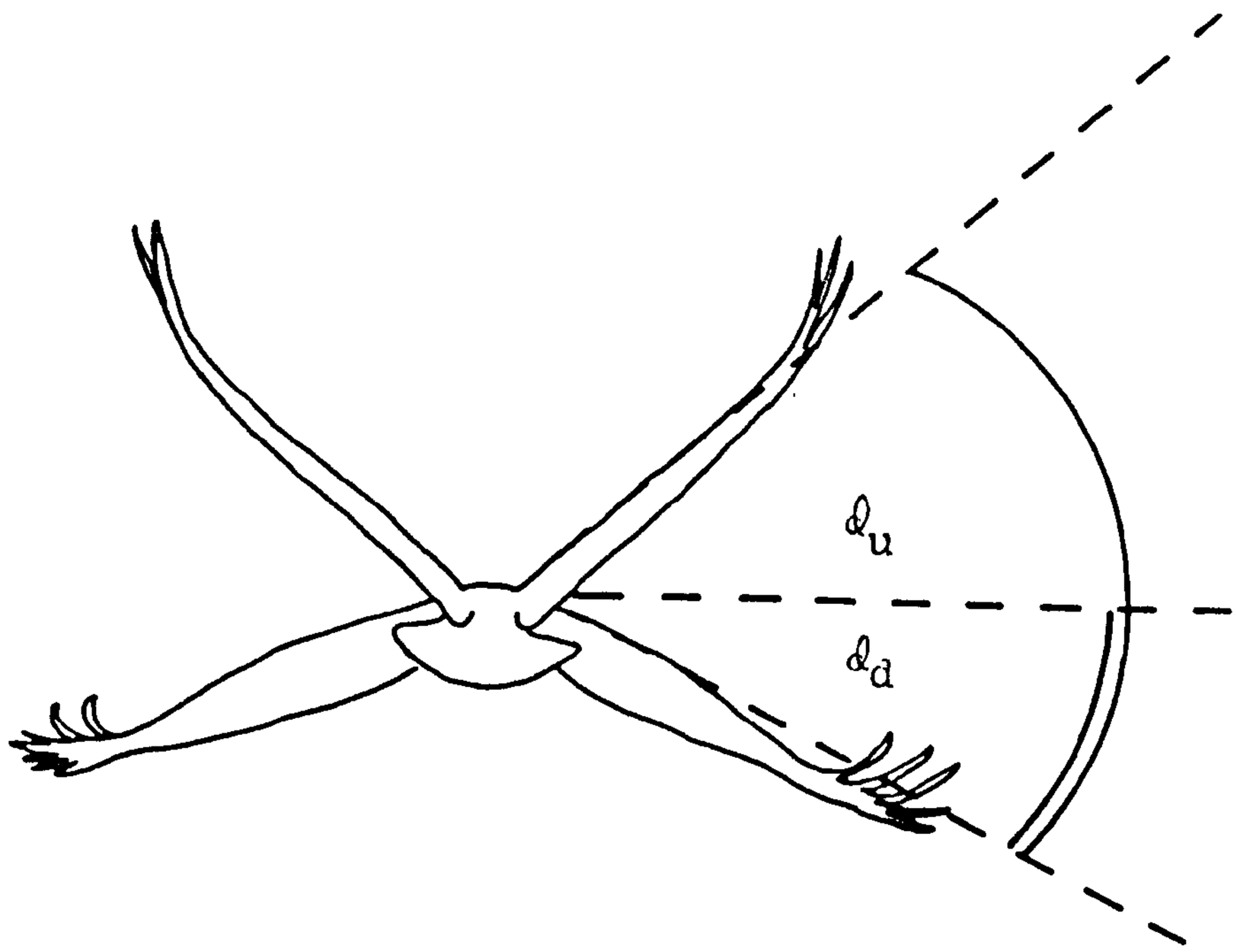

Figure 5.3b

— — — — Proximal wing α_d

— . — . — Distal wing α_d

into the positive elevation θ_u, which is the largest angle subtended between the proximal wing and the horizontal of a level flying bird, and the negative elevation θ_d, which is the corresponding largest angle below the horizontal (Figure 5.3a).

The proximal wing is used because of the complex movements of the distal wing (the section of the wing between wrist and wing tip) at the bottom of the downstroke. The wrist is flexed and the proximal wing rotated (Chapter 6) so that its leading edge is raised, which has the effect of further depressing the wing tip when viewed from behind or in front (Figure 5.3b). The distal wing movements is actually a combination of posterior and downward movement, due to the wrist being flexed horizontally but also rotated upwards. The actual angle through which the distal wing is swept at the base of the downstroke can only be found by a three dimensional analysis. The proximal wing movements, if the stroke plane angle is near to 90^{o} (Chapter 6) is suitable for angle measurement from a two dimensional image, and can be used for this comparative survey.

The angle of camera tilt θ_t required to film a bird flying above or below the camera level will alter the apparent amplitude (Figure 5.4). If a bird has a positive elevation of θ_u and a semi-span $\frac{1}{2}b$, then the true height of the wing tip above the horizontal h will be

$$h = \tfrac{1}{2}b \sin \theta_u$$

Figure 5.4

Distortion of amplitude measurement caused by the bird not being level with the camera. Symbols explained in the text.

Figure 5.4

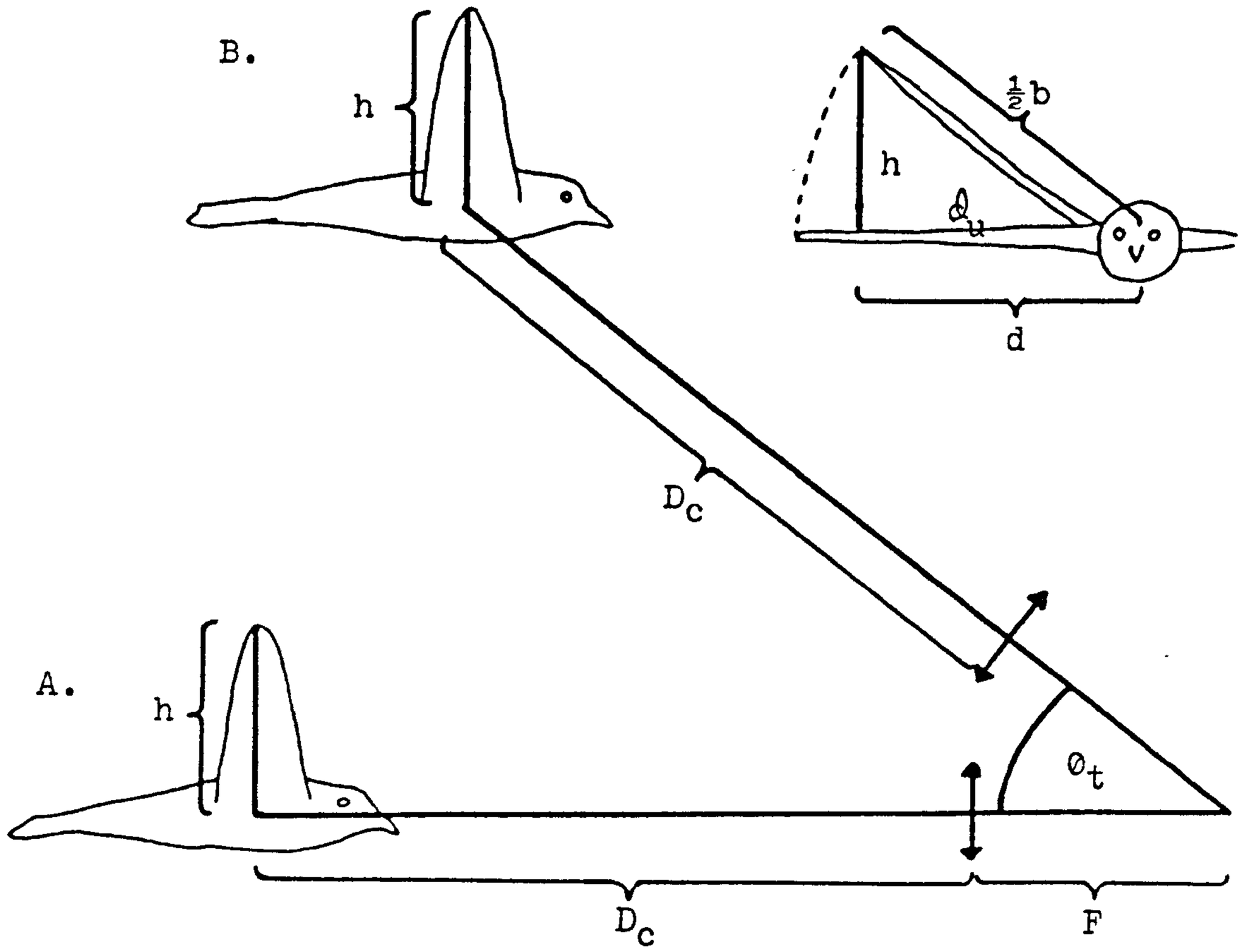

while the horizontal distance of the wing tip to the body d is given by

$$d = \tfrac{1}{2} b \cos \theta_u$$

When the bird is level with the camera, the apparent values of h and d on the focal plane, h' and d' are

$$h' = \frac{F}{D_c} h = \frac{F}{D_c} \tfrac{1}{2} b \sin \theta_u$$

and

$$d' = \frac{F}{D_c} d = \frac{F}{D_c} \tfrac{1}{2} b \cos \theta_u \quad ,$$

when F is the lens focal length and D_c is the distance between the camera and the bird. If the camera must be tilted through an angle θ_t and the bird is still a distance of D_c from the camera, then the images of h and d will be h" and d" given by

$$h'' = \left(\tfrac{1}{2} b \sin \theta_u \cos \theta_t\right) \frac{F}{D_c}$$

and

$$d'' = \frac{\tfrac{1}{2} bF}{D_c} \cos \theta_u \quad ,$$

and so the apparent positive elevation θ_u'' will be

$$\theta_u'' = \arctan \frac{h''}{d''}$$

For amplitudes greater than 30°, θ_t can be up to 20° for the image amplitude to be within 5% error limits; amplitude measurements were only made from film taken within tilt angles of 20°.

5.2.2(iib) Indirect estimate of amplitude

Amplitude can be estimated from views other than those of birds seen head-on or tail-on, provided that the scale of the bird (Section 5.2.2(iii)) and its actual wing span are known. The height of the wing tip above or below the horizontal can then be measured, scaled to the actual value for the bird, and θ_u and θ_d calculated given that

$$\sin \theta_u = \frac{h}{\frac{1}{2}b}$$

5.2.2(iii) Scaling of birds in flight in field conditions

The problem with scaling birds in flight is that it is not possible to judge accurately, on a two dimensionless image, the position of the bird

relative to other objects which may be measured later to provide scale. This problem is usually academic since suitable objects rarely fall into the field of view. Hence, scaling must be done by choosing a dimension of the bird which can be measured accurately from film of it in flight, and which has also been measured on a specimen of the same species. The unavoidable error of this technique is that the animal measured is not the one on film.

The extensive literature survey of Rayner (b, in preparation) gives dimensions of the majority of birds filmed in this survey.

A bird flying directly towards or away from the camera can be scaled by measuring its wing span half-way through the downstroke, when the wings are level and fully extended, and then finding the ratio of this span to the actual wing span of a measured bird of the same species. If more than one measurement was available, the dimensions of the bird with a body mass nearest to the mean were used. When a span measurement was not available, the length of the distal wing of the flying bird was measured and scaled by the species mean ornithological wing length.

A bird flying side-on to the camera could sometimes be scaled if its species mean body length was known. This could only be done for birds with short necks; body length measurements are generally

made with neck outstretched, and the majority of long-necked birds fly with the neck folded. A second method was to measure the thickest vertical body width of a bird flying directly towards the camera, and finding the ratio of this width to the wing span. The equivalent width can be measured from side-view film, and so the scale of the bird can be found.

5.2.2(iv) Flight speed estimation

The flight speed of a bird flying directly towards or away from the camera in still air conditions can be found from the rate of change of the image wing span. If the actual wing span b is known, and the initial span on the film with the wings level and fully extended is b_1', and if the focal length F of the lens is known, then the distance of the bird from the camera D_{c_1} is given by

$$D_{c_1} = \frac{b}{b_1'} F$$

(see Figure 5.5)

If the film, of framing rate R_f, is run forward N frames, the bird's image span is then b_2' and the distance from the camera is D_{c_2}. The flying speed V is then given as

$$V = \frac{D_{c_2} - D_{c_1}}{N / R_f}$$

Figure 5.5

Flight speed estimates from film of a bird flying directly towards (or away from) the camera. Symbols explained in the text.

Figure 5.5

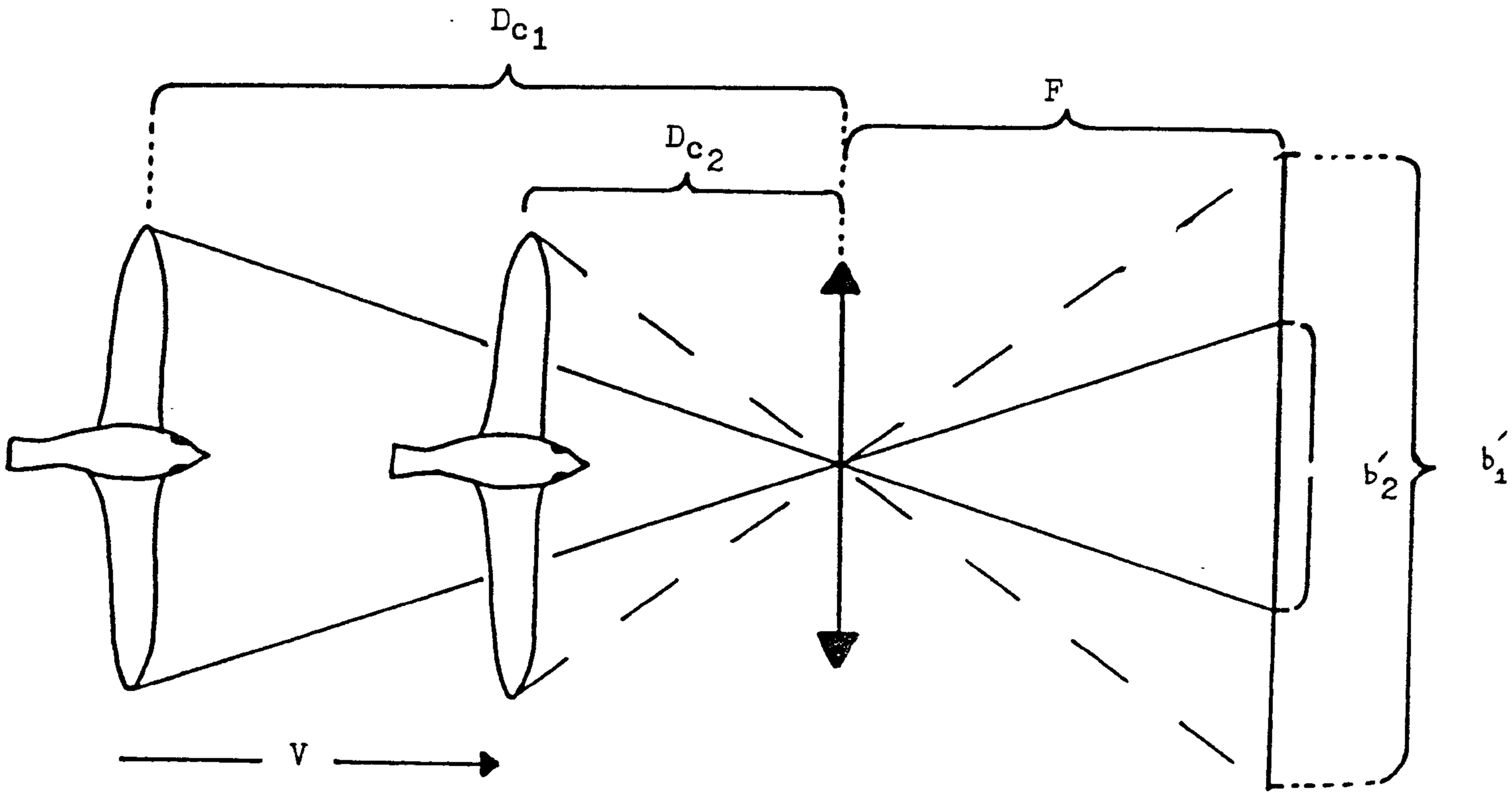

The take-off speed of running vultures was determined by a similar method to that used for running ungulates by Alexander et al (1977) by finding the time for the bird's known body length to pass over an object on the ground. The equivalent take-off speed of a pelican which was side-on to the camera was found by measuring the distance, in known body lengths, from a splash caused by its feet to a position just before its feet re-entered the water, and finding the time required to travel that distance.

5.2.2(v) Frame by frame analysis technique

For each frame a series of points could be digitised, typically wing tips, wrists and a point on the body which was considered as a fixed target. The target co-ordinates could then be subtracted from those of the other points, so positioning them relative to the target. This eliminated any overall body movements of the bird within the field of view to give only the movements of the wings relative to the body, The series of co-ordinates of each point for a complete wing stroke could then be scaled to give actual distances moved in actual time. This data was then plotted as X against Y co-ordinated, X or Y co-ordinates against time, X or Y velocity against time or net speed against time.

5.2.2(va) Head-on or tail-on

A typical head-on 'wing tip trace' in cruise

flight is illustrated in Figure 5.6A. The body target used is the tangent of the highest point on the body. It can be seen that equivalent points in consecutive wing beat cycles (i.e. the point at the beginning of the first downstroke 'A' and the second 'B') do not coincide. This is due to the image wing span becoming smaller as the bird flies away from the camera. If it is assumed that the bird flies at a constant speed throughout a wing beat, then this distortion can be corrected. If the original wing span is b_1 and after one wing beat cycle of N frames the new span is b_2, then the change of scale for each frame Q_α is given by

$$Q_\alpha = \frac{1}{N}\left(\frac{b_1}{b_2} - 1\right)$$

Figure 5.6B is a corrected version of Figure 5.6A.

Such wing traces are limited by camera tilt angles in the same way as amplitude (Section 2.2(ii)). The bird must also be flying directly away or towards the camera for the wing strokes to be symmetrical about the body. Figure 5.6C shows a typical distorted wing trace when the bird's body is at a slight angle to the camera.

If the stroke plane angle is between 72° and 90° then a head-on wing tip trace will give the distances moved during the downstroke to within 5%. If it is

Figure 5.6a

The wing tip trace of a Ruppell's griffon vulture Gyps ruppellii (wing span 2.41m) flying directly away from the camera.

The film speed is 84fps and each solid circle represents the wing tip position for a frame. The trace of the second down stroke is inside that if the first because the image of the bird is reduced as it flies away from the camera.

Figure 5.6b

The wing tip trace as in 5.6a, but having been corrected so that the image of the bird has a constant wing span.

Figure 5.6c

The distorted wing tip trace of a Ruppell's griffon vulture which is not flying directly away from the camera. The traces are no longer symmetrical.

Figure 5.6a

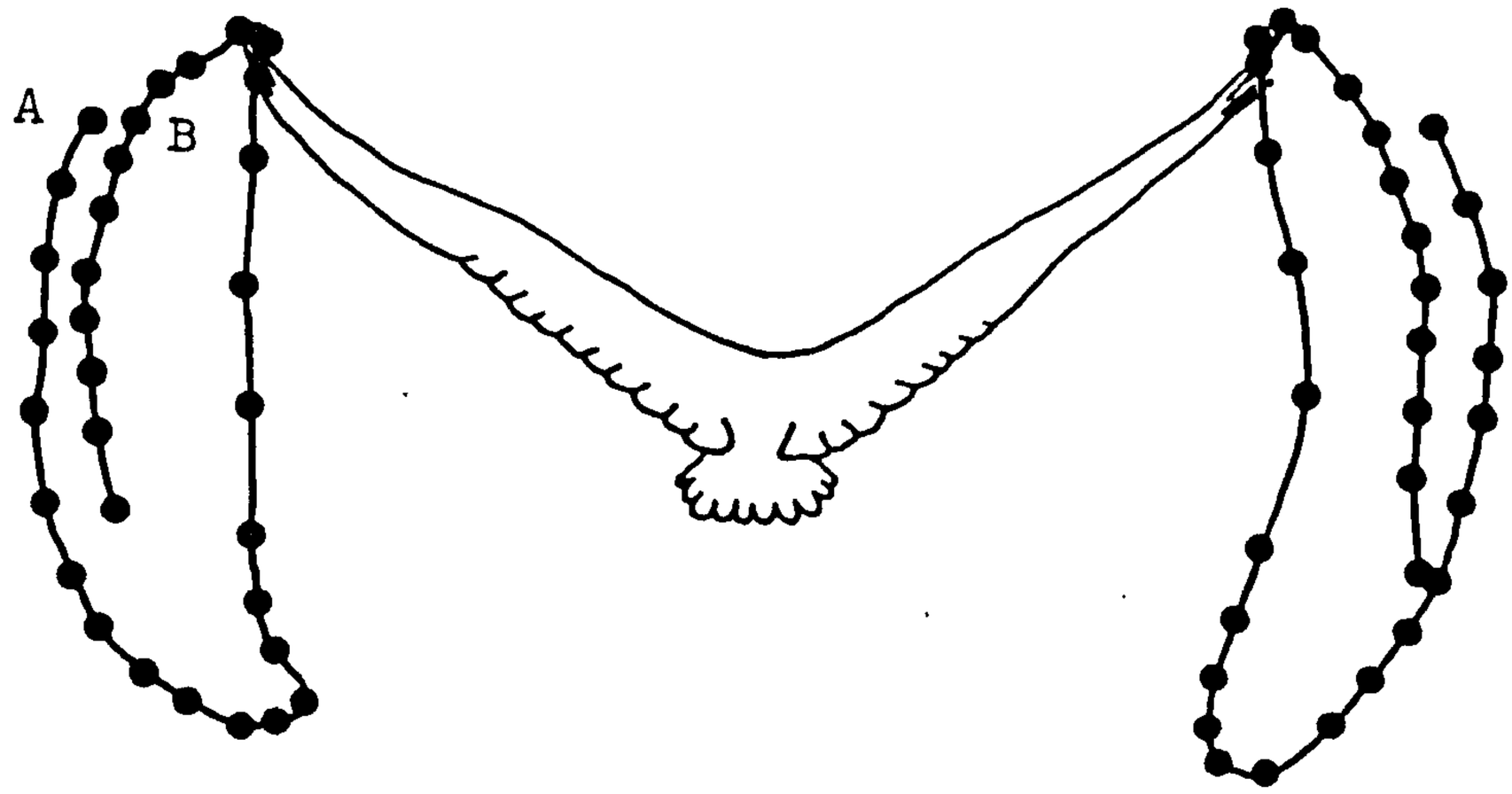

Figure 5.6b

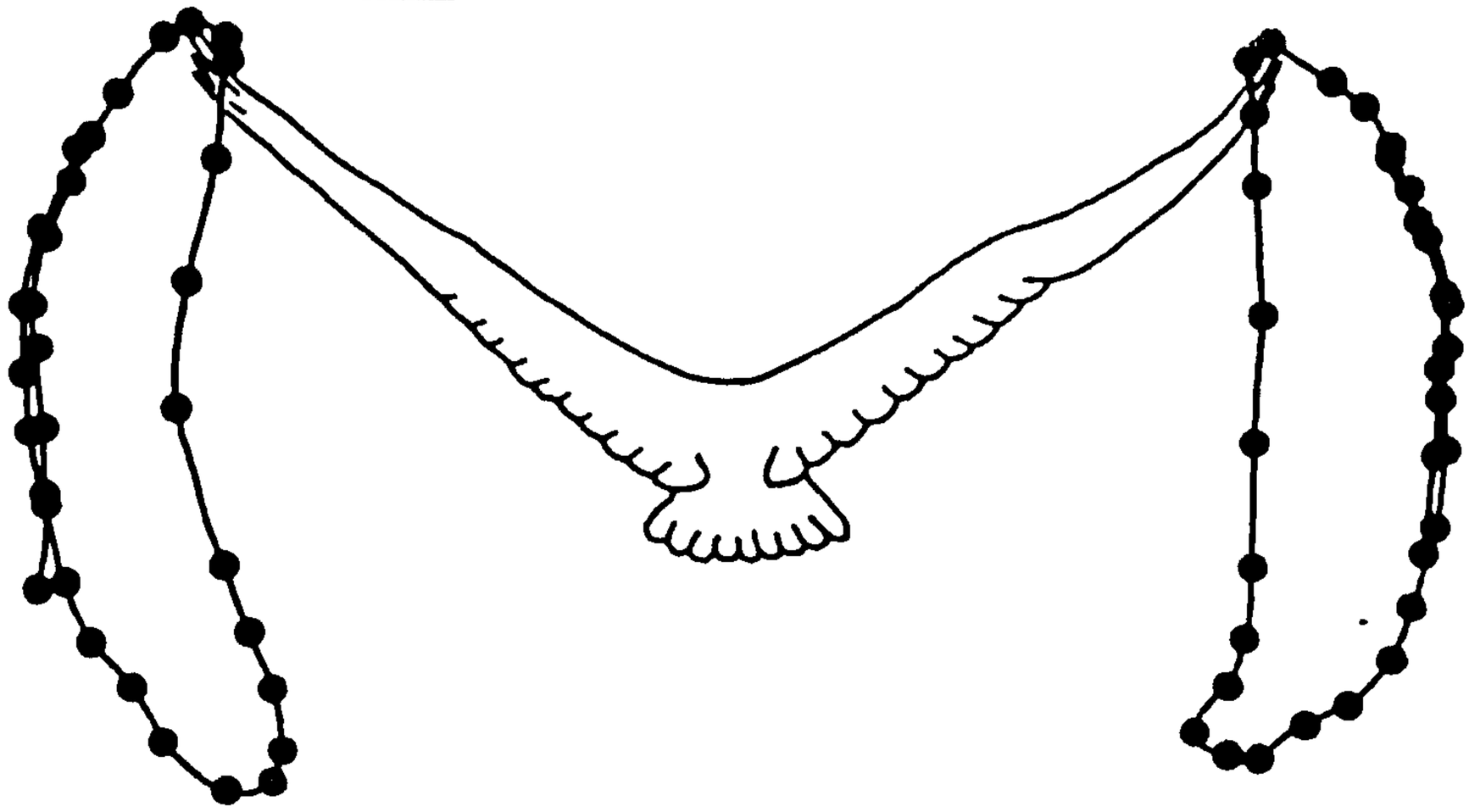

Figure 5.6c

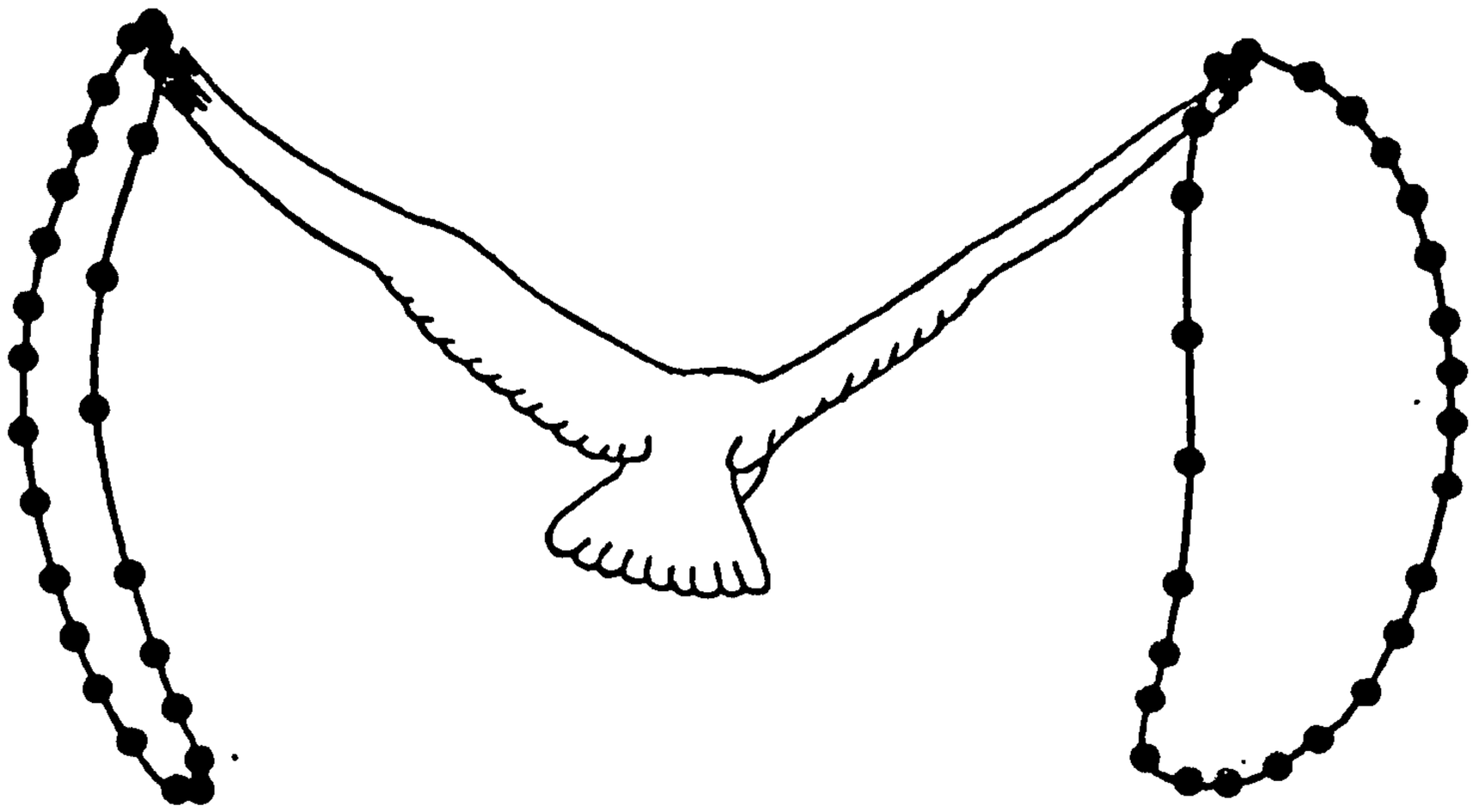

Figure 5.6d

The distribution of wing tip speed with time for one wing cycle of the Ruppell's griffon vulture Gyps ruppellii flying directly away from the camera as in Figure 5.6b. The periods of upstroke and downstroke are indicated by 'up' and 'down' respectively.

Figure 5.6d

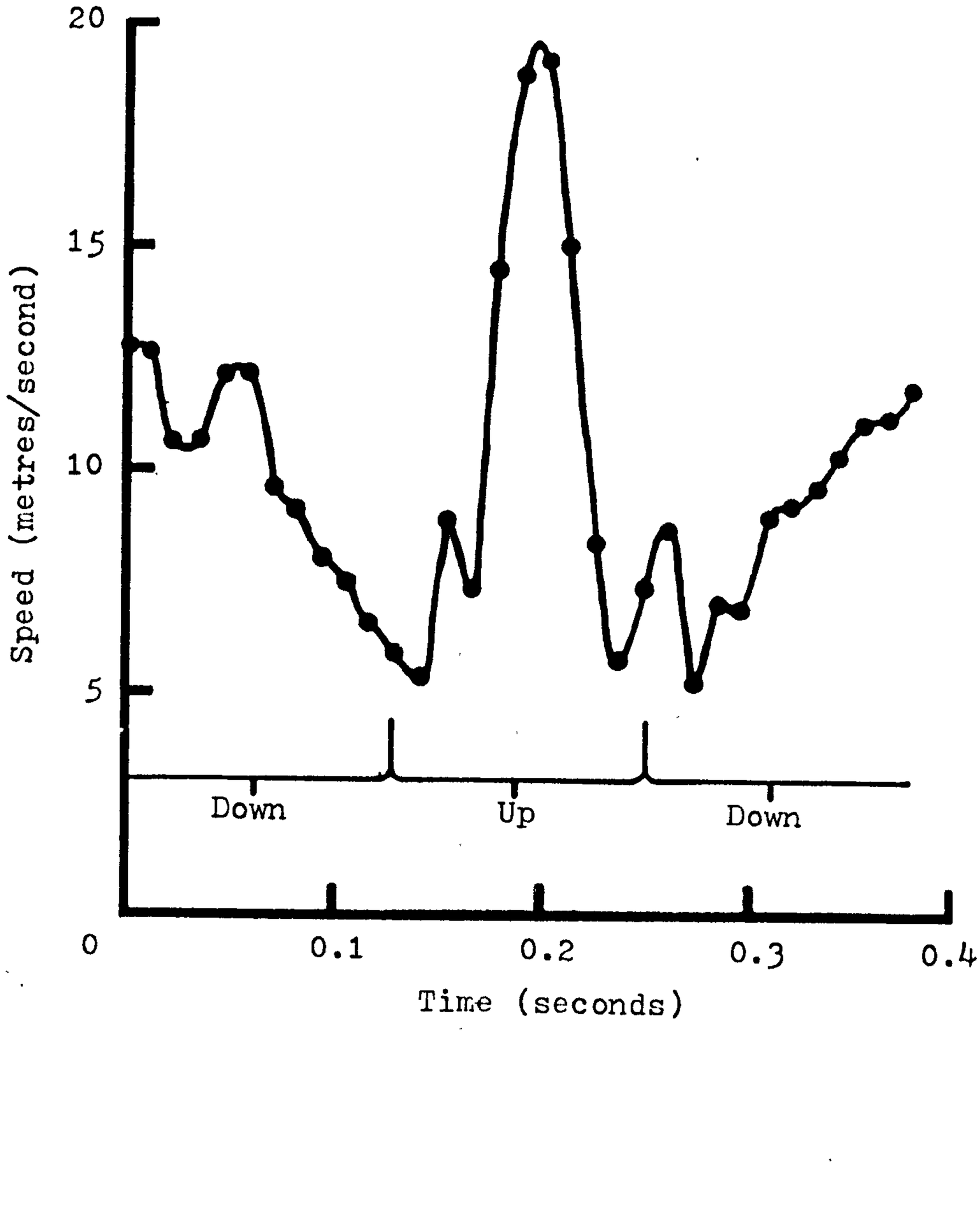
20
15
10
5
0
Speed (metres/second)
Down
Up
Down
0.1
0.2
0.3
0.4
Time (seconds)

assumed that the stroke plane is flat, then this analysis is suitable for investigating the distribution of speed during the downstroke. The speed distribution of the wing stroke shown in Figure 5.6B is given in Figure 5.6D .

5.2.2(vb) Side-on

A typical side-on wing trace is illustrated in Figure 5.7A; it gives the stroke plane angle of the wrist and the wing tip. The eye or the beak were usually used as the target, as they were not usually obscured by the wing movements. It must be assumed that they remain stationary relative to the body which may not necessarily be true.

Side-on frame by frame analysis is subject to parallax distortion caused by the wing tip and the wrist being closer to the camera than the body. As the bird flies past the camera, the relative positions on the image of the wing tip, wrist and body are altered for the same point in each cycle (Figure 5.7B). A typical effect of this form of distortion is illustrated in Figure 5.7C . The distortion is reduced as the distance of the subject from the camera increases, so reducing the ratio of A' to B' in Figure 5.7B . Long focal length lenses are therefore favoured for side-on filming. For side-on analysis only one stroke is suitable, that being the one when

Figure 5.7A

The side on wing tip trace of the common buzzard Buteo buteo (body length approximately 0.54m) in horizontal fast forward flight. Solid circles represent wing tip positions at each frame, and the film speed is 200fps. γ_t is the stroke plane angle of the wing tip and γ_w that of the wrist.

Figure 5.7A

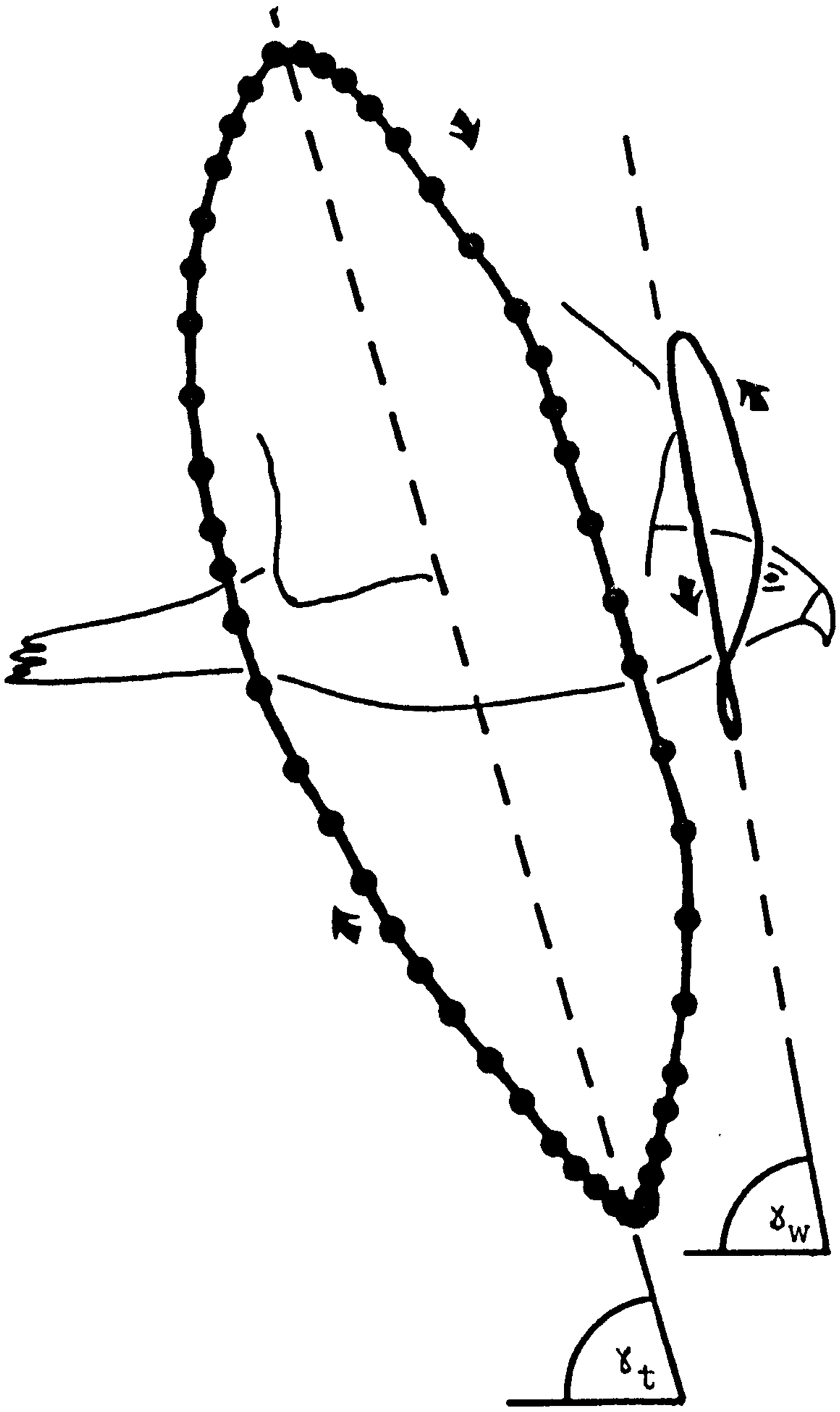

Figure 5.7B

The bird flying past a fixed camera has a distorted image due to parallax. The distance along the body A and B between the beak and a point opposite the wing tip remains constant. The images of A and B as the bird flies past the camera, A' and B' respectively are altered however, with A' being larger than B'. If there is no distortion A' and B' should be equal. The difference between A' and B' is reduced for one wing stroke the further the bird is from the camera, and the shorter the distance it travels during that stroke. Therefore, filming with lenses of long focal length is favoured.

Figure 5.7B

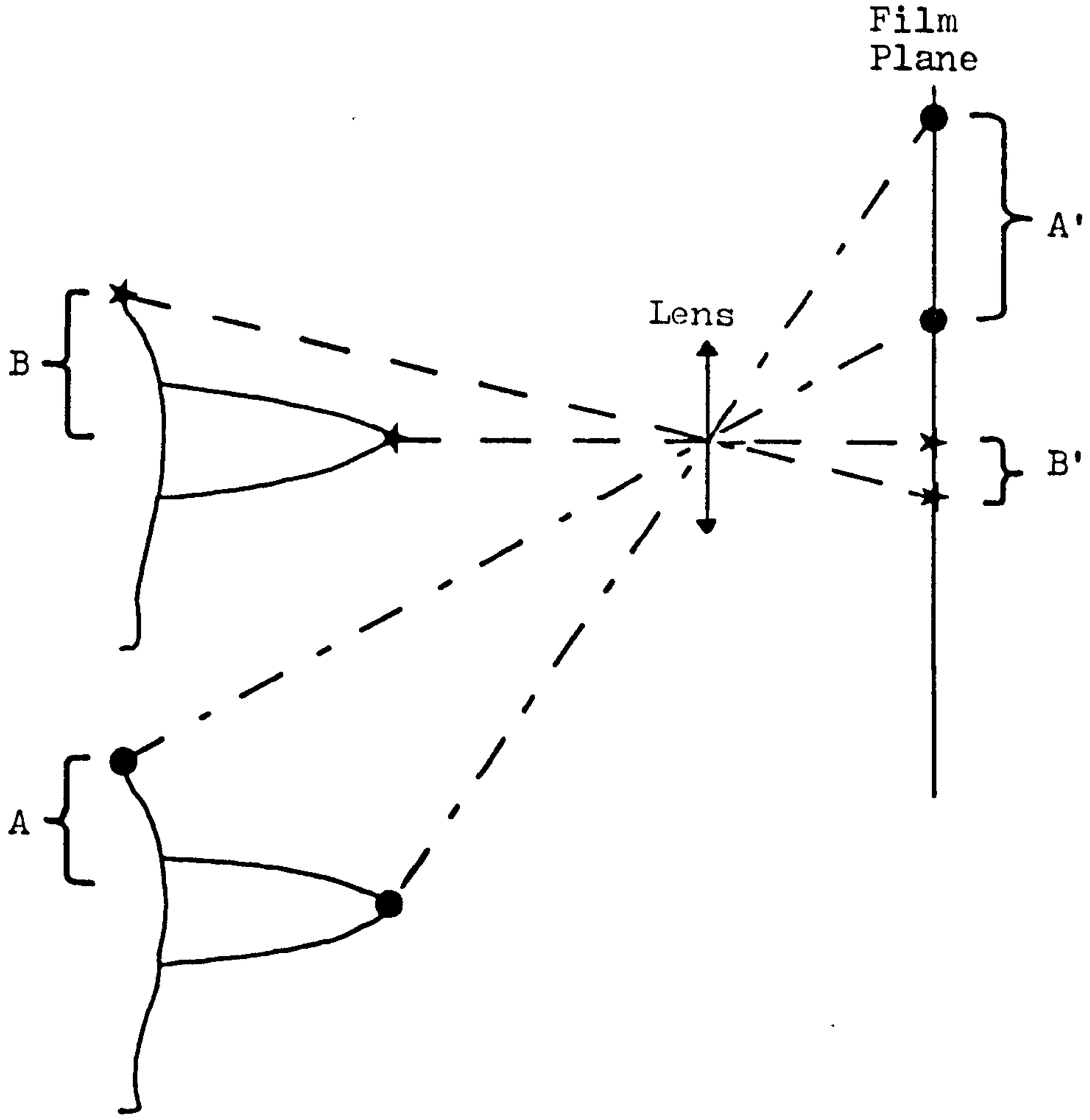

Figure 5.7C

The effect of parallax distortion on a wing tip trace of a grey headed albatross Diomedea chrysostoma. Note how each wing beat trace fails to form a closed ellipse as in 5.7A. Film speed 60fps.

Figure 5.7C

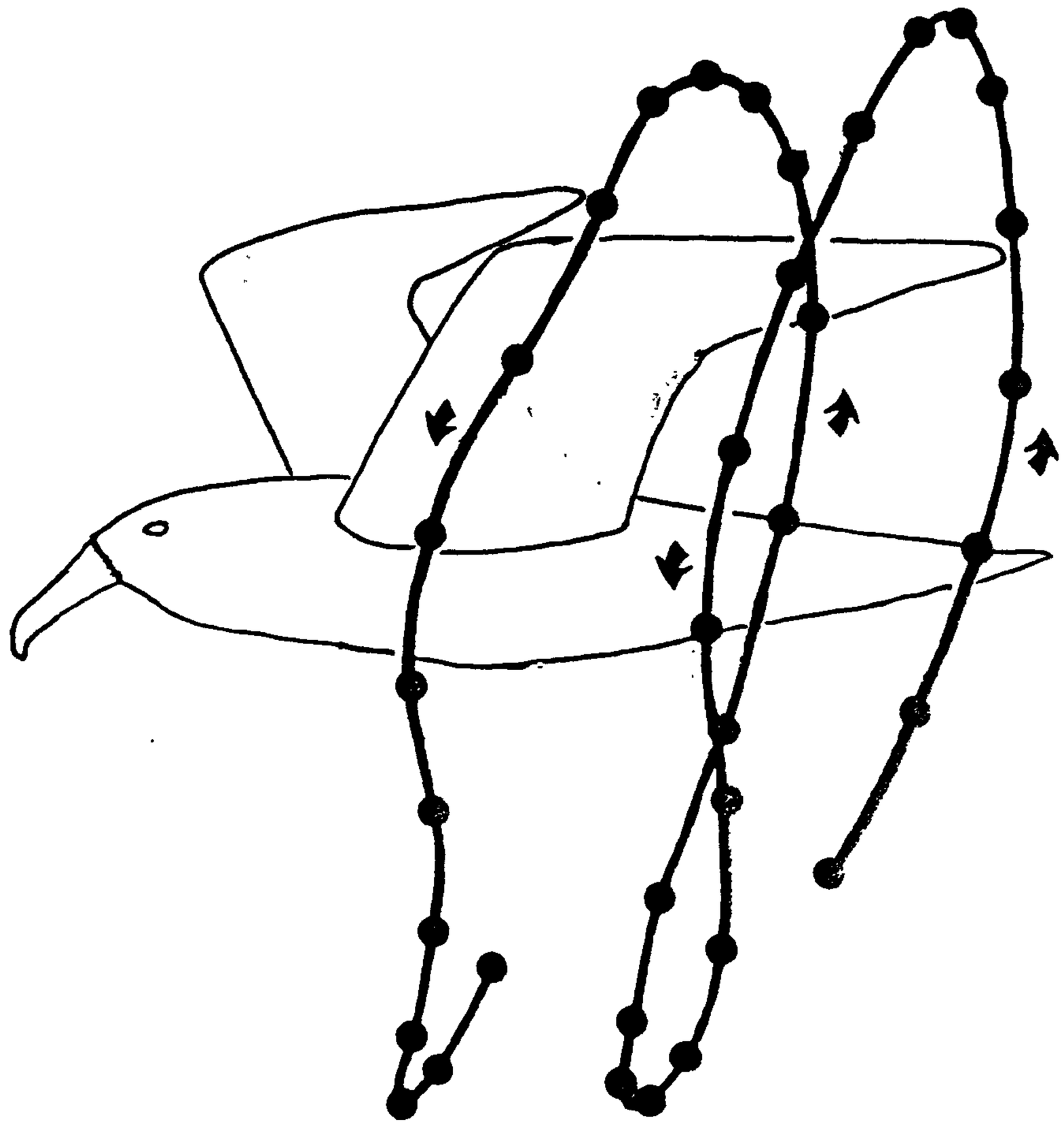

the bird is directly side-on to the camera as it flies past.

The stroke plane angle of the wing tip and the wrist can be estimated from a side-on wing trace as illstrated in Figure 5.7 A .

5.2.2(vi) Repeatability and errors of frame by frame analysis

When recording the movements of a wing point relative to a body target analysis errors may arise in each frame by mis-placing the cross-wires on either point. These errors are dependent upon the size of the image on the screen and on the quality of the image. Image quality can be reduced by soft focusing, inaccurate film exposure and poor contrast between the bird and the background.

The overall errors caused by these factors cannot be calculated as they are dependent upon judgement. An indication of their magnitude has been found by analysing the wing tip movements from the film of head-on views of three birds in cruise flight, one from each of the wing shape groups of Chapters 6 and 7, and repeating the analysis of the downstroke three times. The ranges of image size and quality are typical of the other birds analysed in this survey. The analysed co-ordinates and times were plotted as X against Y and net speed against time with the three traces of each downstroke being plotted together. The errors involvedwere assessed with respect to the

information extracted from each plot. For the traces of X against Y, their general pattern and the distance between the two opposite wings, (the apparent span) is of importance, whereas the distance between successive points is not. The maximum apparent span error was found by finding the point of greatest variation of a span measured between the two opposite wing tips and expressing the error as,

$$\frac{\text{greatest span - least span}}{\text{greatest span}} \times 100\% .$$

Table 5.3 shows this error to be within 3%.

The traces of net speed against time are very sensitive to errors in the distance between successive points. Such traces are used in Chapter 6 to find the peak downstroke speed, and also the overall distribution pattern of speed in the downstroke. The error in the peak speed in each casewas estimated by taking the highest and lowest peak speed of the three traces; the peak speed error is then given by

$$\frac{\text{Highest peak speed - lowest peak speed}}{\text{Highest peak speed}} \times 100\% .$$

Table 5.3 shows this to be within 5% and the traces are illustrated in Figure 5.8. An indication of the greatest error in the value of speed at any

Figure 5.8

Wing tip velocity (metres per second) with time (seconds) for one downstroke analysed three times for;

(A) Lappet faced vulture

Aegypus tracheliotus

(B) Lagger falcon

Falco jugger

(C) Common gull

Larus canus

In each case the frame positions are marked with closed circles for one of the three traces.

FIGURE 5.8

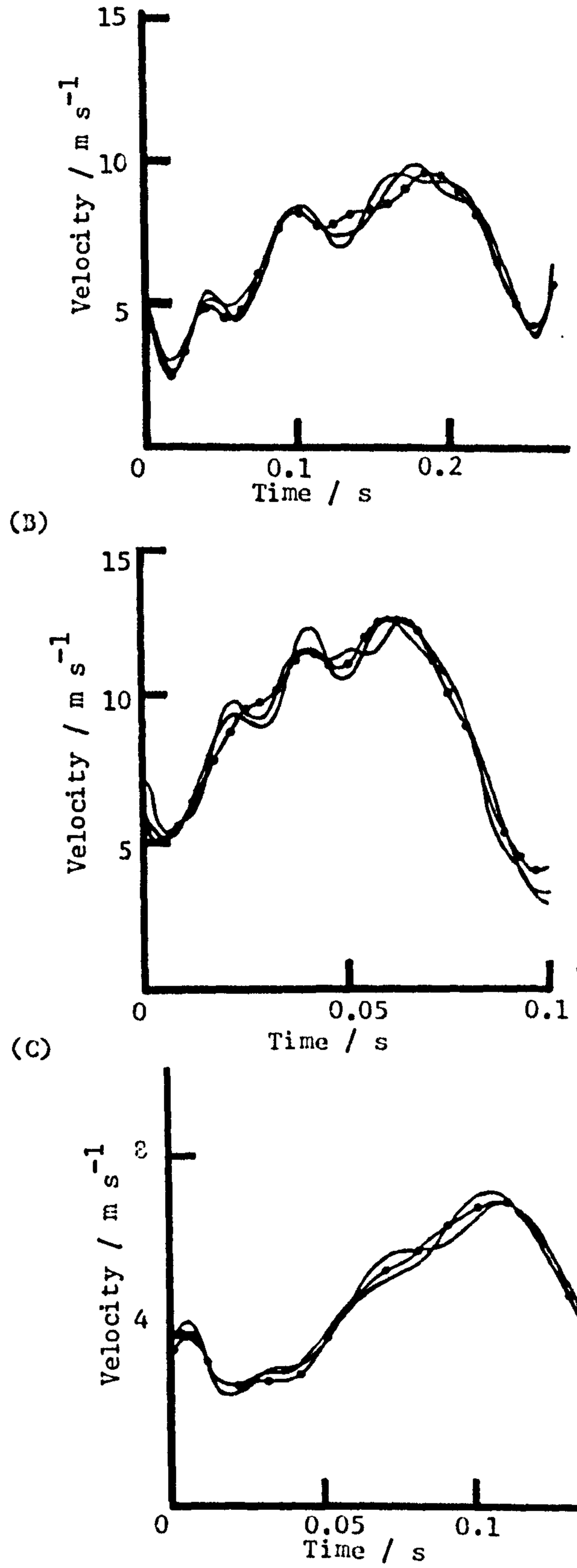
(A)
15
10
5
Velocity / m s-1
0
0.1
0.2
Time / s
(B)
15
10
5
Velocity / m s-1
0
0.05
0.1
Time / s
(C)
8
4
Velocity / m s-1
0
0.05
0.1
0.15
Time / s

time is given, being the maximum vertical separation between the traces. This error is within 15%.

The variation caused by measuring different wing strokes of the same bird is assessed by taking three different downstrokes of the same bird flying away from the camera. The number of downstrokes examined was limited to three, due to the difficulties of finding more than three in the correct orientation. The errors are assessed as above andgiven in Table 5.3. (Speed traces are illustrated in Figure 5.9). All the errors are higher than for the repeat analysis of the same stroke, due probably to slight changes in the orientation of each stroke. Apparent span is within 3% , peak speed within 8% and speed for a particular time within 40% . The latter is unrealistic, as a slight phase separation between the velocity distribution of the two strokes over a period of high acceleration (when the traces are nearly vertical) can lead to very large speed differences for a similar time. It should be noted that the velocity pattern is similar in all cases.

Figure 5.9

Wing tip velocity (metres per second) with time (seconds) for three downstrokes analysed once for;

(A) Lappet faced vulture

Aegypus tracheliotus

(B) Lagger falcon

Falco jugger

(C) Common gull

Larus canus

In each case the frame positions are marked with closed circles for one of the three traces.

FIGURE 5.9

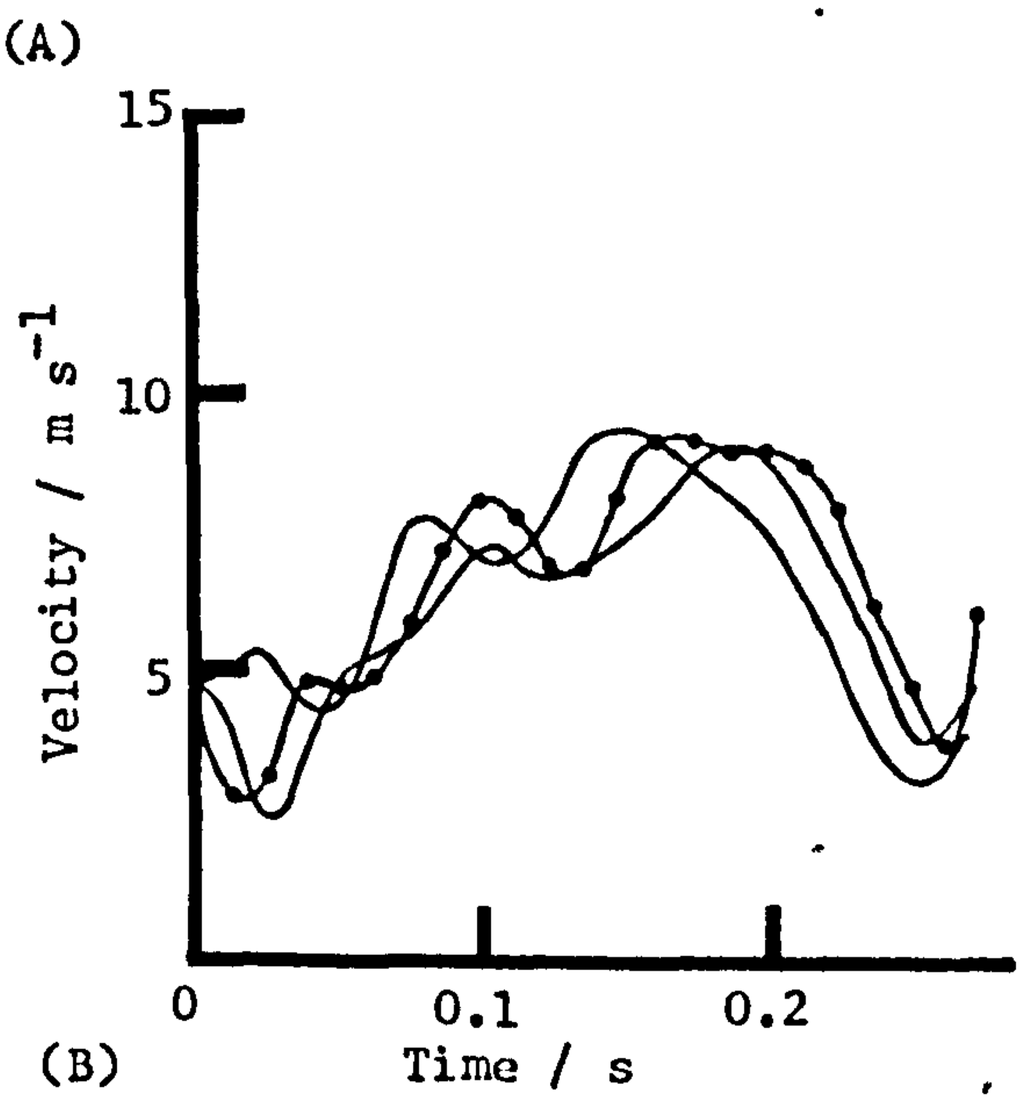
(A)
15
10
5
Velocity / m s-1
0
0.1
0.2
Time / s

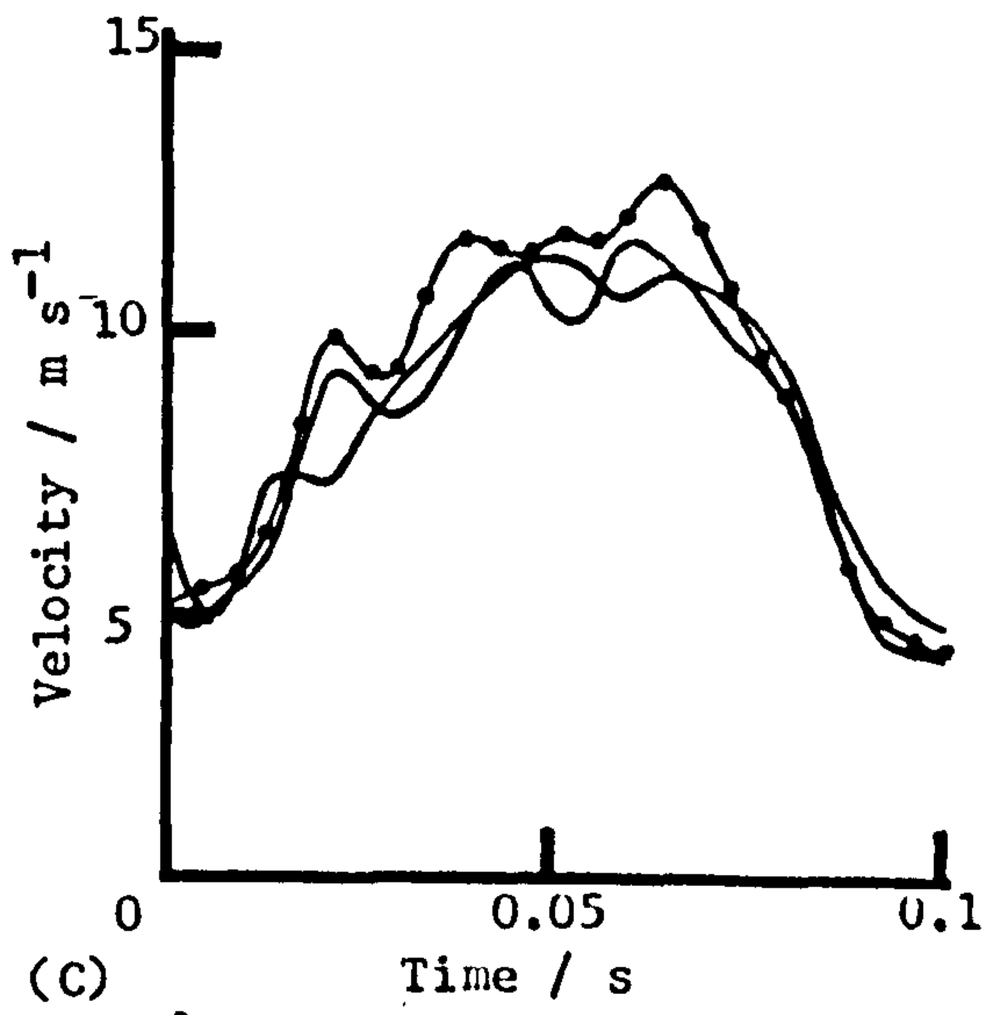
(B)
15
10
5
Velocity / m s-1
0
0.05
0.1
Time / s

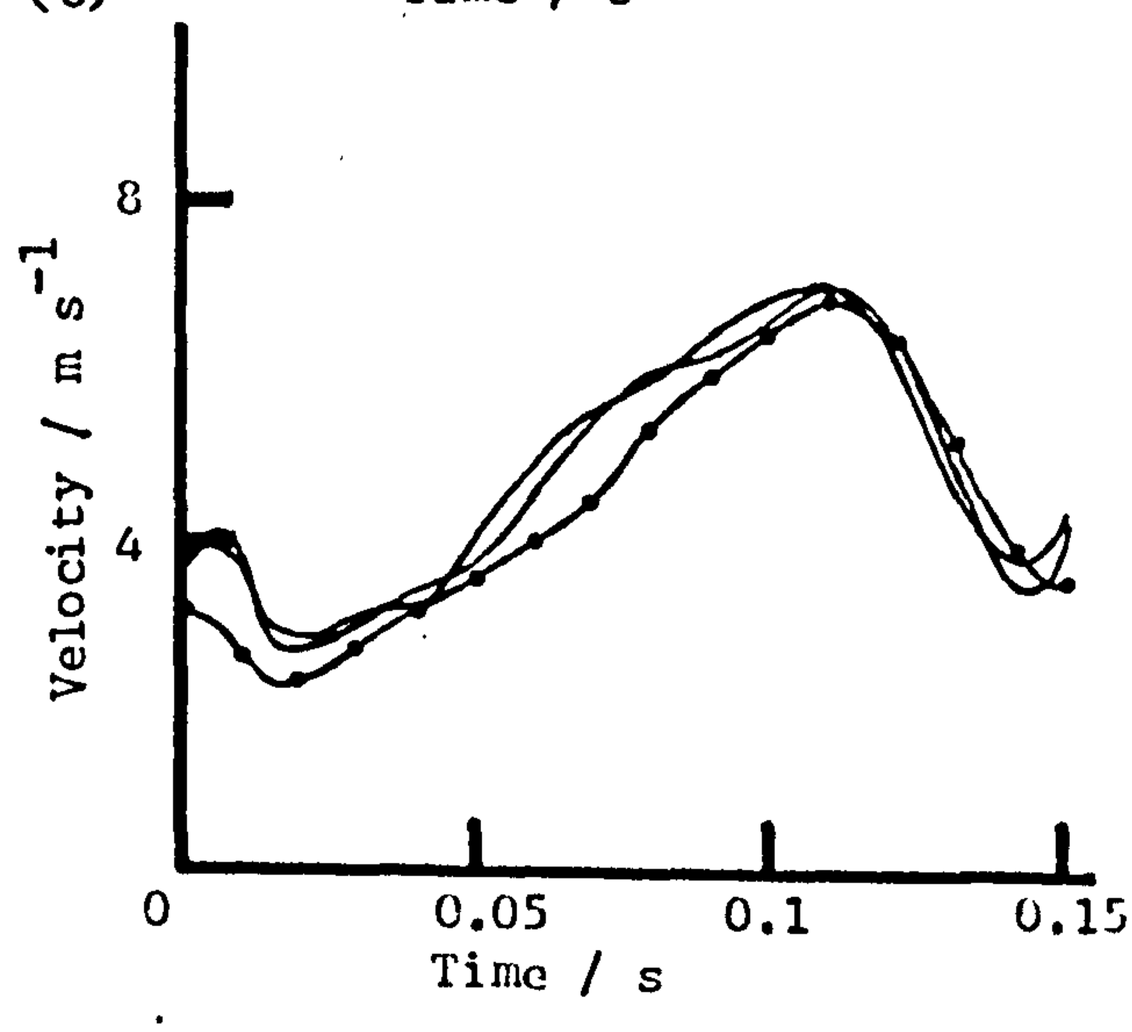
(C)
8
4
Velocity / m s-1
0
0.05
0.1
0.15
Time / s

Table 5.3

Errors in frame by frame analysis. (Details are given in the text.)

Species: English Scientific	Image wing span / Frame width %	X,Y 'Span' Error Greatest - Least / Greatest		Speed Error			
				1 Stroke times 3		3 Strokes times 1	
		1 stroke times 3 %	3 stokes times 1 %	Peak value %	Maximum value %	Peak value %	Maximum value %
Lappet Faced Vulture Aegypus tracheliotus	26	1.5	1.8	4	13	8	38
Common Gull Larus canus	32	2.5	2.9	4	8	4	32
Lagger falcon Falco jugger	41	2	2.8	2	12	8	26

5.2.3 Statistical Analysis

This study is designed to find relationships between bird morphology and wing beat kinematics. Generally in such studies linear regression is used, expressing the relationship of one variable in respect to another in terms of a linear function, given by the equation:

$$Y = \alpha + \beta X$$

where β is the 'slope' and α the intercept of the line with the Y axis. Relationships, both theoretically and empirically determined, between morphological and kinematic features have been found to obey a power law or scaling relation, which is often termed 'allometric' (e.g. Greenewalt, 1975, Weis-Fogh, 1977, Pennycuick, 1978, Rayner, 1979c) and described by the formula

$$Y = \alpha X^{\beta} .$$

Hence, in this study logarithmic transformations of both variables are applied so that

$$\log Y = \log \alpha + \beta \log X .$$

The significance of the regression is found by an analysis of variance and is indicated by the value of F. The confidence limits of α and β (at the 95% level) are determined by a Students' t test and the degree of correlation between the two variables is found by calulating the correlation coefficient r (see Sokal and Rohlf, 1981 for details of calculations).

Regression analysis does not necessarily calculate the line of 'best fit' between any two biological variables (Harvey and Mace, 1982). Regression analysis of Y on X produces a line which minimises the sum of squared distances of points from the line when those distances are perpendicular to the X axis. In the calculation of this line it is assumed that there is no error in the value of X. In this survey both variables, kinematic and morphological, are subject to a degree of 'error'. The kinematic data has a degree of error due to the measuring techniques. The morphology of each bird species is subject to interspecific variation. The dimensions of each species are taken as those of the bird of mean body mass of those individuals of the species compiled by Rayner's survey of bird morphology (Rayner, in prep.b). The bird which has been filmed for kinematic analysis does not necessarily have the same dimensions of this average of Rayner's data. Therefore the morphological data must be considered to have a degree of variation and so error.

There are a number of other techniques for fitting a line between two variables and which account for both variables having a degree of error, Of these, reduced major axis (RMA) is most suitable (Harvey and Mace, 1982, Rayner, personal communication). In RMA analysis a line is fitted between the data points by minimising the sum of the areas of the triangles bounded by this line and lines drawn from it to the data points which are parallel to the original axes. This line of best fit therefore

gives 'weight' to both variables and is considered most suitable for the analysis in this survey. RMA is the geometric mean of Y(X) and X(Y) regressions and so the difference between it and the Y(X) line becomes greater the lower the correlation coefficient. Error bounds for the slope of the RMA line are equal to those for natural regression (Rayner, personal communication).

For each investigation of the relationship between two variables a graph illustrates the data points and the RMA line. The following information is given in the table which accompanies each graph.

i) The titles of the variables

ii) The number of data points : N

iii) The correlation coefficient : r
The probability that $r \neq 1$ is indicated at three levels (N-2) 10% : *
5% : **
1% : ***

iv) The value of F (1, N-2 d.f.) : F

v) For the Y(X) and the RMA values of
a) the intercept of the line with the Y axis : α
b) the slope of the line : β
c) the minimum and maximum 95% confidence limits of α : $\alpha-$, $\alpha+$
β : $\beta-$, $\beta+$

In regression or RMA analysis, with a limited number of data points representing a far larger total number of

possible data, there is always a possibility of an unintentional bias of the collected data affecting the slope of the line. I have tried to collect data on a 'balanced' group of birds covering as wide a range of size (above 0.05kg) and wing shape as is possible within the bounds of my practical limits. However, it is realized that this sample is a very small proportion of all birds and so may well be subject to unintentional bias.

The variance of a kinematic feature may not be totally accounted for by that of one feature of morphology. Further variance may be explained by correlation with more than one morphological feature by using multiple regression analysis. This can be done by a direct extension of the log linear regression equation to

$$Y = \propto X_1^{\beta_1} X_2^{\beta_2} X_3^{\beta_3}$$

where the estimate of the dependent variable Y is a function of the 'independent' variables X_1, X_2 and X_3 (Sokal and Rohlf, 1982).Correlation coefficients r between the kinematic variable and each morphological variable and the overall correlation (termed the product moment correlation) with all three morphological variables can be calculated. The results of the multiple regression analysis are tabulated and in each case the kinematic feature is multiply regressed with body mass m, wing span b and wing area S. Quoted in each table are:

i) the title of the kinematic feature

ii) the number of records : N

iii) the product moment correlation with m, b and S : PMC

iv) the analysis of variance value of
F (3, N - 4 d.f.) : F

v) the correlation coefficients with
m, b and S : r; m, b, S

vi) the intercept with the Y axis : $\propto$

vii) the slopes of the lines with m, b, S :
β ; m, b, S

It should be emphasised that multiple regression is not directly comparable with the RMA of a bivariate sample, although it can be considered as a generalisation of linear or log-linear regression of several independent variables. The multivariate analysis of RMA is principle components analysis but this is not appropriate here as the intention is to test whether kinematic parameters are determined in any sense by morphology. The correlations are of importance in this respect and are the same in multiple regression and principle components analysis.

CHAPTER 6

WING BEAT KINEMATICS IN CRUISE FLIGHT

6.1 Introduction

This chapter is mainly concerned with birds which use 'continuous flapping flight'. Here, this term includes birds which flap continually and those which glide for short periods between flapping, as do many large soaring birds. It does not include birds which body glide between short periods of flapping in so-called 'bounding' or 'intermittant' flight, typical of small passeriformes. A study of the cruise flight of one bounding bird, the zebra finch Poephila guttata, is included for a comparison with continuous flapping flight. The term 'cruise flight' here is defined as the flight of a particular bird, in natural conditions, at the speed it selects for steady horizontal flight. This will generally be between the ranges of the minimum power speed V_{mp} and the maximum range speed V_{mr} of the particular bird.

The Reynolds number of the majority of birds in this study is between 10^5 and 10^6 in flapping flight, with only a few of the smaller species having a Reynolds number below 10^5. A variation in Reynolds number over this range is likely to have only a negligible effect on aerodynamic performance, the boundary layer of the wings probably being turbulent

in all cases. For this reason the Reynolds number is ignored in this analysis.

Greenewalt (1962, 1975) divided the birds of his survey into three groups based on the wing loading at a given body weight. The birds of this survey have also been divided into groups, but on a basis of wing shape. These groups are as follows:

i) Group A : Birds with 'rectangular' wings typical of land soarers, having blunt wing tips and well separated primary feathers. The group includes crows, eagles and storks.

ii) Group B : Birds with wings tapering from the base to the wing tip giving a 'triangular' shape. These are typically birds which fly continuously by powered flight such as pigeons, falcons and waterfowl.

iii) Group C : Birds with very long thin wings which only taper near the wing tip, typically marine soarers such as gulls and albatrosses.

The groupings can be roughly separated by aspect ratio, that of group A being approximately 6 to 8, that of Group B being 8 to 10, and that of Group C being above 10.

As with all such groupings there are some areas of overlap; for example, the white pelican Pelecanus onocrotalus has a Group A wing shape but an aspect ratio of 8.5 . It is also true that some birds have intermediate wing shapes, and can be classified in two groups. However, generally these groupings are distinct; they have been chosen because wing strokes are similar within a group, but differ between groups. The groups are also helpful in later analysis as a reminder of each bird's general wing shape and aspect ratio. Typical wing shapes of each group are illustrated in Figure 6.1A; Figure 6.1B gives symbols for each bird order which are used throughout this chapter and the next in all graphs. The group is indicated by the symbol being enclosed in either a square (Group A), a diamond (Group B) or a circle (Group C).

A number of terms are used to aid the description of wing strokes of these groups. These are defined as follows:

Proximal Wing : The part of the wing supported by the humerus and the radius and ulna, and stretching from the shoulder to the wrist. It supports the secondary flight feathers.

Distal Wing : The wing section supported by the manus and stretching from the wrist to the

Figure 6.1A Typical wing shapes of the three bird groups

Group A. Rectangular wings.
Aspect ratio approximately 6 to 8.

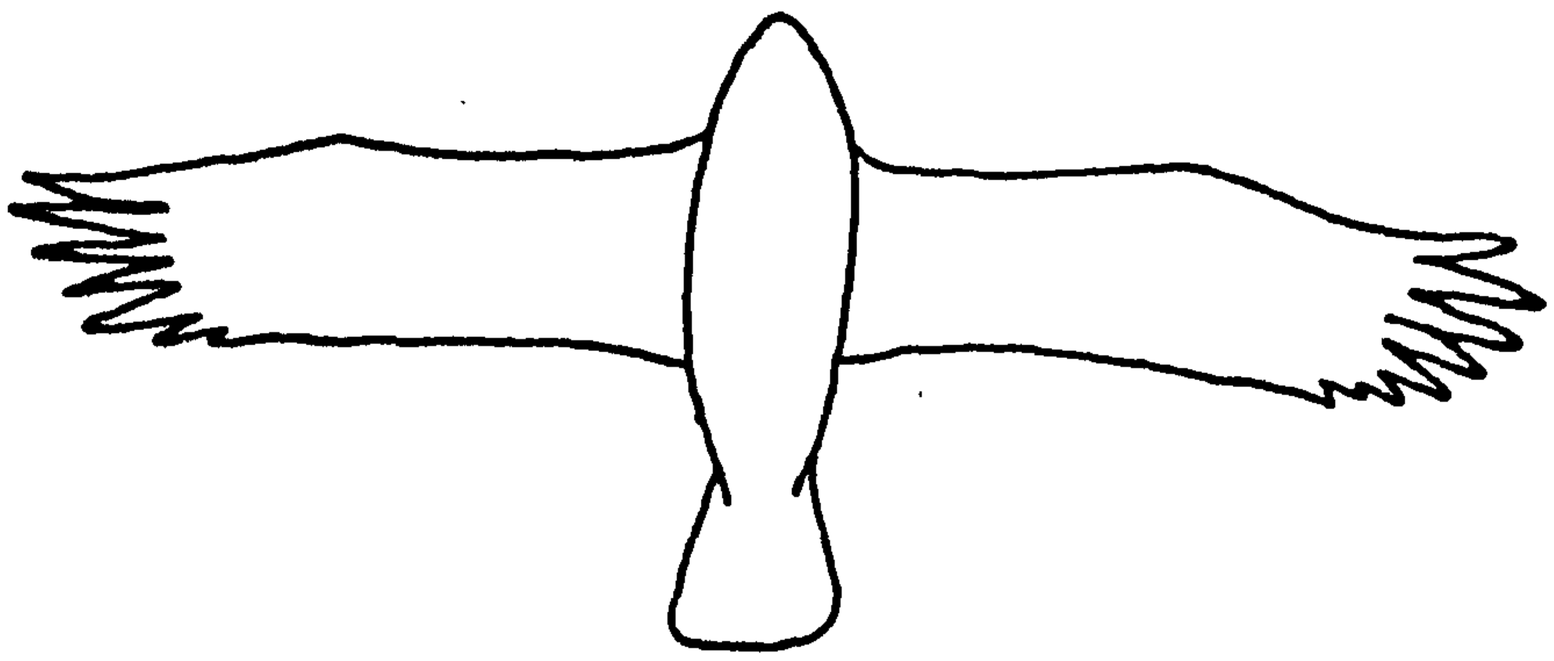

Group B. Tapering triangular wings.
Aspect ratio approximately 8 to 10.

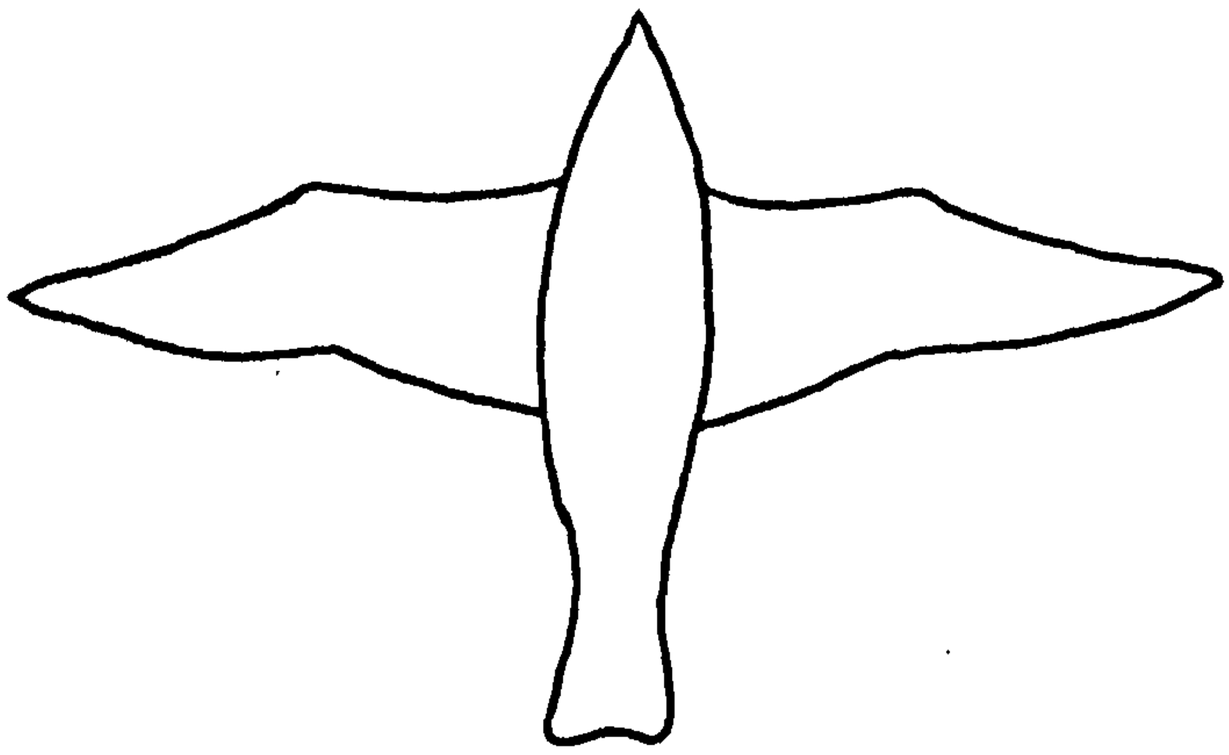

Group C. Long thin tapering wings.
Aspect ratio approximately above 10.

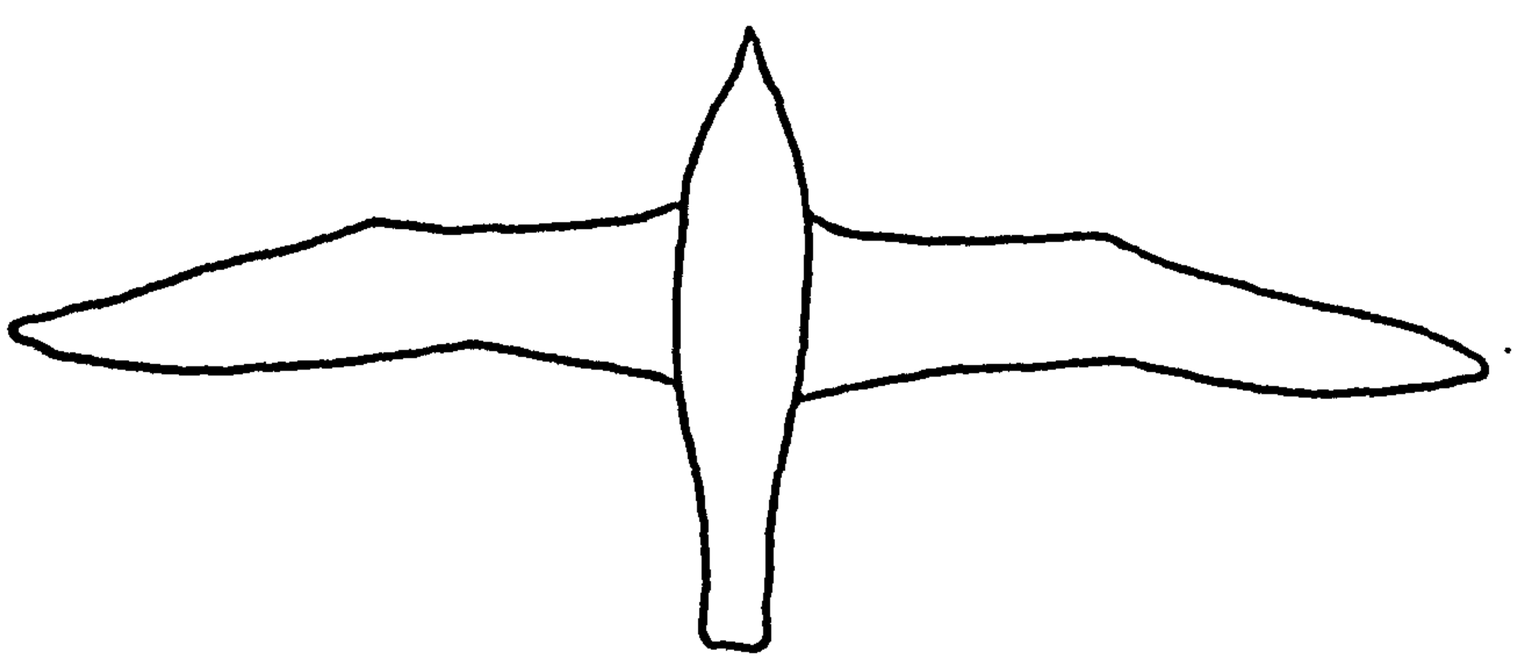

Figure 6.1b Plotting symbols for bird orders.

PROCELLARIIFORMES	+
PELECANIFORMES	×
CICONIIFORMES	□
ANSERIFORMES	◇
FALCONIFORMES	▷
GALLIFORMES	○
GRUIFORMES	◁
CHARADRIIFORMES	△
COLUMBIFORMES	▽
PSITTACIFORMES	●
STRIGIFORMES	✳
APODIFORMES	■
CORACIIFORMES	◆
PASSERIFORMES	▶

wing tip. It supports the primary feathers.

Supination : Twisting along the length of the wing so that the leading edge is raised relative to the trailing edge. It is caused by the radius and ulna moving over each other (Young, 1962; Figure 6.2A3).

Pronation : Twisting in the opposite sense to supination, so that the leading edge is depressed relative to the trailing edge (Figure 6.2A2).

Rotation : The humerus can rotate in the wing stroke causing displacement of the elbow. Hence, rotation is positive in the sense of supination and negative in the sense of pronation (Figure 6.2B).

In this chapter the wing strokes of birds of Groups A, B and C are described, together with the distribution of speed of the wing tip during the downstroke. The latter is recorded by frame by frame analysis of the wing tip of a particular bird, flying directly towards or away from the camera, for a complete downstroke (Chapter 5). The kinematic parameters of wing beat frequency f, amplitude $\mathcal{Q}$, downstroke ratio z, stroke plane angle γ and wing tip downstroke velocity V_{wt}, as defined in Chapter 5, are then related by allometry to the bird's morphology. This is followed by the testing of the prediction of wing beat frequency given by Pennycuick (1978).

Figure 6.2A

Wing Pronation and Supination.

A series of simplified diagrams showing:

1) A non-twisted wing.

2) A pronated wing where the leading edge is depressed relative to the trailing edge by twisting.

3) A supinated wing where the leading edge is raised relative to the trailing edge by twisting.

Figure 6.2B

Wing Rotation.

A series of simplified diagrams showing:

1) A non-rotated wing.

2) A negatively rotated wing where the leading edge is depressed relative to the trailing edge.

3) A positively rotated wing where the leading edge is raised relative to the trailing edge.

Figure 6.2

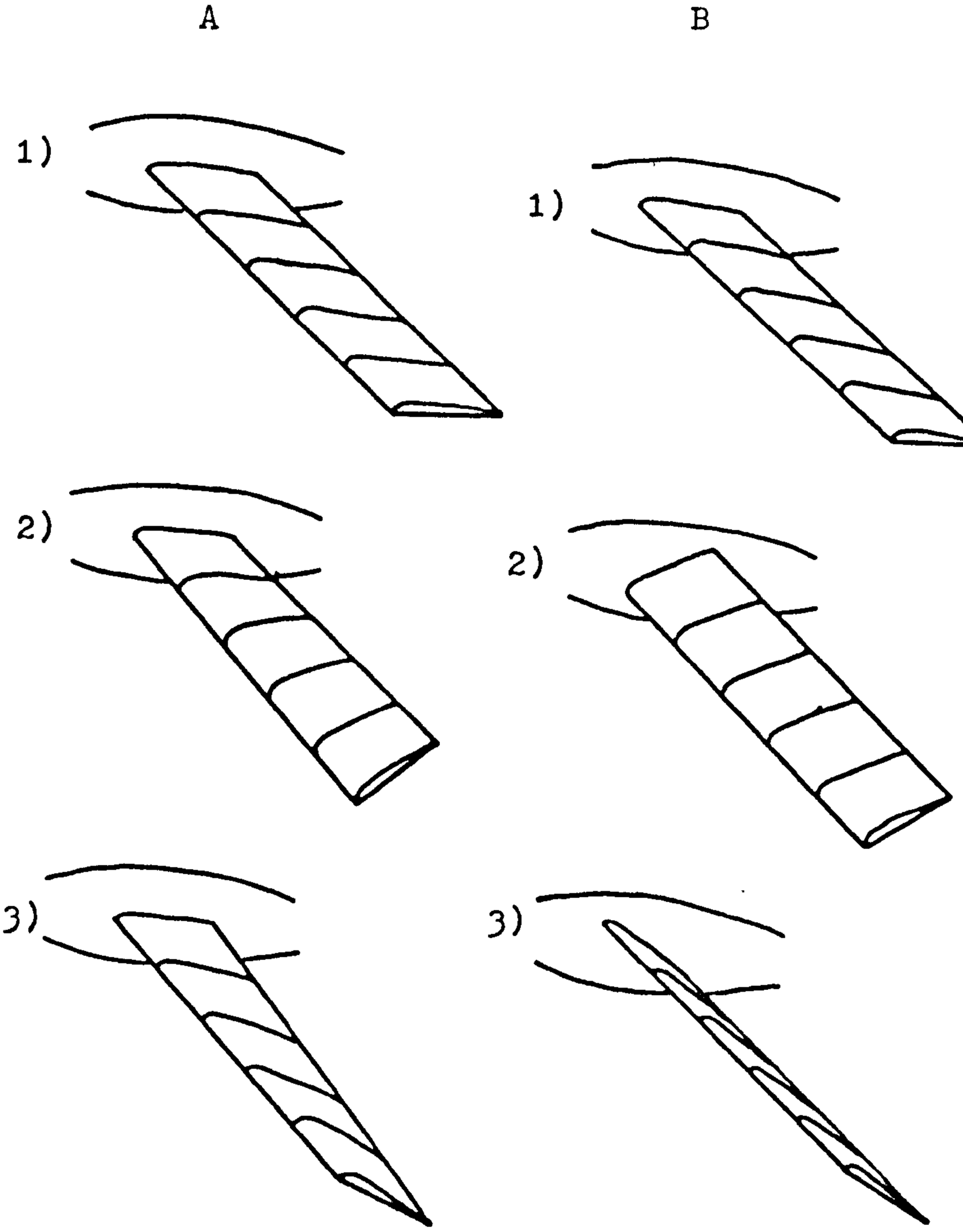

6.2 Descriptions of wing strokes and distribution of speed in the downstroke

6.2.1 Group A

6.2.1(i) Birds larger than 1kg

The downstroke begins with the proximal wing fully extended but the wrist still partially flexed. The wing is held at a high positive elevation (Table 6.1) and the primary feathers are not well separated. The wrist is moved downwards and is simultaneously extended resulting in the wing tip moving upwards and outwards (Figure 6.3A). At the highest position of the wing tip primary feather tip bending occurs and the wing is pronated. Wrist extension continues for the first third of the downstroke period. This extension causes the difference in the apparent stroke planes of the wrist and the wing tip, the latter initially being far shallower (Figure 6.3A). An explanation for the spreading of the distal wing during the downstroke is given in Section 6.4 . For the next third of the downstroke period the wrist and the wing tip follow approximately the same stroke plane. The primary feathers are now well spread. The humerus then reaches its maximum negative elevation, which is considerably less than the positive elevation (Table 6.1).

The upstroke begins with the proximal wing being sharply rotated in the positive sense and the elbow is

Figure 6.3A

A series of illustrations of the Ruppell's griffon vulture Gyps ruppellii, which is a typical Group A bird, larger than 1kg, in cruise flight. Wing span 2.41m. Film speed 84fps.

a) Tail on and side on drawings from film of stages of the wing stroke at four frame intervals. Each side on illustration is approximately at the same position in the wing stroke as the opposite tail on view. Side on and tail on views are not to scale.

Figure 6.3A (a) Ruppell's Griffon Vulture

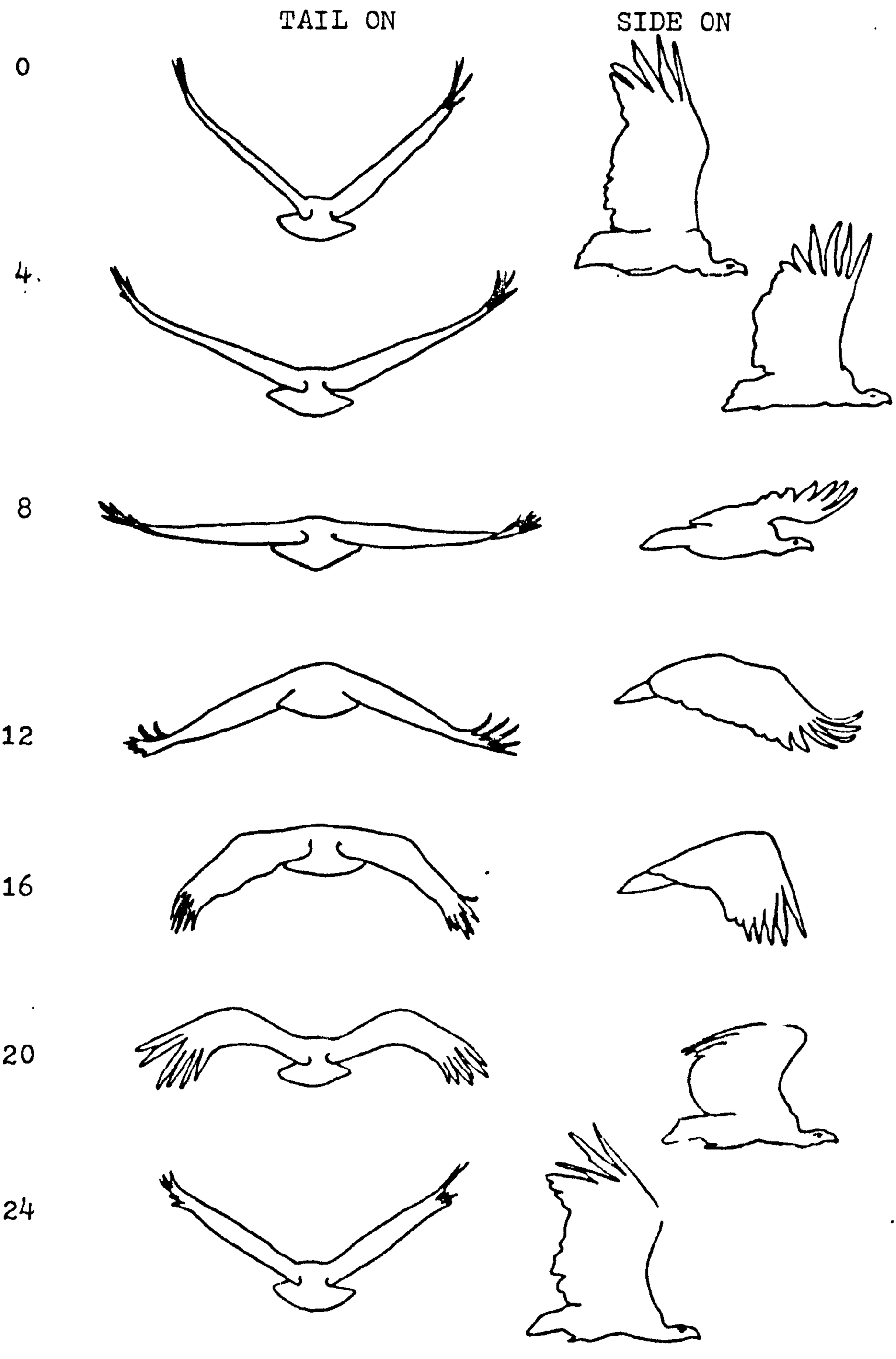

Figure 6.3A

b) Wing tip traces for tail on and side on views of a complete wing stroke. Each solid circle on the trace represents the position of the wing tip at each frame. The trace of the wrist is also shown. The direction of movement of the wing tips and the wrist is shown by arrows. The two views are not to scale.

Figure 6.3A

(b) Ruppell's Griffon Vulture

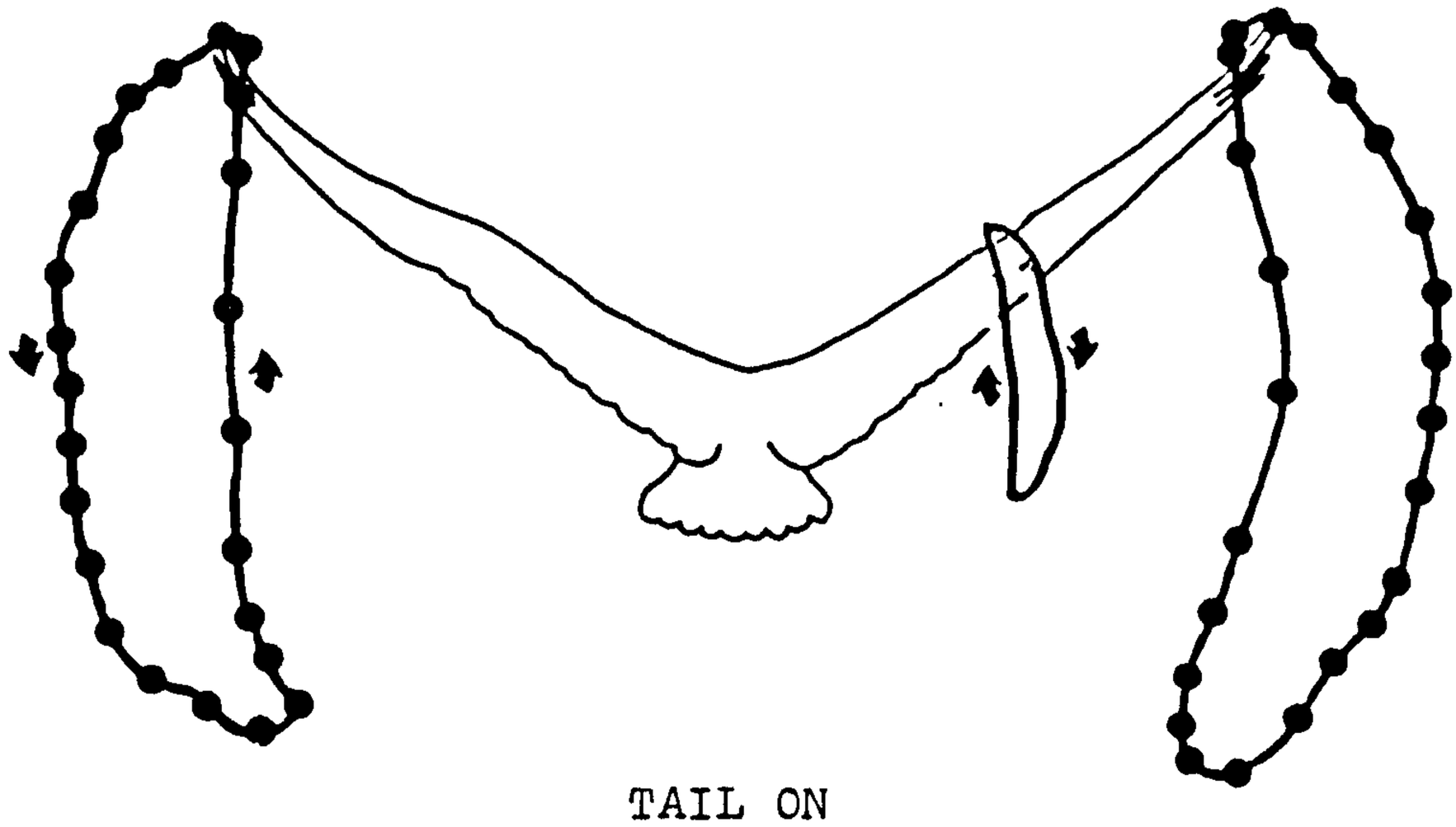

TAIL ON

SIDE ON

Figure 6.3A

c) Graph of the vertical position of the wing tip and the wrist (broad and narrow lines respectively) against time. The vertical X coordinates are relative to a fixed body target. Each frame is marked by a solid circle. It can be seen that the vertical movement of the wrist always proceeds that of the wing tip.

Figure 6.3A (c)

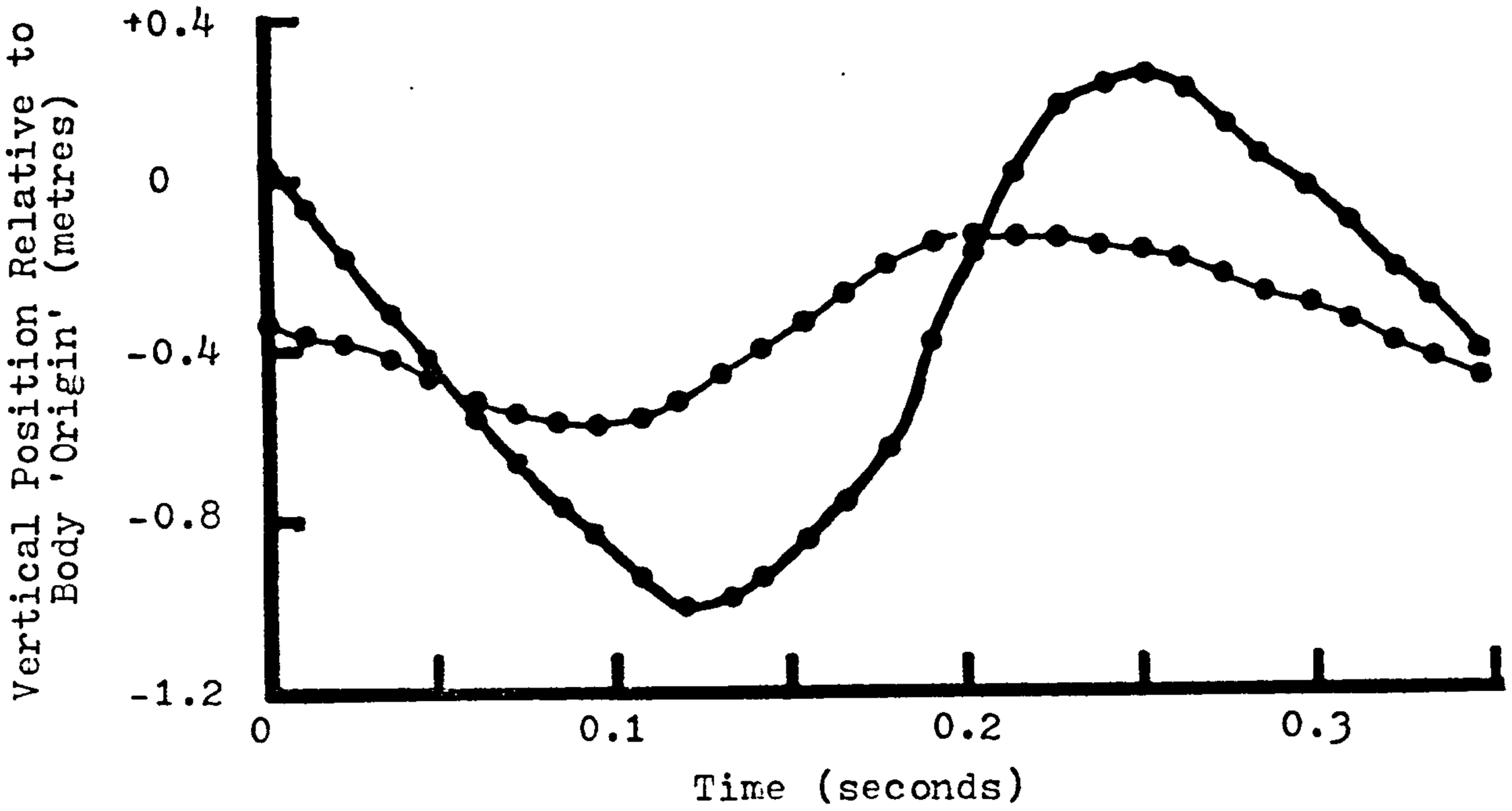
Vertical Position Relative to Body 'Origin' (metres)
+0.4
0
-0.4
-0.8
-1.2
0
0.1
0.2
0.3
Time (seconds)

flexed and depressed, and so the wrist is raised and moved forwards. The span of the proximal wing is thus reduced, and the wrist is raised in a path anterior to that of the downstroke. As the wrist begins to move upwards it is flexed, and this action combined with proximal wing positive rotation and supination results in the primary feathers continuing to move downwards, but at a steeper stroke plane angle than before (Figure 6.3A). At this stage the primary feathers are still bent, and bending ends only when the wing tip reaches its lowest position and begins to move upwards. This process at the end of the downstroke causes the delay between the start of the upstroke for the wrist and that for the wing tip (Figure 6.3A). The considerable wing flexing causes the wing tip to be swept posteriorly.

The wing tip moves upwards, posteriorly to its down-stroke path during the initial stages of its upstroke (Figure 6.3A). This is due to a combination of the raising of the wrist and the gradual negative rotation of the proximal wing from its original position of extreme positive pitch. Flexion of the wrist and elbow result in the overall wing span in the mid-upstroke being considerably reduced (Table 6.1). The wrist then reaches its greatest positive elevation, and at this point the proximal wing is rotated negatively and the wrist begins to extend from its fully flexed position. This combination of actions causes a very rapid upward

flick of the wing tip bringing it into position for the next downstroke.

Group A birds appear to show large vertical body movements through the wing stroke, with the body moving upwards in the latter stages of the downstroke and down during the upstroke. As the camera was panning in most of the sequences, and because there was no fixed reference point on the ground, these movements cannot be measured and confirmed here.

The downstroke speed distribution of Group A birds (Figure 6.4) generally show a steady increase in speed (with superimposed fluctuations sometimes giving a humped effect) until the peak velocity is achieved, approximately 60% to 70% of the way through the downstroke period. Generally there is a distinct velocity 'hump' soon after the beginning of the downstroke. This is probably caused by the high degree of wrist extension exhibited by this group during this period, and it is discussed in detail in Section 6.4 . The deceleration from peak speed is very rapid. It should be noted that, because of the high degree of wrist flexion and extension exhibited by this group, the wing tip always has some speed even at the beginning and end of the downstroke.

6.2.1(ii) Group A birds weighing less than 1kg

The Corvidae (Passeriformes) have similarly shaped wings to those mentioned above, but have smaller body

Figure 6.3B

A series of illustrations of the rook Corvus frugilegus, which is a typical Group A bird, smaller than 1kg, in cruise flight. Wing span 0.9m. Film speed 100fps.

a) Head on and side on drawings from film of the stages of the wing stroke at four frame intervals. The other details are as in Figure 6.3A(a). Side on and head on views are not to scale.

Figure 6.3B

(a) Rook

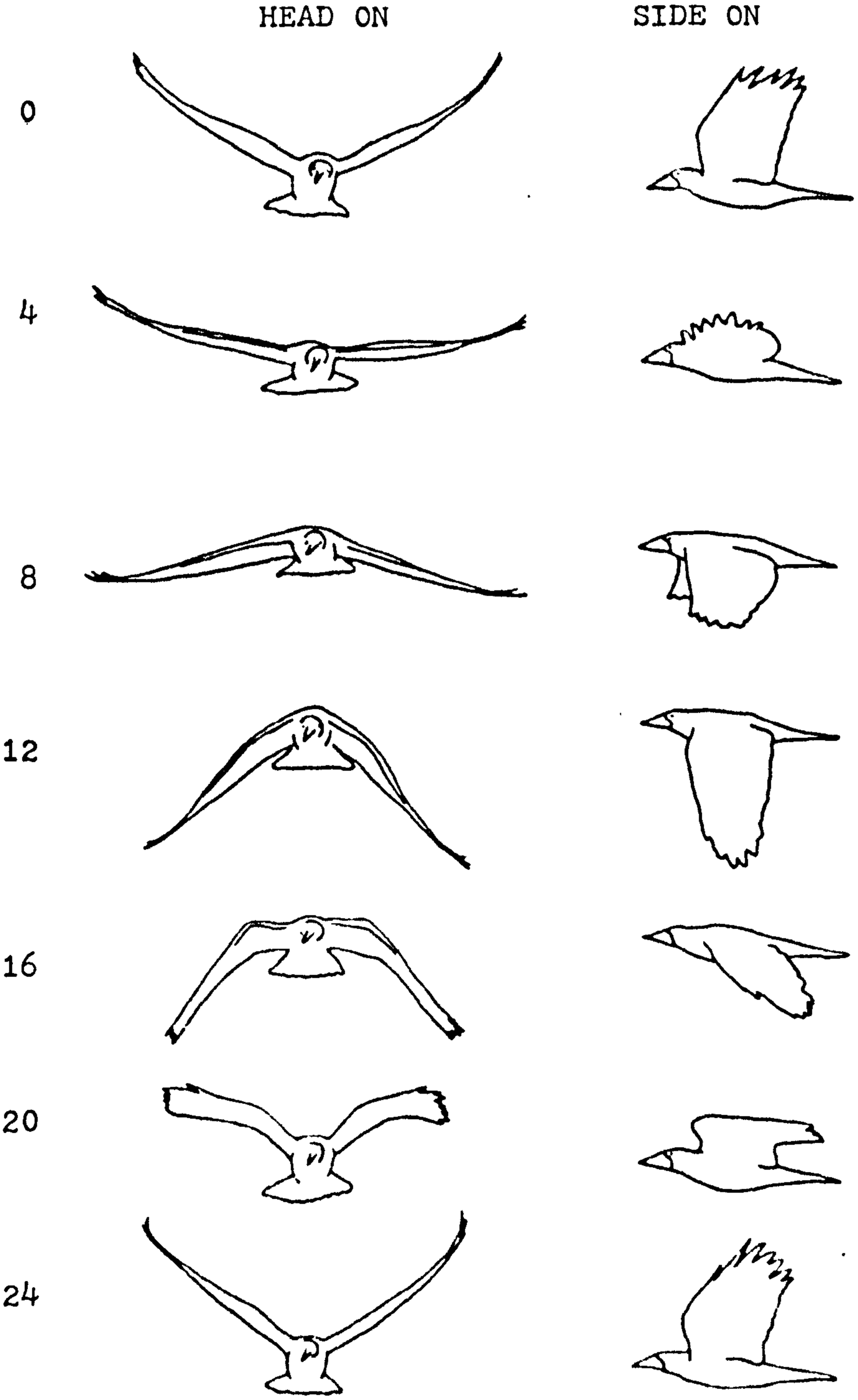

Figure 6.3B

b) Wing tip traces for head on and side on views of a complete wing stroke. Details as in Figure 6.3A(b). The two views are not to scale.

Figure 6.3B (b) Rook

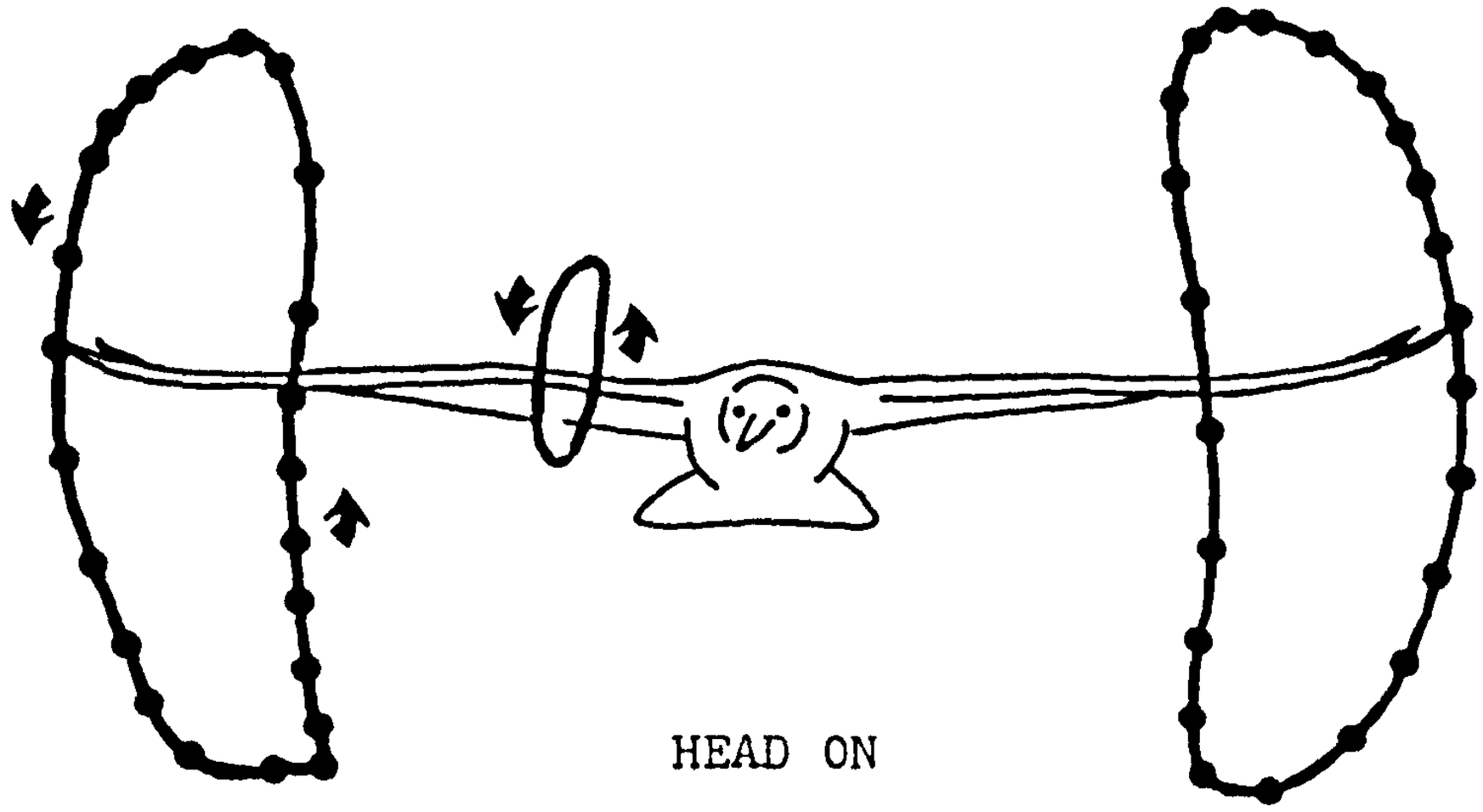

HEAD ON

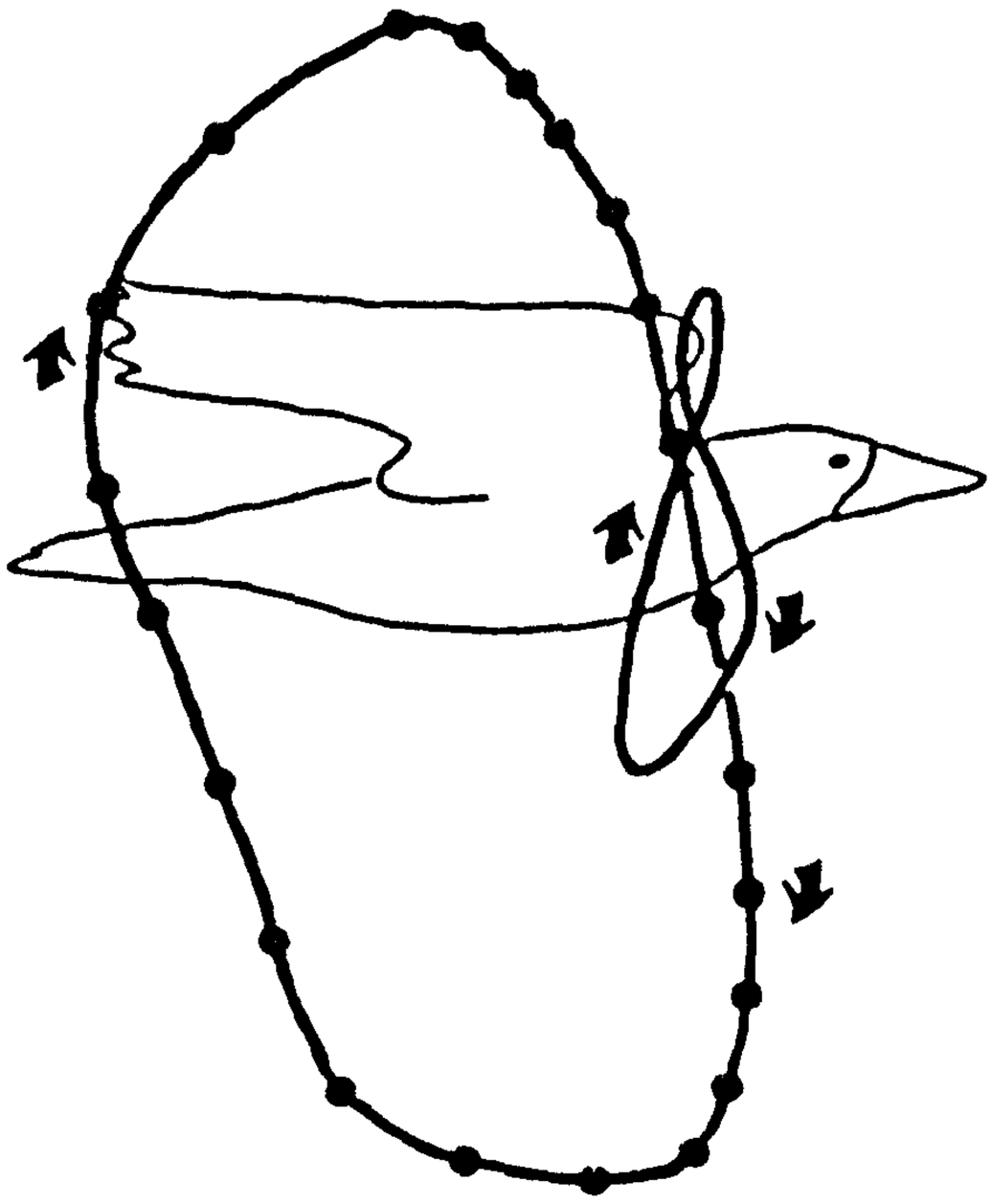

SIDE ON

Figure 6.3B

c) Graph of the vertical position of the wing tip and wrist (broad and narrow lines respectively) against time. X axis coordinates are relative to the fixed body target. Other details as in 6.3A(c).

Figure 6.3B (c)

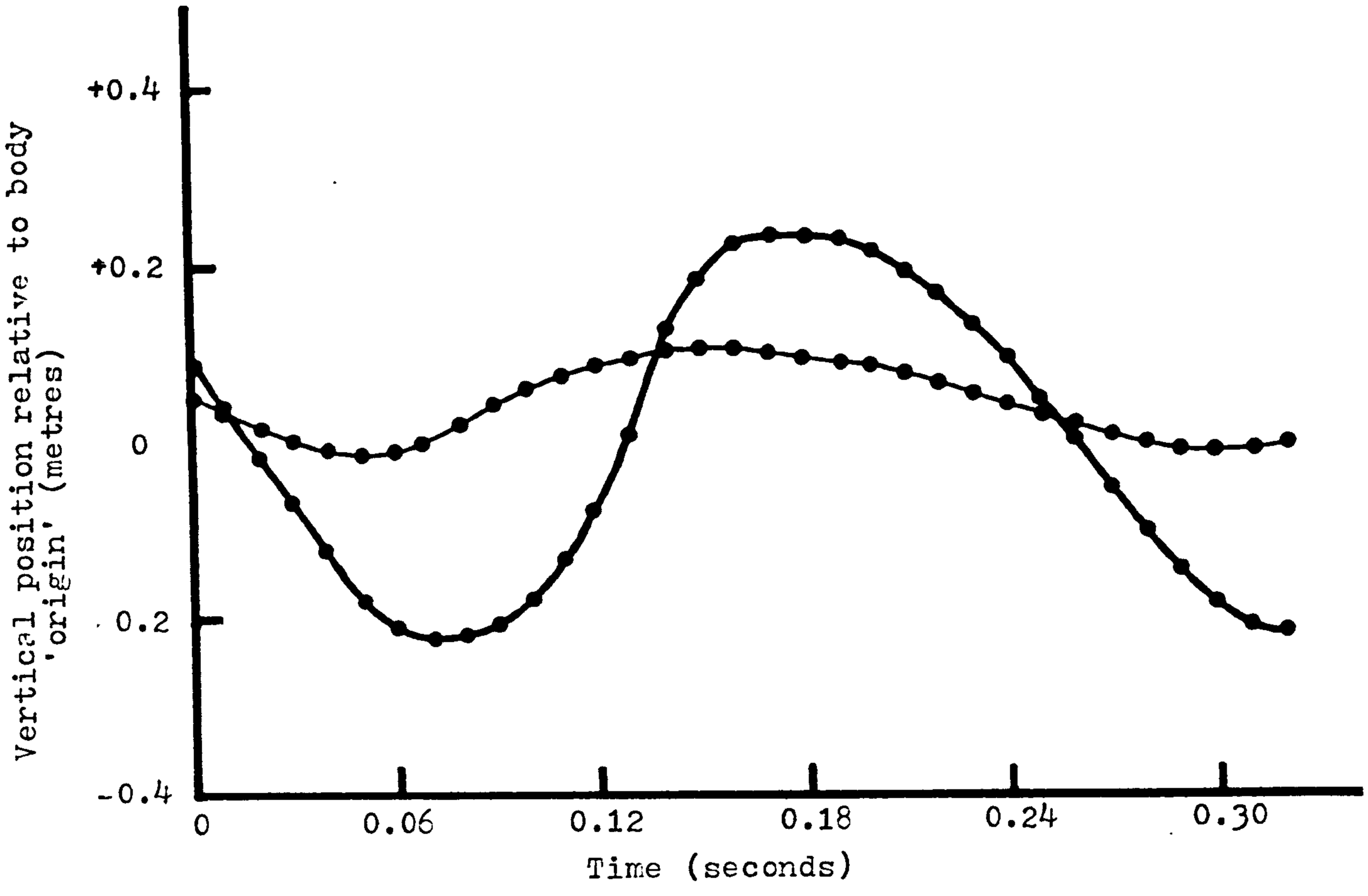
+0.4
+0.2
0
-0.2
-0.4
Vertical position relative to body 'origin' (metres)
0
0.06
0.12
0.18
0.24
0.30
Time (seconds)

Explaination for Tables 6.1, 6.2 and 6.3.

Species: English and scientific names

Average morphology:

m: Body mass

b: Wing span

S: Wing area

Stroke periods:

n: Number of recordings

f: Wing beat frequency and S.D.

ƨ: Downstroke ratio and S.D.

Stroke angles:

n : Number of recordings

Φ_u : Positive elevation and range

Φ_d : Negative elevation and range

Φ : Amplitude

γ : Stroke plane angle estimate

Peak V_{m_t} : Peak downstroke wing tip velocity

$\frac{b_d - b_u}{b_d}$: $\frac{\text{Downstroke span - upstroke span}}{\text{Downstroke span}}$ (X 100)

TABLE 6.1 Wing Beat Kinematics of Group A Birds.

Species	Average Morphology			Stroke Periods					Stroke Angles (degrees)							Peak V_{mt} m s^{-1}	$\frac{b_d - b_u}{b_d}$ %
					f(Hz)		z			θ_u		θ_d		θ	γ		
	m(kg)	b(m)	$S(m^2)$	n	mean	SD	mean	SD	n	mean	R±	mean	R±				
WHITE PELICAN *Pelecanus onocrotalus*	8.5	2.92	0.997	22	2.76	0.11	0.57	0.02	7	35	2	22	3	57	70	-	28
GREY HERON *Ardea cinerea*	1.35	1.61	0.343	24	2.46	0.35	0.56	0.04	-	-	-	-	-	-	-	-	-
GREAT EGRET *Egretta garzetta*	1.18	1.45	0.283	11	3.40	0.17	0.54	0.02	-	-	-	-	-	-	-	-	-
MARABOU STORK *Leptoptilus crumeniferus*	7.1	2.62	0.935	20	2.63	0.16	0.63	0.02	4	44	4	22	5	66	-	9.5	20
ANDEAN CONDOR *Vultur gryphus*	8.4	2.78	0.97	6	2.30	0.10	0.59	0.02	2	34	2	24	2	58	-	-	11
SECRETARY BIRD *Sagittarius serpentarius*	4.15	2.0	0.627	29	3.19	0.25	0.65	0.03	4	48	4	32	3	80	-	9.5	20
BLACK KITE *Milvus migrans*	0.964	1.2	0.233	48	3.70	0.23	0.51	0.04	7	32	3	24	4	56	80	7.5	21
HOODED VULTURE *Neophron monachus*	2.0	1.71	0.436	9	3.14	0.30	0.56	0.04	3	44	4	27	3	71	-	8.5	24

TABLE 6.1 continued.

	m(kg)	b(m)	S(m^2)	f(Hz) n	f(Hz) mean	f(Hz) SD	z mean	z SD	α_u° n	α_u° mean	α_u° R±	α_d° mean	α_d° R±	α°	γ°	V_{mt} m s^{-1}	$\frac{b_d - b_u}{b_d}$ %
WHITE BACKED VULTURE *Pseudogyps africanus*	5.38	2.18	0.69	33	3.24	0.16	0.60	0.03	8	43	2	18	4	61	70	11.5	27
RUPPELL'S GRIFFON VULTURE *Gyps ruppellii*	7.57	2.42	0.83	25	3.23	0.23	0.58	0.04	8	41	3	22	3	63	70	10	26
LAPPET FACED VULTURE *Aegypius tracheliotus*	6.6	2.64	1.03	28	2.53	0.07	0.59	0.02	8	38	2	26	3	63	-	8.5	22
WHITE HEADED VULTURE *Trigonoceps occipitalis*	3.7	2.24	0.667	39	2.70	0.09	0.55	0.03	4	41	4	21	3	62	70	9	32
BATELEUR *Terathopius ecuadatus*	2.10	1.54	0.358	21	5.0	0.32	0.50	0.01	-	-	-	-	-	-	-	-	-
COMMON BUZZARD *Buteo buteo*	0.80	1.25	0.221	21	3.91	0.10	0.50	0.03	-	-	-	-	-	-	80	-	-
STEPPE EAGLE *Aquila rapax*	2.0	1.78	0.447	14	3.34	0.07	0.50	0.01	5	31	4	30	4	61	80	-	20
OSPREY *Pandion haliaetus*	1.11	1.57	0.281	48	3.10	0.21	0.50	0.04	4	38	4	15	3	53	80	-	26
EAGLE OWL *Bubo bubo* (BBC film)	2.0	1.34	0.34	20	2.96	0.25	0.56	0.04	-	-	-	-	-	-	-	-	-
ROOK *Corvus frugilegus*	0.47	0.972	0.139	35	4.29	0.37	0.30	0.03	3	36	3	23	2	59	80	6	33

Figure 6.4

Wing tip downstroke speed distributions (velocity m s^{-1} with time s) for four Group A birds:

(A) Ruppell's griffon vulture

Gyps ruppellii

(B) Hooded vulture

Neophron monachus

(C) White backed vulture

Pseudogyps africanus

(D) Black kite

Milvus migrans

Figure 6.4

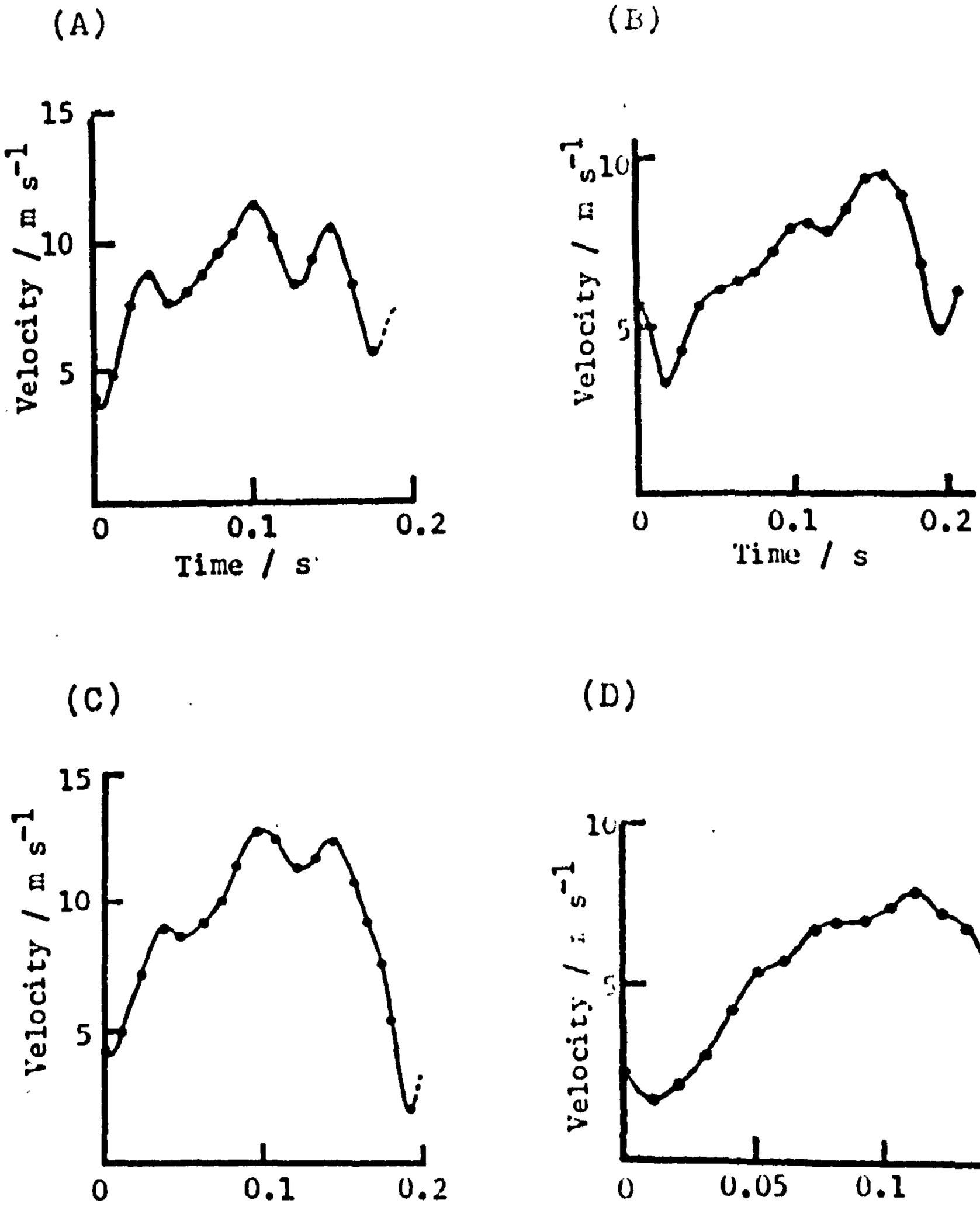
(A)
15
10
5
Velocity / m s-1
0
0.1
0.2
Time / s
(B)
10
5
Velocity / m s-1
0
0.1
0.2
Time / s
(C)
15
10
5
Velocity / m s-1
0
0.1
0.2
Time / s
(D)
10
Velocity / m s-1
0
0.05
0.1
0.15
Time / s

masses and a few differences in their wing strokes. The downstroke is the same as above, the differences only arising when the wrist begins the upstroke. Here, it is moved posteriorly and this, combined with wrist flexion, causes the wing tip to have a rounded posterior path unlike that of (i). The upstroke flick arises in the same manner, the only difference being that, as the proximal wing is swept backwards, the wing tip during the flick is more posterior.(Figure 6.3B)

6.2.2 Group C

At the beginning of the downstroke the positive elevation is relatively low (Table 6.2) and the wrist is far less flexed than in Group A birds. The action during the initial stages of the downstroke is similar to that of Group A, but the degree of distal wing spreading is less and occurs over a smaller period of the downstroke; hence the wrist and the wing tip follow a similar, near vertical, stroke plane (Figure 6.5) for most of this half of the wing beat cycle. There is no separation of the primary feathers at the wing tip, and only slight tip bending. The wing is pronated during most of the downstroke.

The upstroke is distinctly different from that of Group A birds in that the proximal wing positive rotation and the elbow and wrist flextion are all far less than in birds of Group A. As a result, the overall span of the wings is only slightly reduced in

the upstroke (Table 6.2) and there is only a slight upstroke 'flick'. This is because, when proximal wing negative rotation and elbow and wrist extension occur at the top of the upstroke, they are low in magnitude; so too is the enhancement of the speed of the wing tip. Throughout the upstroke all Group C birds show supination. Apparent vertical body movements during the cycle are not noticeable in the available film.

Group C birds (Figure 6.6) exhibit two separate downstroke speed distribution trends. The gulls of the Charadriiformes show a speed profile similar to those of Group A birds with the absence of the 'wrist extension hump'. The velocity increases steadily to a peak, approximately 60% to 70% of the way through the downstroke period. The Procellariiformes, however, show a very rapid acceleration to a period of near constant velocity for the middle third of the downstroke. Deceleration is relatively slow. The initial acceleration may appear exaggerated due to the small degree of wrist flexion and extension during the wing stroke, so causing the wing tip to have very low speeds at the start and finish of the downstroke compared with Group A and Group B birds. Nevertheless, this is the same for gulls who exhibit far slower initial accelerations than the similarly shaped Procellariiformes.

Figure 6.5A

A series of illustrations of the Black headed Gull Larus ridibundus, which is a typical small Group C bird, in cruise flight. Wing span 0.82m. Film speed 100fps.

a) Head on and side on drawings from film of the stages of the wing stroke at every fourth frame. The side on and head on views are not to scale. Other details are as in Figure 6.3A(a).

Figure 6.5A (a) Black headed Gull

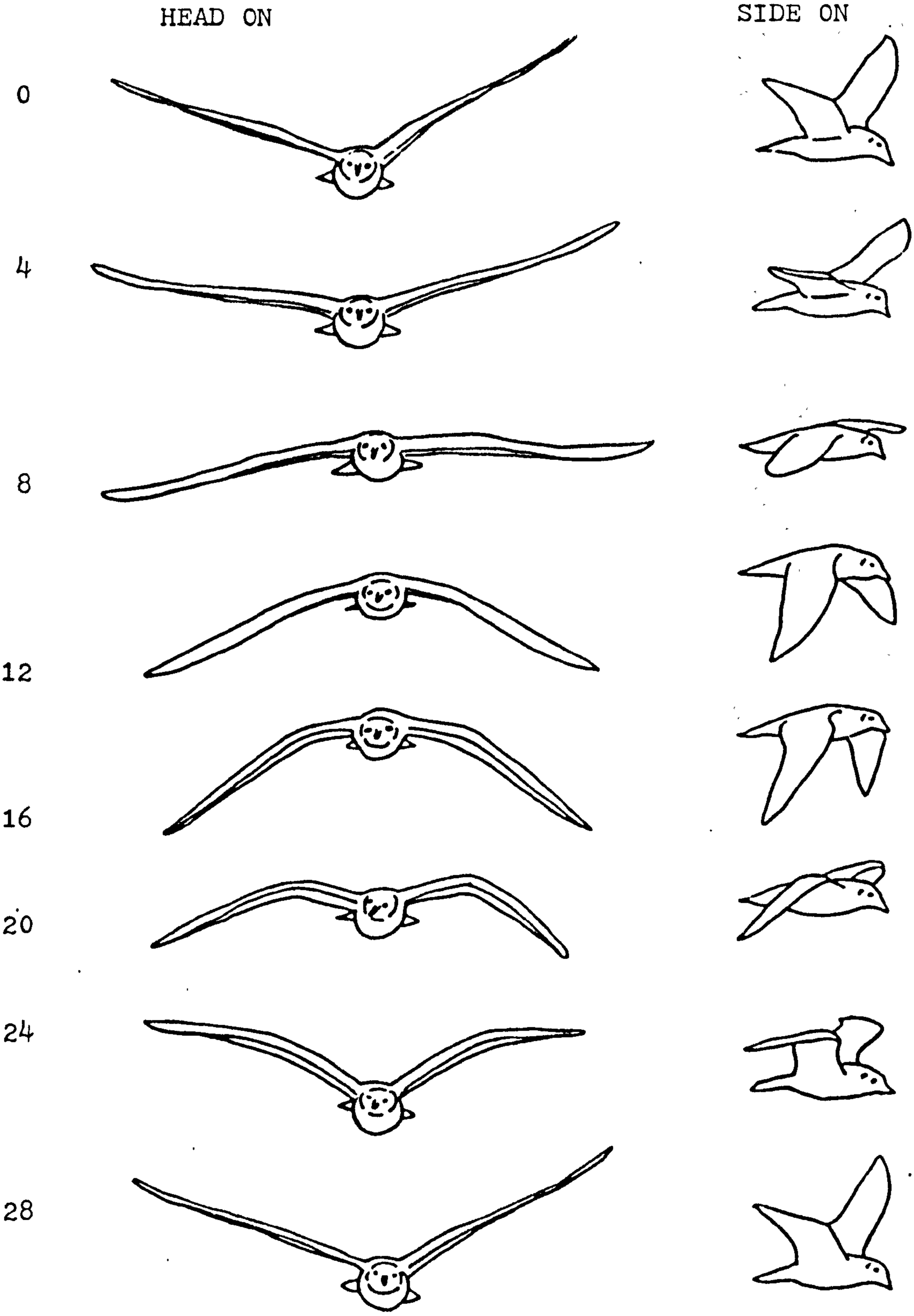

Figure 6.5A

b) Wing tip traces for head on and side on views of a complete wing stroke as in Figure 6.3A(b). Head on and side on views are not to scale.

Figure 6.5A (b) Black headed Gull

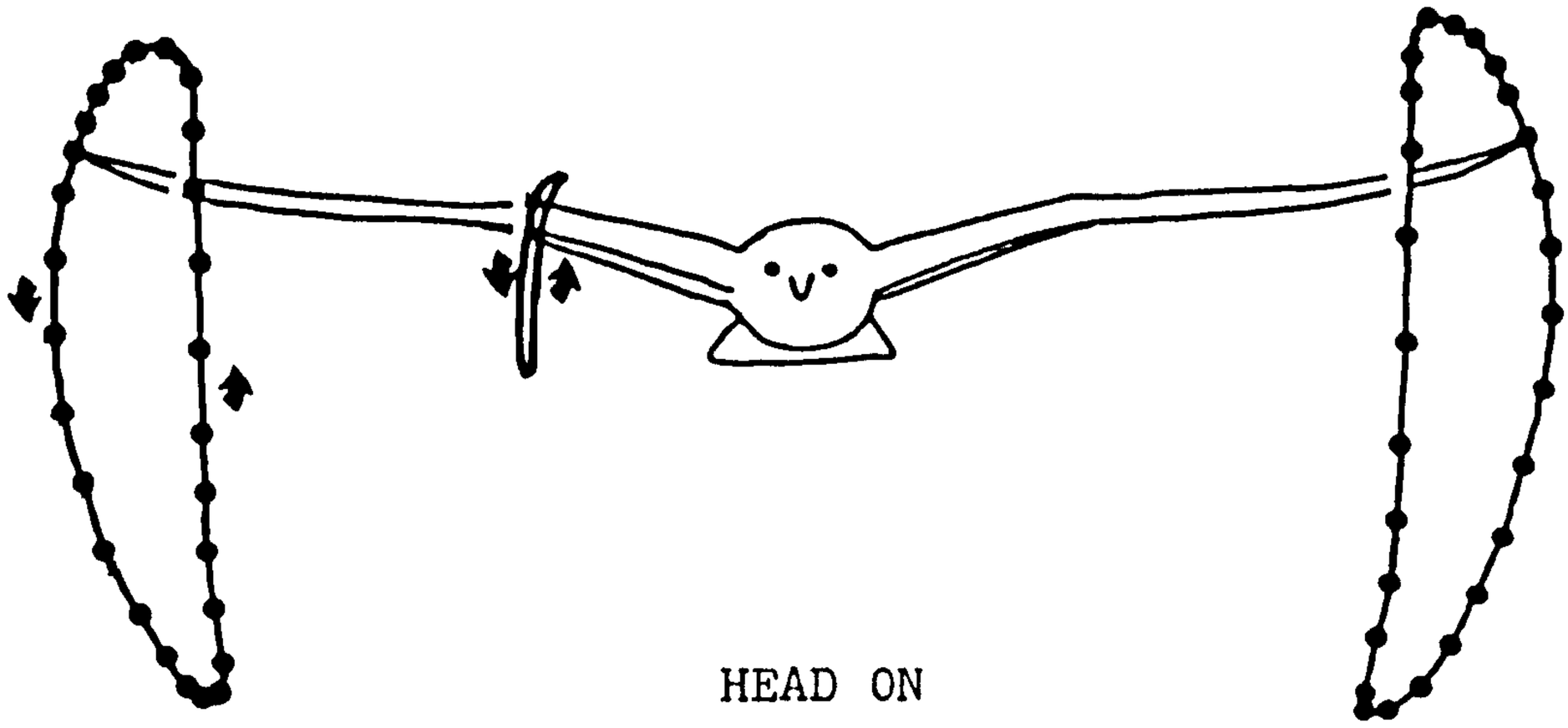

HEAD ON

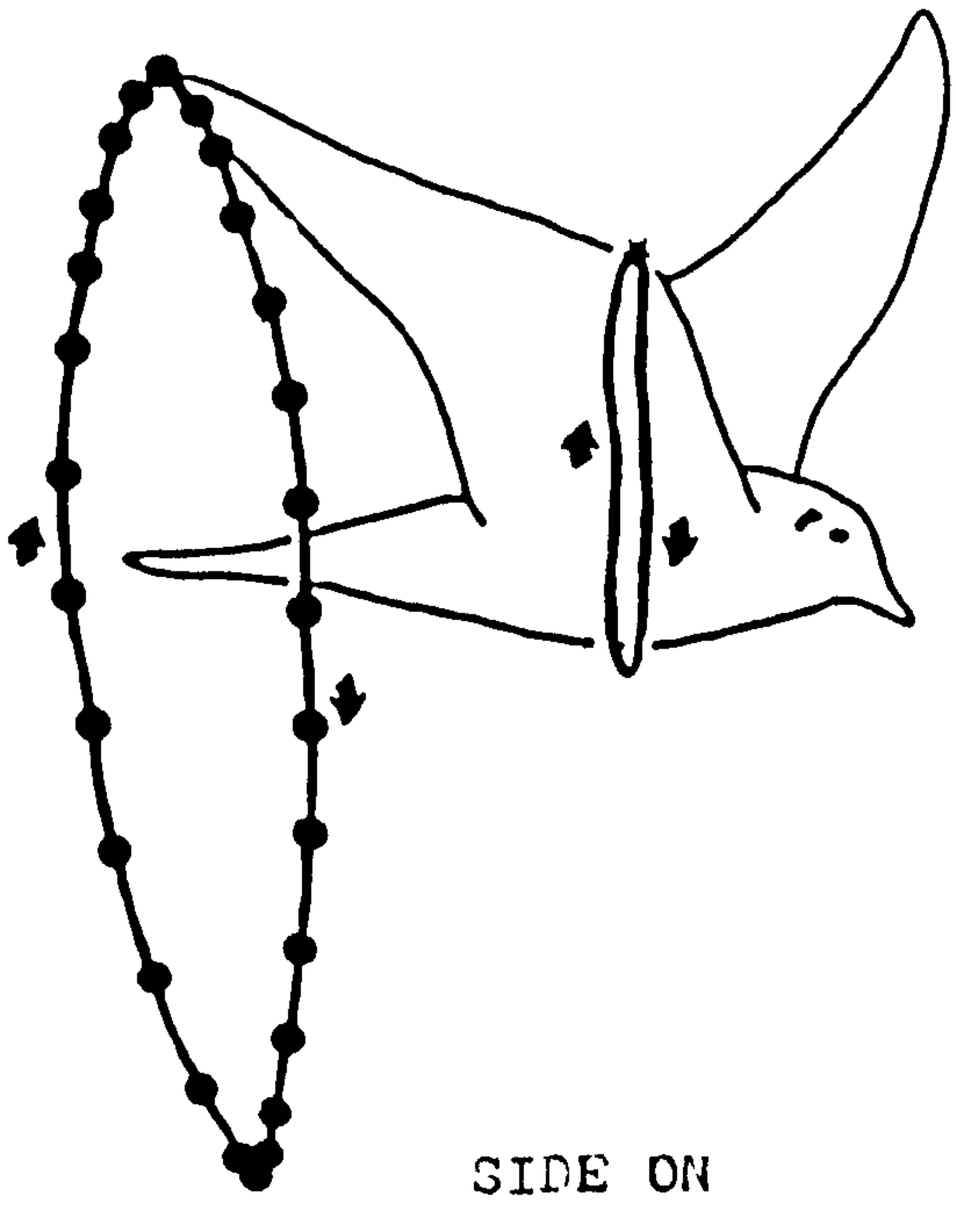

SIDE ON

Figure 6.5A

c) Graph of the vertical position of the wing tip and the wrist (broad and narrow lines respectively) against time. The X coordinates, as in Figure 6.3A(c), are relative to the fixed body target.

Figure 6.5A (c) Black headed Gull

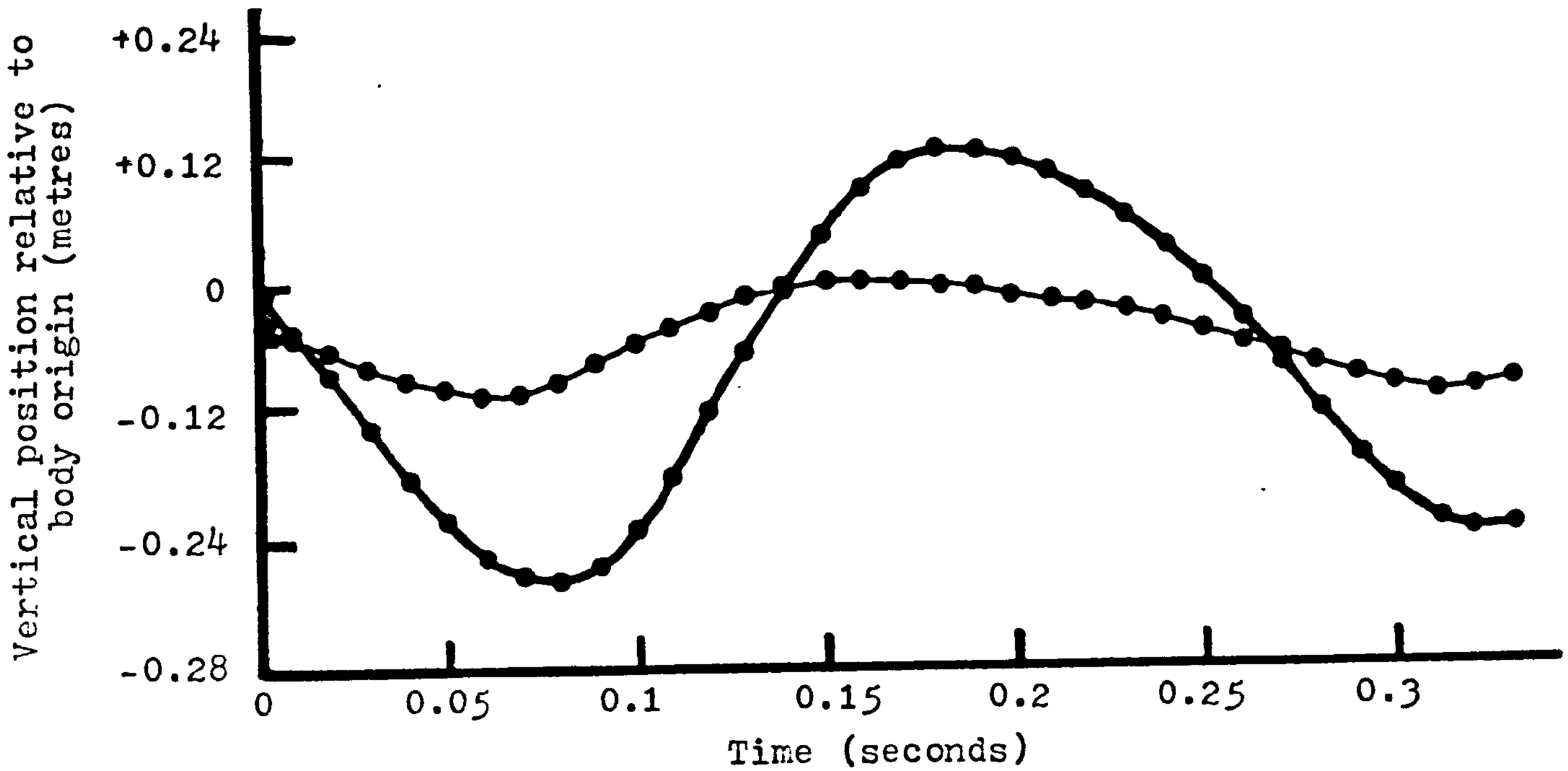

Figure 6.5B

A series of illustrations of the black browed albatross Diomedea melanophris, which is a typical large Group C bird,in cruise flight. Wing span 2.09m. Film speed 60fps.

a) Head on and side on drawings from film of the stages of the wing stroke at every third frame. The side on and head on views are not to scale. Other details as in Figure 6.3A(a).

Figure 6.5B a) Black Browed Albatross

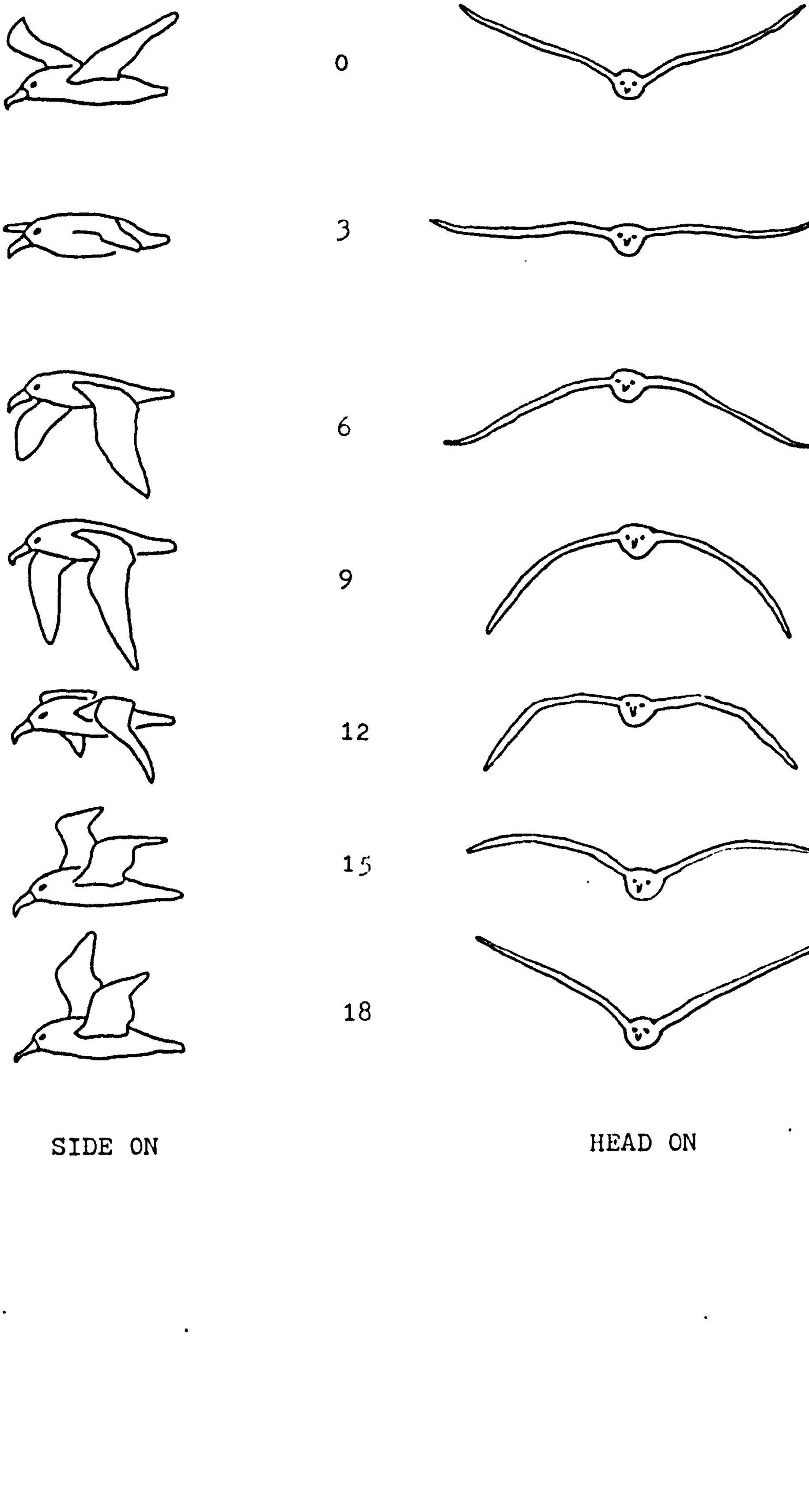

SIDE ON HEAD ON

Figure 6.5B

b) Wing tip traces for a complete wing stroke viewed from head on and from the side as in Figure 6.3A(b). The two views are not to scale.

Figure 6.5B (b) Black browed albatross

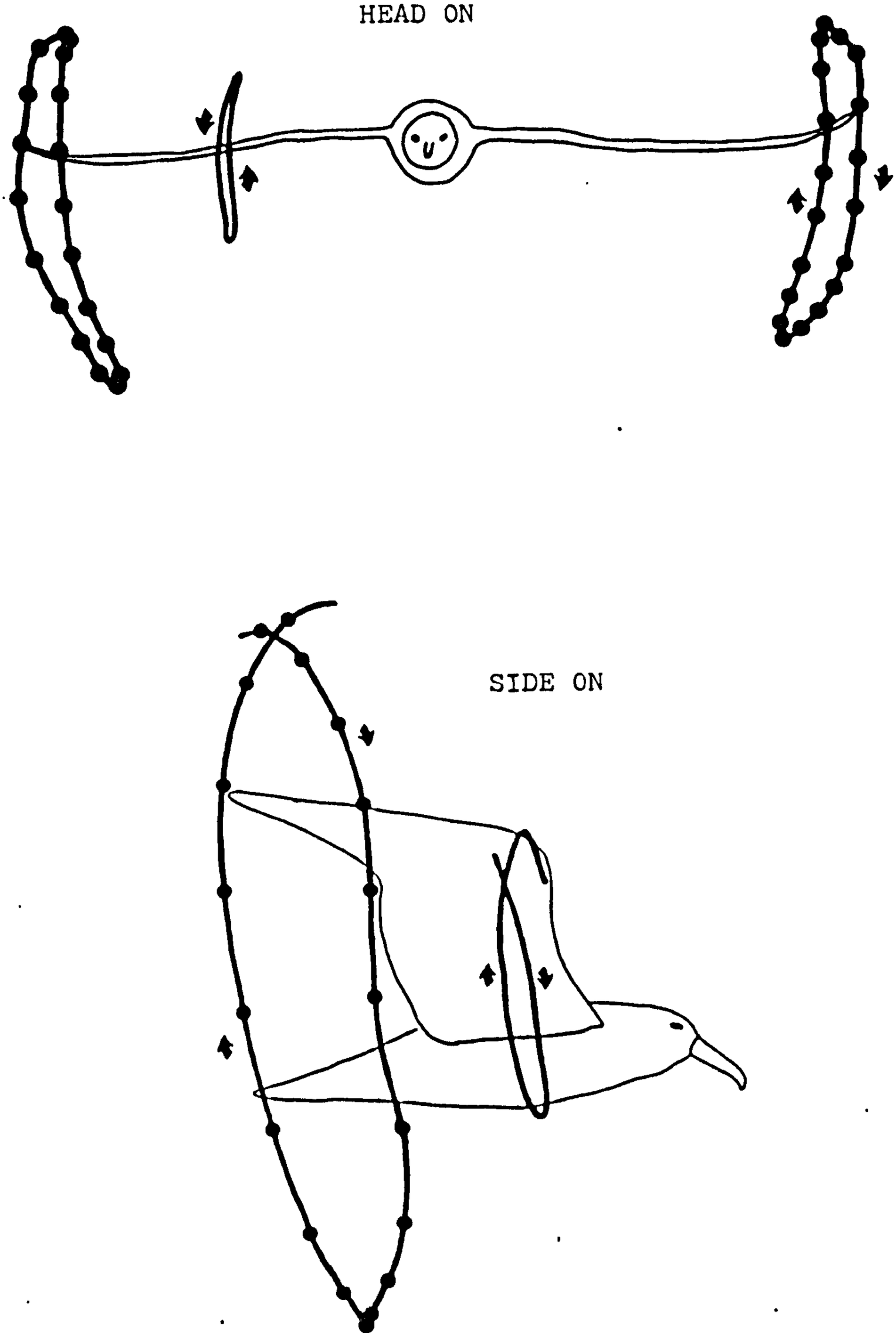

Figure 6.5B

c) Graph of the vertical position of the wing tip and the wrist (broad and narrow bones respectively) against time. These X coordinates, as in 6.3A(c) are relative to a fixed body target.

Figure 6.5B (c) Black browed albatross

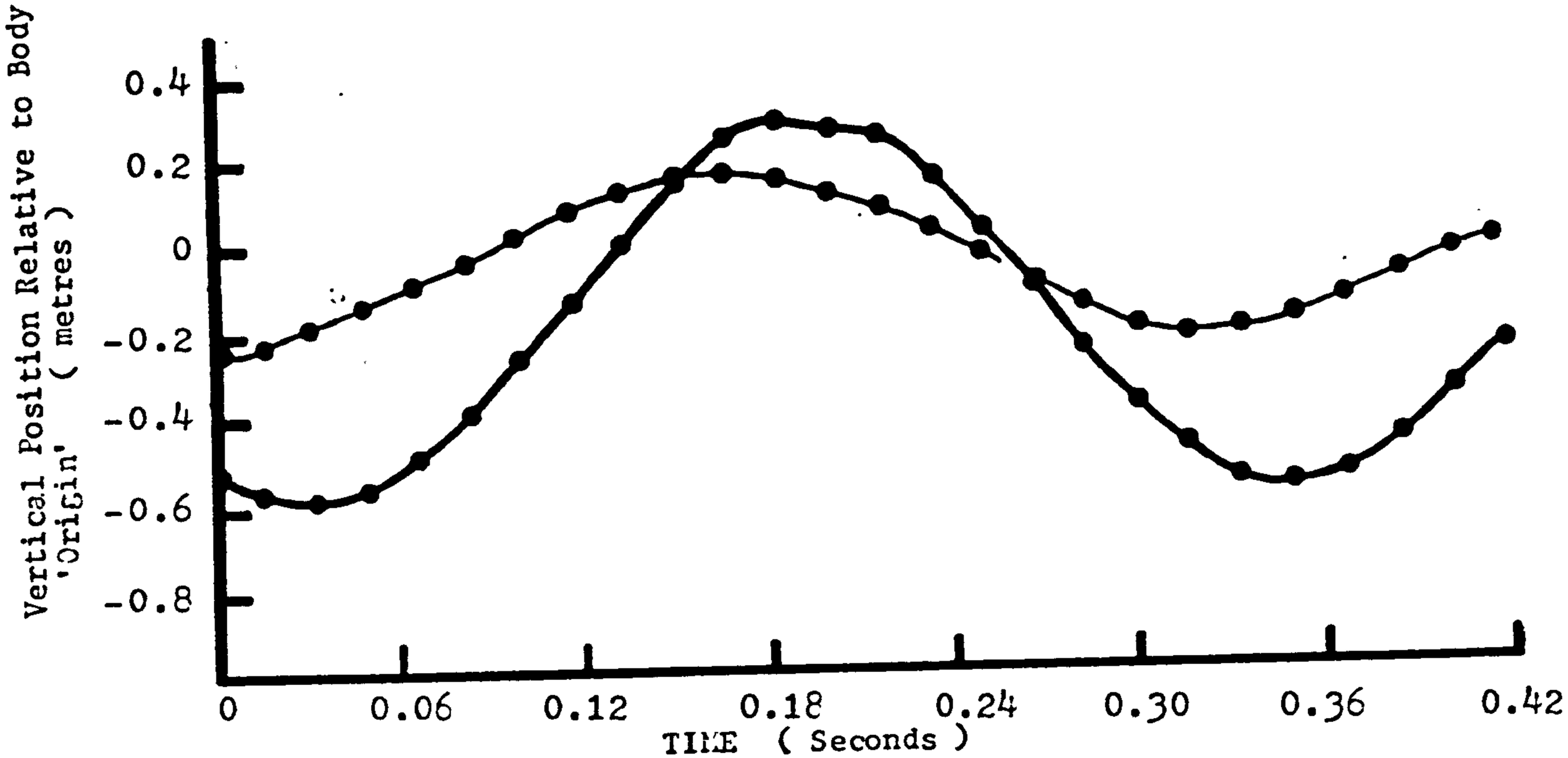

TABLE 6.2 Wing Beat Kinematics of Group C Birds.

Species	Average Morphology			Stroke Periods					Stroke Angles (degrees							Peak V_{wt} $m\,s^{-1}$	$\frac{b_d - b_u}{b_d}$ %
					f(Hz)		z			Φ_u		Φ_d		Φ	γ		
	m(kg)	b(m)	$S(m^2)$	n	mean	SD	mean	SD	n	mean	$R^{\pm}$	mean	$R^{\pm}$				
GREY HEADED ALBATROSS *Diomedea chrysostoma*	3.75	2.16	0.316	12	3.00	0.14	0.50	0.04	5	25	3	24	3	49	-	8.5	12
WANDERING ALBATROSS *Diomedea exulans*	8.5	3.42	0.621	23	2.61	0.26	0.51	0.04	4	24	2	24	4	48	-	9.5	12
BLACK BROWED ALBATROSS *Diomedea melanophris*	2.91	2.1	0.268	16	3.11	0.15	0.51	0.04	4	23	4	25	3	48	85	8	10
GIANT PETREL *Macronectes giganteus*	3.8	1.93	0.313	15	3.2	0.18	0.50	0.03	3	26	2	19	3	45	-	7	9
FULMAR *Fulmarus glacialis*	0.795	1.13	0.118	9	4.51	0.21	0.51	0.03	5	31	4	30	3	61	90	-	16
WHITE CHINNED PETREL *Procellaria aequinoctialis*	1.0	1.42	0.162	25	4.30	0.61	0.50	0.04	6	32	4	28	4	60	-	7	11
COMMON GULL *Larus canus*	0.388	1.13	0.125	29	3.76	0.27	0.51	0.04	5	35	3	17	2	52	-	-	20

TABLE 6.2 continued

	m(kg)	b(m)	S(m^2)	f(Hz) n	f(Hz) mean	f(Hz) SD	z mean	z SD	Q_u n	Q_u mean	Q_u R±	Q_d mean	Q_d R±	Q	γ	V_{mt} ms^{-1}	$\frac{b_d - b_u}{b_d}$ %
BLACK HEADED GULL Larus ridibundus	0.251	0.94	0.087	18	3.84	0.26	0.50	0.04	6	32	4	20	3	52	90	4.5	16
LITTLE TERN Sterna albifrons	0.053	0.50	0.0185	37	4.60	0.68	0.47	0.03	5	64	4	37	4	101	85	5	40
SWIFT Apus apus	0.043	0.37	0.0127	22	8.56	1.24	0.50	0.03	8	35	5	35	4	70	-	-	32

Figure 6.6

Wing tip downstroke speed distribution (velocity m s^{-1} with time s) for six Group C birds:

(A) Wandering albatross

Diomedea exulans

(B) Grey headed albatross

Diomedea chrysostoma

(C) Black browed albatross

Diomedea melanophris

(D) Giant petrel

Macronectes giganteus

(E) Black headed gull

Larus ridibundus

(F) Common gull

Larus canus

Figure 6.6

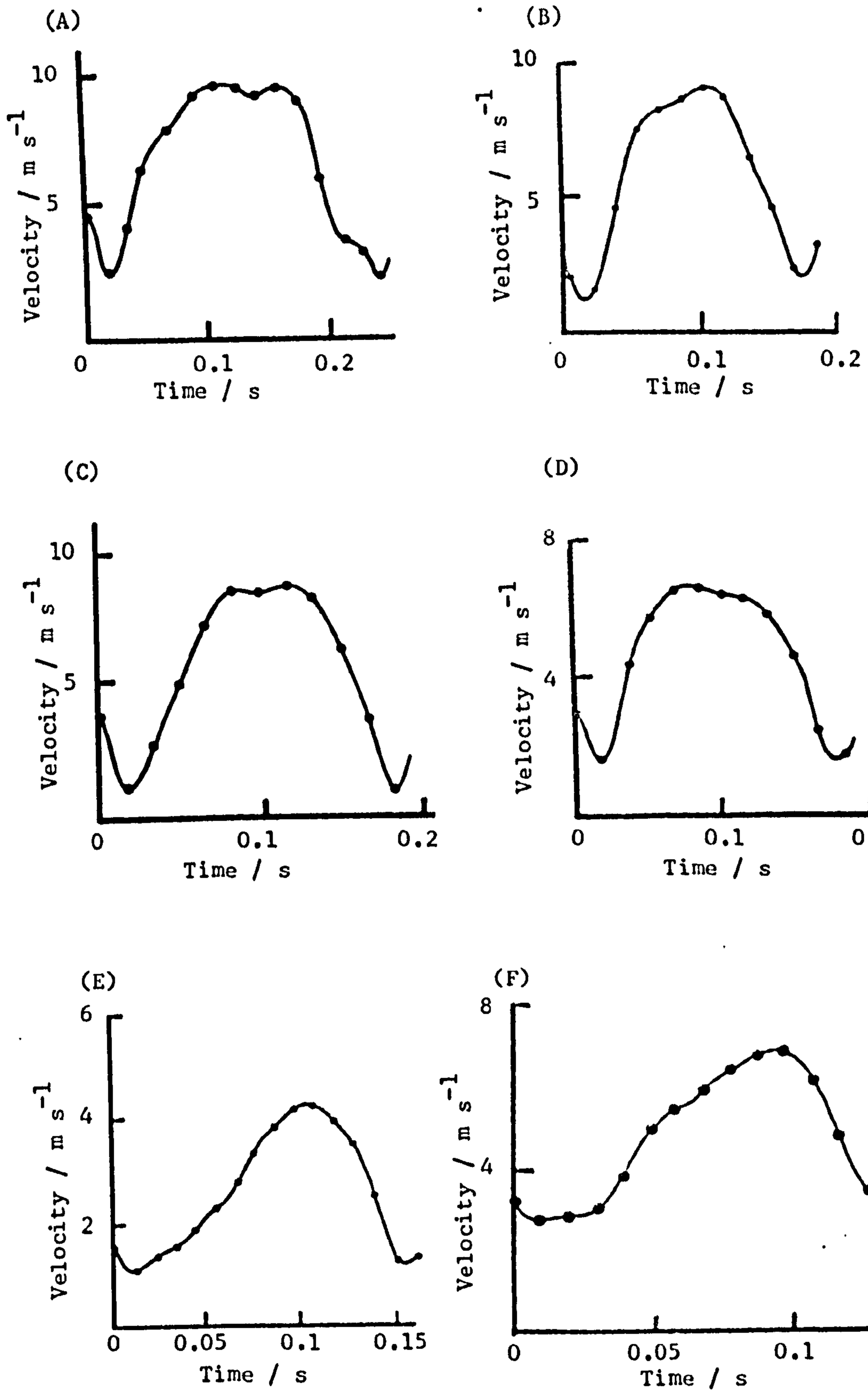
(A)
10
5
Velocity / m s-1
0
0.1
0.2
Time / s
(B)
10
5
Velocity / m s-1
0
0.1
0.2
Time / s
(C)
10
5
Velocity / m s-1
0
0.1
0.2
Time / s
(D)
8
4
Velocity / m s-1
0
0.1
0.2
Time / s
(E)
6
4
2
Velocity / m s-1
0
0.05
0.1
0.15
Time / s
(F)
8
4
Velocity / m s-1
0
0.05
0.1
Time / s

6.2.3 Group B

Broadly speaking, this group can be considered to have wing tip patterns intermediate between those of Group A and Group C birds. The positive elevations are generally between those of Group A and Group C birds. Wrist extension during the downstroke is generally pronounced, and therefore initial differences in the stroke plane of the wrist and the wing tip occur. The stroke plane of the wrist is generally close to vertical (Table 6.3). The pattern of events at the base of the downstroke is similar to those described for Group A, except that the wrist generally moves upwards along the same path as it descended, and this causes the wing tip to have a more rounded upstroke path (Figure 6.7) as in corvids. The wing is pronated in the downstroke and a small degree of primary feather separation may occur. During the upstroke the elbow is flexed and the wing supinated. The degree of elbow and wrist flexion is intermediate between that of Groups A and C, and this is reflected in their span reductions (Table 6.3). The upstroke movements show considerable variation within the group, but generally the upstroke velocities of the flick are intermediate between those of similar sized members of Groups A and C. Vertical movements of the body are apparently small although, as they cannot be measured, this cannot be confirmed.

The downstroke speed distribution of Group B birds

Figure 6.7

A series of illustrations of the lagger falcon Falco jugger, which is a typical Group B bird, in cruise flight. Wing span 1.01m. Film speed 300fps. a) Tail on and side on drawings from film at eight frame intervals during one wing stroke. The two views are not to scale. Other details are as in Figure 6.3A(a).

Figure 6.7 a) Lagger falcon

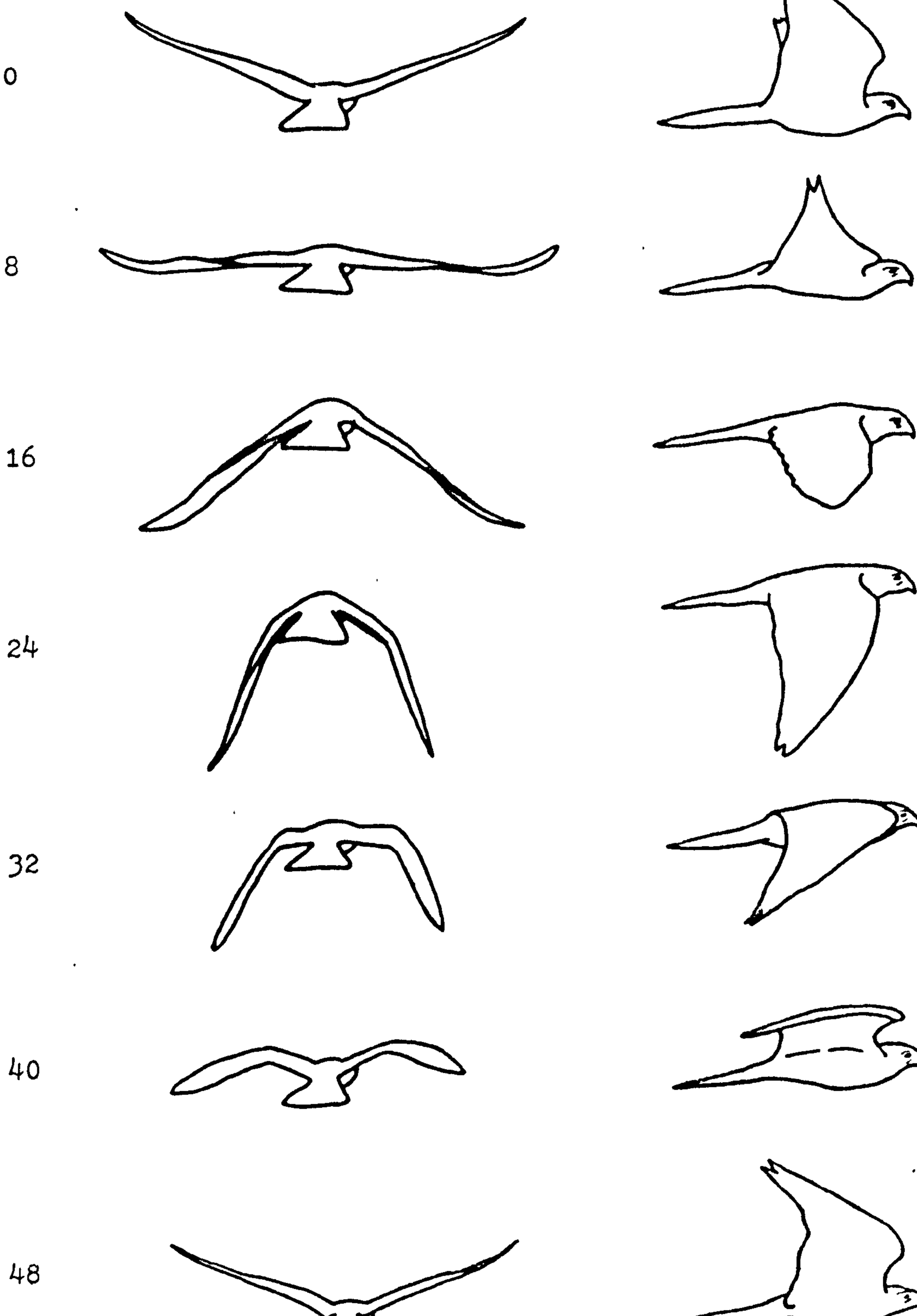

TAIL ON

SIDE ON

Figure 6.7

b) Wing tip traces for head on and side on views of a complete wing stroke. Only every other frame has been marked with a solid circle. Other details are as in Figure 6.3A(b). The two views are not to scale.

Figure 6.7 b) Lagger falcon

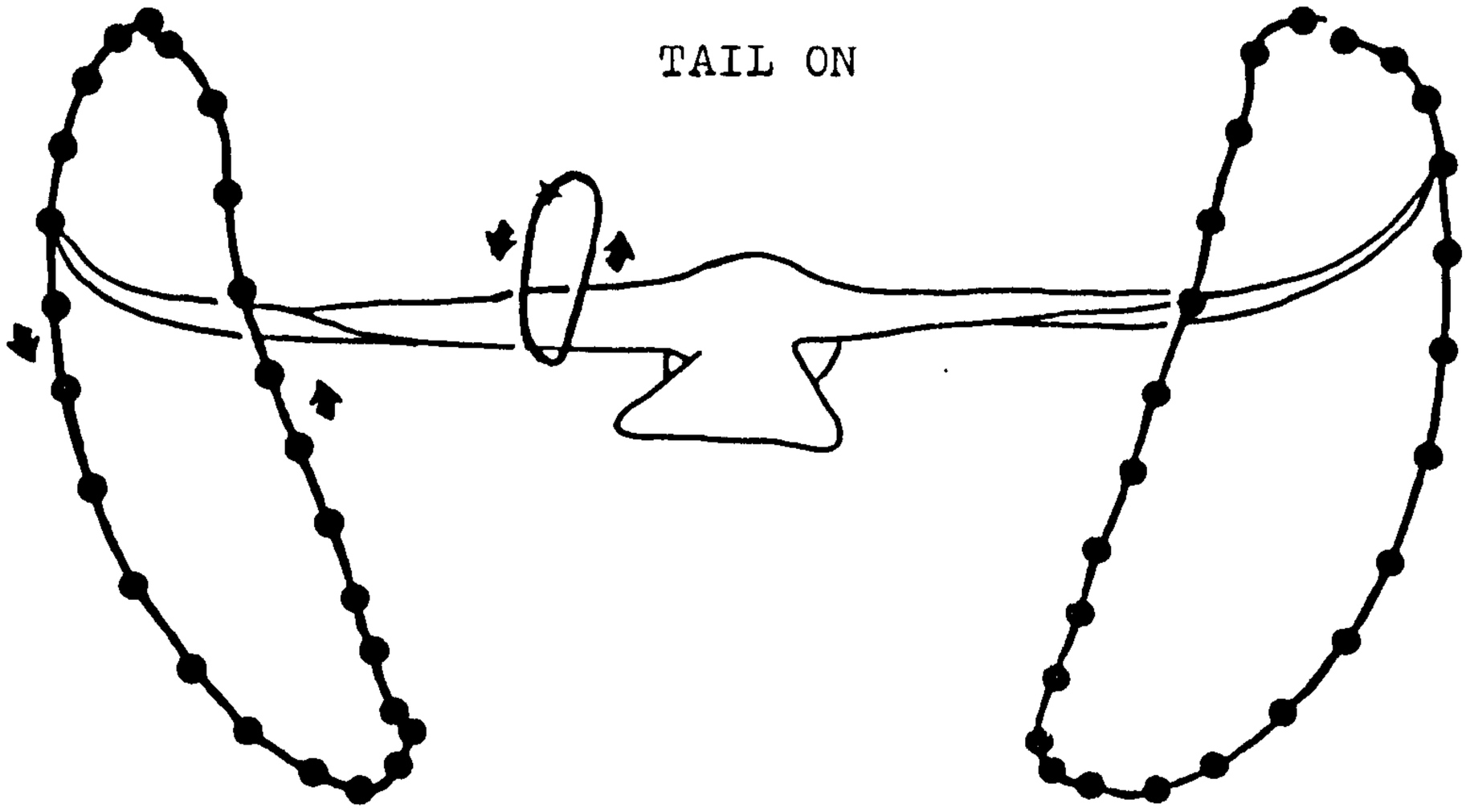

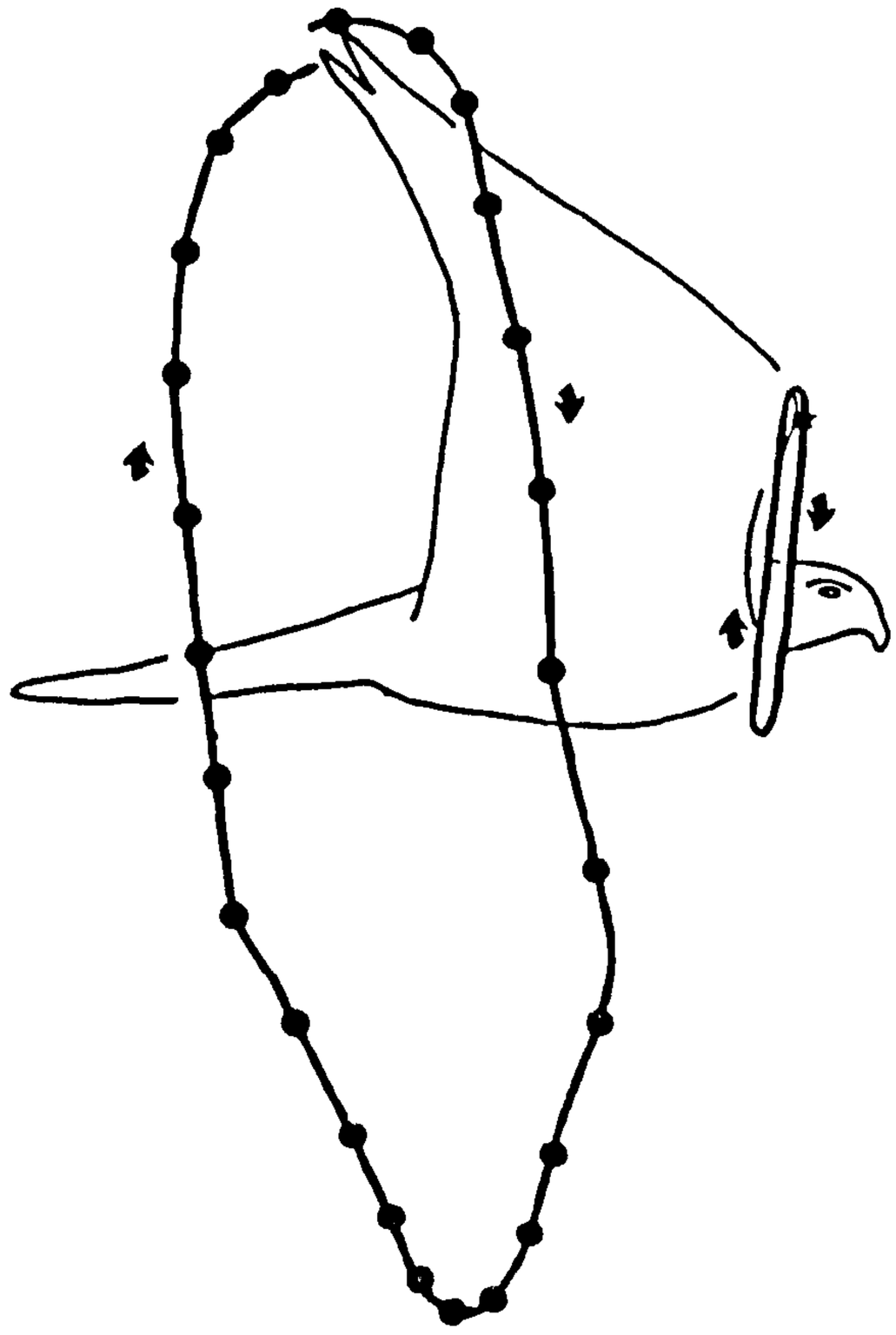

Figure 6.7 (c)

c) Graph of the vertical position of the wing tip and the wrist (broad and narrow lines respectively) against time. X axis coodrinates are relative to the fixed body target. Other details are as in 6.3A(c).

Figure 6.7 (c)

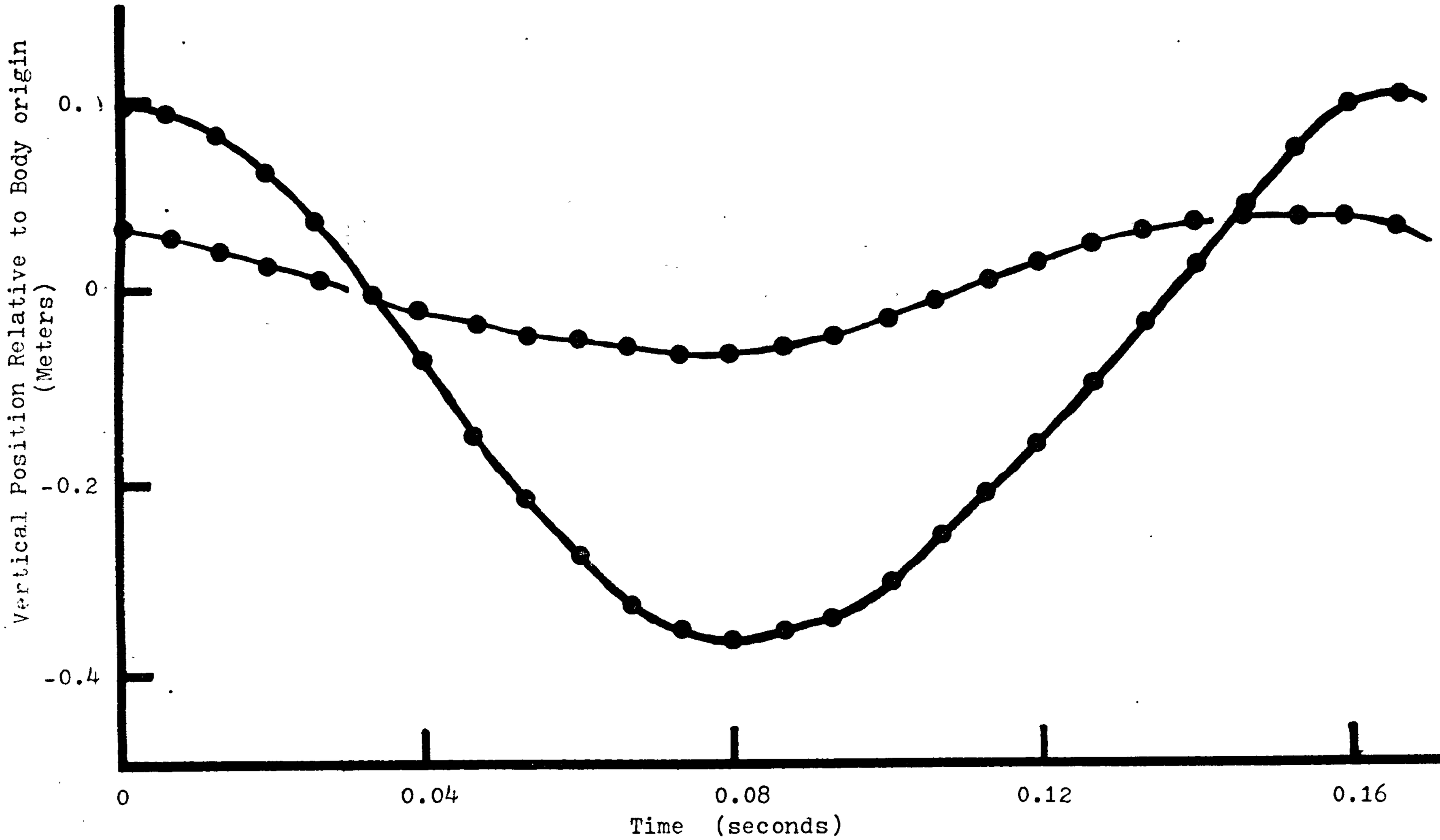
Vertical Position Relative to Body origin (Meters)
0.
0
-0.2
-0.4
0
0.04
0.08
0.12
0.16
Time (seconds)

TABLE 6.3 Wing Beat Kinematics of Group B Birds.

Species	Average Morphology			Stroke Periods					Stroke Angles (degrees)							Peak V_{mt} m s -1	$\frac{b_d - b_u}{b_d}$ %
					f(Hz)		τ			Φ_u		Φ_d		Φ	γ		
	m(kg)	b(m)	$S(m^2)$	n	mean	SD	mean	SD	n	mean	R±	mean	R±				
WHITE NECKED CORMORANT *Phalacrocorax carbo*	1.87	1.44	0.251	65	5.43	0.35	0.54	0.03	4	44	4	13	3	57	-	7.5	33
ANHINGA *Anhinga anhinga*	1.21	1.18	0.168	39	5.66	0.58	0.60	0.04	3	46	3	15	3	61	-	8	37
LESSER FLAMINGO *Phoeniconaias minor*	1.16	1.38	0.188	60	5.23	0.35	0.54	0.03	3	38	2	15	2	53	-	-	26
BEWICK SWAN *Cygnus columbianus*	6	1.76	0.377	15	4.0	0.16	0.58	0.02	5	31	3	22	3	53	80	8	19
WHOOPER SWAN *Cygnus cygnus*	11.3	2.33	0.603	14	3.70	0.20	0.60	0.03	5	34	3	22	2	56	-	10	18
MUTE SWAN *Cygnus olor* (film of E:C.G.)	11.6	2.33	0.603	16	3.60	0.17	0.61	0.03	6	29	3	26	3	45	80	8	21
BARNACLE GOOSE *Branta leucopsis*	1.15	1.08	0.115	15	4.47	0.34	0.50	0.03	4	37	3	21	3	58	-	-	22
PINTAIL *Anas acuta*	0.955	0.916	0.084	63	7.54	0.78	0.56	0.04	6	36	5	30	2	66	90	9	21

TABLE 6.3 continued.

	m(kg)	b(m)	S(m^2)	n	f(Hz) mean	f(Hz) SD	τ mean	τ SD	n	θ_u° mean	θ_u° R±	θ_d° mean	θ_d° R±	θ°	γ°	V_{mt} $m\ s^{-1}$	$\frac{b_d - b_u}{b_d}$ %
MALLARD *Anas platyrhynchos*	1.1	0.90	0.093	22	6.25	0.42	0.53	0.03	8	26	5	32	4	58	-	7	16
LANNER FALCON *Falco biarmicus*	0.571	1.02	0.131	18	5.63	0.26	0.51	0.03	4	36	2	36	3	72	-	10	34
LAGGER FALCON *Falco jugger*	0.571	1.02	0.131	20	6.0	0.20	0.50	0.02	5	23	3	35	3	58	90	11	36
KESTREL *Falco tinnunculus*	0.216	0.73	0.0705	16	7.14	0.26	0.50	0.02	3	34	2	38	2	72	-	-	27
OYSTER CATCHER *Haematopus ostralegus*	0.438	0.82	0.062	62	7.77	0.95	0.49	0.03	4	35	3	17	2	52	80	7	10
GUILLIMOT *Uria aalge*	0.99	0.704	0.052	40	9.43	1.16	0.51	0.03	-	-	-	-	-	-	-	-	-
ROCK DOVE *Columba livia* (film by BBC)	0.34	0.724	0.0733	25	6.70	0.54	0.50	0.03	3	40	5	40	5	80	80	-	-
WOOD PIGEON *Columba palumbus*	0.447	0.73	0.0744	10	5.71	0.35	0.50	0.02	-	-	-	-	-	-	-	-	-
COLLARD DOVE *Streptopelia decaocto*	0.202	0.53	0.0398	12	7.54	0.94	0.45	0.03	-	-	-	-	-	-	-	-	-
PIED KINGFISHER *Ceryle rudis*	0.09	0.458	0.0327	25	6.88	0.56	0.51	0.04	4	42	6	54	5	96	75	5	65

Figure 6.8

Wing tip downstroke speed distribution (velocity m s^{-1} with time s) for four Group B birds:

(A) Bewick swan

Cygnus columbianus

(B) Mallard

Anas platyrhynchos

(C) Lanner falcon

Falco biarmicus

(D) Lagger falcon

Falco jugger

Figure 6.8

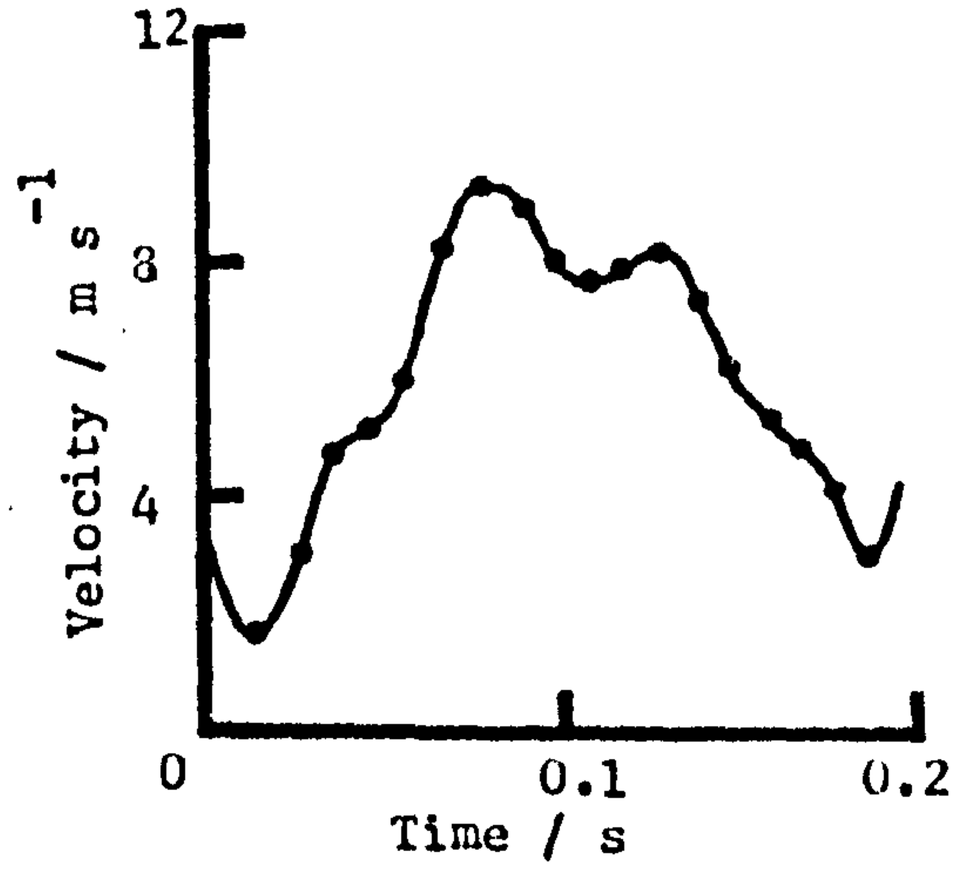
(A)
12
8
4
Velocity / m s-1
0
0.1
0.2
Time / s

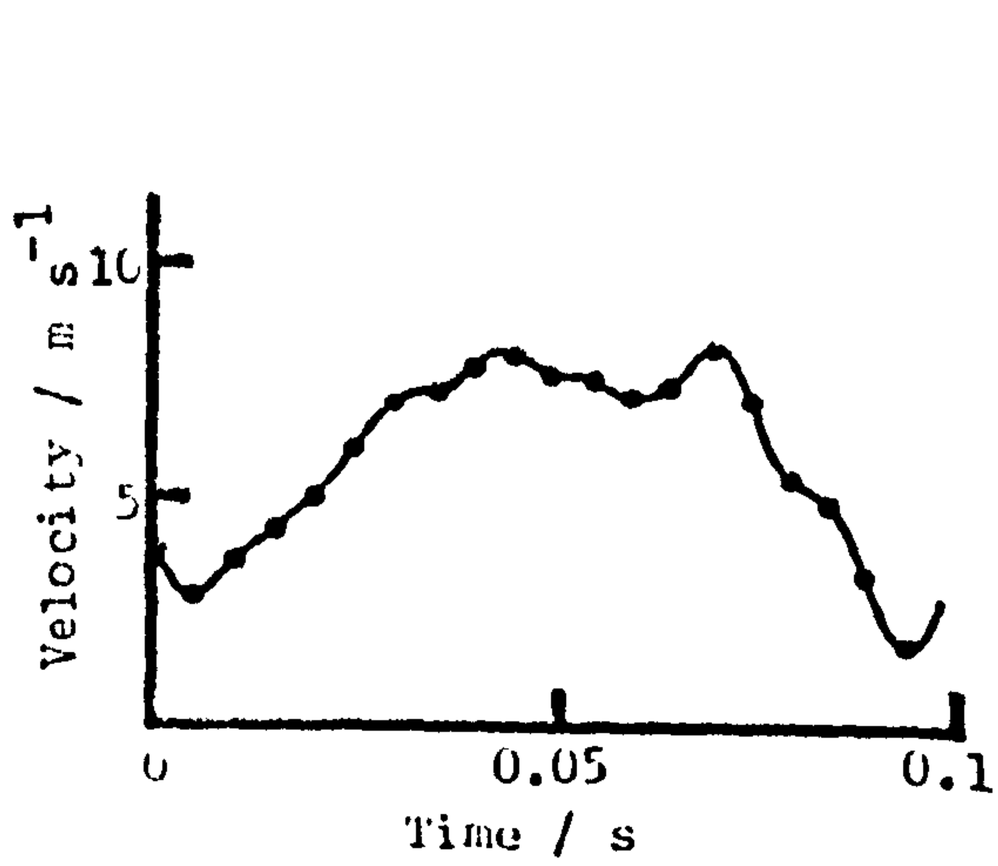
(B)
10
5
Velocity / m s-1
0
0.05
0.1
Time / s

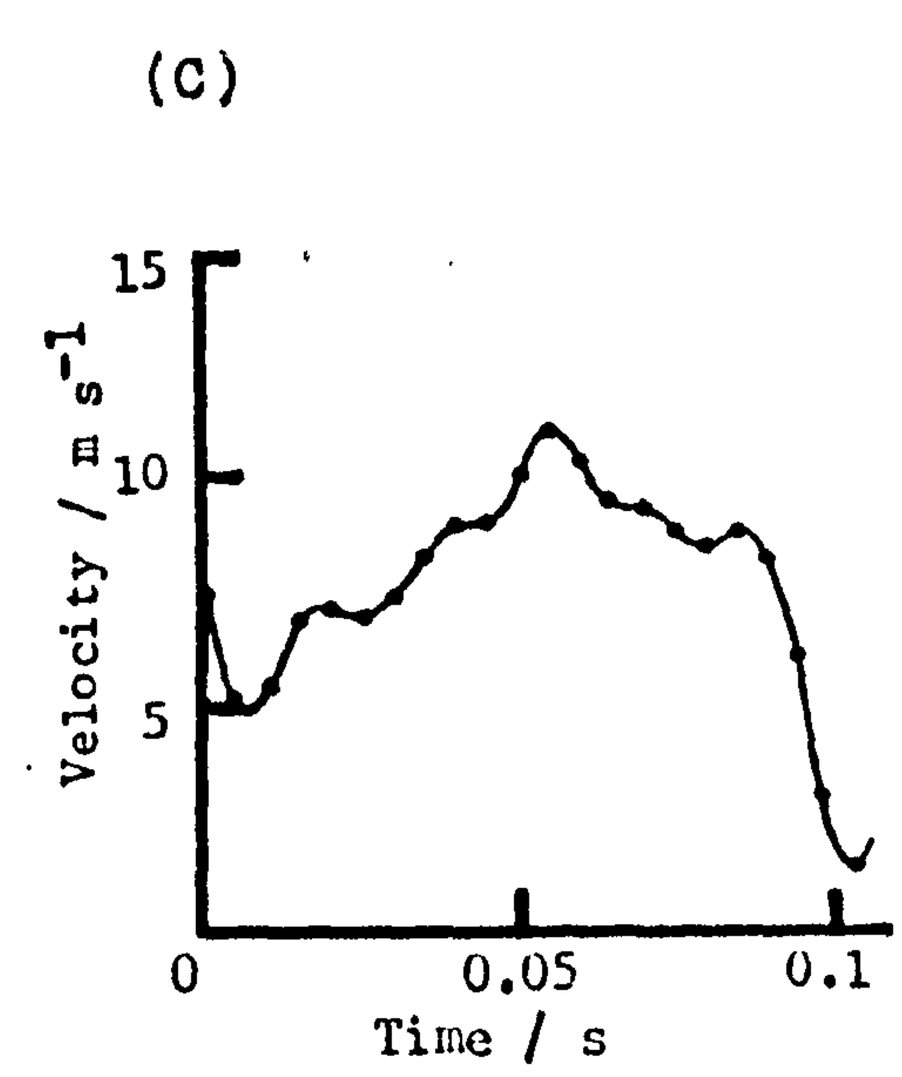
(C)
15
10
5
Velocity / m s-1
0
0.05
0.1
Time / s


(D)
15
10
5
Velocity / m s-1
0
0.05
0.1
Time / s

(Figure 6.8) generally exhibit peak speeds 50% of the way through the downstroke period, and the middle third of this period has a high, fairly constant velocity on either side of the peak. Deceleration is rapid.

6.3 Zebra finch cruise flight: Wing stroke description

The zebra finch is typical of small passerines in that it uses bounding or intermittent flight. Its flight can be divided into the flapping period and the body glide period.

In cruise flight the zebra finch beats its wings 3 or 4 times between body glides. The wing stroke is similar to that of the hovering pied flycatcher (Ficedula hypoleuca) described by Norberg (1975). The downstroke begins with the wrist still slightly flexed, and it is extended during the initial stages of the downstroke, causing the spreading of the primary feathers in a similar manner to that described for larger birds (Section 6.2). The wing is slightly pronated and the primary feathers are bent upwards. The upstroke is similar to that described for Group A birds, although the actions are more exaggerated. The elbow is flexed and the proximal wing section is positively rotated as it begins to move upwards close to the body. The wrist is greatly flexed and the primaries, separated and forming a 'venetian blind' effect, are moved close to the body. As the wrist approaches its highest elevation it is rotated negatively causing the primary feathers to move up and past the body. In the latter stages of this rotation the wrist is extended, bringing the wing into position for the next downstroke (Figure 6.9a). The secondary feathers of the two wings do not appear to come into contact at the top of the upstroke.

Figure 6.9a

Side on view of the zebra finch Poephila guttata in fast forward flapping flight showing one wing stroke. The film speed is 500fps. The frame numbers are indicated by each illustration.

Figure 6.9a Zebra Finch

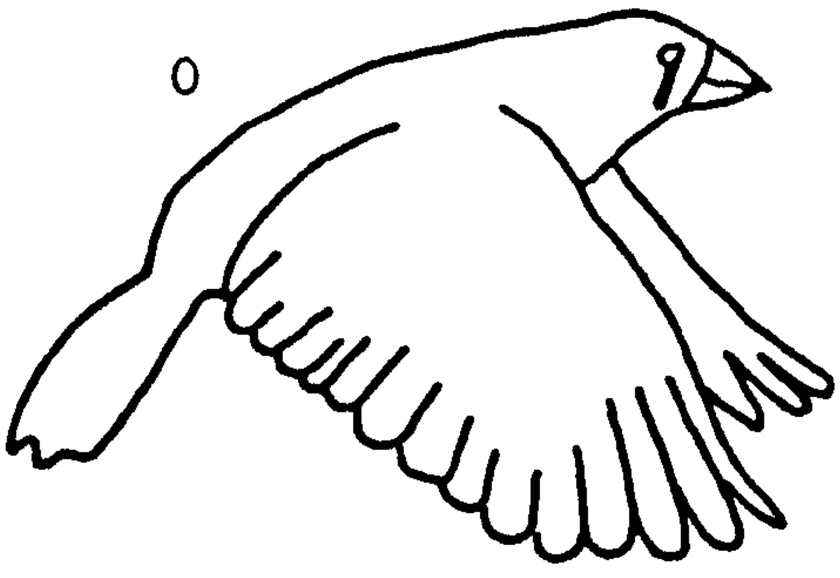

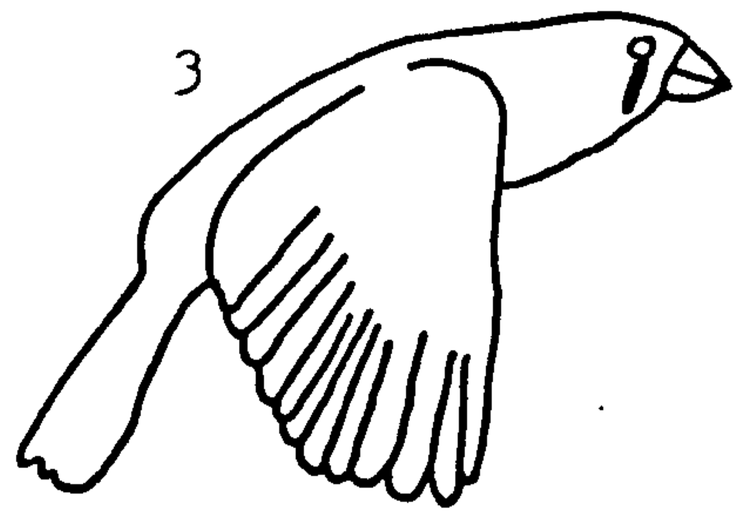

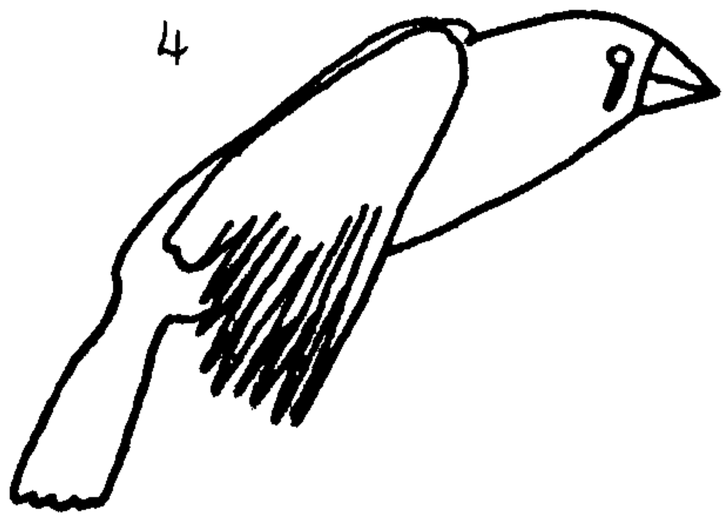

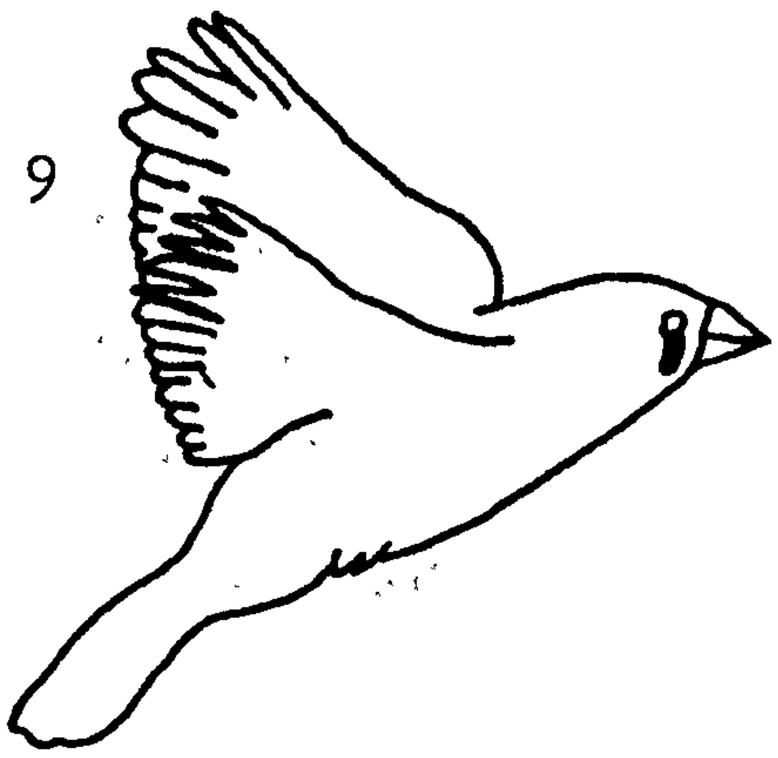

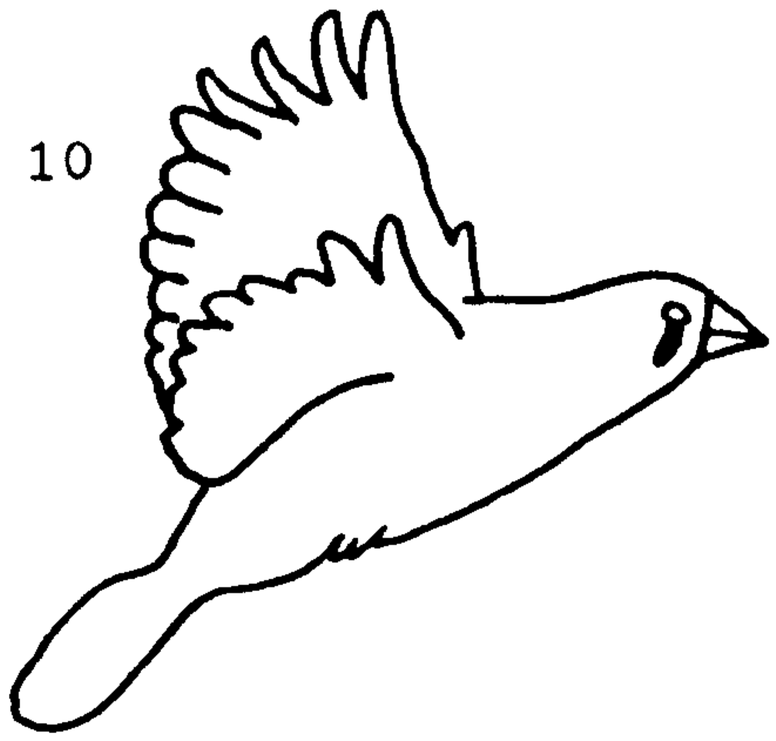

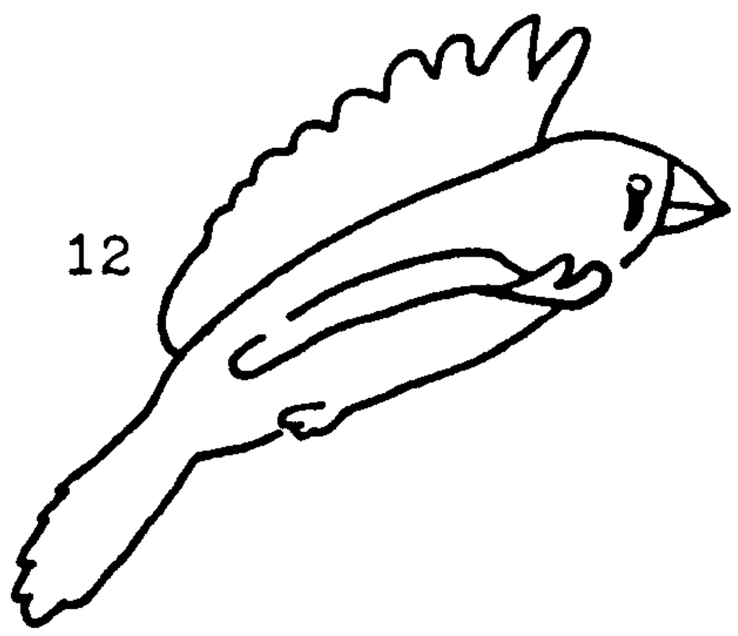

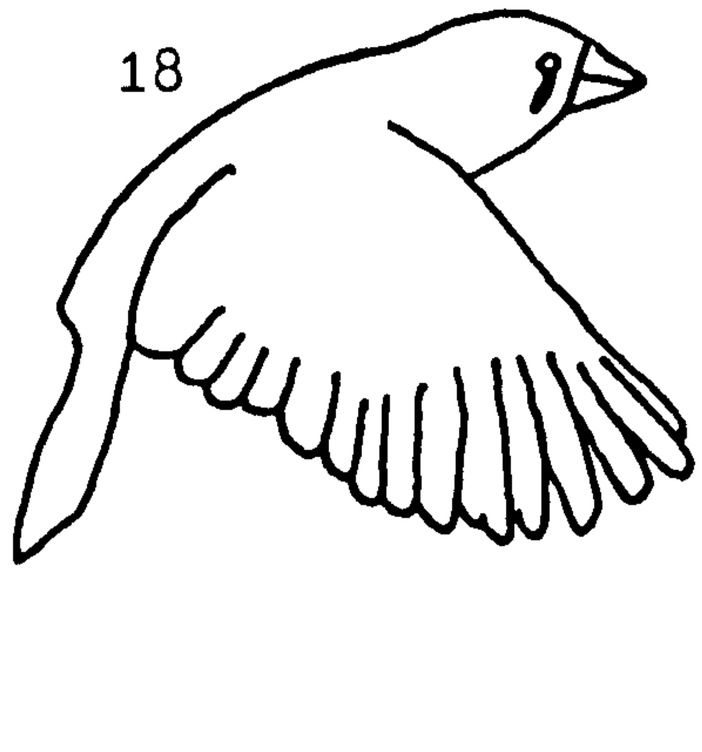

The kinematics are given as follows. Positive elevation varied for the two cruise flapping sequences between the ranges of 57 ± 3^{o} and 40 ± 6^{o}, whereas the negative elevation was always approximately 55 ± 5^{o}. Stroke plane angle relative to the body was constant at 62 ± 2^{o}, but the body tilt varied through the three or four wing beat cycles between body glides, from about 15^{o} to 20^{o} at the start of a beat sequence to 30^{o} to 37^{o} at the end. The stroke plane angle relative to the horizontal varied accordingly. Wing beat frequency was 27.8 ± 3 Hz and the downstroke ratio was 0.47 ± 0.06 at a flying speed of 5 ± 0.2m s^{-1}

At the end of a flapping sequence the finch folds its wings close to the body and begins the 'bound'. This is usually characterised by being a shallow parabola as illustrated in Figure 6.9B. During the end of a flapping sequence the body is tilted at an angle of about 35^{o}, and the bird moves upwards at an angle of about 18^{o}. The angle of incidence decreases during the bound, but the body always remains at a positive angle of attack. The body gliding of the zebra finch has been fully described by Csicsaky (1977).

Figure 6.9b

Side on trace of the 'bound' of the zebra finch Poephila guttata. The body of the finch is represented by a solid line with a star at one end denoting the position of the tip of the beak and a solid circle at the other denoting the tip of the tail. The trace of the beak is given by a solid line, the direction of movement being from left to right and indicated by arrows. The film speed was 500fps and body symbols represent the position of the finch at 20 frame intervals. The points of the beginning and end of the bound are indicated.

Figure 6.9b

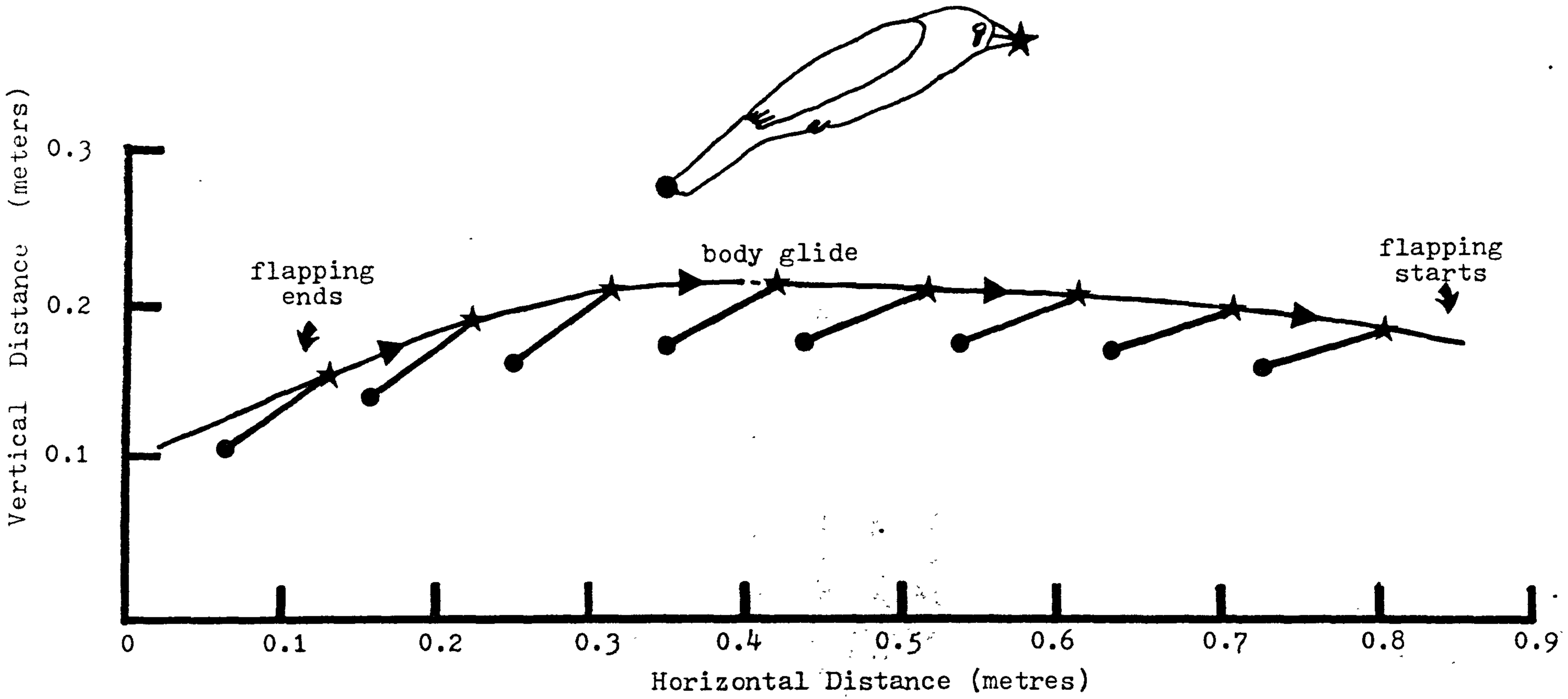
Vertical Distance (meters)
0.3
0.2
0.1
flapping ends
body glide
flapping starts
0
0.1
0.2
0.3
0.4
0.5
0.6
0.7
0.8
0.9
Horizontal Distance (metres)

6.4 Kinematic variation with morphology: An analysis by correlation

The variation of each kinematic parameter with morphology (body mass m, wing span b and area S) is investigated by first assuming that mass is the dominant feature of morphology; each kinematic parameter is then correlated with it to find the equation of the R.M.A. line (Chapter 5). Each kinematic parameter is then correlated with mass, span and area by multiple regression to find the degree to which it is affected by span and area.

6.4.1 Wing beat frequency f

Graph 6.1A shows f plotted against mass for all the data acquired in this survey, together with that found in the literature survey carried out by Rayner (in preparation b). The R.M.A. line gives f proportional to $m^{-0.353}$ (Table 6.4) which is close to $m^{-\frac{1}{3}}$. It can be seen that birds with high wing loadings, such as the Galliformes and Anseriformes, have high wing beat frequencies for their size, while birds with low wing loading, such as the Ciconiiformes and the gulls of the Charadriiformes have relatively lower wing beat frequencies. The Passeriformes have generally high wing beat frequencies, so possibly making the R.M.A. line steeper. The multiple regression (Table 6.5) gives a high product-moment correlation of 0.93, and it is interesting to note that frequency correlates better with span and

GRAPH 6.1A

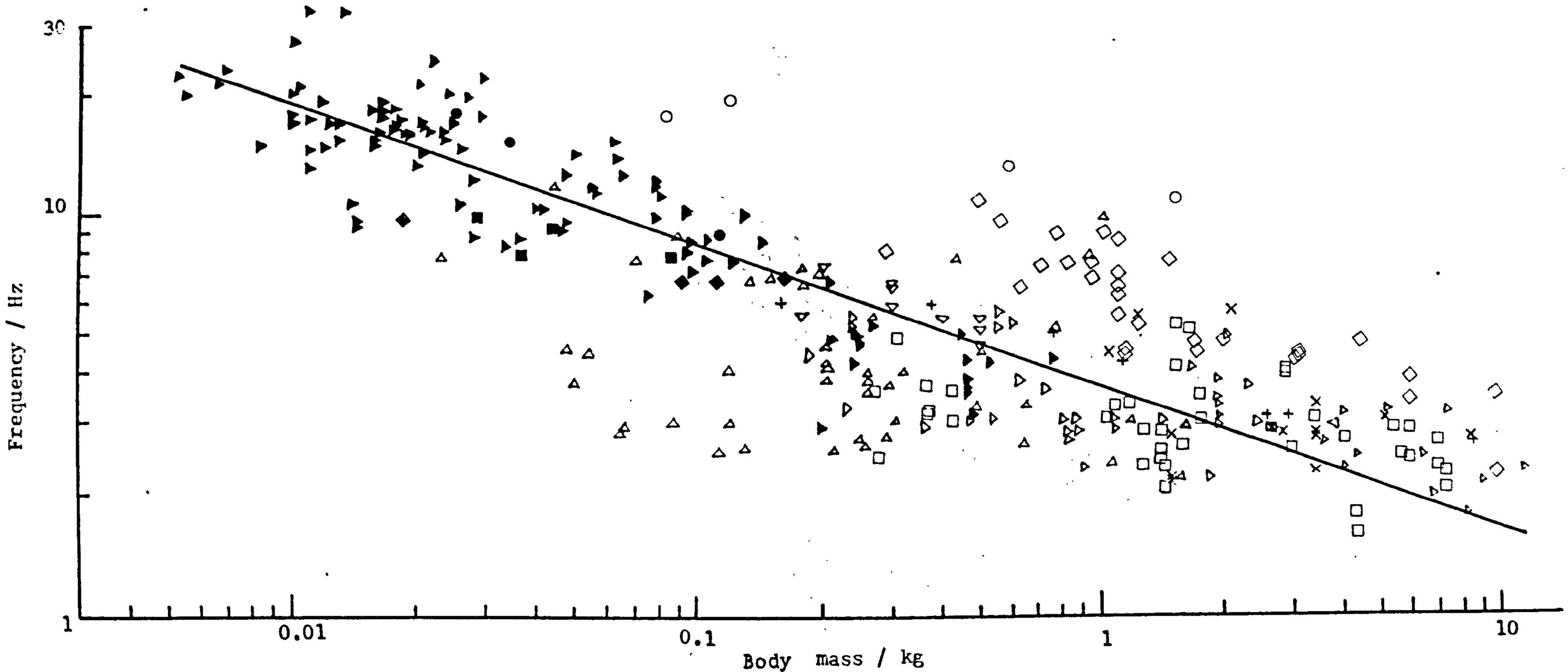

GRAPH 6.1A

Wing beat frequency f (Hz) and body mass m (kg) for all the data of this survey and that from the literature survey by Rayner (in preparation). The R.M.A. is shown and the symbols are as in Figure 6.1B. The equations are given in Table 6.4.

NOTE : Outer 'Group' symbols are not given.

GRAPH 6.1B

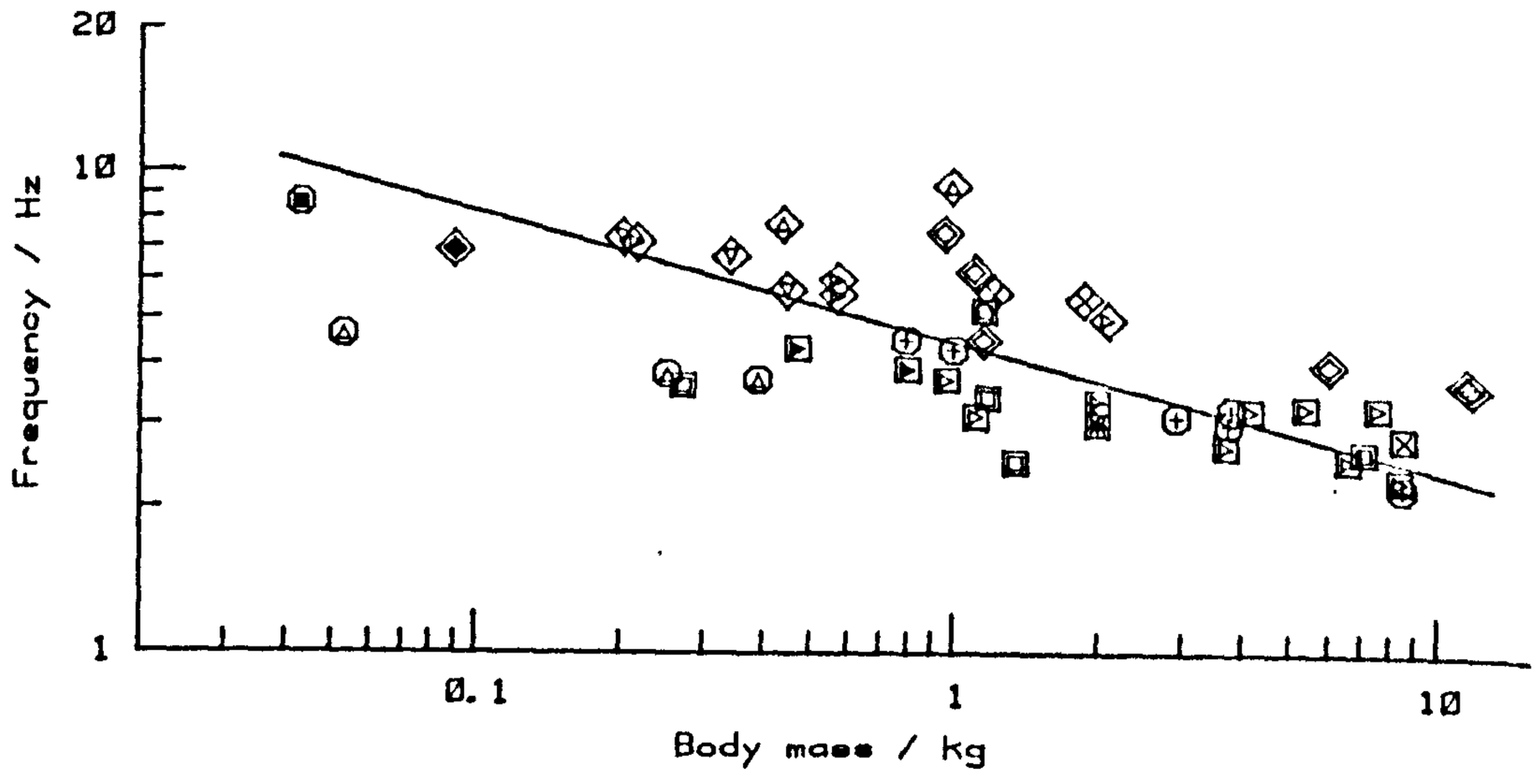

GRAPH 6.1C

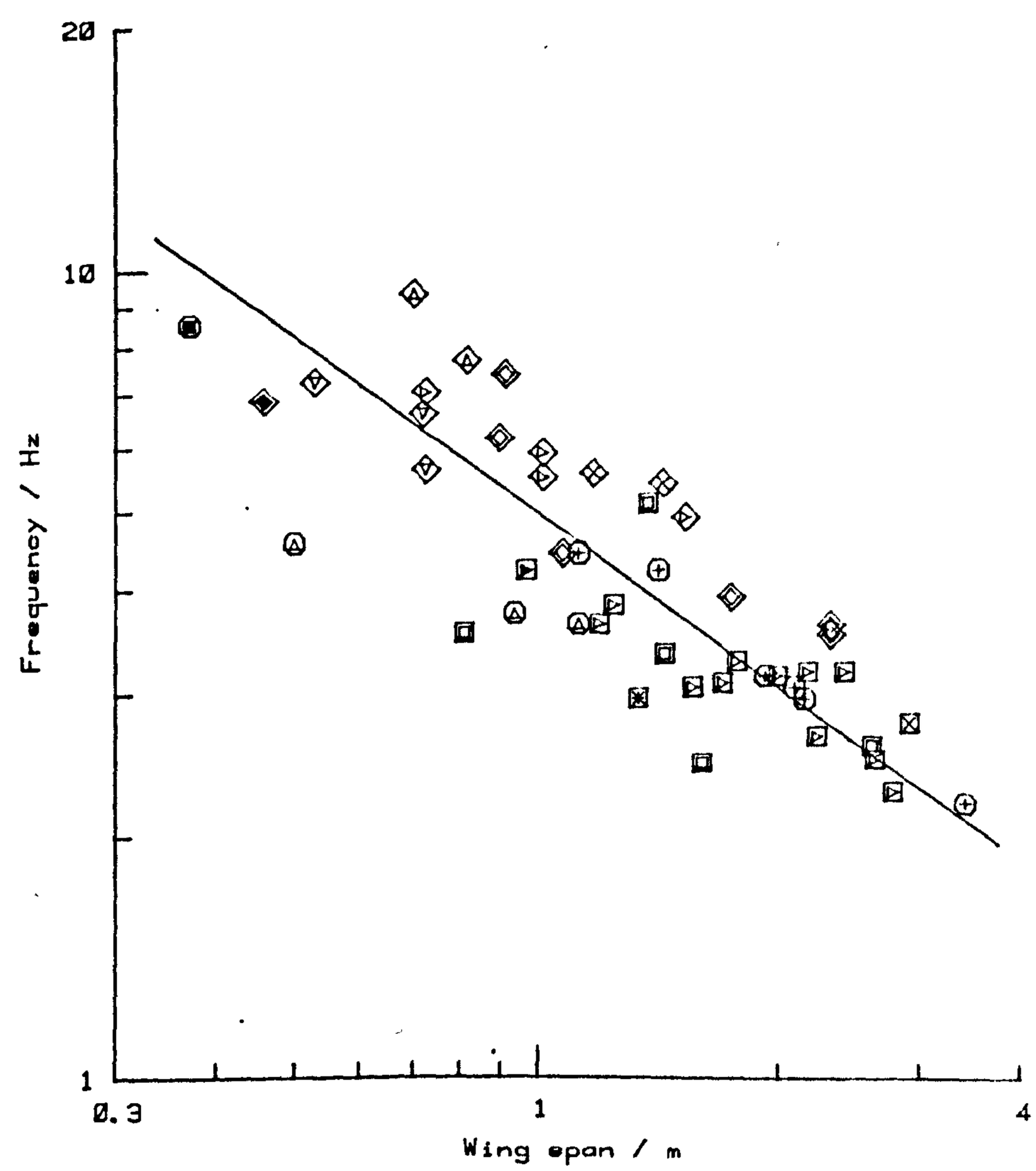

GRAPH 6.1B

Wing beat frequency f (Hz) and body mass m (kg) for the data of this survey. The R.M.A. is shown and the symbols are as in Figure 6.1B. The equations are qiven in Table 6.4.

GRAPH 6.1C

Wing beat frequency f (Hz) and wing span b (m) for the data of this survey. The R.M.A. is shown and the symbols are as in Figure 6.1C. The equations are given in Table 6.4.

area than does mass, the correlation coefficients being 0.89, 0.87 and 0.80 respectively.

Graph 6.1B (Table 6.4) shows only the data for this survey, and here f is proportional to $m^{-0.27}$. This shallower slope, when compared with that of Graph 6.1A, is largely due to the absence of the Passeriformes. The correlation coefficient is slightly lower than in Graph 6.1A. The multiple regression again shows that frequency is more dependent on wing span and area than mass, with respective coefficients of 0.83, 0.81 and 0.67 (Table 6.5). Graph 6.1C shows f against wing span, and the equation gives f proportional to $b^{-0.71}$, but with some scatter around the R.M.A. line, the correlation coefficient being only 0.83.

6.4.2 Downstroke ratio z

Graph 6.2A is of downstroke ratio z against body mass; it indicates a tendency for z to increase with mass as $m^{0.065}$. The multiple regression shows z to be slightly more dependent on mass and wing area than is span (correlation coefficients of 0.69, 0.66 and 0.61 respectively). There are two interesting observations to be made from Graph 6.2A; firstly, z does not begin to increase from 0.5 until body mass exceeds about 0.5kg and secondly, the Procellariiformes larger than 0.5kg are exceptional in that they show no trend to increase z as size increases.

Graph 6.2B is of z against body mass for birds

GRAPH 6.2A

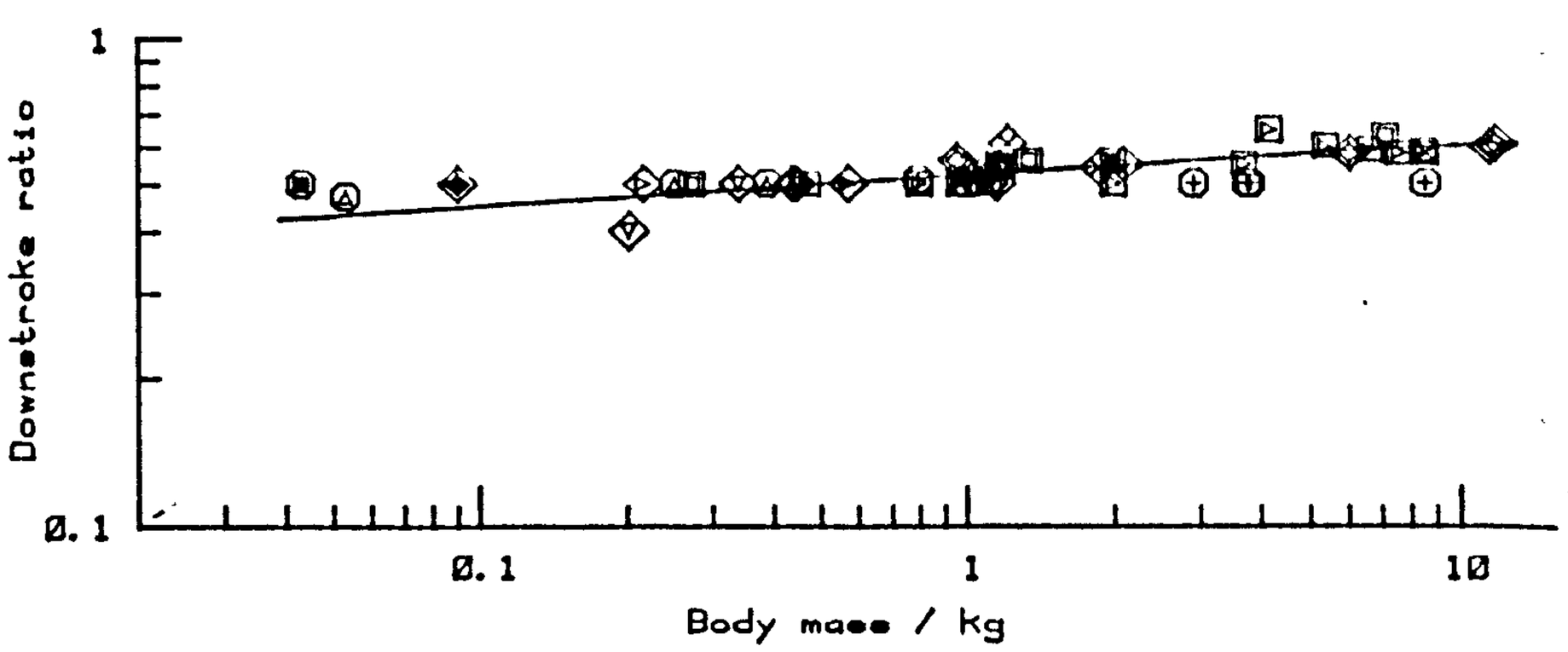

GRAPH 6.2B

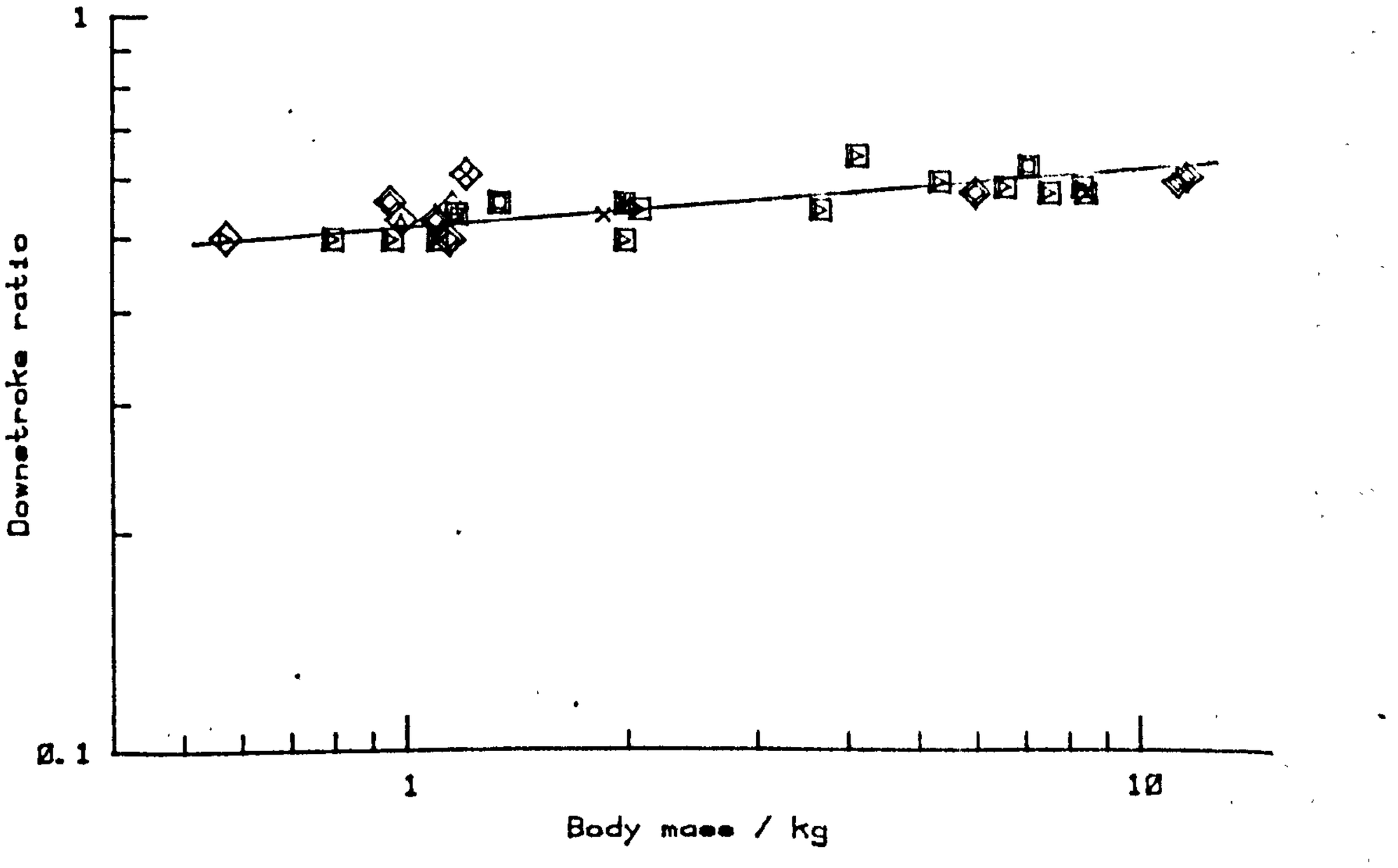

GRAPH 6.2A

Downstroke ratio τ and body mass m (kg) for all the data of this survey. The R.M.A. is shown and the symbols are as in Figure 6.1B. The equations are given in Table 6.4.

GRAPH 6.2B

Downstroke ratio τ and body mass m (kg) for birds greater than 0.5kg and excluding the Procellariiformes. The R.M.A. is shown and the symbols are as in Figure 6.1B. The equations are given in Table 6.4.

greater than 0.5kg excluding the Procellariiformes The correlation equation slope increases as $m^{0.082}$, and the correlation coefficient increases from 0.69 in Graph 6.2A to 0.76 in Graph 6.2B. The multiple regression now shows mass to be of the greatest importance in determining z, the correlation coefficient for mass being 0.76, while for span and area it is 0.62 and 0.60 respectively (Table 6.5).

6.4.3 Stroke amplitude Φ

Graph 6.3 is of amplitude against mass; it has a very low correlation coefficient of-0.49, but does indicate a trend for amplitude to decrease with mass, being proportional to $m^{-0.12}$ (Table 6.4). The multiple regression has a very low product-moment correlation of 0.66, and indicates that amplitude is slightly more dependent on mass and span than on area. It can be clearly seen from Graph 6.3 that Group A birds, particularly those above 1kg, have considerably higher amplitudes than Group C birds, with those of Group B birds being intermediate.

6.4.4 .Stroke plane angle γ

The R.M.A. line for stroke plane angle against body mass (Graph 6.4) gives γ proportional to $m^{-0.062}$ with a low correlation coefficient of -0.41. Stroke plane angle also correlates poorly with span and area, the coefficients being 0.41 and 0.53 respectively. It

GRAPH 6.3

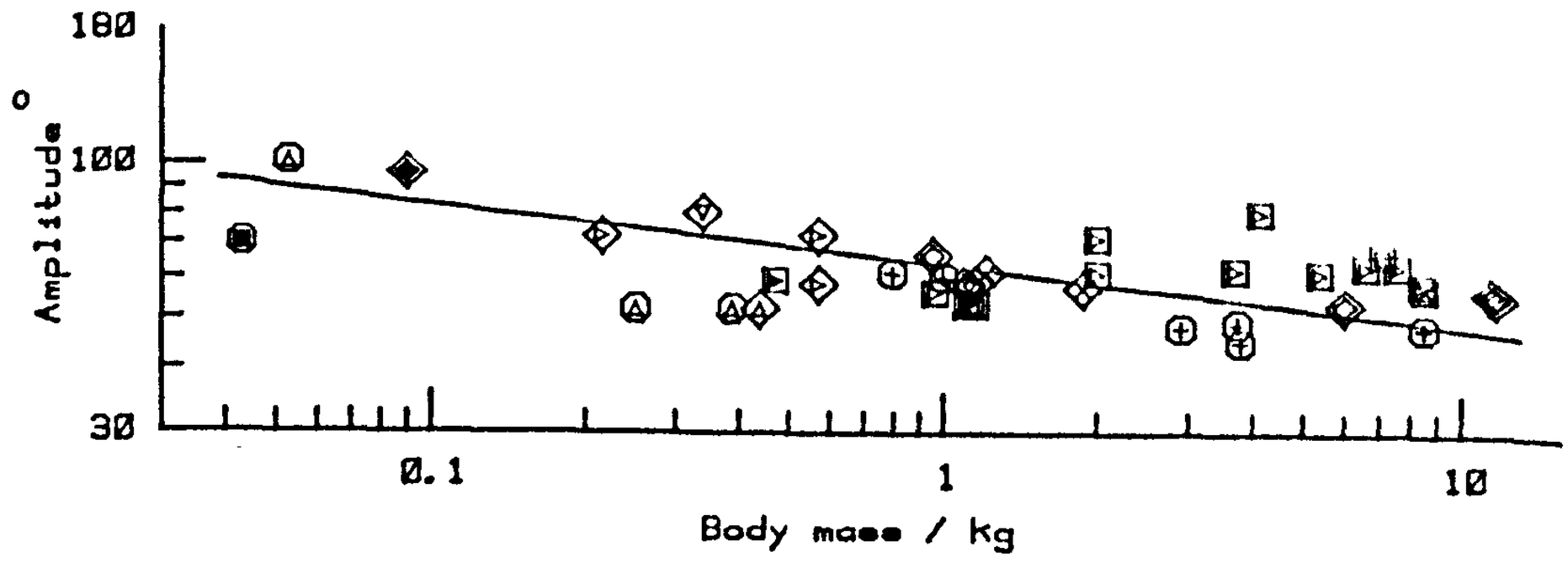

GRAPH 6.4

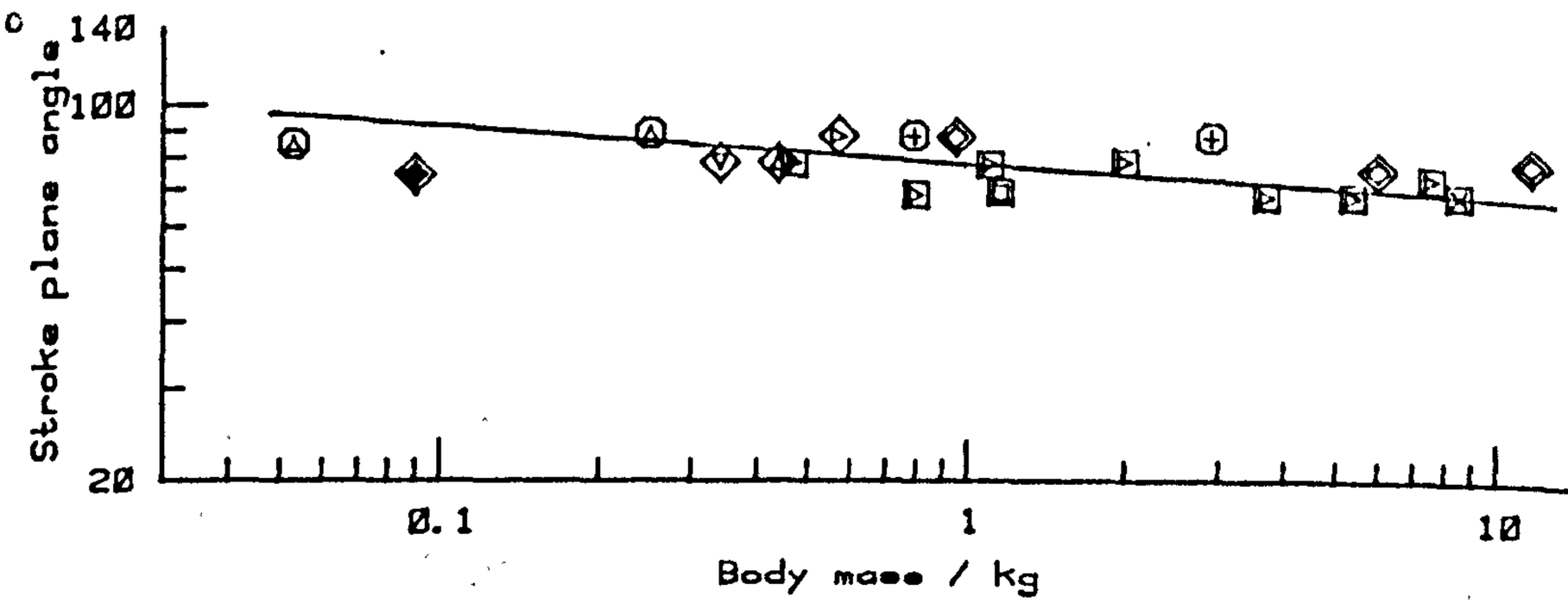

GRAPH 6.3

Stroke amplitude Φ (degrees) and body mass m (kg). The R.M.A. is shown and the symbols are as in Figure 6.1B. The equations are given in Table 6.4.

GRAPH 6.4

Stroke plane angle γ (degrees) and body mass m (kg). The R.M.A. is shown and the symbols are as in Figure 6.1B. The equations are given in Table 6.4.

appears that Group A birds tend to have slightly shallower (i.e. nearer to the horizontal) angles than do those of Group C. This analysis shows that there is little alteration of δ with increasing size (δ proportional to m^{o}), but alterations in aspect ratio may have some effect, the higher the aspect ratio the steeper the stroke plane.

6.4.5 Wing tip downstroke velocity V_{wt}

Graph 6.5 is of calculated mean downstroke velocity (Chapter 5) against body mass; it gives an R.M.A. line with a slope of 0.14 and a low correlation coefficient of 0.53 . Span and area have poorer correlation coefficients of 0.43 and 0.47 respectively. The measurements of peak downstroke velocity are displayed in a similar manner in Graph 6.6; although the intercept of the line is higher, the slope of the R.M.A. line is similar at 0.165 with a correlation coefficient of 0.70 . The correlation with span and area is higher for peak downstroke velocity, the values being 0.66 and 0.69 respectively. The lanner falcon Falco biarmicus and the lagger falcon Falco jugger have exceptionally high downstroke velocities. On Graph 6.6 there is little scatter from the R.M.A. line, and so the peak wing tip velocity of birds of the same mass are similar, regardless of their aspect ratio.

GRAPH 6.5

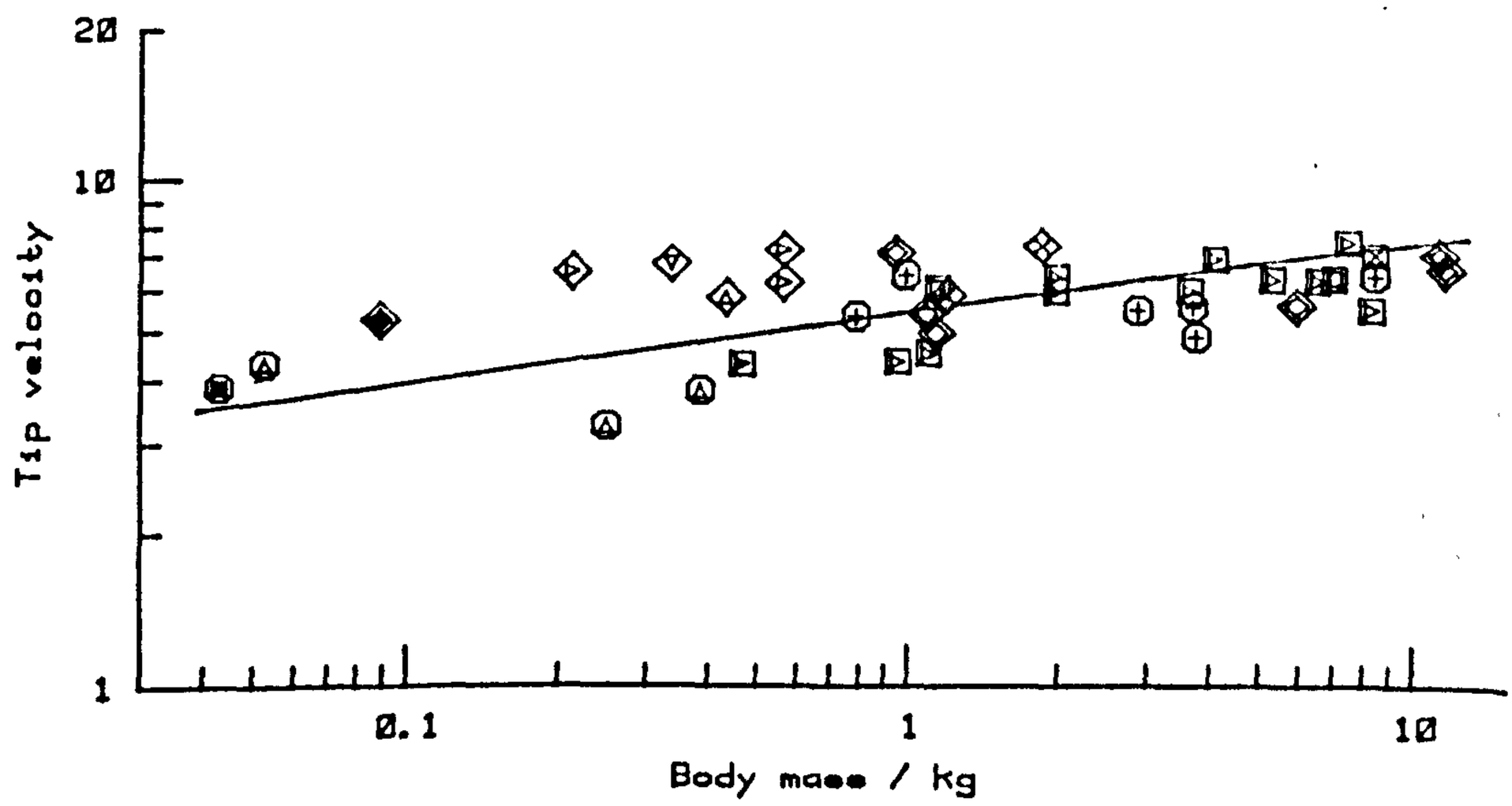

GRAPH 6.6

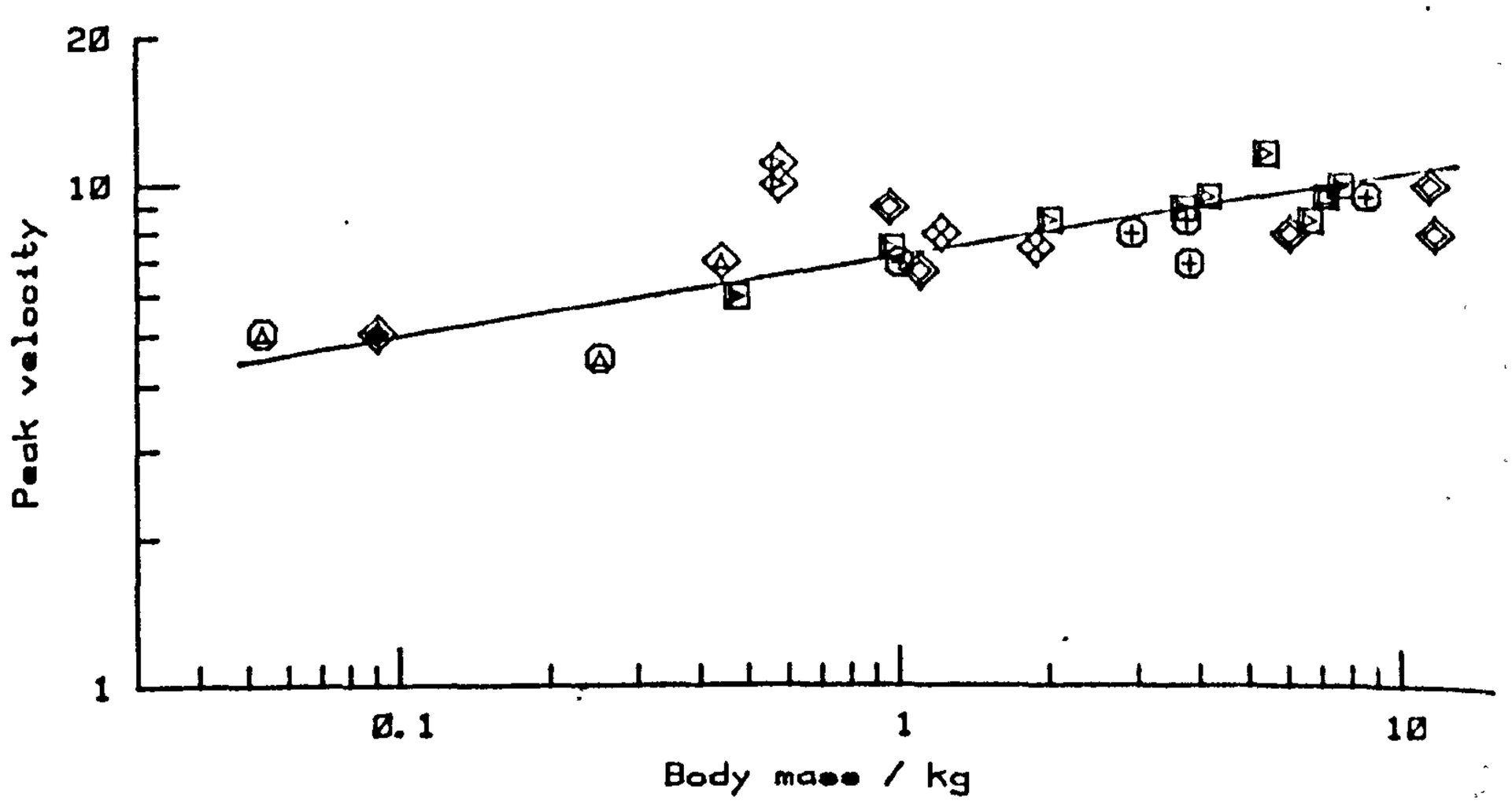

GRAPH 6.5

Mean wingtip downstroke velocity ('tip velocity') (m s^{-1}) and body mass m (kg). The R.M.A. is shown and the symbols are as in Figure 6.1B. The equations are given in Table 6.4.

GRAPH 6.6

Measured peak wingtip downstroke velocity ('peak velocity') (m s^{-1}) and body mass m (kg). The R.M.A. is shown and the symbols are as in Figure 6.1B. The equations are given in Table 6.4.

TABLE 6.4 Equations for Graphs 6.1A to 6.6

		n	r	F	α	β	$\alpha-$	$\alpha+$	$\beta-$	$\beta+$	Graph
FREQUENCY (Hz) AND	Y(X)	343	-0.829***	751	4.06	-0.293	3.87	4.26	-0.314	-0.272	6.1A
BODY MASS (Kg) (ALL DATA)	RMA				3.78	-0.353	3.60	3.97	-0.374	-0.332	
FREQUENCY (Hz) AND	Y(X)	47	-0.671***	36.9	4.38	-0.182	4.02	4.75	-0.242	-0.122	6.1B
BODY MASS (Kg) (KDS DATA)	RMA				4.46	-0.271	4.07	4.89	-0.331	-0.210	
FREQUENCY (Hz) AND	Y(X)	47	-0.828***	98.3	4.91	-0.589	4.58	5.27	-0.709	-0.469	6.1C
WING SPAN (m)	RMA				5.08	-0.711	4.72	5.46	-0.831	-0.592	
DOWNSTROKE RATIO	Y(X)	47	0.688***	40.4	0.525	0.0447	0.514	0.535	0.0306	0.0589	6.2A
AND MASS (Kg)	RMA				0.522	0.0650	0.511	0.534	0.0508	0.0792	
DOWNSTROKE RATIO	Y(X)	29	0.760***	36.8	0.527	0.0620	0.513	0.541	0.0410	0.0829	6.2B
AND MASS (Kg)[1]	RMA				0.519	0.0816	0.505	0.533	0.0606	0.103	
AMPLITUDE (Degrees)	Y(X)	38	-0.491***	11.4	61.9	-0.0587	58.7	65.3	-0.0938	-0.0235	6.3
AND BODY MASS (Kg)	RMA				63.3	-0.119	59.5	67.2	-0.155	-0.0843	
STROKE PLANE ANGLE (Degrees)	Y(X)	20	-0.414*	3.73	79.9	-0.0258	76.7	83.3	-0.0540	-0.00228	6.4
AND BODY MASS (Kg)	RMA				80.3	-0.0624	76.5	84.4	-0.0905	-0.0342	

1. Birds larger than 0.5kg, excluding Procelariiformes

TABLE 6.4 continued

MEAN WING TIP VELOCITY ($m\ s^{-1}$) AND BODY MASS (kg)	Y(X)	38	0.529***	14.0	5.53	0.0718	5.22	5.87	0.0329	0.111	6.5
	RMA				5.41	0.136	5.06	5.78	0.0967	0.174	
MEASURED PEAK WING TIP VELOCITY ($m\ s^{-1}$) AND BODY MASS (kg)	Y(X)	27	0.699***	23.9	7.45	0.115	6.92	8.01	0.0669	0.164	6.6
	RMA				7.24	0.165	6.69	7.84	0.117	0.214	-

TABLE 6.5 Multiple Regression of Kinematic Features with Body Mass, Wing Span and Wing Area.

	N	PMC	F	r			α	β		
				m(kg)	b(m)	$S(m^2)$		m(kg)	b(m)	$S(m^2)$
FREQUENCY(Hz) (ALL DATA)	143	0.930	297.6	-0.796	-0.893	-0.871	3.47	0.361	-1.219	-0.233
FREQUENCY(Hz) (KDS DATA)	47	0.905	65.2	-0.671	-0.828	-0.813	3.86	0.310	-1.01	-0.177
DOWNSTROKE RATIO	47	0.745	17.9	0.688	0.613	0.656	0.642	0.0547	-0.211	0.0916
DOWNSTROKE RATIO 0.5kg NO PROCELARIFORMES	29	0.772	12.3	0.760	0.624	0.605	0.581	0.0827	-0.145	0.0422
AMPLITUDE (Degrees)	38	0.664	8.96	-0.491	-0.517	-0.404	115.6	-0.0427	-0.612	-0.279
STROKE PLANE ANGLE (Degrees)	20	0.713	5.52	-0.414	-0.413	-0.535	51.4	0.0141	0.326	-0.215

Table 6.5 cont.

				r			α	β		
	n	PMC	F	m(kg)	b(m)	$S(m^2)$		m(kg)	b(m)	$S(m^2)$
Mean wing tip velocity ($m\ s^{-1}$)	38	0.606	6.58	0.529	0.432	0.474	7.18	0.181	-0.491	0.0895
Measured peak wing tip velocity ($m\ s^{-1}$)	27	0.716	8.06	0.699	0.659	0.694	9.67	0.0992	-0.20	0.123

6.5 The variation of a kinematic parameter with morphology, flying speed and remaining kinematics: An aerodynamic approach

In this section one kinematic parameter, that of wing beat frequency f, is taken and its variation with flying speed, morphology and kinematics investigated. This is done by using the Pennycuick (1978) prediction of frequency which accounts for morphology, lift coefficients and flying speeds, and then using a Rayner modification of Pennycuick's prediction which includes downstroke ratio and amplitude.

6.5.1 The Pennycuick prediction

Pennycuick (1975) derives the angular velocity of a bird's wing in cruise flight as

$$\omega^2 = 24\left(\frac{F - \tfrac{1}{2}\rho V^2 S C_L}{\rho C_L S^2 \Lambda}\right), \qquad (6.1)$$

where ρ is the air density, v is air speed, S is the wing area, Λ is the aspect ratio, C_L is the lift coefficient and F is the total force on the wing. He assumes that the wing sweeps through an angle of $\frac{1}{2}\pi$ radians at a constant angular velocity and that the downstroke always occupies two-thirds of the wing beat cycle, and so

$$f = \frac{4\omega}{3\pi} \qquad (6.2)$$

During the downstroke the total force F must support the weight and overcome parasite drag, weight alone being balanced throughout the cycle, so

$$F^2 = W^2 + \left[1.5\left(\tfrac{1}{2}\rho A V^2\right)\right]^2 , \qquad (6.3)$$

where A is the equivalent flat plate area of the body. Frequency can be expressed as

$$f^2 = \left(\frac{4}{3\pi}\right)^2 \frac{24}{\rho C_L S^2 N}\left\{\left[W^2 + \left(\frac{1.5\rho A V^2}{2}\right)^2\right]^{\frac{1}{2}} - \tfrac{1}{2}\rho V^2 S C_L\right\}, \qquad (6.4)$$

and velocity can be given in terms of the stalling speed V_s as $V/V_s = \varphi$ where

$$V_s^2 = \frac{2W}{\rho S C_{L_o}} , \qquad (6.5)$$

W being the weight and C_{L_o} the lift coefficient before stalling. Frequency is therefore given as

$$f^2 = \frac{4.32 W}{\rho S^2 N}\left\{\frac{1}{C_L}\left[1 + \left(\frac{1.5\varphi^2}{C_{L_o}}\frac{A}{S}\right)^2\right]^{\frac{1}{2}} - \frac{\varphi^2}{C_{L_o}}\right\} . \qquad (6.6)$$

Now for the range of birds considered here

$$\left[1+\left(\frac{1.5\,\varphi^2}{C_{L_o}}\,\frac{A}{S}\right)^2\right]^{1/2} = k \simeq 1 \qquad (6.7)$$

Since C_{L_o} is taken as 1.6 (Pennycuick, 1978), the right hand side of the expression is very small in magnitude, and so Equation (6.6) can be given as

$$f^2 = \frac{4.32\,W}{\rho S^2 \lambda}\,Q\,, \qquad (6.8)$$

where

$$Q = \frac{k}{C_L} - \frac{\varphi^2}{C_{L_o}}\,. \qquad (6.9)$$

Pennycuick (1978) assumes that C_L, C_{L_o} and φ remain constant and gives them suitable values. Here, Q is left as a variable. In this investigation I am not concerned that the absolute values of Pennycuick's prediction are correct, but am interested in finding out how each variable affects frequency.

Graph 6.7 is a plot of a double logarithmic scale of wing beat frequency against W/S^2, and it can be seen

GRAPH 6.7

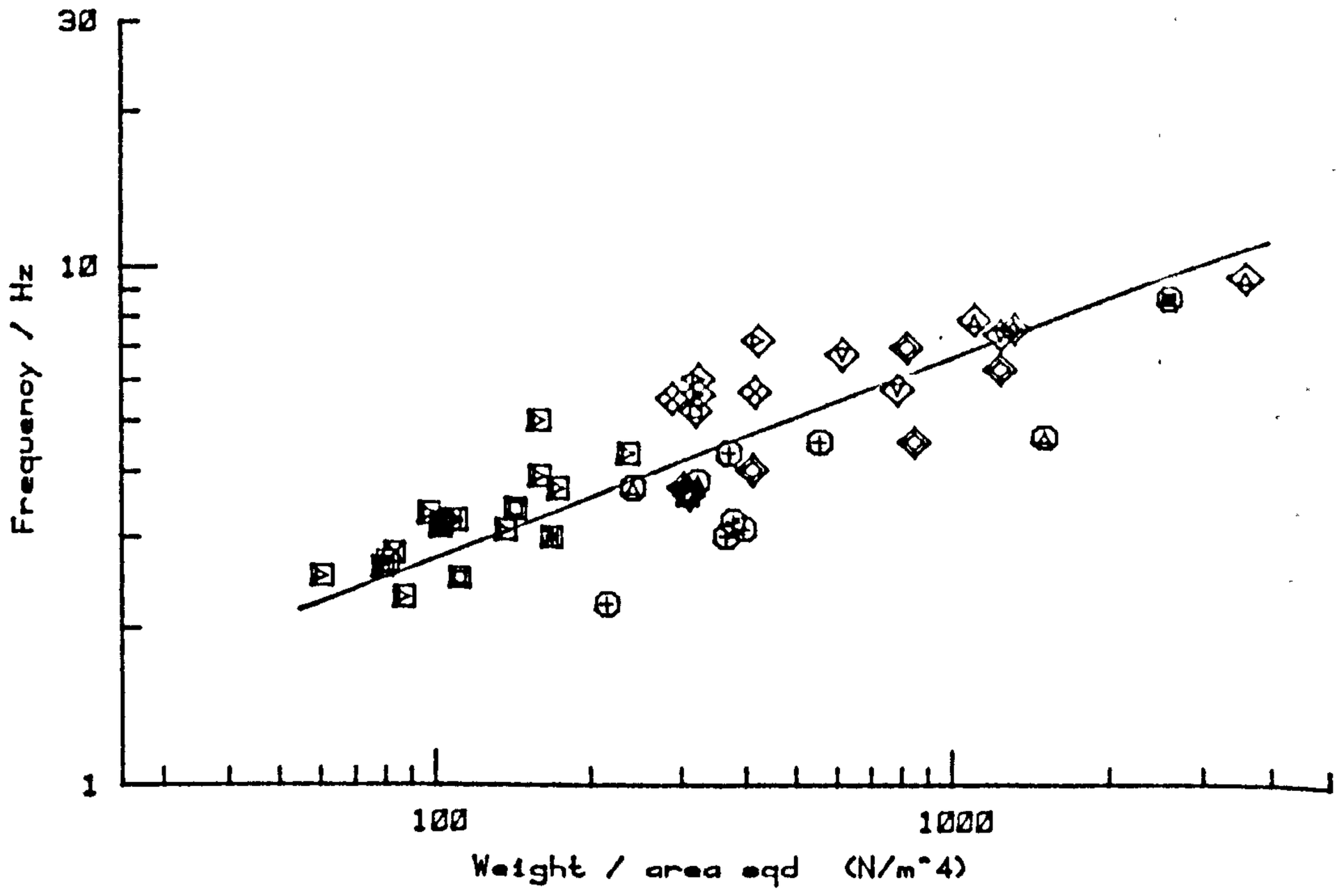

GRAPH 6.8

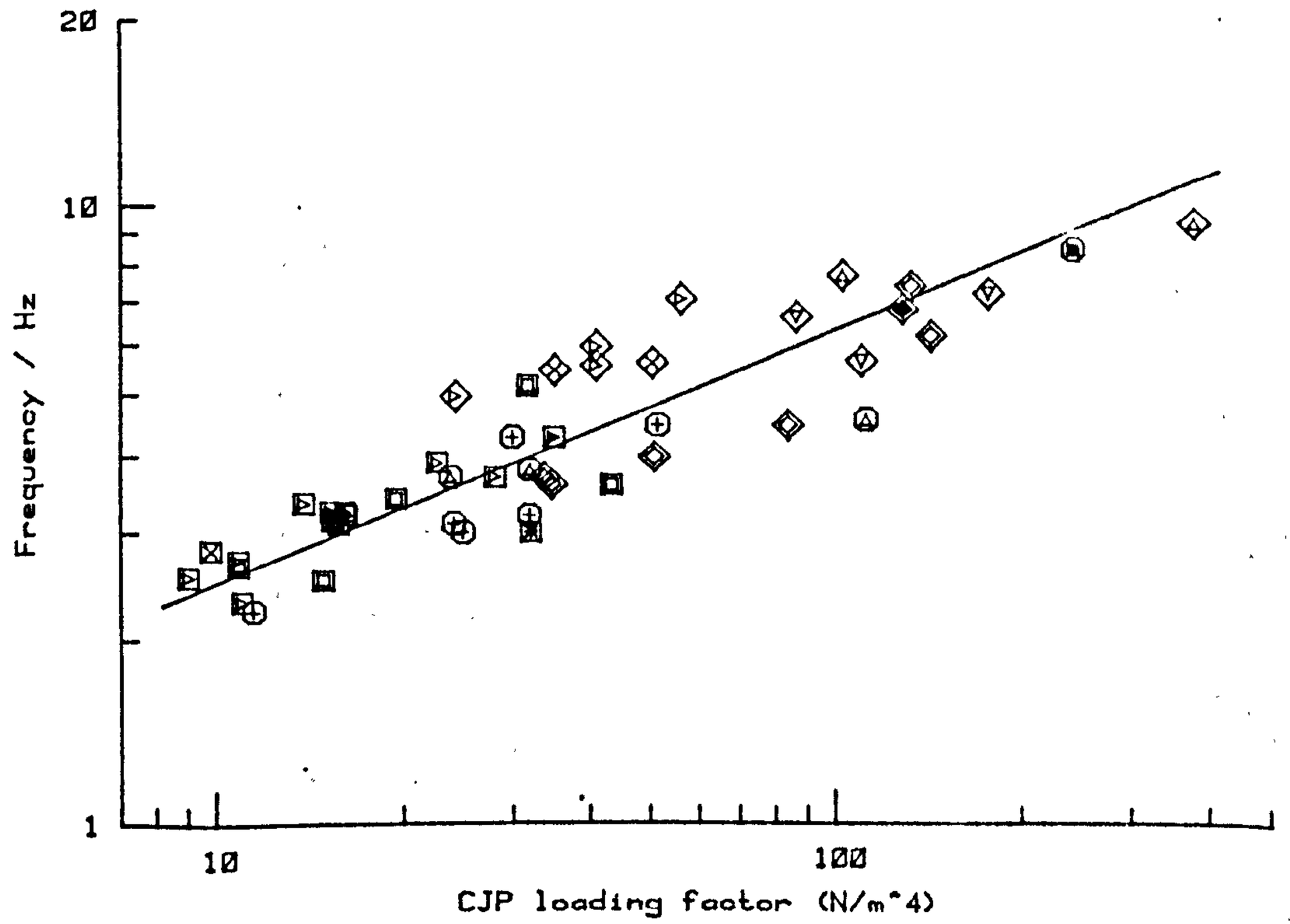

GRAPH 6.7

Wing beat frequency f (Hz) and body weight/ wing area squared mg/S^2 (N/m^4). The R.M.A. is shown and the symbols are as in Figure 6.1B. The equations are given in Table 6.6.

GRAPH 6.8

Wing beat frequency f (Hz) and body weight/ wing area squared * aspect ratio ('CJP loading factor') $mg/S^2\mathcal{W}$ (N/m^4). The R.M.A. is shown and the symbols are as in Figure 6.1B. The equations are given in Table 6.6.

that, as Pennycuick (1978) predicted, the birds of each aspect ratio range (Groups A, B and C) broadly fall on separate, near parallel lines. Increasing aspect ratio decreases the wing beat frequency. If frequency is only determined by body mass, wing span and area with Q remaining constant, as Pennycuick assumes, then all the points should be on the same line in Graph 6.8 of f against $W/S^2\nu$ (on logarithmic scales) and the slope of the line should be 0.5 . This is clearly not the case as there is a fairly low correlation coefficient of 0.84 (Table 6.5) and some scatter about the R.M.A. The R.M.A. slope is 0.41, significantly different from 0.5 which indicates either variation in Q or variations in the kinematics with $W/S^2\nu$ or both.

6.5.2 A modification including amplitude and downstroke ratio

The above argument can be extended to incorporate the downstroke ratio z and the amplitude ϕ as independent variables (Rayner, personal communication).

The angular velocities of the upstroke ω_u and downstroke ω_d can be expressed as

$$\omega_u = \frac{2\phi f}{1-z} \quad , \qquad (6.10)$$

$$\omega_d = \frac{2\phi f}{z} \quad , \qquad (6.11)$$

for respective values of C_{L_u} and C_{L_d}

If it is assumed that lift is only generated during the downstroke as in Rayner (1979a,b) then

$$\omega_d^2 = 24\left(\frac{2L_d - \frac{1}{2}\rho V^2 S C_{L_d}}{\rho C_{L_d} S^2 \Lambda}\right) , \qquad (6.12)$$

where L_d is the total lift generated on the downstroke, and so

$$f^2 = \frac{6z^2}{Q^2} \frac{W}{\rho S^2 \Lambda} \left(\frac{k}{z C_{L_d}} - \frac{\varphi^2}{C_{L_o}}\right) . \qquad (6.13)$$

If lift is equally developed during the upstroke then

$$f^2 = \frac{6z(1-z)}{Q^2} \frac{W}{\rho S^2 \Lambda} \left(\frac{k}{C_L} - \frac{\varphi^2}{C_{L_o}}\right) . \qquad (6.14)$$

(full derivations are given in the appendix)

The effects of the kinematics on wing beat frequency can now be included. In Section 4.2 it was shown that z systematically increased with body masses above 0.5kg for all birds other than those with very high aspect ratios. This trend could account for the variation in Graph 6.8., and so in Graph 6.9 amplitude is assumed

to be constant and f is plotted against $\tau^2 W/S^2\Lambda$ in the previous manner. It can be seen that Groups A and C become condensed for low values of $\tau^2 W/S^2\Lambda$ and the slope increases to 0.44 . In Graph 6.10 amplitude Q is accounted for with f being plotted logarithmically with $\tau^2 W/S^2\Lambda Q^2$. Here, as opposed to improving the correlation coefficient and the level of significance, this modification reduces both dramatically (Table 6.6). The slope of the R.M.A. line is increased to 0.49 however, being closer to Pennycuick's prediction of 0.5 . Closer consideration of Graph.6.10 shows that the different aspect ratio groups A, B and C fall approximately into separate near parallel lines, reminiscent of Graph 6.7 . There are, however, definite exceptions, for example the Anseriformes. As morphology and wing beat kinematics have now been accounted for, deviations from the mean regression line must be due to variations in Q_d where

$$Q_d = \left(\frac{h}{\tau C_{L_d}} - \frac{\psi^2}{C_{L_o}}\right) \quad . \qquad (6.15)$$

Graph 6.11 is a plot of Q_d' against aspect ratio where Q_d' is given by

$$Q_d' = \frac{\beta^2}{\tau^2 W/S^2\Lambda Q^2} \qquad (6.16)$$

GRAPH 6.9

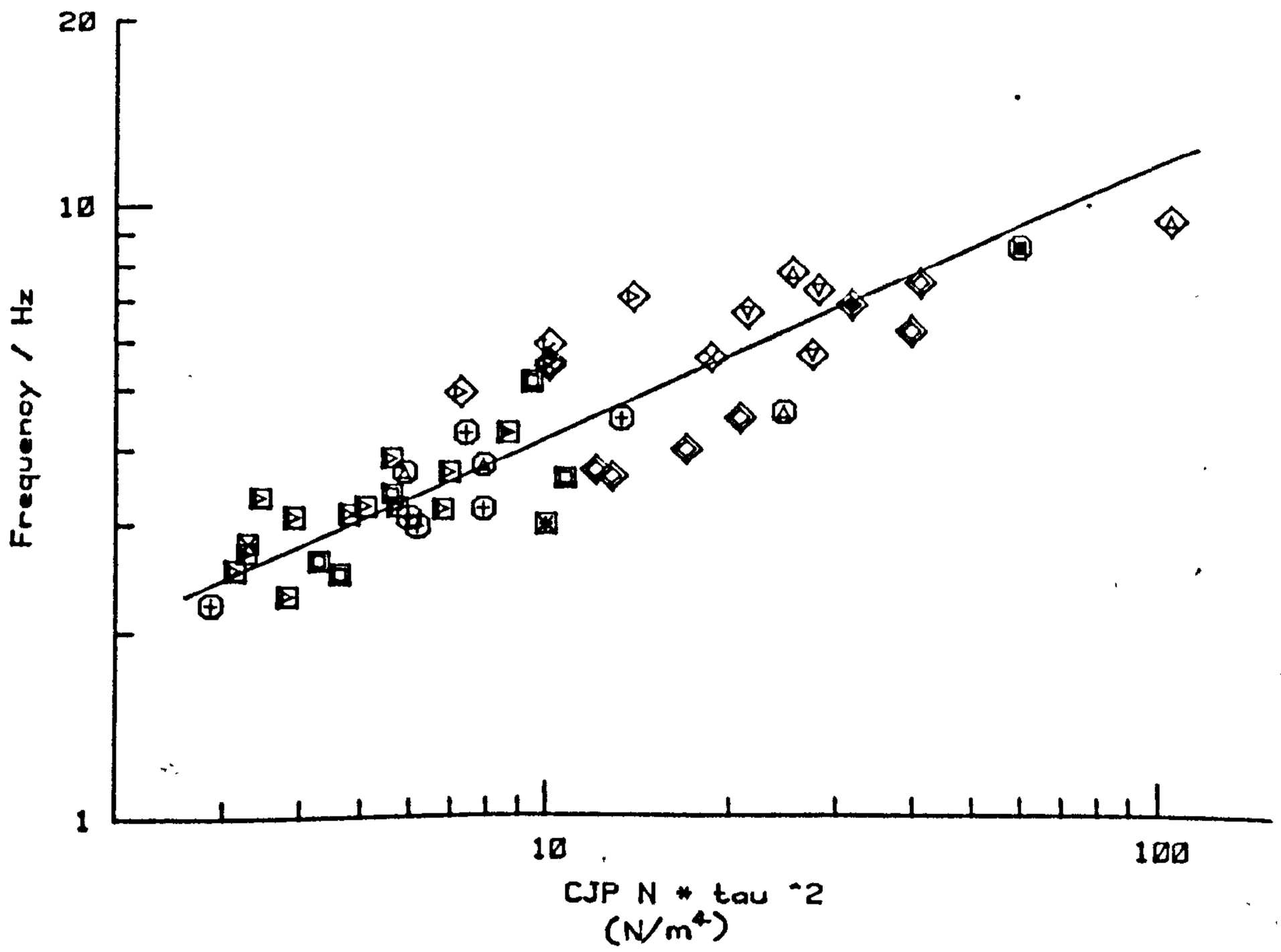

GRAPH 6.10

GRAPH 6.11

Q_d' and aspect ratio $\sqrt{\nu}$ where,

$Q_d' = f^2/(\varepsilon^2 mg/S^2\sqrt{\nu}\,Q^2)$. The R.M.A. is shown and the symbols are as in Figure 6.1B. The equations are given in Table 6.6.

GRAPH 6.11

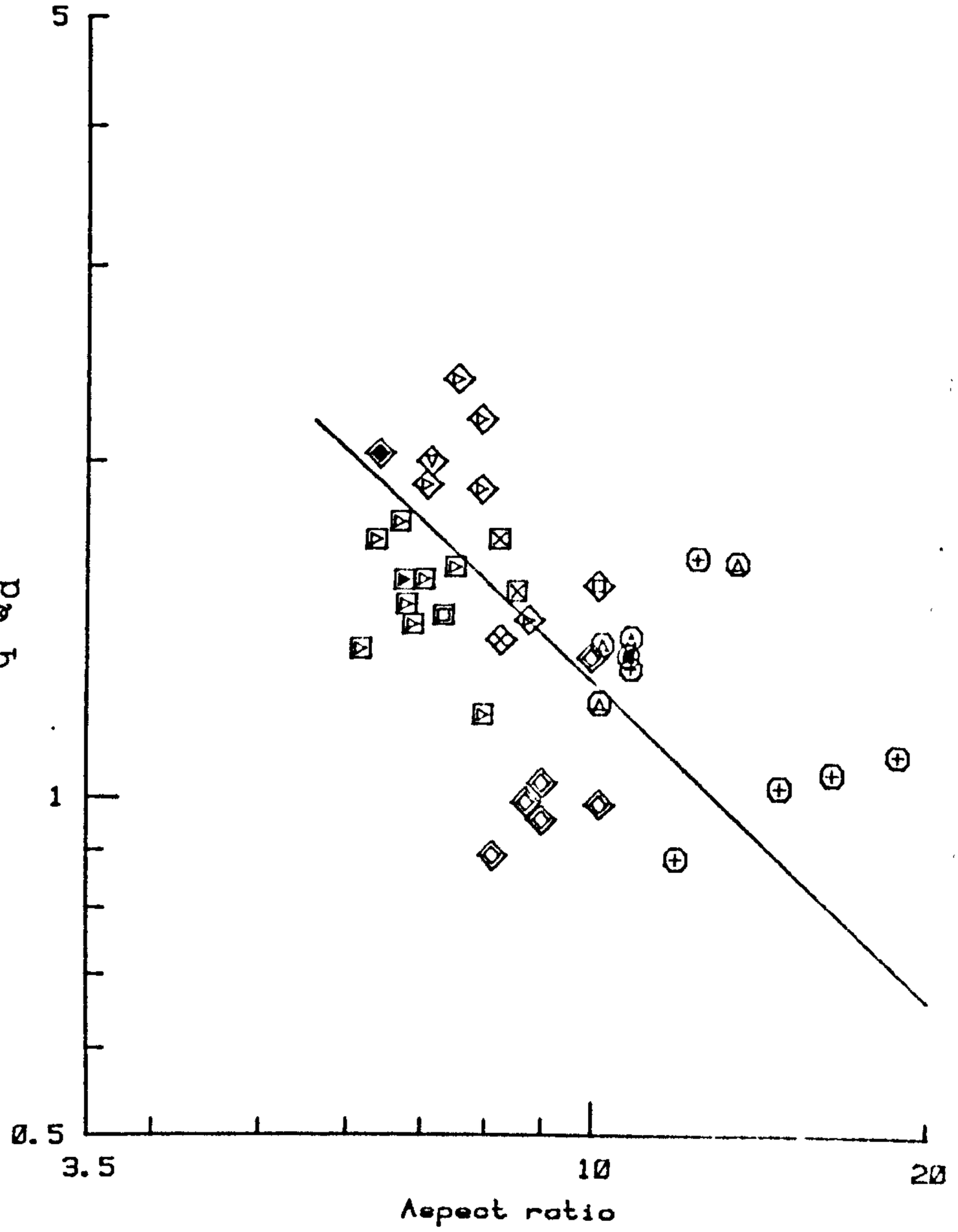

GRAPH 6.11

Q_d' and aspect ratio $\sqrt{\nu}$ where, $Q_d' = f^2/(\varepsilon^2 mg/S^2\sqrt{\nu}\,Q^2)$. The R.M.A. is shown and the symbols are as in Figure 6.1B. The equations are given in Table 6.6.

and although there is a very large degree of scatter with the correlation coefficient as only -0.49, it can be seen that Q_d' tends to decrease with aspect ratio, being proportional to $\Lambda^{-0.93}$. This scatter is not surprising since variations in Q_d' can be caused by variations in C_L, z , C_{L_o} and ϕ .

Rayner (1979a) gives a method for calculating average lift coefficients in cruise flight, assuming that lift is only generated during the downstroke. To emphasise that this is a calculated mean and may not be similar to the actual lift coefficients C_L of the wing it is given by the symbol Γ_L . (Rayner, personal communication).

The value of Γ_L is calculated for each bird flying at its maximum range speed V_{mr}, and Graph 6.12 shows these Γ_L values plotted logarithmically against aspect ratio. This gives a significant correlation coefficient of 0.88 and shows Γ_L to be proportional to $\Lambda^{0.78}$. This dependence of Γ_L upon aspect ratio accounts for the general trend towards a decrease in Q_d' with Λ. It is interesting to note that values for the Anseriformes fall well above the mean regression line, indicating the use of abnormally high lift coefficients in cruise flight. This may be because Graph 6.12 does not account for variations in individuals' flying speeds relative to their specific power curves.

Table 6.7 lists the birds for which the flying speeds were estimated for the same flights for which the

GRAPH 6.12

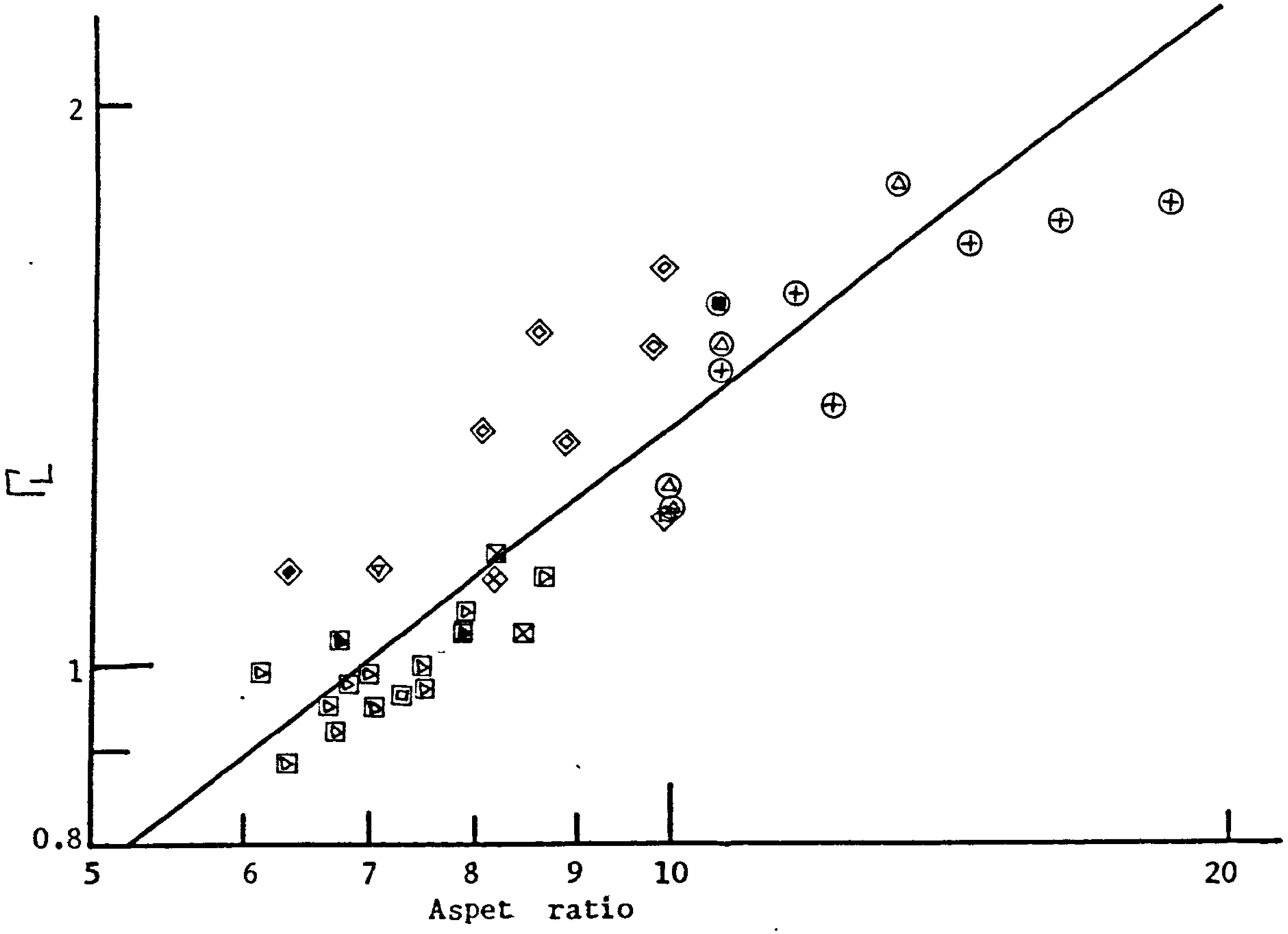

GRAPH 6.12

Calculated mean lift coefficient $\bar{C}_L$ and wing aspect ratio $\sqrt{\nu}$. The R.M.A. is shown and the symbols are as in Figure 6.1B. The equations are given in Table 6.6.

TABLE 6.6 Equations for Graphs 6.7 to 6.12

		n	r	F	α	β	$\alpha-$	$\alpha+$	$\beta-$	$\beta+$	Graph No.
f and W/S^2	Y(X)	47	***	96.63	0.684	0.316	0.470	0.990	0.251	0.381	6.7
	RMA		0.826		0.467	0.383	0.321	0.681	0.318	0.448	
f and $W/S^2\sqrt{\nu}$	Y(X)	47	***	176	1.12	0.368	0.914	1.38	0.312	0.423	6.8
	RMA		0.893		0.958	0.412	0.780	1.18	0.356	0.467	
f and $W\tau^2/S^2\sqrt{\nu}$	Y(X)	47	***	153	1.70	0.391	1.45	1.98	0.327	0.454	6.9
	RMA		0.879		1.50	0.444	1.28	1.75	0.381	0.508	
f and $W\tau^2/S^2\sqrt{\nu}\,Q^2$	Y(X)	38	***	52.0	1.85	0.374	1.46	2.35	0.270	0.479	6.10
	RMA		0.769		1.46	0.487	1.15	1.85	0.381	0.592	
$f^2/[W\tau^2/S^2\sqrt{\nu}\,Q^2]$ AND $\sqrt{\nu}$	Y(X)	38	***	11.6	3.88	-0.461	2.12	7.11	-0.735	-0.187	6.11
	RMA		-0.494		10.9	-0.932	5.96	20.0	-1.21	-0.659	
Γ_L and $\sqrt{\nu}$	Y(X)	38	***	126.7	0.268	0.687	0.204	0.353	0.564	0.811	6.12
	RMA		0.882		0.219	0.779	0.167	0.288	0.655	0.903	

Table 6.7

Measured flight speeds and calculated V_{mp} and V_{mr}.

Species	Measured V ($m\ s^{-1}$)	Cal V_{mp} ($m\ s^{-1}$)	Cal V_{mr} ($m\ s^{-1}$)
Lappet faced vulture *Aegypius tracheliotus*	12	12	19
Ruppell's griffon vulture *Gyps ruppellii*	12	13	21
Hooded vulture *Neophron monachus*	11	10	16
Marabou stork *Leptoptilus crumeniferus*	14	12	20
Kestrel *Falco tinnunculus*	8	7	12
Lagger falcon *Falco jugger*	13	9	14
Bewick swan *Cygnus columbianus*	14	14	23
Mallard *Anus platyrhynchos*	19	11	18
Pintail *Anus acuta*	16	11	17
White necked cormorant *Phalacrocorax carbo*	14	13	21
Common gull *Larus canus*	8	7	12

the kinematics were also analysed (Chapter 5). The calculated values of V_{mp} and V_{mr} from Rayner's simplified power model are also given. It can be seen that the majority of these birds are flying at about V_{mp}, with the Anseriformes being largely an exception.

The density of air was assumed to be 1.22kg m^{-3} in the calculation of C_L. For some of the species filmed in East Africa, at altitudes of 1000m or more, the density of the air would have been less, in the region of 1.05 to 1.1kg m^{-3}. However, there is no systematic variation of the C_L values of these African birds from the rest. It is likely that reductions in air density result in an increase in cruise flying speed with the kinematics and C_L remaining the same. This, however, warrants further controlled investigation.

6.6 Discussion

6.6.1 The allometric analysis

The allometric analysis of the kinematic data permits the testing of some of the predictions on how angular velocity of the wing ω scales with body mass m. It has been predicted that, on purely aerodynamic considerations, the minimum angular velocity ω_{min} is proportional to $m^{-1/6}$. If, however, the strength of materials governs angular velocity, presumably at its maximum ω_{max}, then it should scale as $m^{-\frac{1}{3}}$ (Pennycuick, 1975; Lighthill, 1977; Weis-Fogh, 1977). It is generally assumed that the wing beat frequency f is proportional to ω. Lighthill (1977) suggests that, for hovering, for a given body mass, f may be bound by a number of other constraints in addition to those mentioned above.

It has been found in this analysis that, if the wing beat frequency data of small passerines are included, the scaling of f approximates to $m^{-\frac{1}{3}}$, suggesting that the strength of materials predominantly governs f. A similar slope was found by Greenewalt (1962, 1975) for insects and birds. This does not appear to be the case for the scaling of continuously flapping birds only, where f is proportional to $m^{0.27}$. It would appear here that f, and hence ω, is a compromise between the strength of materials and aerodynamic scaling predictions. The steeper slope of the line when the passeriformes

data are included is caused by many of the passeriformes having abnormally high wing beat frequencies. This is probably related to their 'bounding flight' and is discussed further in Chapter 8.

It is not necessarily true that ω is proportional to f, since ω is dependent on the stroke amplitude $\mathcal{Q}$ and the downstroke ratio τ as well. For continuously flapping birds it has been shown that $\mathcal{Q}$ and τ vary, with $\mathcal{Q}$ scaling as approximately $m^{-0.12}$ while τ scales as $m^{0.065}$. The wing tip velocity is a product of $f, \tau, \mathcal{Q}$ and wing semi-span $\frac{1}{2}b$ and so is more suitable for testing the scaling predictions of Pennycuick (1975), Weis-Fogh (1977) and Lighthill (1977). If $\frac{1}{2}b$ is proportional to $m^{\frac{1}{3}}$, then the wing tip velocity would be expected to scale as

Aerodynamic prediction: $\omega_{min}\frac{1}{2}b = m^{-1/6} \times m^{1/3} = m^{1/6}$

Strength of materials prediction: $\omega_{max}\frac{1}{2}b = m^{-1/3} \times m^{1/3} = m^{0}$

The calculated average downstroke tip velocity and the measured peak tip velocity are both dependent on f, τ and $\mathcal{Q}$ and have been shown to scale as $m^{0.14}$ and $m^{0.17}$ respectively. Both of these values are close to $m^{1/6}$ and so it is clear that aerodynamic considerations largely govern the scaling of cruise flight ω, as was predicted for continuously flapping birds by Pennycuick (1975). This demonstrates that f is not necessarily proportional

to ω and so f alone should not be used to test aerodynamic theory which predicts ω. Since the aerodynamic rule predicting that ω scales as $m^{-\frac{1}{6}}$ is based on the assumption that lift coefficient remains constant with variations of mass, the above findings indicate that this assumption is correct.

The allometric analysis shows that although f, $\mathcal{Q}$ and z vary with m they are not totally dependent upon it. The value of f for a given mass varies considerably with wing loading and aspect ratio. Birds with high wing loading such as the guillemot Uria aalge have very high frequencies for their body mass, whereas herons and egrets (Ciconiformes) with low wing loadings have correspondingly low values of f for their size. High aspect ratio apparently reduces f. Greenwalt (1960) postulates that span is of great importance in determining f in birds and insects, but this data suggests that mass, span and area are of nearly equal importance in this respect. It is apparent that birds with high aspect ratio do not increase their downstroke ratio with sizes above 0.5kg, which is a trend which occurs with all other birds with aspect ratios below 10. Large span or high aspect ratio seem also to be of importance in limiting $\mathcal{Q}$ but here again all three morphological features appear to cause some variation. It is only stroke plane angle which apparently is almost unaffected by mass ($\delta \propto m^0$) though possibly slightly altered by span and area. The

shallower stroke plane angles of Group A birds may be artificial due to the distortion of downstroke wrist extension which is prominent in these birds. It is by no means clear if the so-termed 'stroke plane angle' is in fact a plane, as many of the side-on traces have a curved appearance even after the downstroke wrist extension is accounted for. So none of the kinematic parameters are predominantly dependent on one morphological parameter. Also, morphology alone does not appear to be adequate in accounting for all the variation in each kinematic parameter, with the product-moment correlation for the multiple regressions of z and Q, with mass span and area, being only 0.76 and 0.66 respectively. Even this value for frequency, 0.91, implies that other factors besides morphology may be involved. These may include data errors and the kinematic parameters interacting with each other as well as morphology. Furthermore, the kinematics may vary with the relative flying speed of the bird relative to the stalling speed.

6.6.2 The aerodynamic analysis

Group A and Group C birds show distinct differences in the shape of the wing beat cycle; Group B birds have cycles which are, broadly speaking, intermediate between the two. These differences can be simplified to variations in the degree of upstroke rotation and wrist flexion. Generally speaking, the higher the aspect ratio of the bird, the less the rotation and the

wrist flexion, and consequently the smaller the reduction in wing span during the upstroke (Tables 6.1,2,3) and the lower the wing tip upstroke velocity. Birds with low aspect ratios, including the 'bounding' passerines (Section 3, Rayner, 1977) tend to reduce the profile of the wing towards the relative air flow as greatly as possible, whereas birds with high aspect ratios do not. Large birds with low aspect ratios are not capable of such great span reductions during the upstroke as are smaller birds with similar aspect ratios. This may be due to the higher wing inertias of large birds allowing less stroke flexibility, and also to the tendency for the proximal part of the wing to increase in proportion to the distal part with increasing size. Upstroke span reductions in the proximal section of the wing, by elbow flexion, are more difficult to achieve. The degree of apparent body recoil observed during a wing stroke varies with the aspect ratio, it appearing to be very pronounced in Group A birds and only slight in those of Group C.

In Section 5 it has been demonstrated that, even when morphology and kinematics are accounted for, the modified Pennycuick prediction does not hold true, suggesting variations in lift coefficient and flying speed relative to stalling speed in individual birds. The calculated values of C_L from Rayner's power model increase dramatically with aspect ratio, and there may be two causes for this.

1) The polar of C_L against C_D varies with aspect ratio (Prandtl and Tietjens, 1957) as in Graph 6.13 . A bird optimising its lift to drag ratio and so flying at V_{mr} should have a value of C_L given by the tangent of the respective curve and the origin. This optimum value of C_L will therefore increase with aspect ratio. However, for the range of aspect ratios considered here (5 to 20) this increase will be very small, the curves becoming closer to each other as the aspect ratio increases. This slight increase in C_L is therefore insufficient to totally explain the variations found.

2) Rayner (1979a) calculated $\bar{C}_L$ during the wing beat cycle by assuming that only the downstroke is used to generate lift. A bird which also uses the upstroke to produce lift would not have to develop as much lift during the downstroke as would a bird relying on the downstroke alone. This would be reflected in the downstroke kinematics, with the former bird probably having a lower amplitude and downstroke period that the latter. If the mean lift coefficient for a beat cycle is calculated assuming that only the downstroke is used, then a bird that also uses the upstroke, and so has diminished downstroke kinematics, will have an artificially high lift coefficient. Hence the apparent high calculated lift coefficient $\bar{C}_L$ with high aspect ratio is probably artificial and caused by a corresponding increase in the use of the upstroke.

Graph 6.13

Polar of Lift Coefficient C_L against Drag Coefficient C_D for wings of the same profile and aspect ratios from 1 to 7. (After Prandtl and Tietjens, 1957).

Graph 6.13

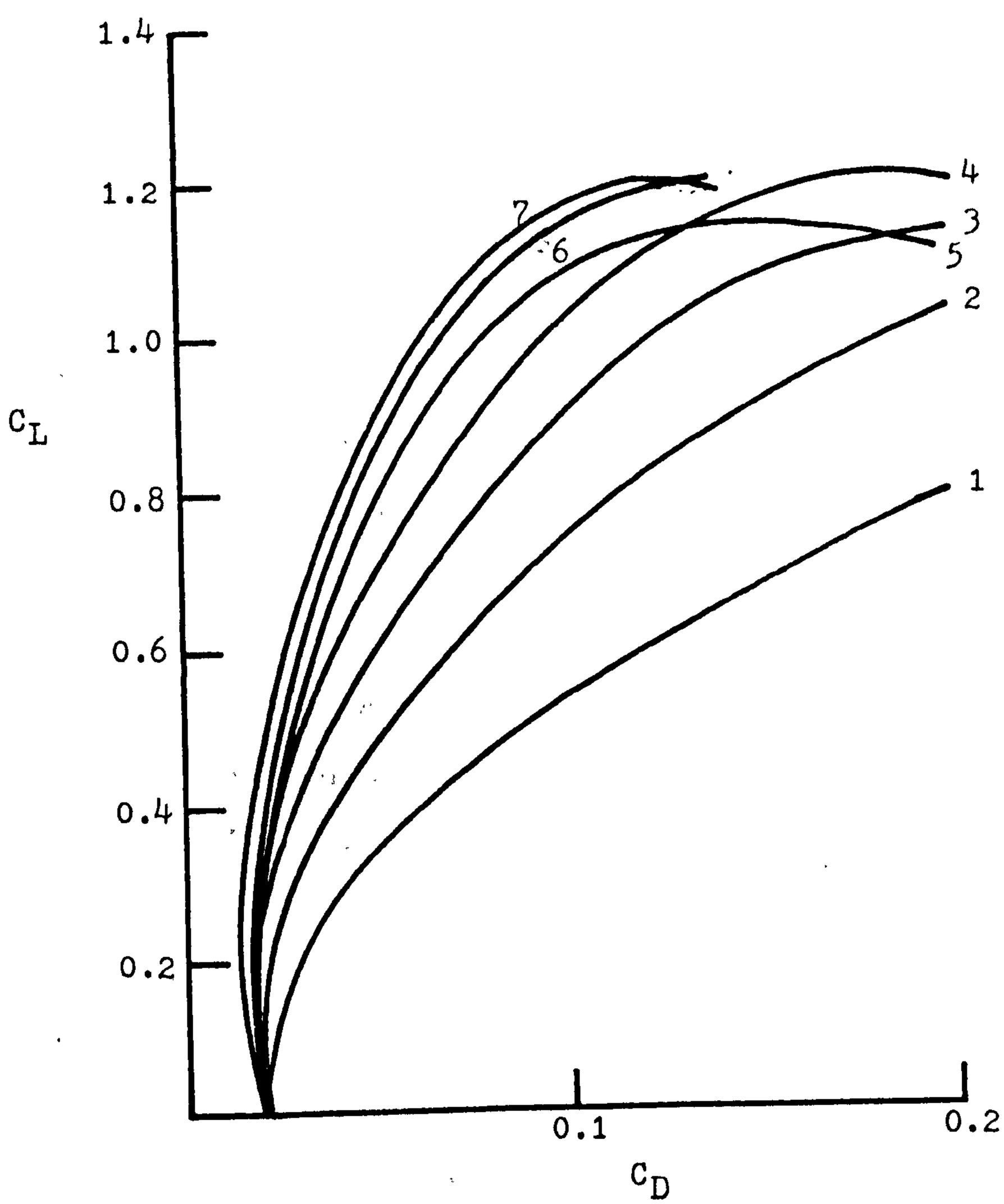

There are distinct differences in the variation of the downstroke ratio τ with increasing body mass between Groups A and C. For birds of Group A, τ can be as high as 0.7, but generally scales as $m^{0.082}$ for those above 1kg. With birds of Group C there is little variation in τ from 0.5 for those of the same size range. With no upstroke lift, decreasing the upstroke period has the advantage of reducing that part of the cycle where there is no weight support, and also of increasing the wing beat frequency. Pennycuick (1971, 1975) argues that the muscular power output of a bird is dependent upon its wing beat freqency, and hence increasing τ could have important benifits to large birds whose power requirements for cruise flight are approaching the total amount of muscular power that they can produce. The scaling of for Group A birds, and to a lesser extent those of Group B, is therefore similar to that expected for birds which do not rely greatly upon the upstroke for lift generation.

A bird which uses the upstroke for weight support probably benifits by keeping the air speed of the wing, or of that section of it that generates lift, similar in the upstroke and the downstroke, by keeping τ close to 0.5. Too high an upstroke speed would require a large amount of supination which would be detremental (see below). Also, in equation 6.14, which assumes the extreme case where the mean

lift coefficient of the wing on the upstroke is the same as the downstroke, f is maximised if τ is 0.5. Hence it would seem that the large birds of Group C do rely to some extent on the upstroke to generate lift.

The above findings suggest that there is variation in the degree to which non-bounding birds use the upstroke, and that this variation is largely dependent upon the aspect ratio of the bird. Birds of Group A having a low aspect ratio tend not to use the upstroke, whereas those of Group C are probably very dependent upon its use. These findings contradict Brown's (1963) suggestion that the wing strokes of all continually flapping birds in fast forward flight are the same.

It is the conclusion of many researchers who have studied flight using high speed cinematography (Brown, 1963; Storer, 1948; Shestakova, 1956) that large birds use the upstroke in fast forward flight. These authors believe that only the proximal wing is used to produce upstroke lift, and my own observations support this. The wing tips, even in the Procelariiformes which have very high aspect ratios, never exhibit up-bending during the upstroke which suggests that no lift generation occurs on the distal wing.

The recent work of G.R.Spedding (1981) investigating the wake behind a kestrel Falco tinnunculus in fast forward flight, shows that the proximal wing is producing a vortex pattern typical of gliding, whereas

no vorticity is associated with the distal wing. The reason why birds use only the proximal wing for upstroke lift is as follows: The velocity of the flapping wing increases along its length to a maximum at the tip. If the whole wing is to have a positive angle of attack then the wing must be supinated along its length (Figure 6.10) This means that the resultant force produced by the wing sections near to the body will have a large vertical component, whereas those near the wing tip will have a large horizontal backward component. On the downstroke this horizontal component produces forward thrust, but if it were present on the upstroke it would have a large retarding effect. Consequently, birds using the upstroke probably angle the proximal wing to produce lift, but keep the distal wing at a zero angle of attack and so reducing this retardation.

Any use of the upstroke to produce lift, even by only the proximal wing, must have a slight retardation effect on the forward motion of the bird. The degree to which it is used must therefore be determined by the balance of the amount of benefit which can be gained by supporting the weight during this part of the cycle and so reducing the amount of work done on the downstroke, against the degree of retardation caused by the upstroke lift, and associated profile and induced drag, which must be overcome by downstroke thrust. It seems that this balance favours the use of the upstroke at higher aspect ratios, and the reason for this could be as follows.

Figure 6.10

During an upstroke this simplified wing has been supinated so that a positive angle of attack is maintained along the whole length of the wing. The resultant force produced by the wing near to the body, where the upward movement of the wing is small, has a large vertical component, whereas that produced near the wing tip, where the upward movement of the wing is greatest, has a large horizontal backward component..

Figure 6.10

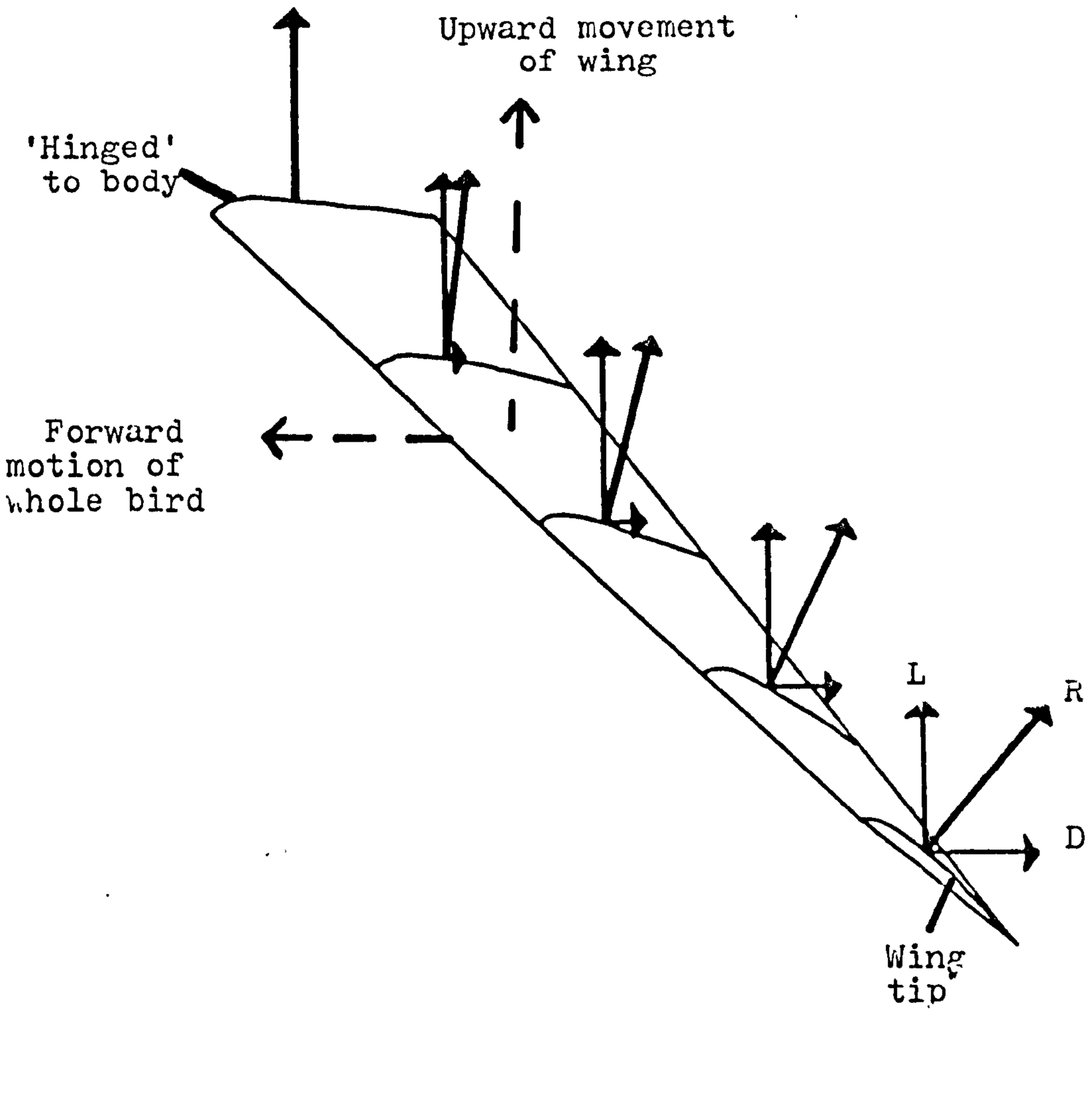
Upward movement
of wing
'Hinged'
to body
Forward
motion of
whole bird
L
R
D
Wing
tip

Wings having a low aspect ratio have proximal wings of low span and wide chord which will have high profile and induced drag during an 'upstroke glide', whereas wings having a higher aspect ratio will have increasingly more favourably shaped proximal wings. Separated wing tip primary feathers, typical of many low aspect ratio birds, may reduce this induced drag in the unfavourably shaped complete wing (Hummel, 1980). However, during an upstroke, when the distal wing cannot be used, this drag reduction device will not be available, making the proximal wing very unfavourable for use in an 'upstroke glide'.

6.6.3 Distribution of speed of the wing tip in the downstroke

Variation in the kinematic parameters with wing morphology may also be associated with the acceleration and deceleration of the particular wing. The downstroke wing tip speed profiles show general similarities to the angular velocity descriptions of the downstroke by Oehme and Kitzler (1975) although the latter seem to be oversimplified. Oehme and Kitler show the angular velocity increasing constantly to a level, beyond which it remains constant. Here it is found that the wing tip accelerates to a peak velocity although, especially amongst Group B birds, the rate of velocity increase or decrease about the peak can be low. This is presumably the period Oehme and Kitzler assume to be constant.

The causes of the variation in the wing tip speed profiles may be related to wing shape. Relatively large wing areas will have high profile drag and therefore require a long period of acceleration. Certainly Group A birds, with their high area, low aspect ratio wings, appear to require a greater percentage of the downstroke to accelerate the wing than the higher wing loading birds of Group B. Pennycuick (1969) suggested that the unsymmetrical elevation distribution of the pigeon wingstroke, having a higher elevation up than down, was largely due to the need to accelerate the wing and that only the middle section of the stroke was at a useful speed for lift generation. If a proportion of the positive elevation is used in this way it would be expected that the Group A birds, requiring long acceleration periods, should exhibit higher positive elevation than the rapidly accelerated wings of Group B birds. Graph 6.14 shows this to be generally the case. The wing shape and low area of Group B birds appear to permit the wing tip to be near its peak velocity for a far greater proportion of its downstroke than Group A and so reducing the required 'acceleration amplitude'. In this respect Group B birds are far more suitable for flapping flight than the square winged Group A.

The gulls (Laridae) of Group C have a similar velocity profile to Group A, presumably due to their relatively high wing areas. Although their amplitudes are less than those of Group A, they show a similar asymmetrical

Graph 6.14A

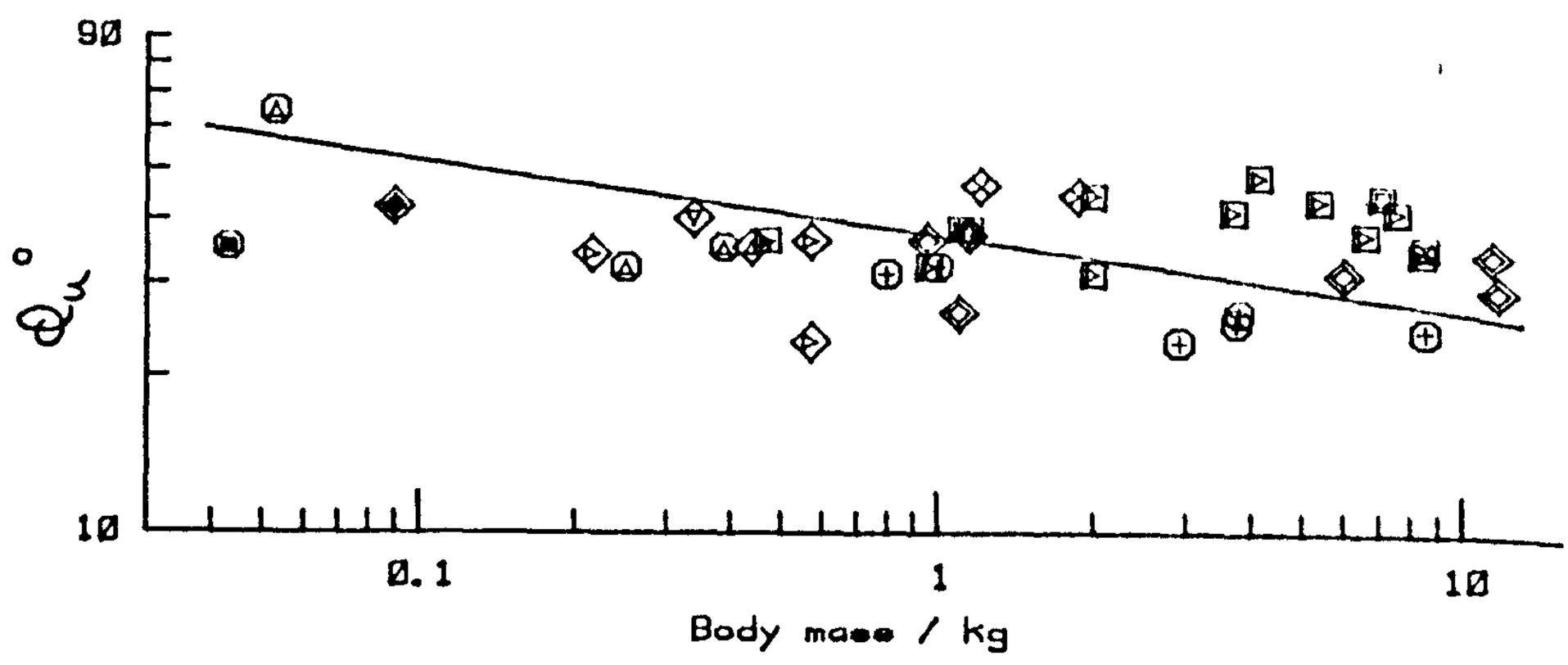

Graph 6.14B

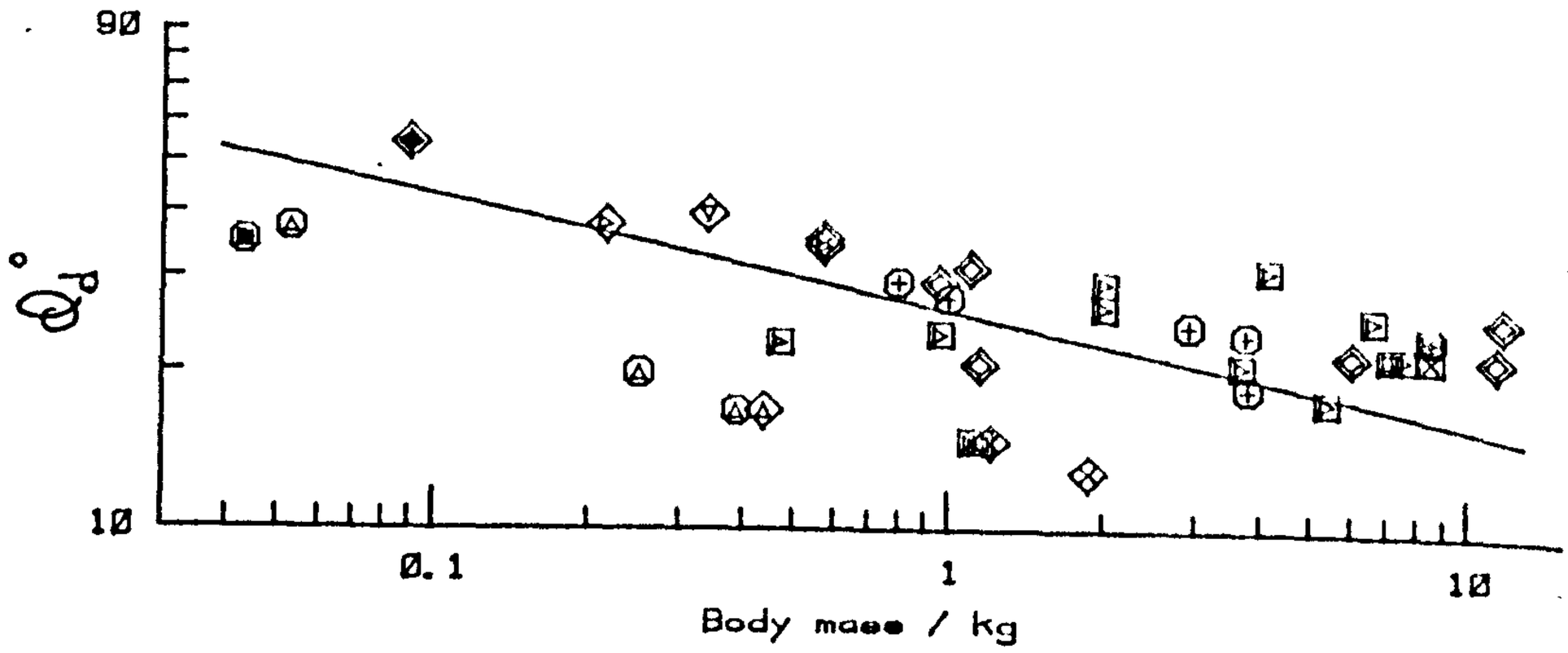

GRAPH 6.14A

Positive (up) elevation (degrees) and body mass m (kg) to illustrate the variation in positive elevation between groups A, B and C.*

GRAPH 6.14B

Negative (down) elevation (degrees) and body mass m (kg) to illustrate the variation in negative elevation between groups A, B and C.*

* The symbols are as in Figure 6.1B and the R.M.A. is shown in all cases.

distribution of positive and negative elevation to facilitate wing acceleration. As the Procellariiformes have a similar wing shape, it would be expected that their wing tip speed profiles would be similar to the gulls. Clearly the acceleration rates of the Procellariiformes are far greater and this is reflected in the positive and negative elevations being symmetrical (Graph 6.14). These high accelerations may be due to the high moments of inertia of the large wing spans of these birds. A second possible explanation is that Pennycuick (. 1982 b .) has found a lock system in albatross and giant petrel pectoral girdles which enable them to fix their wings in the horizontal position during gliding. This lock, he suggests, may reduce the positive elevation and also store elastic energy from the upstroke which is released during the initial stages of the downstroke. This could cause a rapid acceleration in the downstroke. Pennycuick found no such lock in the white chinned petrel Procellaria aequinoctialis which exhibits a similar speed profile to the albatrosses, which suggests that other factors may be involved besides the pectoral lock. In order that this elastic mechanism can be confirmed, a detailed anatomical study of the lock and how it may function in flapping is required, linked to a detailed study of the relevant kinematics. This would include far higher framing rates of cine film than the 60fps used here, so that the velocity profile at the beginning of the downstroke can be investigated in detail.

The patterns of deceleration are not as clear as those of acceleration due to the complex movements of the wing tip at the base of the downstroke (Section 6.2). Group A birds generally show rapid deceleration and correspondigly low down amplitudes. Their low aspect ratio wings, with relatively small spans, have low moments of inertia compared to Group C birds of similar size. Also the wing chord is large near the wing tip, consisting of separated primary feathers which can generate a large aerodynamic force. The combination of low inertia and the ability to generate a large force near to the wing tip should facilitate rapid distal wing deceleration. The separated primary feathers of Group A exhibit considerably tip bending in cruise flight and Pennycuick and Lock (1976) suggest that elastic energy stored in the bent feathers can be released to produce useful aerodynamic work to decelerate the wing. If so, Group A birds may be of an ideal design to utilise the mechanism, but on the other hand their very flexible feathers may be unsuitable for storing large amounts of elastic energy. The deceleration periods of Group B birds are also rapid and it is only the Procellariiformes which exhibit deceleration periods of a similar length to those of acceleration, This long deceleration may be a consequence of the very high moments of inertia of these long span birds coupled with the tapered distal wing being unsuitable for generating a large aerodynamic force near the wing tip.

Pennycuick (1969, 1975) assumes that at the end of the downstroke the downward motion can be entirely stopped by aerodynamic lift. Whether this is true or not is not clear in all cases. The final stopping of the distal wing appears to be a combination of the end of wrist flexion and the upward movement of the wrist itself. Both could require muscular work. It is also not clear how the proximal wing is decelerated. The similarity in the deceleration rates of all the birds, except those of very high span, is contrary to what would be expected if aerodynamic forces were solely involved. Wing deceleration probably involves a certain amount of muscular work.

6.6.4 Downstroke wrist extension

It was shown in Section 6.2 that the wrist is still slightly flexed at the beginning of the downstroke and is extended during approximately the first third of the downstroke period. The degree of flexion at the beginning of the downstroke is greatest in Group A birds and least in Group C birds. The function of delaying the full extension of the wrist until well into the downstroke is probably twofold. Firstly, the bulk of the downstroke wing acceleration must occur in this period and initially little aerodynamic force can be generated by the distal wing due to its relatively low speed. It may therefore benefit the bird to keep the wrist flexed and so reduce the distal wing area at the beginning of the stroke to reduce its profile drag and

allow more rapid accelation. If so it would be expected that the degree of flexion at the beginning of the downstroke should be related to the relative area of the distal wing which is, broadly speaking, true.

The second function could be to enhance the velocity of the distal wing during the early stages of the downstroke and so initiate circulation at an earlier stage. The degree of wing tip velocity enhancement by downstroke wrist extension is illustrated in Figure 6.11 on a two dimensional basis by the side-on view of a buzzard Buteo buteo in cruise flight. The actual stroke plane angle is taken as the solid line which is parallel to the wrist's stroke plane angle and that of the middle section of the wing tip's downstroke, after wrist extension is complete. The plane of the wing tip during the wrist extension period is approximated by the dotted line. The distance the wing tip travels when its movement is enhanced by wrist extension is some 24% more than if the wrist was fully extended at the beginning of the downstroke. As the time taken to travel this distance is the same, the wing tip velocity is enhanced by an equal magnitude by wrist extension. This two dimensional illustration does not account for the distance moved horizontally outwards from the body by the wing tip (but only downwards and forwards) during wrist extension and so the velocity enhancement can be assumed to be even greater. The degree of velocity increase is obviously reduced the closer a distal wing chord is to the wrist. The rate at which the wrist is extended is probably

a balance between the needs to reduce the distal wing profile drag and these requirements to enhance distal wing circulation.

Figure 6.11

Wrist extension in the downstroke of the buzzard Buteo buteo. During the period of wrist extension the wing tip travels a distance of 1.24 units whereas if it were to remain fully extended throughout this period the wing tip would only travel through 1 unit.

For each frame the position of the wing tip is marked by a closed circle and the position of the wrist by a star.

Figure 6.11 Buzzard

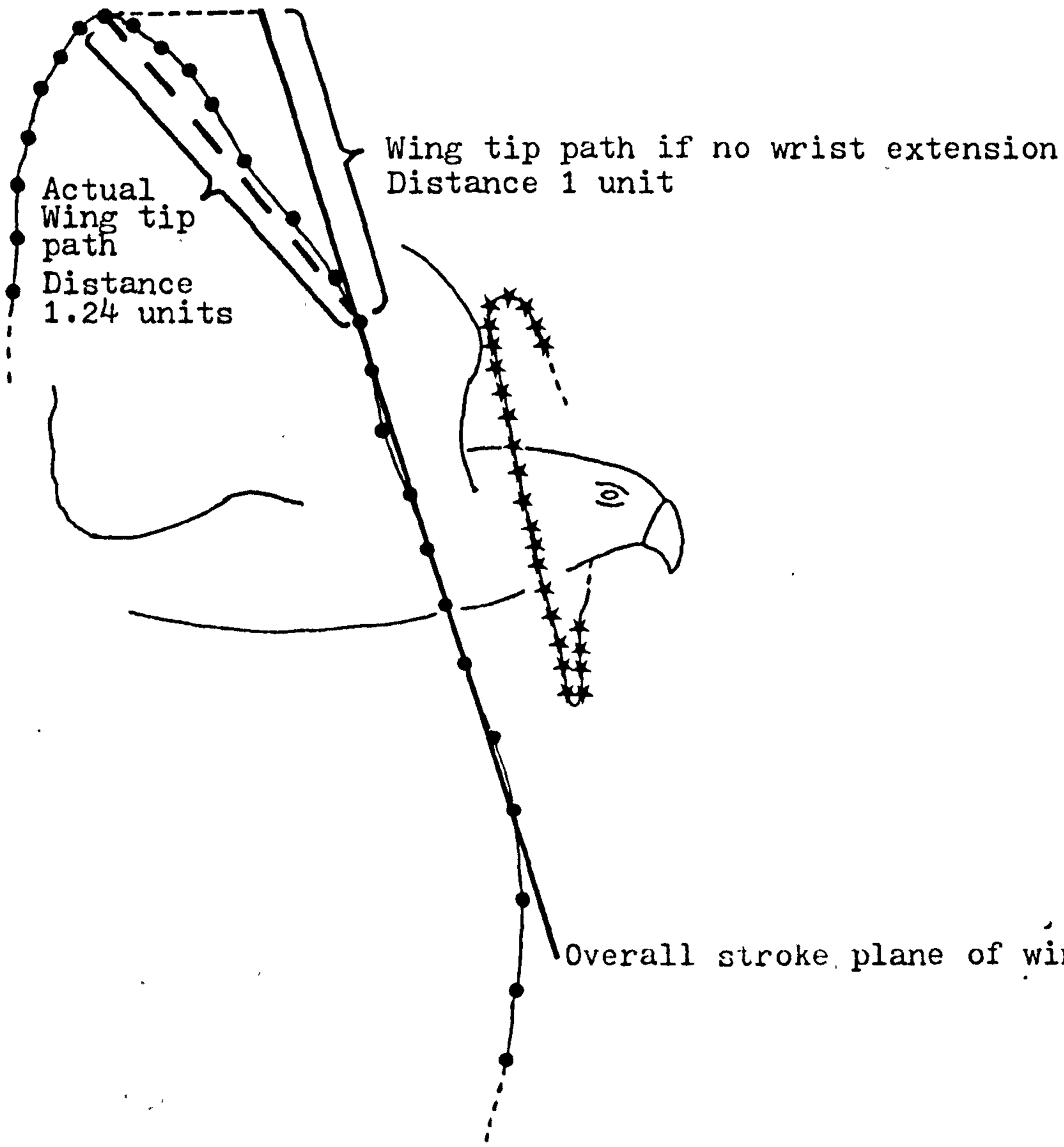

CHAPTER 7

HOVERING AND SLOW FORWARD FLIGHT

7.1 Introduction

This chapter is primarily concerned with the kinematics of birds at their slowest flying speeds, when they are generally flying at their maximum power. This initially involves a study of hovering of birds up to 0.25kg, and then take-off of birds as large as 8.5kg . In the study of hovering the three types of hovering wing stroke (Brown, 1963; Darthe and Oehme, 1978) are investigated; they are those of a) humming birds, b) birds using a 'feathered' (passive, producing no lift and little drag) upstroke, and c) birds using a 'tip reversal' upstroke (Brown, 1963).

With the exception of the film of the humming bird Chlorostilbon melanorhynchus, taken by Ruppell (1972a) and obtained from the Encyclopaedia Cinematographica of Gottingen, all the species described here were filmed during this survey.

In hovering, the stroke plane angle is often close to the horizontal and the wing may be moving upwards or downwards relative to the horizontal. In this chapter, stroke planes where the wing moves downwards are referred to as negative, and those where it moves upwards as positive.

The kinematics of the wandering albatross Diomedea exulans during landing, and of the kestrel Falco tinnunculus flying slowly into wind, are described. In both cases these birds are unlikely to be flying at maximum power and therefore the data are not included in the scaling analysis of maximum power kinematics.

7.2 Hovering

7.2.1 Humming bird (Chlorostilbon melanorhyncus)

The wing stroke of Chlorostilbon melanorhyncus is illustrated in Figure 7.1 , showing views from side on and from above . The stroke is as described for Melanotrochilus sp. by Stolpe and Zimmer (1939), except that here the wing tip path, viewed from the side, is not symmetrical. The downstroke has, for the majority of its period, a negative stroke plane angle of about -17^{o} ; -28^{o} for the first half and -9^{o} for the second , whereas the upstroke stroke plane has a negative angle for only the first third of the period, the angle being only -11^{o}, and for the remaining period it is positive at about 26^{o}. Ruppell (1972a) describes an asymmetrical stroke for the same film. The remaining kinematic parameters of stroke frequency, downstroke ratio and stroke amplitude are given in Table 7.1 .

7.2.2 Birds using the 'feathered' upstroke

Here the stroke of the pied kingfisher (Ceryle rudis) of body mass 90g and of the zebra finch (Poephila guttata) of body mass 13g are described.

The stages of the wing stroke of the pied kingfisher are illustrated in Figure 7.2A . At the end of the upstroke the secondary feathers are joined

Figure 7.1

Humming bird Chlorostilbon melanorhynchus hovering.

Film taken by Ruppell and details are given in Ruppell (1972a).

7.1A Side on view of the complete hovering wing stroke with every tenth frame illustrated. Film speed 2,500fps.

Figure 7.1A Humming bird

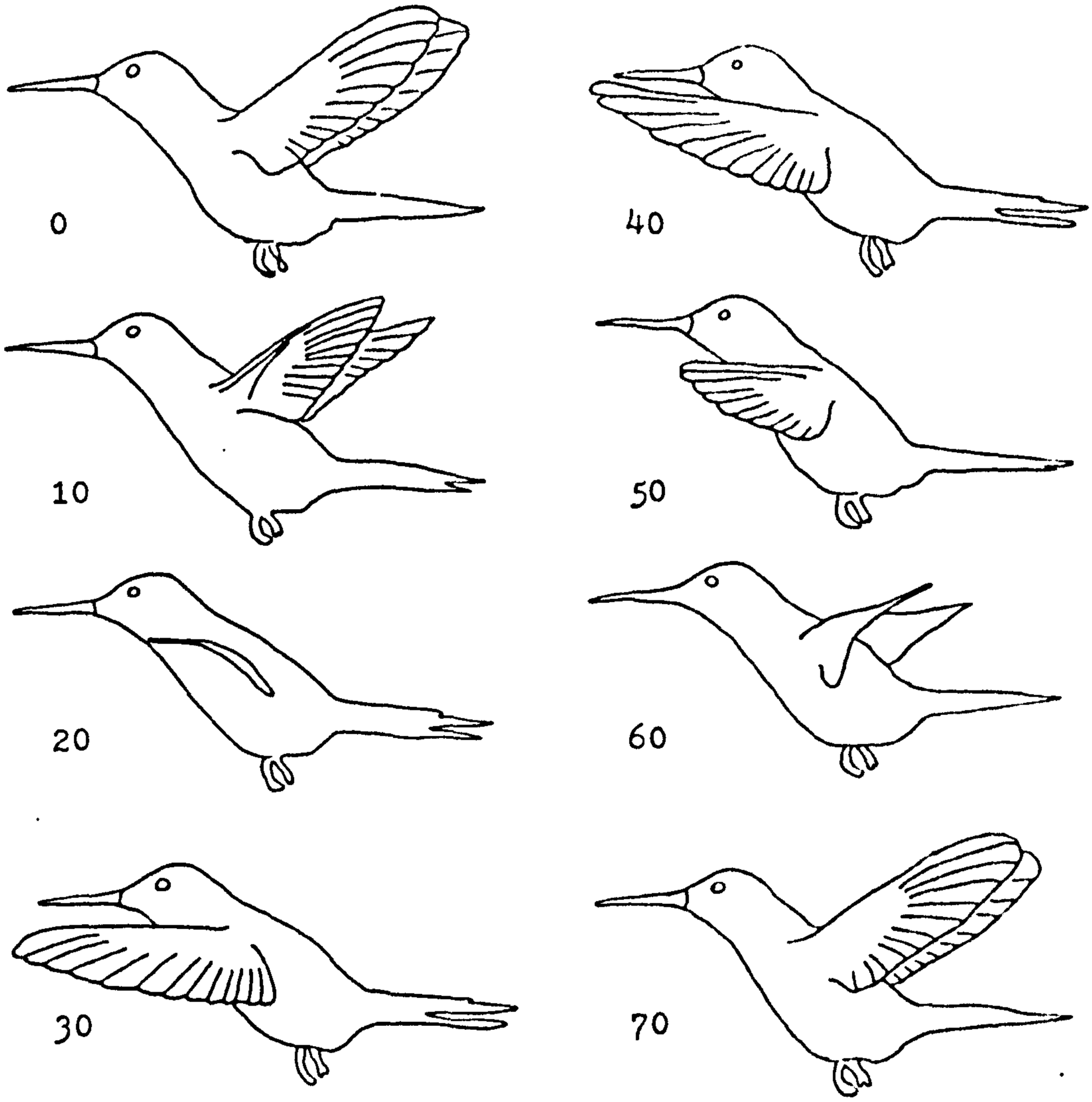

Figure 7.1B

Dorsal view of the downstroke and the upstroke in hovering. The frame time base has been approximately fitted to be equivalent to 7.1A, as the film speed for this view was not clear.

Figure 7.1B

Humming bird

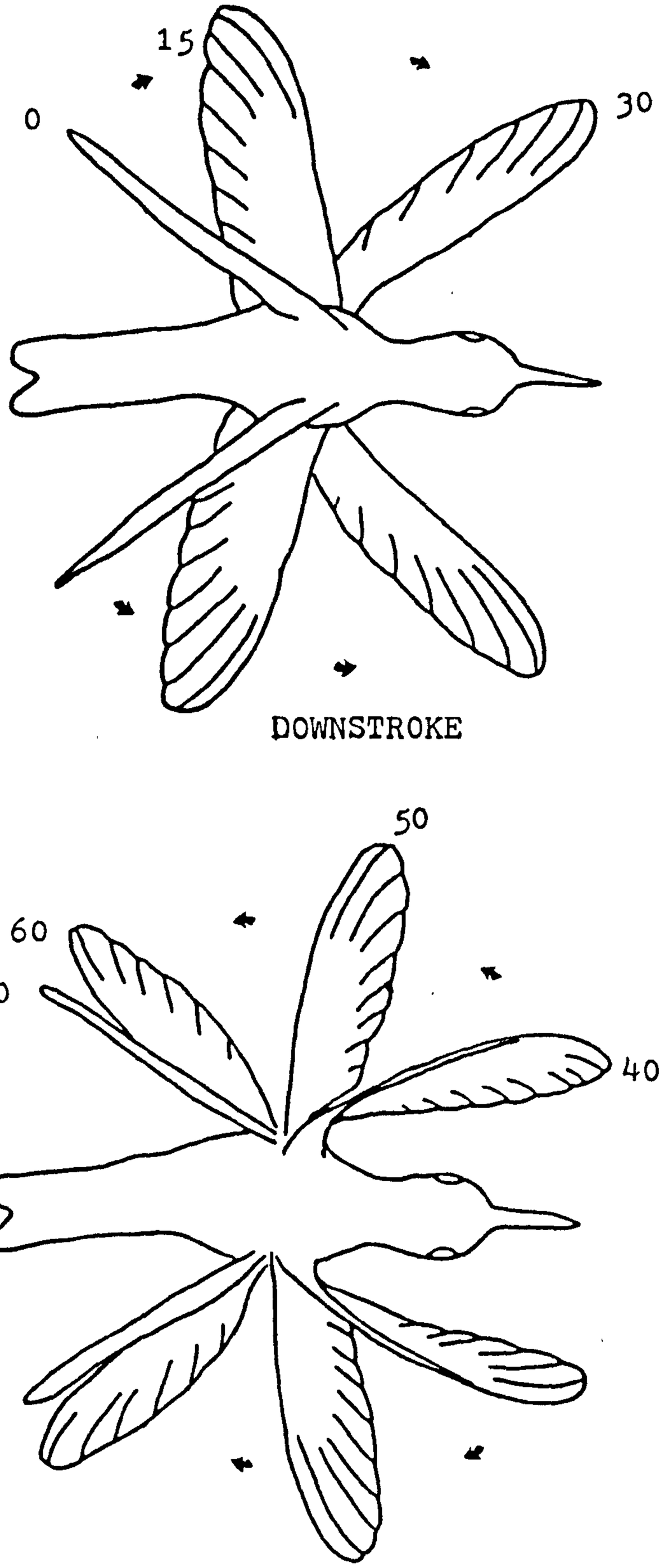

at their trailing edges and are moved apart during the initial stages of the downstroke as in the clap-and- fling (Weis-Fogh, 1973). During this period the wrist is fully extended. For the majority of the stroke the primary feathers are multislotted at the wing tip, the anula raised and the wing tip slightly pronated. The upstroke begins with the proximal section of the wing being negatively rotated and the elbow and wrist begin to flex and move upwards. This causes the primary feathers, which have previously been bent upwards at their tips, to snap straight. The wrist is moved upwards close to the body, so pulling upwards the primary feathers which are now slotted, giving the 'Venetian blind' appearance. The proximal wing section, nearest its highest elevation, is positively rotated causing the wing tip to swing backwards and upwards past the body in an upstroke flick which is enhanced by elbow and wrist extension in the latter stages of the upstroke. The wing is thus brought into position for the next downstroke.

The tail is furled during the first half of the downstroke and then full spread during the second. It remains so throughout the first half of the upstroke and is then refurled during the remaining upstroke period (Figure 7.2A). The kinematic measurements for the hovering pied kingfisher are given in Table 7.1 .

The hovering stroke of the zebra finch is

Figure 7.2A

Pied kingfisher Ceryle rudis hovering viewed from head on and approximately side on. Every fourth frame is illustrated. Film speed is 300 fps and the wing span 0.46m. The two views are not to scale.

Figure 7.2A Pied kingfisher

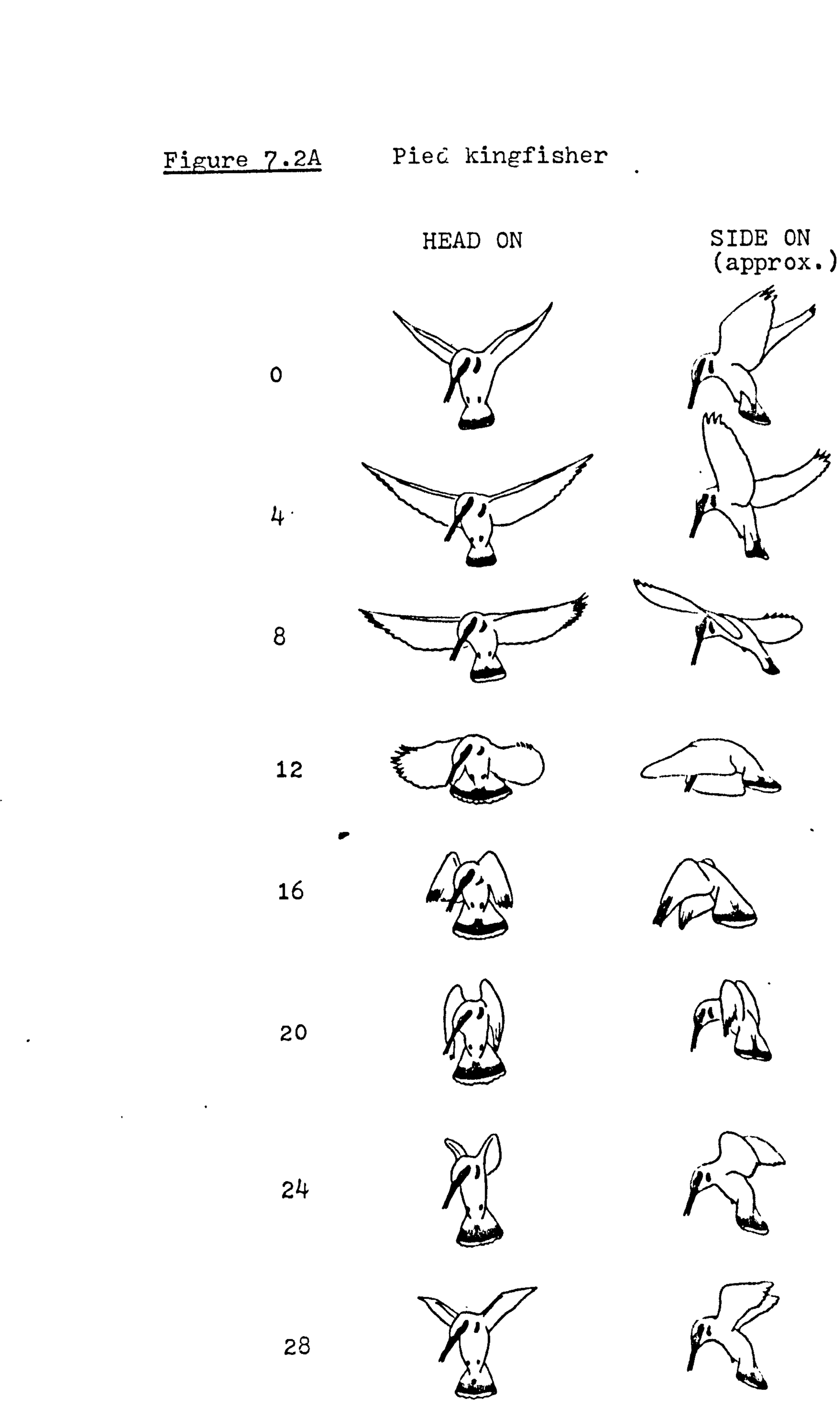

Figure 7.2B

Zebra finch Poephila guttata hovering, viewed approximately side on and head on. Every fourth frame is illustrated and the film speed is 500fps. The wing span is 0.18m.

Figure 7.2B Zebra finch

SIDE ON HEAD ON

0

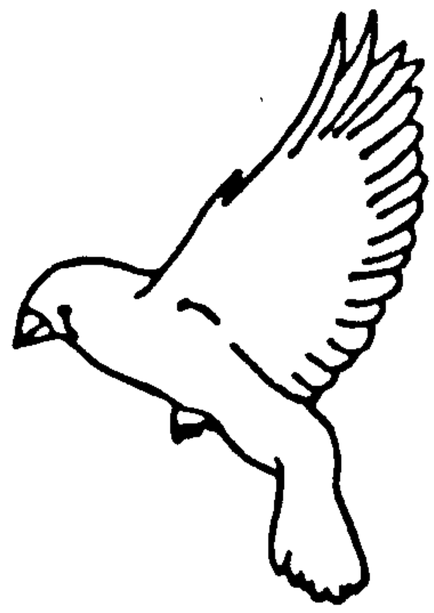

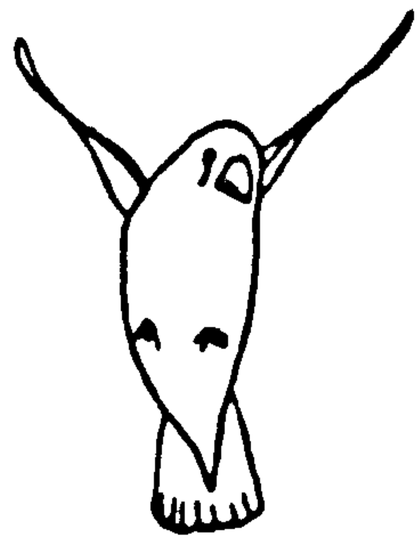

4

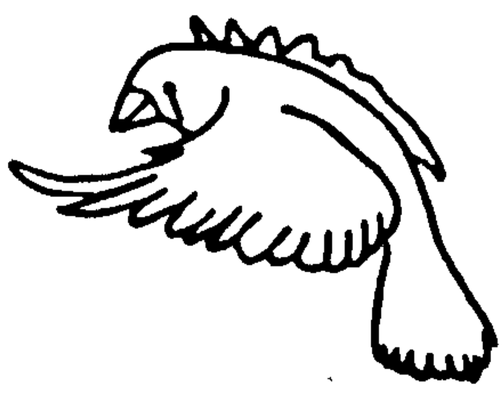

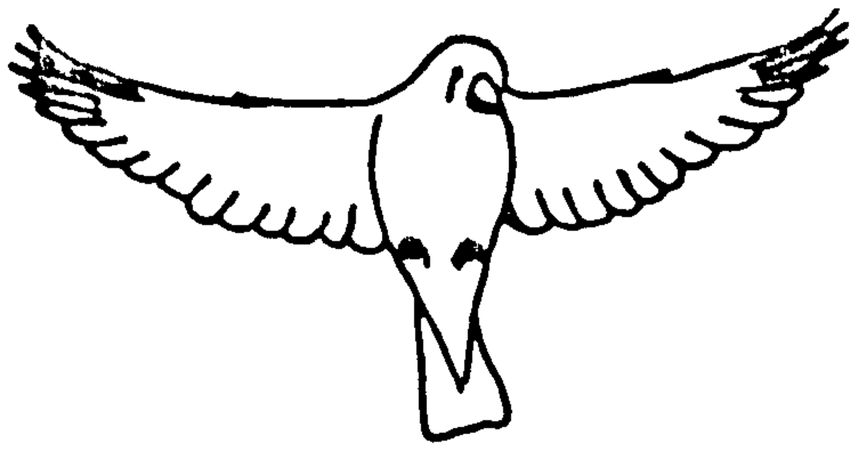

8

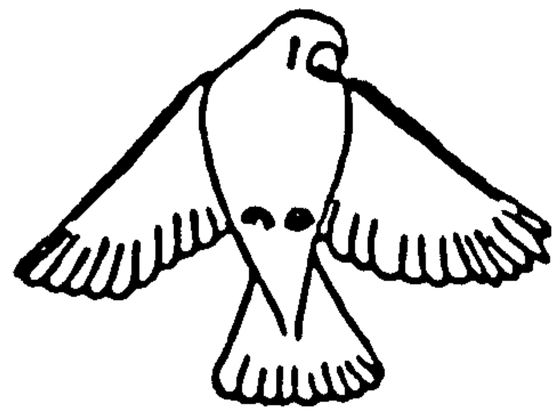

12

16

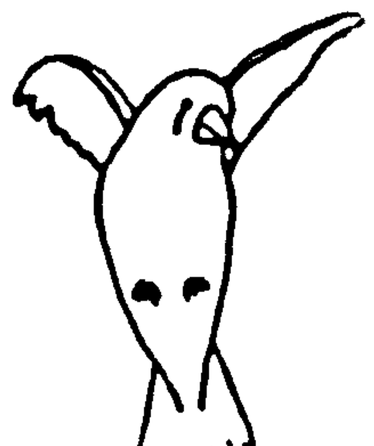

illustrated in Figure 7.2B , and is similar to that described for the pied kingfisher. It is apparently almost identical to that described for the zebra finch in fast forward flight (Chapter 6.3). The body tilt is within the range of 31 ± 4° and the stroke plane relative to the body is approximately-63°, the same as in fast forward flight. The remaining kinematic measurements are listed in Table 7.1 . In a similar manner to the pied kingfisher, the tail is spread during the latter stages of the downstroke and furled halfway through the upstroke (Figure 7.2B). This pattern is also found in the wing stroke of the hovering redstart (Ruppell, 1972b).

The zebra finch does not flap continuously when hovering, but periodically folds its wings into the bound position. The 'bound' is always of similar duration, between 0.034 seconds and 0.05 seconds (mean 0.043 seconds) whereas the longer flapping period greatly varies from 0.11 seconds to 0.27 seconds (mean 0.15 seconds).

7.2.3 Birds using the tip reversal upstroke

The hovering wing stroke is illustrated for the budgerigar (Melopsittacus undulatus) and for the black headed gull (Larus ridibundus) in Figures 7.3A and 7.3B, and can generally be described as follows.

The downstroke is similar to that of birds using

feathered upstrokes, except that the stroke plane angle is distinctly shallower (Table 7.1) and consequently the downstroke ends with the wing tips extended in front of the animal and level with, or slightly higher than, its head. The downstroke ends when slight flexion of the elbow and wrist occurs, followed by a rotation of the humerus which moves the elbow down and towards the body, and causes the wrist to move upwards and close to the head. The primary feathers are retracted posteriorly and wing tip bending ceases. These movements of the elbow and wrist produce a dramatic reduction in the span of the proximal wing section and also arrange the distal section so that the leading edge is uppermost and the ventral wing surfaces face each other. The wrist is moved horizontally past the head during the middle of the upstroke and the primary feathers, which lie in a horizontal stack with each feather distinctly separated from its neighbour, are flicked backwards. This flick is enhanced in the latter stages of the upstroke by the extension of the elbow and wrist bringing the wing into position for beginning the downstroke. The overall effect of the upstroke is that the wrists pass close to each other, over the head, and the wing span is composed mainly of multislotted primary feathers. The path of the wing tip during the middle of the upstroke is higher than during the downstroke and is nearly horizontal. The tails of the black headed gull and the pigeon

Figure 7.3A

Budgerigar Melapsittacus undulatus hovering, viewed approximately from side on and tail on. Every fifth frame is illustrated except for the tail on view where the second frame in the wing beat is also shown to illustrate the peeling apart of the trailing edges of the wings in the clap and fling. The film speed is 500fps and the wing span is 0.28m.

Figure 7.3A Budgerigar

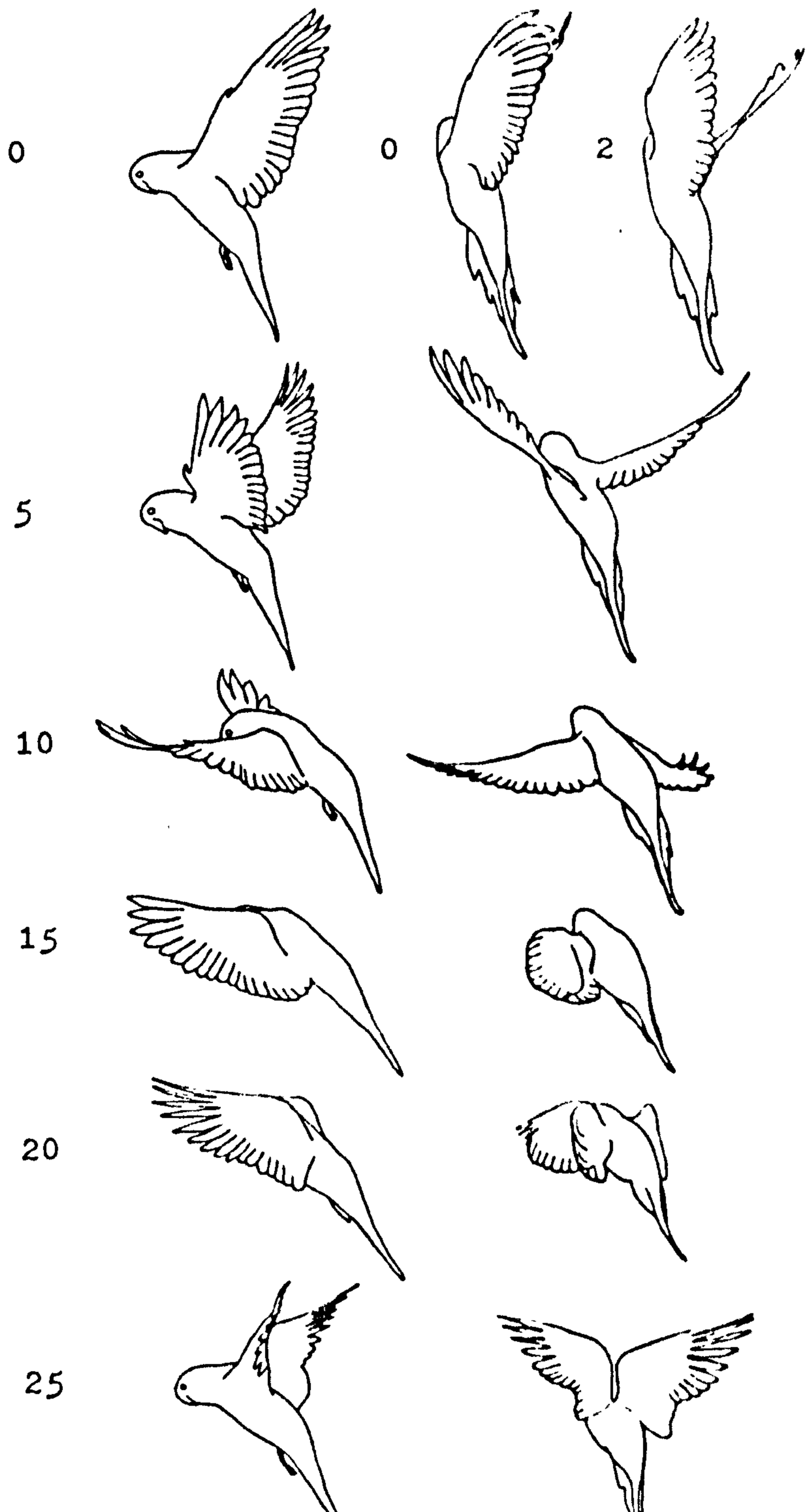

Figure 7.3B

Black headed gull Larus ridibundus hovering viewed from tail on, side on and approximately head on. Frames o, 4, 6, 8, 10 and 14 are illustrated. The film speed is 100fps and the wing span 0.82m. The three views are not to scale.

Figure 7.3B Black headed gull.

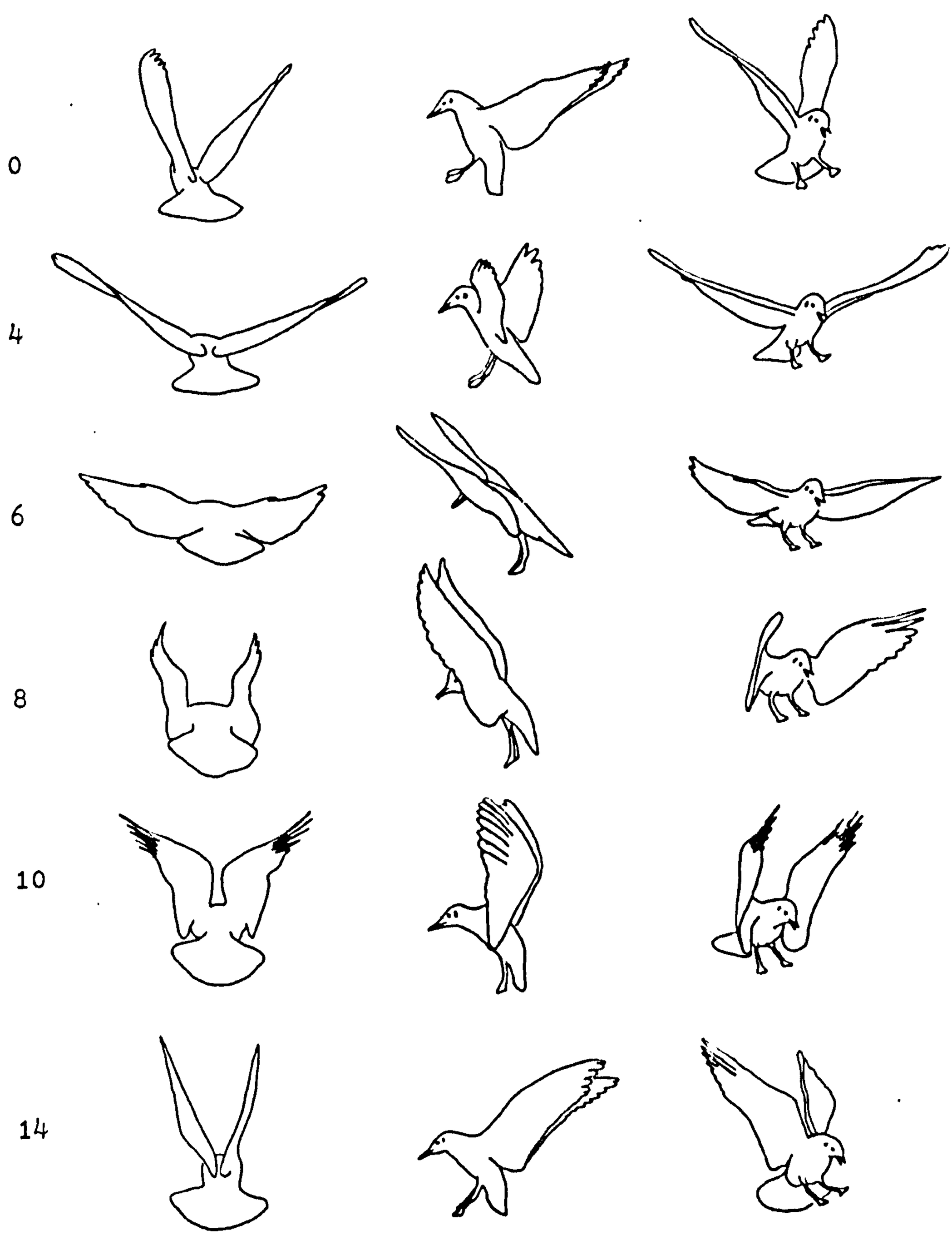

TABLE 7.1 Wing beat kinematics in hovering.

Special name English/Scientific	MORPHOLOGY				STROKE PERIODS					STROKE ANGLES			
	m kg	b m	S m^2		N	f Hz	fS.D. Hz	τ	τS.D.	N	Φ Degrees	Φ range Degrees $\pm$	γ * Degrees
Humming bird CHLOROSTILBON MELANORHYNCUS					35	49.7	7.0	0.50	0.021	10	129	5	-17
Pied kingfisher CERYLE RUDIS	0.09	0.458	0.0327	6.4	38	9.41	0.22	0.570	0.022	4	115	10	-48
Zebra finch POEPHILA GUTTATA	0.0138	0.176	0.0052	6.0	25	26.4	1.42	0.513	0.029	8	125	12	-32
Budgerigar MELOPSITTACUS UNDULATUS	0.0323	0.276	0.0097	7.9	27	16.4	1.73	0.502	0.032	4	170	10	-17
Black headed gull LARUS RIDIBUNDUS	0.251	0.94	0.087	10.2	17	6.26	0.43	0.494	0.031	6	115	15	-15

* Approximate values

(Guidi, 1938) remain spread throughout the stroke. It is difficult to determine whether the tail of the budgerigar is spread or not due to its thinness.

The budgerigar carries out a clap and fling at the beginning of the downstroke, with the trailing edge of the secondary feathers and all but the first four primary feathers joining before the downstroke begins. The black headed gull sometimes brings the secondary feathers, near the base of the wing, into contact before the downstroke. The kinematic measurements of the black headed gull and of the budgerigar are given in Table 7.1 .

7.2.4 Discussion

The wing strokes of the humming bird and of feathered upstroke birds are distinctly different in that the humming bird maintains a fully extended wing during the upstroke and inverts it, while feathered upstroke birds reduce the wing span to a minimum and draw the wing up close to the body in the upstroke. It is generally considered that the feathered type of upstroke produces little or no useful vertical force (Brown, 1962; Norberg, 1975; Dathe and Oehme, 1978) and the upstroke is arranged to reduce aerodynamic drag to a minimum. Birds only using the downstroke have relatively steep downstroke planes (Table 7.1 and Graph 7.1) whereas the humming bird has a relatively shallow stroke plane.

The tip reversal wing strokes have shallow downstroke planes, similar to the humming birds, and the distal wing section is fully extended during the upstroke. This, coupled with the near horizontal upstroke plane and the upward bending of the wing tip feathers during the upstroke, has been suggested by Brown (1961) as evidence that this upstroke produces lift. I agree with this conclusion since, if the primary feathers were not producing beneficial lift in the upstroke, they would be brought close to the body to reduce profile drag. The pigeon, as it accelerates after take-off, initially uses a tip reversal upstroke but then, as its speed increases, it uses a feathered upstroke. Forward motion reduces the speed of the air flow over the backward flicking primary feathers, and there must be a critical forward air speed when a tip reversal upstroke is no longer effective.

The differences in the tail spreading between birds using a feathered or tip reversal upstroke are probably related to the distribution of lift generation through the cycle. The tail may have two functions; as a structure to balance the turning moment of the body, or as an extra lifting surface aiding in maintaining an attached air flow over the wings. In either case, the cyclical spreading and furling of the tail in birds using a feathered upstroke suggests that the stroke is

producing force intermittently, whereas the continual spread by birds using the tip reversal stroke indicates a more continual generation of force. The period of the wing stroke in which the tail is spread, for birds using a feathered upstroke, is curious, it being spread halfway through the downstroke and remaining so until halfway through the upstroke. Spedding (1981) has found that the vortex ring produced by the pigeon in slow forward flight (using a feathered upstroke) is not shed from the bird until the middle of the upstroke. The tail spreading could be of importance in the vortex ring generation.

Dathe and Oehme (1978) found no reason to explain why certain birds should use a feathered upstroke or one of tip reversal. Table 7.1 and Graph 7.1 show that body mass is of no relevance but that, generally, birds with aspect ratios below 7 tend to use feathered upstrokes while those with aspect ratios above that value use tip reversal. The kestrel is an exception, but its aspect ratio is close to the 'transition' value. The shape of the distal wing section is probably of importance as it is only this part of the wing which is used in the tip reversal upstroke. Birds with low aspect ratio wings tend to have rounded wing tips composed of relatively short primary feathers but having a large surface area. Birds with high aspect ratios generally have tapered wing tips with a large

Graph 7.1

Bar chart to show the (a) Aspect ratios, (b) Body masses and (c) Stroke plane angles for a selection of birds that hover using either the 'feathered' or the 'tip reversal' upstroke. The information for these charts was taken from the film of this survey for the zebra finch, pied kingfisher, kestrel, black headed gull, pigeon and budgerigar. Information for the remaining birds was from the following sources:

redstart : Ruppell, 1972b, sun bird : Zimmer, 1943 and jackdaw : Dathe and Oehme, 1978.

Graph 7.1

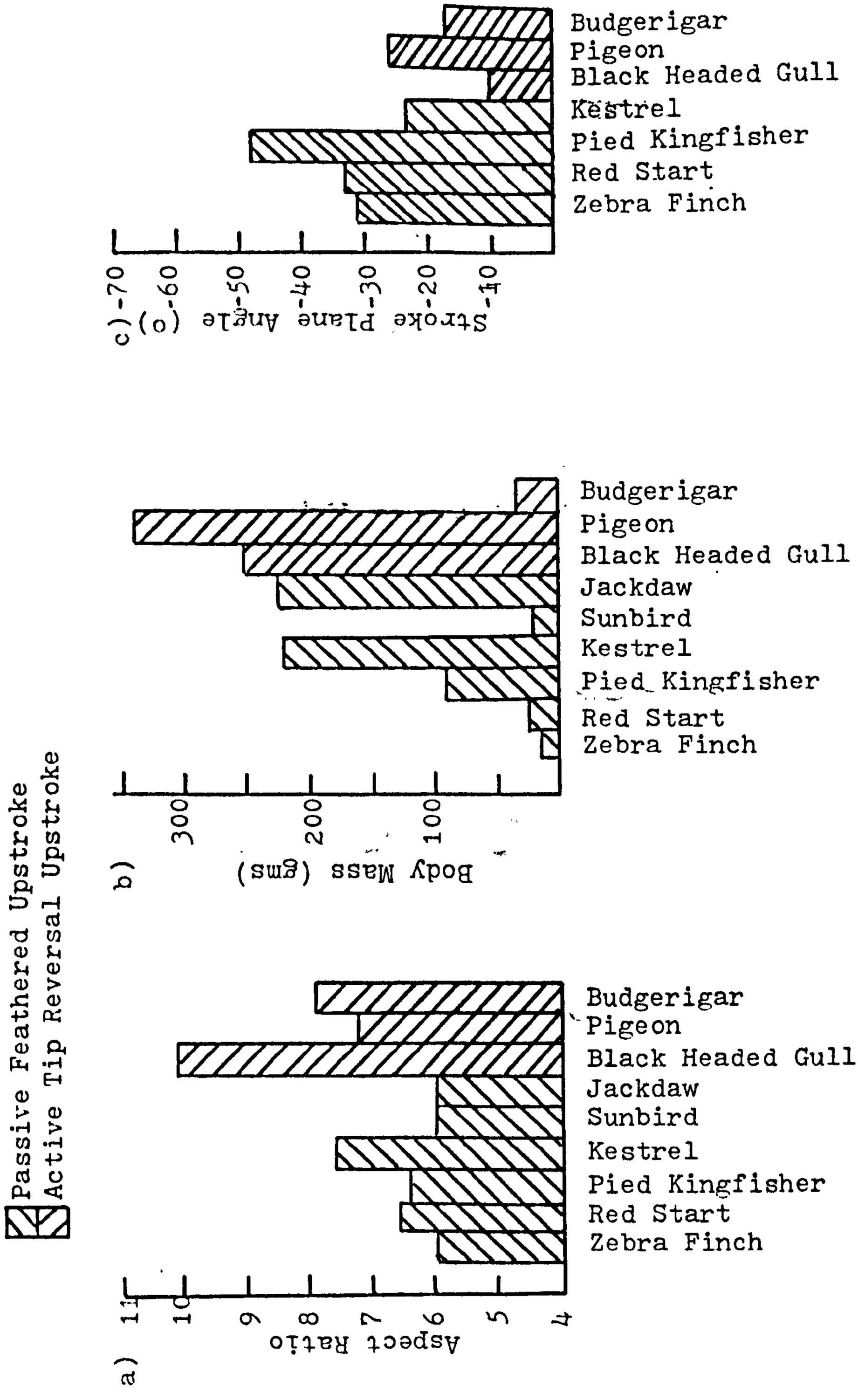
Passive Feathered Upstroke
Active Tip Reversal Upstroke
Budgerigar
Pigeon
Black Headed Gull
Jackdaw
Sunbird
Kestrel
Pied Kingfisher
Red Start
Zebra Finch
Aspect Ratio
11
10
9
8
7
6
5
4
Body Mass (gms)
300
200
100
Stroke Plane Angle (°)
-70
-60
-50
-40
-30
-20
-10

distal wing span of relatively small area. Such a distal section would have a relatively low induced and profile drag, whereas the distal section of a low aspect ratio bird would have high profile and induced drag if they were used in a tip reversal manner. There must be a critical shape of the distal wing section as aspect ratio is increased, when the induced and profile drag is sufficiently low for a tip reversal upstroke to be beneficial.

Determining the degree of upstroke used in cruise flight was done by investigating the variation of the mean calculated lift coefficient Γ_L in Chapter 6.5 . This approach is not possible in hovering because, although humming bird flight may conform to steady or quasi-steady state aerodynamic theory (Weis-Fogh, 1972), that of the pied flycatcher does not (Norberg, 1975), and this is probably the case for most hovering birds with inclined stroke planes (Ellington, 1977).

Is the ability to use the upstroke in hovering distinctly advantageous? Generally it is believed that the humming bird hovering wing cycle is very superior to the feathered upstroke wing cycle (Hertel, 1966). If the advantages are very great, it is surprising that other birds reliant on hovering, such as the pied kingfisher and the sunbird, have not developed a humming bird type cycle. A bird using only the downstroke can select an optimum downstroke plane angle,

which is probably not possible for a bird using both halves of the cycle which would tend to have shallower downstroke planes. For birds using the upstroke, the shallower downstroke plane may be necessary so that the wing tip does not have to be moved far upwards to begin the upstroke of horizontal or negative stroke plane. Rayner (1979c) describes how vortex rings may be produced in 'normal' (symmetrical, as in humming birds) and in 'avian' (feathered upstroke) hovering, in both cases producing a vertical stack of horizontal equally sized rings. From the above observations it would be predicted that birds using the feathered upstroke probably produce vortex rings in the manner described by Rayner. Those using tip reversal will produce one large ring on the downstroke and a smaller one on the upstroke. If tip reversal birds require a compromise stroke plane angle for the downstroke, these two rings may not be horizontal but shed at a slight angle opposite to each other, so that any horizontal ring momentum of the large and small rings is balanced. This may also be the case for humming birds. These questions can only be successfully answered by flow visualisation techniques as used by Spedding (1981) (See figure 7.3C).

Figure 7.3C

A simplified diagram to show the predicted wakes produced by a bird hovering using (a) feathered upstroke and (b) tip reversal upstroke. It is suggested that the bird using the 'feathered upstroke' produces a vertical stack of vortex rings as predicted by Rayner (1979C). The bird using the 'tip reversal upstroke' is suggested to produce one large ring on the downstroke and a small one during the upstroke. Both are shed at a slight angle to the vertical. This diagram is probably greatly simplfied as the small and large rings are likely to interfere with each other.

Figure 7.3C

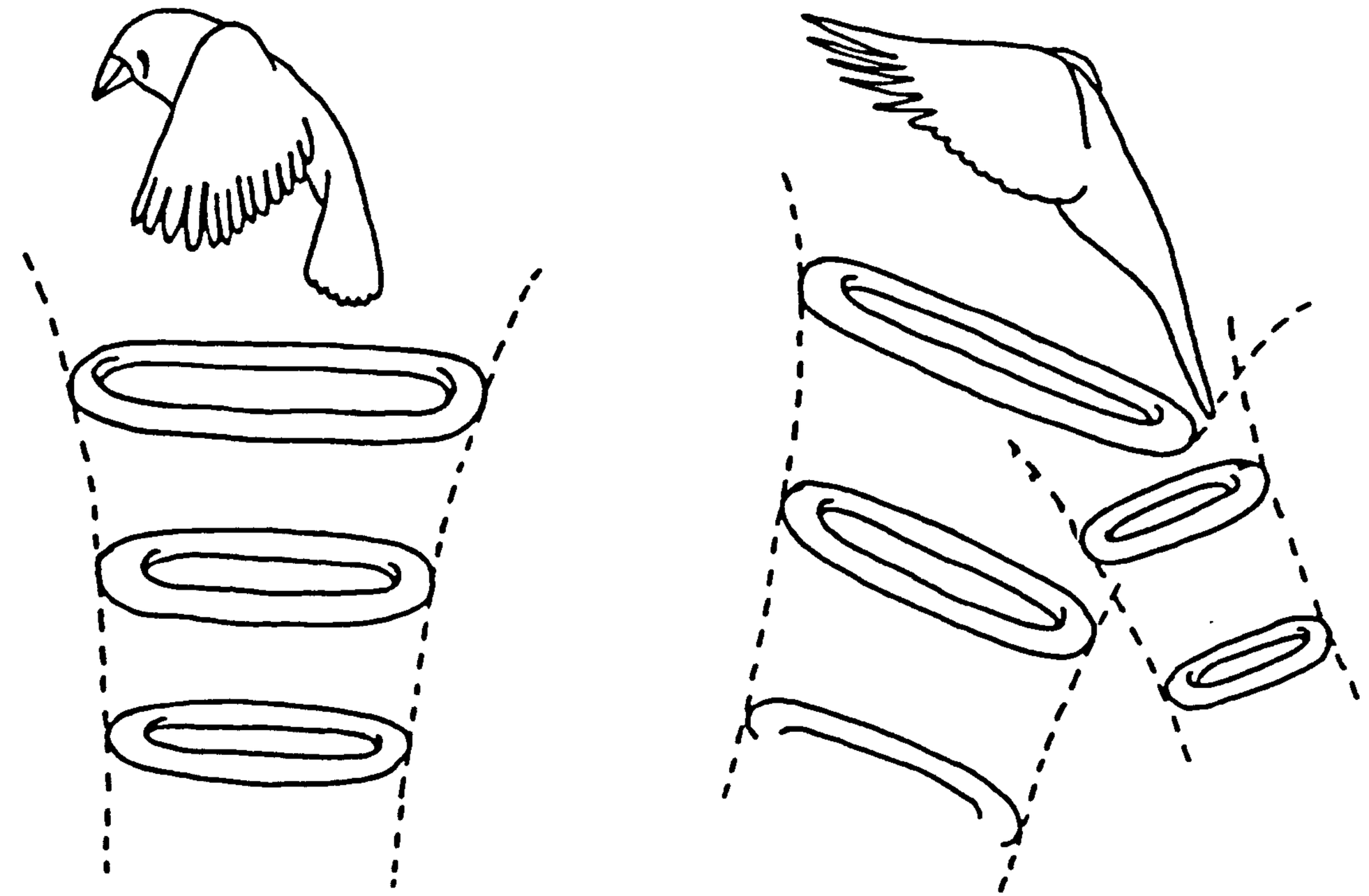

7.3 Take-off requiring running

7.3.1 Introduction

Very large terrestrial birds (approximately larger than 5kg) are incapable of taking off immediately by jumping, so require a take-off run to gain sufficient air speed for flight. Pennycuick (1975) relates the need for a take-off run in large birds to their insufficient available power to overcome the demands of very slow forward flight. The problem of take-off is accentuated for birds which must take off from water, a medium which does not provide a firm base for an initial take-off jump.

Here the running take-off technique of a large terrestrial bird, the Ruppell's griffon vulture Gyps ruppellii (approximately 7.6kg) and that of a large aquatic bird, the white pelican Pelecanus onocrotalus (approximately 8.5kg) are compared. Other types of running take-off are briefly discussed.

7.3.2 Ruppell's griffon vulture (Gyps ruppellii)

This vulture has a characteristic asymmetrical gait, illustrated in Figure 7.4 , with the left foot slightly preceding the right by about 0.02 seconds, with a phase difference of about 0.08 of the stride frequency. The vulture pushes off the ground with its left foot at the end of the upstroke, and with the right

Figure 7.4

Ruppell's griffon vulture Gyps ruppellii taking off. Frame numbers are given above each illustration and the film speed is 84fps. The scale is as given on the diagram.

Figure 7.4 Ruppell's griffon vulture

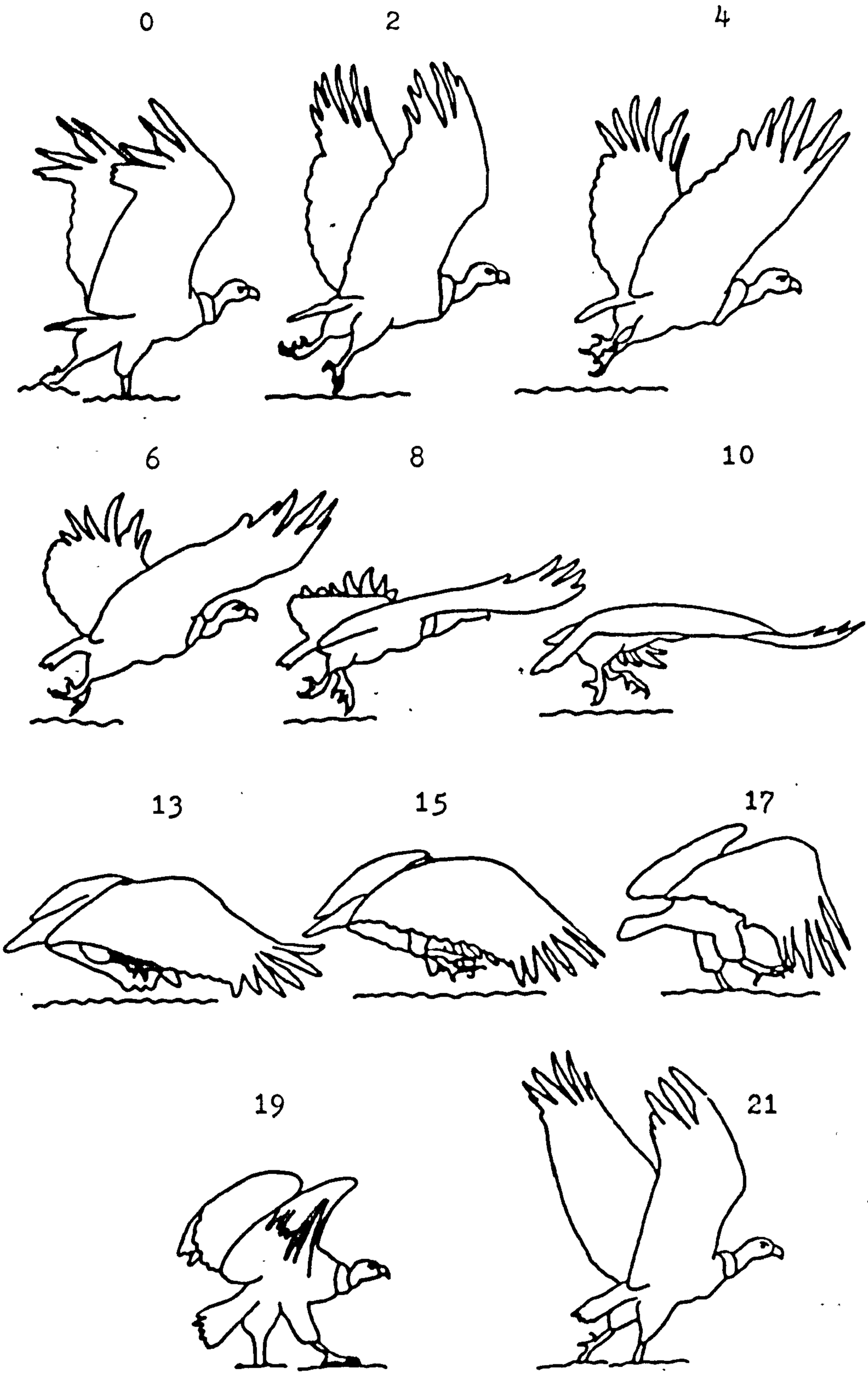

as the downstroke is initiated. During the downstroke both legs are moved forwards and the left foot is placed on the ground as the primary feather bending ceases. The right foot comes into contact with the ground shortly afterwards, and so both feet are on the ground for most of the upstroke. Throughout the take-off canter the vulture remains close to the ground.

During the final stride of the take-off run in apparently still air, the Ruppell's griffon vulture has a ground speed of approximately 6m s^{-1}. The air density was estimated to be 1.1kg m^{-3}. The stride frequency is the same as the wing beat frequency, 3.9 $\pm$ 0.1 Hz at take-off. During the final stride the stride length is approximately 1.5m, step length is 0.4m and duty factor is 0.24 (gait terms are as defined by Alexander et al 1977)

Wing beat frequency (Graph 7.2A) is at its maximum at the point of take-off, then decreases slightly to 3.7Hz for 8 wing cycles, and then gradually decreases to the cruise frequency of 3.2Hz. Downstroke ratio does not vary significantly from that of cruise flight during take-off and acceleration to cruise flight.

The stroke plane angle for the wing strokes before take-off is vertical for the wrist (-75° to -80° for the wing tip) but becomes shallower for the take-off wing stroke, with the wrist plane at -60° and the wing tip at approximately -45°. The wing beat positive

Graph 7.2

Changes in wing beat kinematics during the take-off and the acceleration to approximately cruise flight of the Ruppell's griffon vulture Gyps ruppellii.

(a) Wing beat frequency against wing stroke number. The vertical broken line denotes the wing stroke of take-off in this graph and in graphs (b) and (c). The standard deviation of cruise flight wing beat frequency is given at the right of the graph.

(b) Downstroke ratio against wing stroke number. The standard deviation of cruise downstroke ratio is given at the right of the graph.

(c) Left axis : Wing elevation against wing stroke number. Negative elevation is given by solid stars joined by a dotted line while positive elevation is given by circles enclosing clear stars and joined by a narrow continuous line.

Right axis : Wing amplitude against wing stroke number given by the solid circles joined by a wide continuous line.

*Note; This data is from film of only one take-off and should be interpreted accordingly.

Graph 7.2

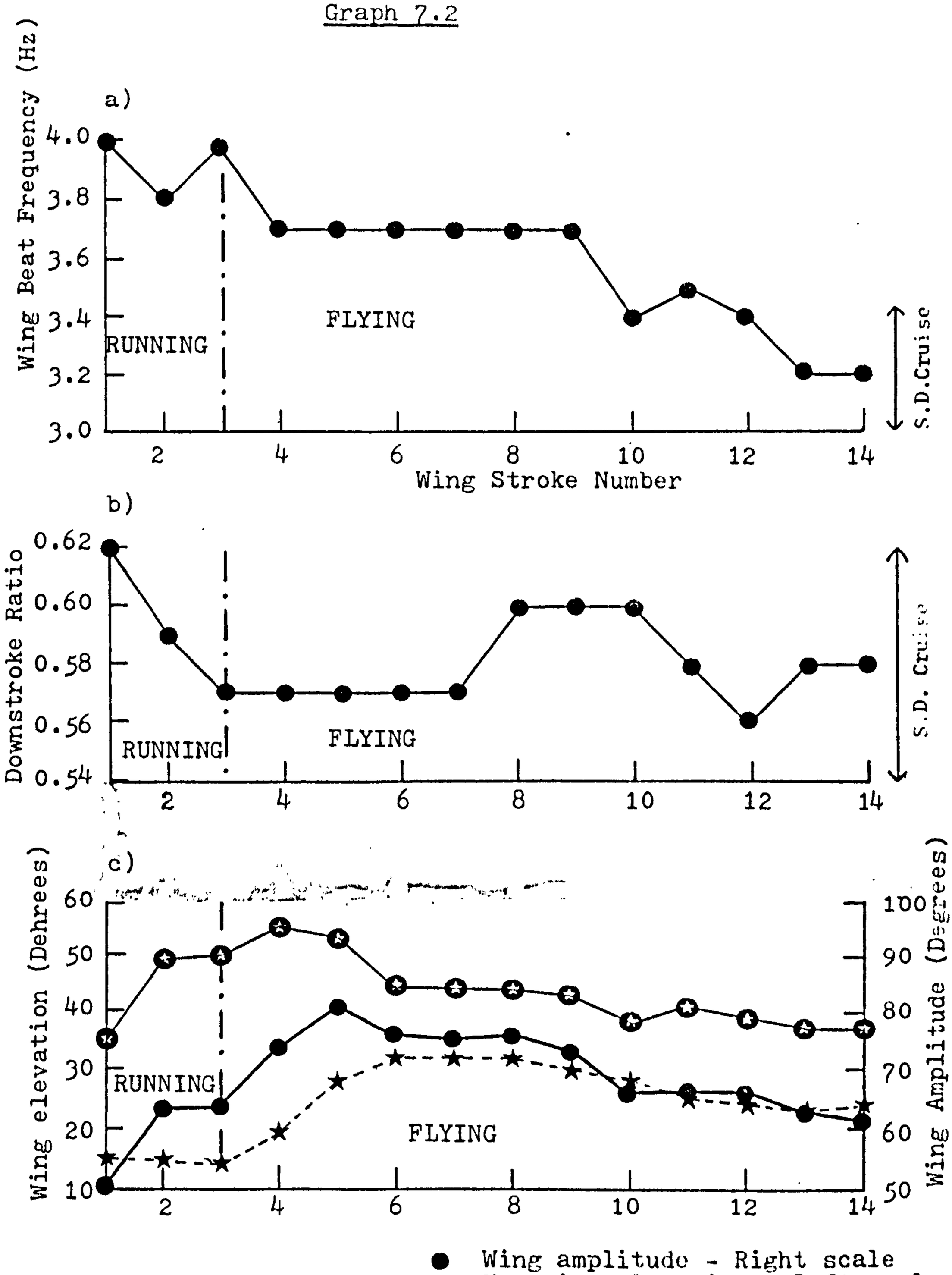
a)
Wing Beat Frequency (Hz)
4.0
3.8
3.6
3.4
3.2
3.0
RUNNING
FLYING
S.D.Cruise
2
4
6
8
10
12
14
Wing Stroke Number
b)
Downstroke Ratio
0.62
0.60
0.58
0.56
0.54
RUNNING
FLYING
S.D. Cruise
2
4
6
8
10
12
14
c)
Wing elevation (Dehrees)
60
50
40
30
20
10
RUNNING
FLYING
Wing Amplitude (Degrees)
100
90
80
70
60
50
2
4
6
8
10
12
14
● Wing amplitude - Right scale
★ Negative elevation - Left scale
✪ Positive elevation - Left scale

elevation gradually increases during the take-off run to a maximum for the take-off stroke of 55°. It then initially decreases rapidly to 44°, after which it gradually decreases to about 40° during cruise flight (Graph 7.2B). Negative elevation during the run is restricted to 15° owing to the animal's close proximity to the ground at the end of the downstroke and its near vertical stroke plane. During the take-off stroke the negative elevation is increased, and this increase continues for two strokes after take-off when negative elevation reaches its maximum of 32°. This is gradually decreased as the bird accelerates, until the cruise negative elevation is achieved. The overall amplitude (Graph 7.2B) therefore increases during the take-off run and reaches a maximum one stroke after the take-off stroke, remains level at about 75° for a short period during the acceleration, and then gradually decreases to the cruise amplitude level of about 62°.

7.3.3 White pelican Pelecanus onocrotalus

A white pelican taking off in shallow water (depth approximately 0.2 - 0.5m) is illustrated in Figure 7.5 . These actions are the same for the similarly sized chilean pelican Pelecanus thagus taking off in deep water. The feet are moved together, with both feet being immersed at the beginning of the downstroke and remaining so until the wings are approximately horizontal.

Figure 7.5

White Pelican Pelecanus onocrotalus taking off from shallow water. Every fourth frame is illustrated and the film speed is 100fps. The scale is as indicated

FIGURE 7.5

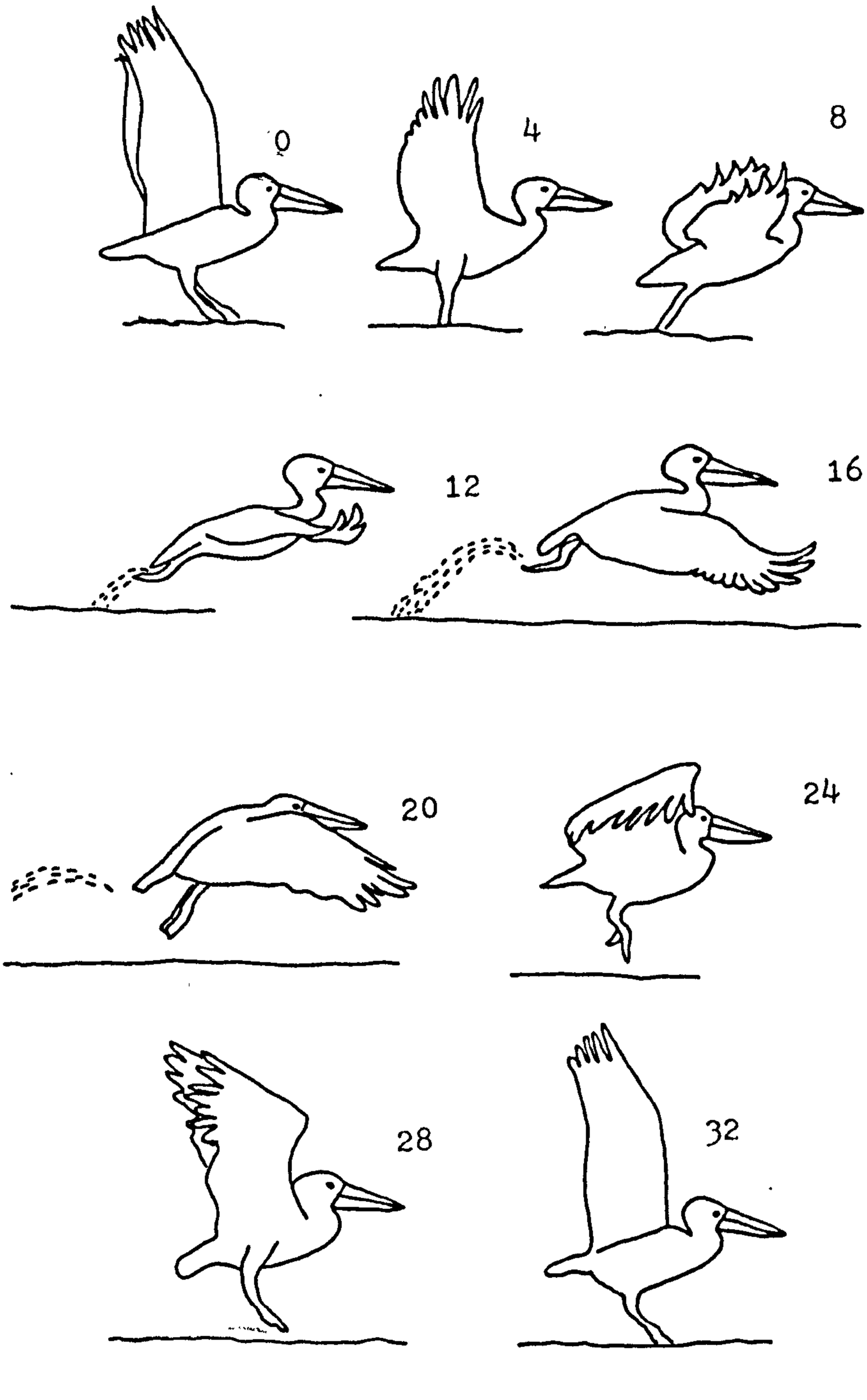

Graph 7.3

Changes in wing beat kinematics during the take-off and the acceleration to approximately cruise flight of the White pelican Pelicanus onocrotalus.
(a) Wing beat frequency against wing stroke number. The vertical broken line denotes the wing stroke of take-off in this graph and in graphs (b), (c) and (d). The standard deviation of cruise flight wing beat frequency is given on the right.
(b) Downstroke ratio against wing stroke number. The standard deviation of cruise downstroke ratio is given on the right.
(c) Left axis; Wing elevation against wing stroke number. Negative elevation is given by the solid stars and positive elevation is given by circles enclosing clear stars.

Right axis; Wing amplitude against wing stroke number given by solid circles.
(d) Stroke plane angle (wrist) with wing stroke number.
Note: Broken lines in (c) and (d) are for wing strokes were angles could not be measured due to the pelican turning.
This data is from film of only one take-off and should be interpreted accordingly.

GRAPH 7.3

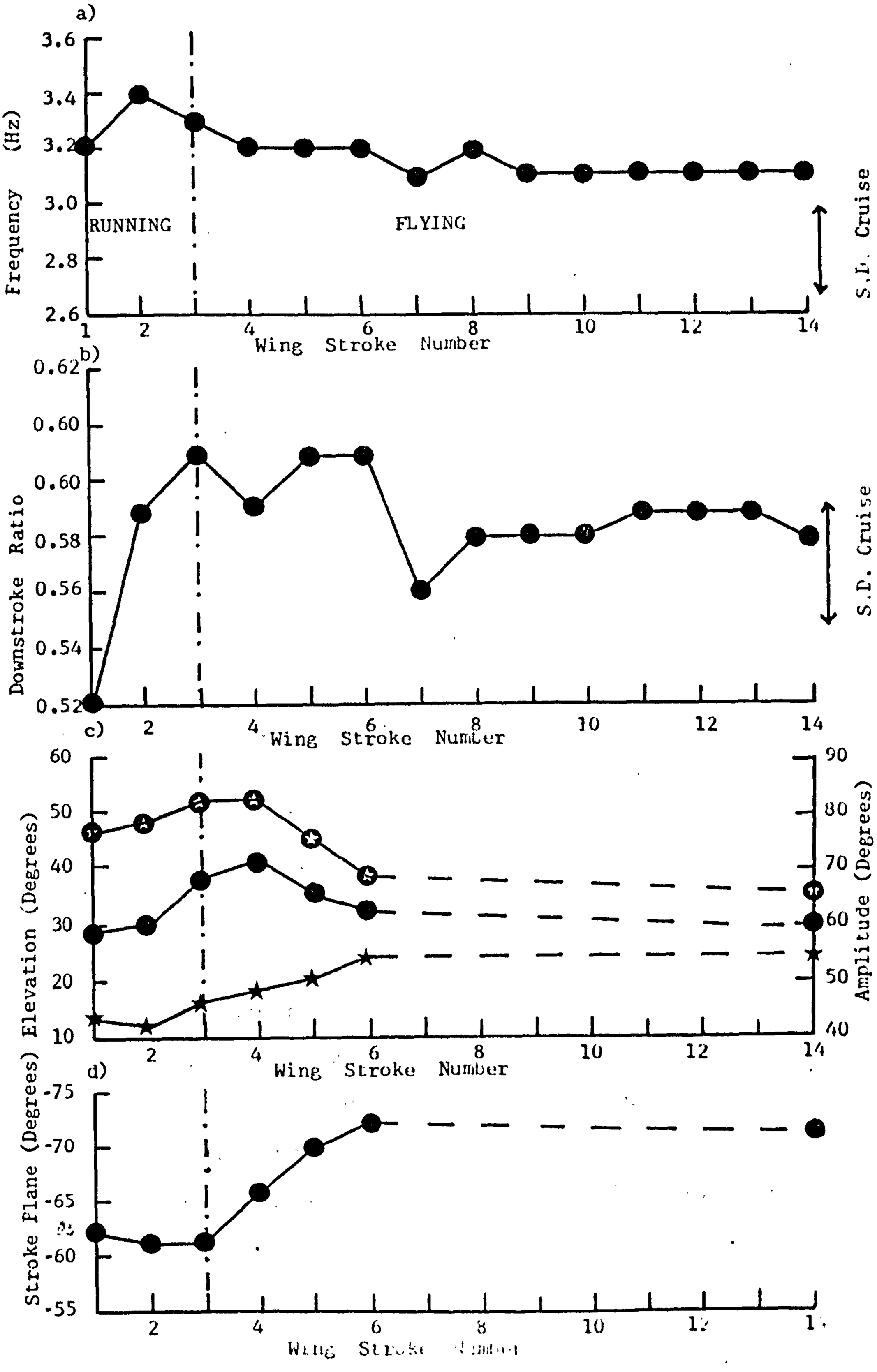
a)
3.6
3.4
3.2
3.0
2.8
2.6
Frequency (Hz)
RUNNING
FLYING
S.D. Cruise
1
2
4
6
8
10
12
14
Wing Stroke Number
b)
0.62
0.60
0.60
0.58
0.56
0.54
0.52
Downstroke Ratio
S.D. Cruise
2
4
6
8
10
12
14
Wing Stroke Number
c)
60
50
40
30
20
10
(Degrees) Elevation
90
80
70
60
50
40
Amplitude (Degrees)
2
4
6
8
10
12
14
Wing Stroke Number
d)
-75
-70
-65
-60
-55
Stroke Plane (Degrees)
2
4
6
8
10
12
Wing Stroke Number

The feet are then pushed out of the water leaving behind them an arc of spray water. The feet remain out of the water throughout the upstroke, and are brought forwards to enter the water just at the end of the upstroke. The pelican's body movements up and down are considerably more pronounced during the take-off 'bound' than those of the Ruppell's griffon vulture.

For the final stride before take-off, the white pelican studied had a ground speed of approximately 7m s^{-1}, a stride frequency (equal to wing beat frequency) of 3.4Hz, a stride length of approximately 2.2m, a step length of 0.5m and a duty factor of 0.25 . The air was still during the take-off, and the air density was estimated to be 1.05 kg m^{-3}.

Wing beat frequency increases to a maximum one stroke before take-off, and then gradually decreases to a level (3.1Hz)slightly above the cruise wing beat frequency (Graph 7.3A). The estimates of stroke plane angle show that it is relatively shallow throughout the take-off run (Graph 7.3D), increasing in steepness as the pelican accelerates. Wing beat positive elevation increases during the take-off run to a maximum at take-off, and then steadily decreases to the cruise positive elevation. Negative elevation starts to increase just before take-off and continues to do so for three strokes after to 24^{o}. Hence amplitude increases to a peak of approximately 72^{o} at take-off and

then varies in the same way as does positive elevation during the pelican's acceleration to cruise speed (Graph 7.3C).

7.3.4 Comparison of the take-off of the white pelican and the Ruppell's griffon vulture

The take-off techniques of these two similarly sized birds (the body mass and aspect ratio of the white pelican being 8.5kg and 8.6 respecitvely, and those of the Ruppell's griffon vulture being 7.6kg and 7 respectively) are distinctly different, probably as a result of differences in the medium from which they take off. The vulture, taking off from the ground, can support its weight with its feet during the upstroke, when little or no lift is generated. Lift for weight support during the upstroke does not have to be generated during the downstroke, and so the downstroke can be used primarily for generation of thrust. This is indicated by the very steep stroke plane angle during the take-off run. The white pelican, if taking off in deep water, cannot support its weight with its feet during the upstroke. Hence the feet are raised out of the water during the upstroke, and are in the water only during the downstroke when weight support is supplied by the wings. The take-off technique is therefore probably adapted for deep water, from which the pelican would normally have to take off.

In this case, although the pelican is taking off from shallow water, the same technique is still used.

The downstroke must also supply sufficient lift for the upstroke, and this emphasis on weight support by the wings is reflected in the shallower stroke plane angle of the pelican during its take-off bound. As the pelican must remain 'air borne' throughout the upstroke, it gains considerable height during the downstroke, whereas the vulture does not.

The feet of the pelican must mainly provide thrust during take-off, whereas for the vulture they provide primarily weight support, plus a certain amount of thrust. The vulture's asymmetrical gait has probably arisen as a compromise between having to have both feet on the ground during the upstroke of take-off and needing a certain amount of stability, particularly when moving at slower speeds. The pelican, since its weight is largely supported by the wings, gains its stability from the wings and so can move both feet together. This subject is in need of greater investigation, if possible under controlled conditions.

7.3.5 Other running take-off techniques

Norberg and Norberg (1971) describe the take-off of the diver Gavia stellata, where the 'skittering' feet are alternately pushed through the water synchronously with the wing stroke. One foot pushes

during the downstroke and the other during the upstroke, the feet contributing the extra vertical force to keep the diver out of the water while acceleration is accomplished by the feet and the wings. A similar take-off technique has been observed in the mallard Anas platyrhynchos, the Bewick swan Cygnus columbianus and the mute swan Cygnus olor.

The white necked cormorant Phalacrocorax carbo and the Peruvian booby Sula variegata (Figure 7.6) move the feet together similarly to the white pelican, having the feet immersed in water during the downstroke, pushing them out of the water at the end of the downstroke, and then bringing them forwards in the upstroke. This take-off technique is apparently characteristic of the Pelecaniformes. The lesser flamingo Phoeniconaias minor (Figure 7.7) has a stride frequency which is half that of its wing beat frequency. This bird takes of from very shallow water and so can support its weight with its leg throughout the upstroke, alternate feet being on the ground for each upstroke. Both legs are 'floated' during the downstroke. The relatively low stride frequency of the lesser flamingo is probably related to its long leg length.

Figure 7.6

Peruvian booby Sula variegata taking off. The film speed is approximately 40fps and the frame numbers are as shown.

Figure 7.6 Peruvian booby

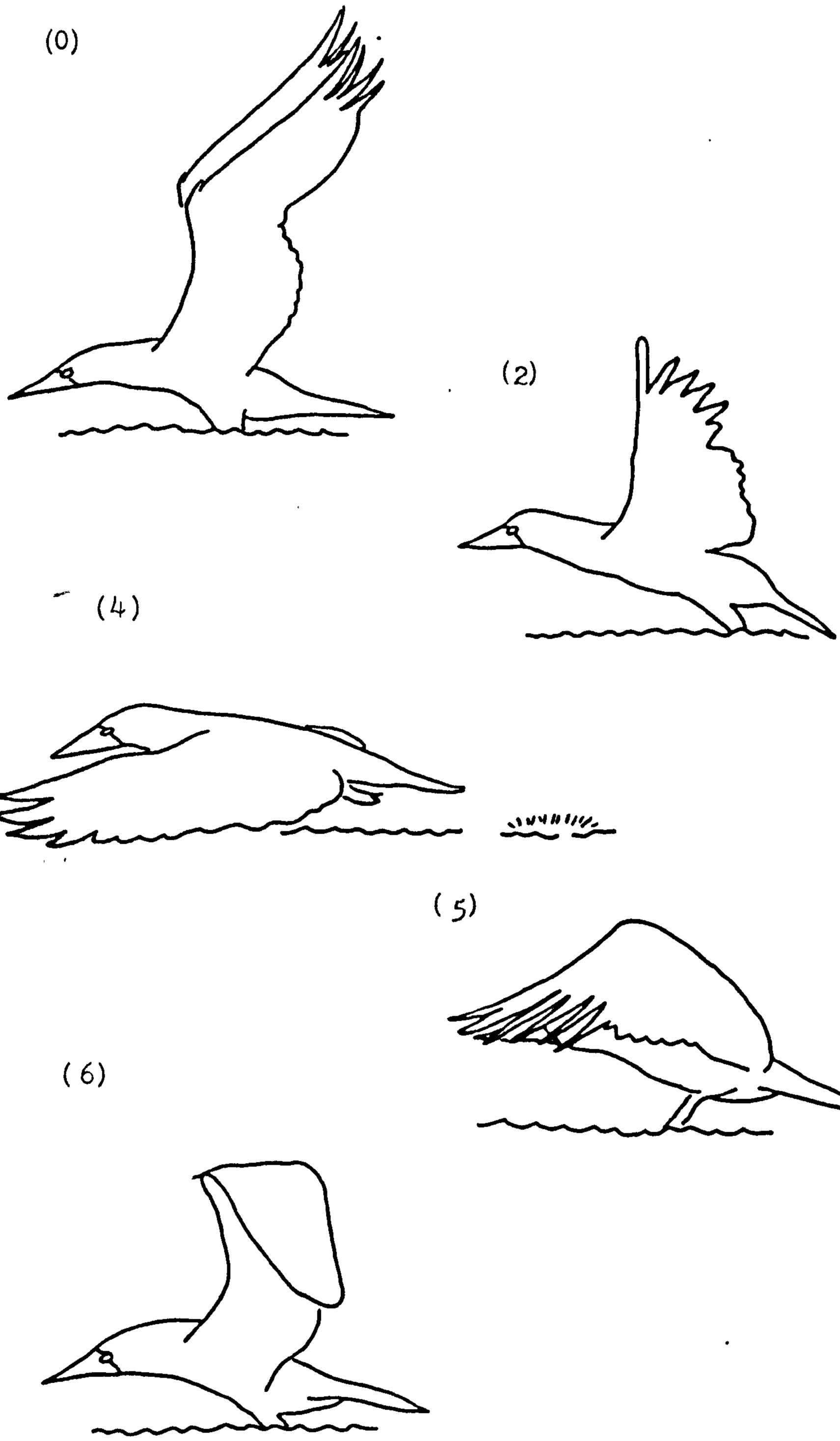

Figure 7.7

Lesser flamingo Phoeniconaias minor taking off in shallow water. Every tenth frame is illustrated and the film speed is 200fps. The approximate scale is given.

Figure 7.7 Lesser Flamingo

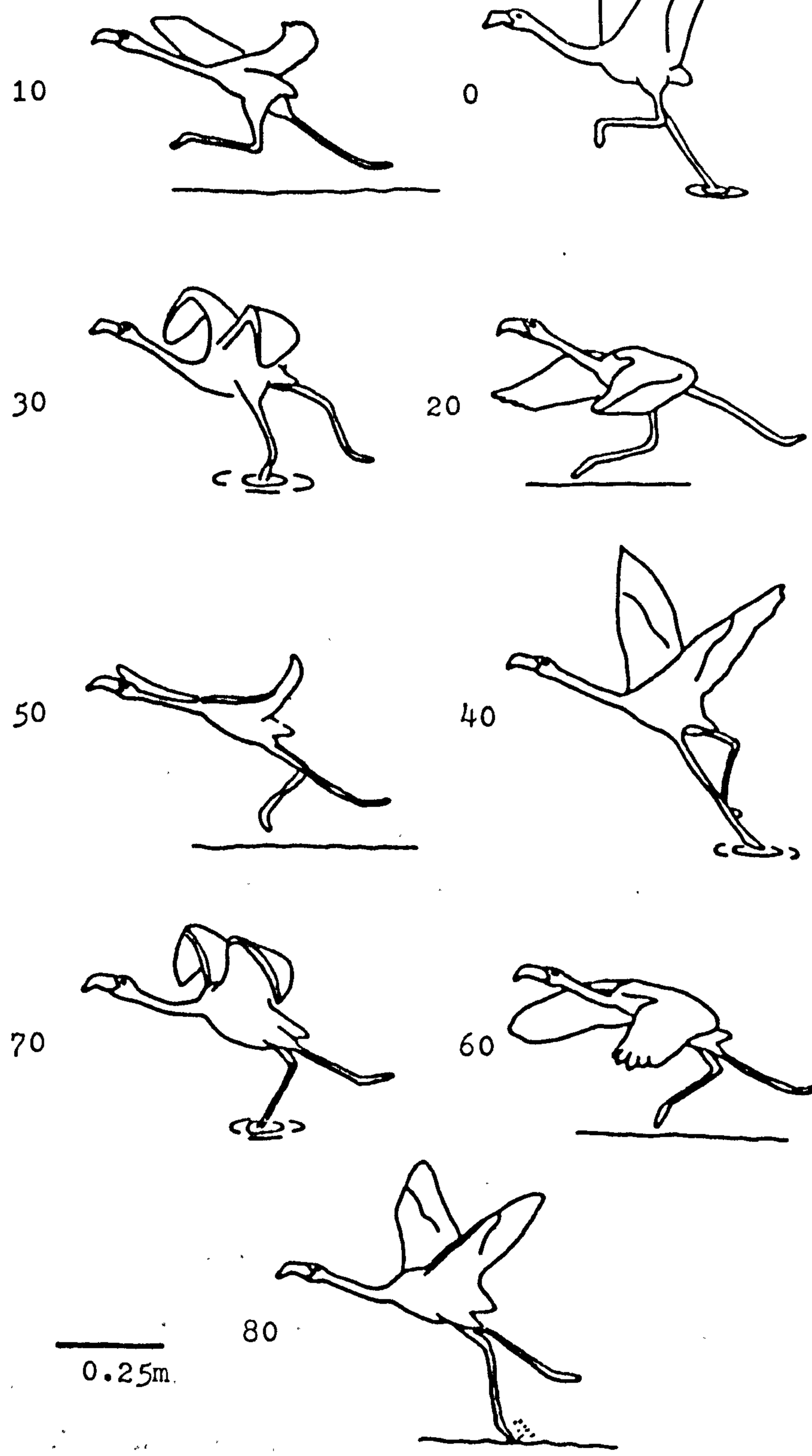

7.4 Landing in the wandering albatross

A wing stroke which is distinctly different from anything so far described is used by the wandering albatross Diomedea exulans when landing (Figure 7.8). At the beginning of the downstroke the wing is positively rotated at the humerus, and pronated. Approximately half-way through this part of the cycle the humerus is rotated negatively, bringing the wing into a position of high angle of incidence. The feathers along the leading edge of the proximal wing section show 'ruffling' as the wing reaches the end of the downstroke. Throughout the downstroke the primary feathers are well bent at their tips and the alula is raised. The amplitude of the downstroke is very small, the wing elevation moving from approximately $+20^{o}$ to $+5^{o}$.

The upstroke begins with the proximal section being raised, and the wrist being slightly flexed. The elbow apparently remains extended throughout the stroke. During the upstroke the trailing edge of the secondary feathers often shows ruffling, the feather tips being raised upwards. When the proximal section reaches its highest elevation, the humerus is positively rotated, the wrist extended and the manus pronated for the next downstroke.

The wing beat frequency of this stroke is very high, measured within the ranges of 5.1 ± 0.3Hz and 5.8 ± 0.3Hz for the two individuals filmed. This is

Figure 7.8

Wandering albatross Diomedea exulans landing viewed from approximately head on and tail on. Every second frame is shown and the film speed is 60fps. The wing span is 3.4m.

Figure 7.8 Wandering albatross

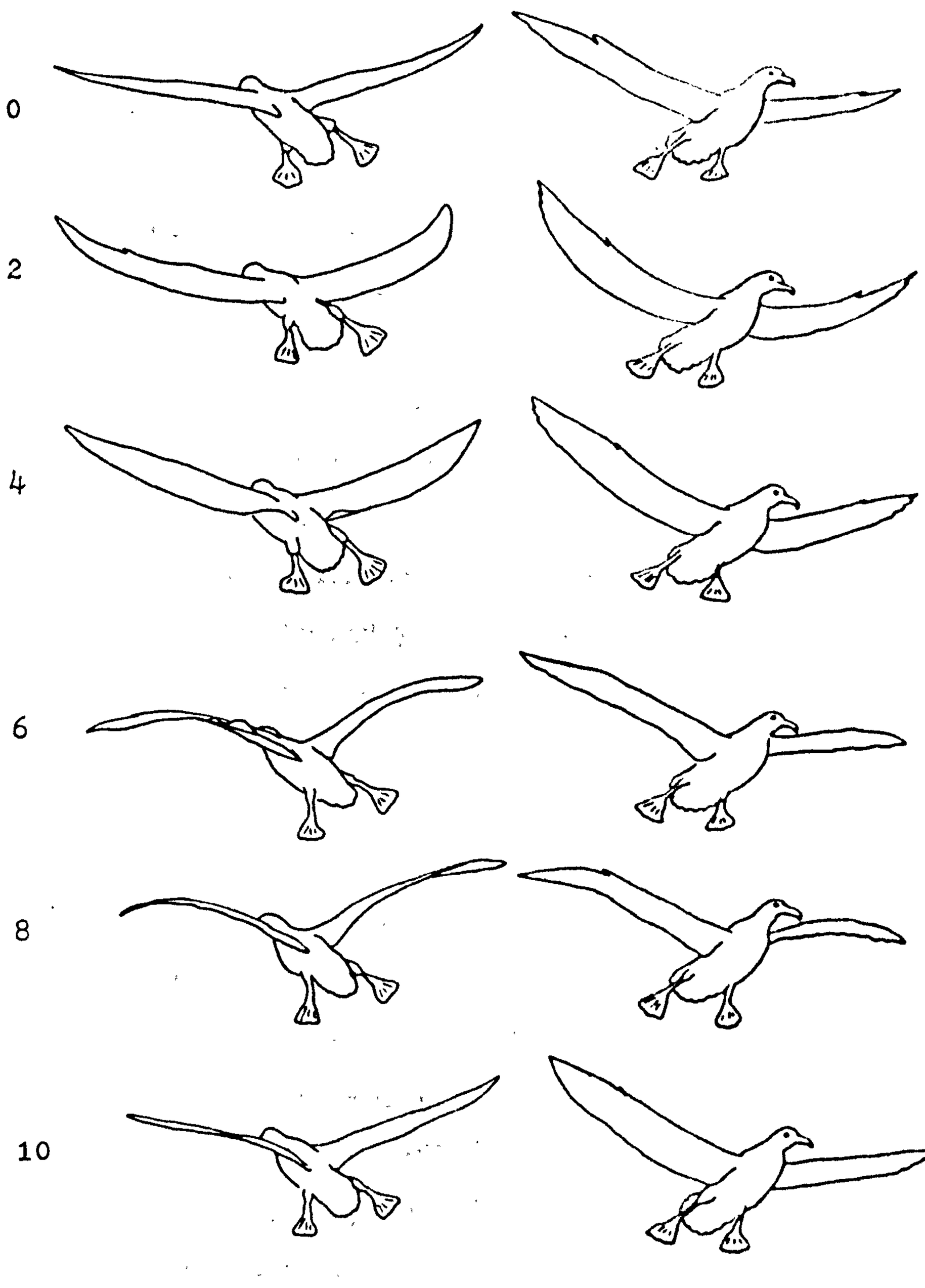

approximately twice the cruise frequency of 2.5Hz. Throughout the stroke the tail is fully spread and the feet are extended backwards, presumably to extend the 'lifting' surface area.

Lift is apparently generated on the downstroke and, from the amount of leading edge feather ruffling at the base of the downstroke, it appears that the wing is very close to the stall. Trailing edge lifting of the secondary feathers during the upstroke implies that this wing section is providing lift. This would have a large backward component, and so would be useful for braking the bird before landing. The very small amplitudes may have two causes. Firstly, the very high wing inertia (moment of inertia scales crudely as l^5) of the albatross may make a large amplitude prohibitive. Secondly, the positive elevation may be limited by the locking device described by Pennycuick (1982 b) (Chapter 6.6.3).

To compensate for the low amplitudes, the wing beat frequency has been raised to maintain the required airflow over the wings, and to maintain a mean lift coefficient below the maximum. This may have the added advantage that, if frequency causes specific power increases (power per unit mass of muscle) as argued by Pennycuick (1975), then the landing technique of the albatross may make it possible to utilise the maximum available power output from the muscles.

7.5 Clap and fling

Weis Fogh (1973) proposed a novel lift mechanism to explain the very high lift coefficients $\bar{C}_L$ of the hovering chalcid wasp Encarsia, whereby the wings are clapped together above the body and then flung apart about their trailing edges. Air is sucked into the spaces between the wings and creates circulation around them. This eliminates the Wagner effect which is the lag in circulation, and so to lift, when a wing is suddenly set in motion. Lighthill (1973) confirmed that the mechanism is theoretically feasible. Clap and fling has been observed in all small insects so far studied, and also in a number of larger ones (Ellington, 1977). Up to this date it has only been identified amongst birds in the pigeon (Weis Fogh, 1973) and the pied flycatcher (Norberg, 1975). Ellington (1977) also suggests that a near clap and fling, whereby the wings are separated by less than half a wing chord at the beginning of the downstroke, can also help to eliminate the Wagner effect.

In this study, film has been obtained showing the use of clap and fling, and of near clap and fling, by numerous birds during hovering, take-off and landing. These species are listed in Table 7.2 which also gives each individual's body mass, aspect ratio, the degree to which the primary and secondary feathers come into contact, and the type of flight for which the observation was made. Illustrations are given for a selection of

these cases in Figure 7.9 . It can be seen that in the majority of cases only the secondary feathers come into contact, the primaries being sometimes positioned for a near clap and fling, but generally being too far apart. Norberg (1975) believes that as only the proximal or 'arm' wing is involved in the clap and fling of the pied flycatcher Ficedula hypoleuca, the mechanism is probably of little importance. This is probably not the case, as the proximal wing section, in slow forward flight, has a very low velocity relative to the air, and so the creation of circulation for this part of the wing by clap and fling may be of great importance in enabling it to produce lift in the downstroke.

Some degree of clap and fling appears to be used very widely in hovering, and for the first wing stroke of birds which take off with an initial jump. Birds using take-off runs apparently do not use this technique, probably because their forward speed makes it unnecessary. However, the vast majority of birds are likely to be capable of bringing the wings into the clap and fling or the near clap and fling positions when the need arises, regardless of their size or wing shape (Table 7.2) with the probable exception of the larger, very high aspect ratio Procellariiformes.

TABLE 7.2 Clap and fling.

The degree of feather tip contact and the type of flight where the listed species exhibit a clap and fling.

Species Name	Body Mass(kg)	Aspect Ratio	Type of Flight	Type of contact between feather tips	
				Primaries	Secondaries
Budgerigar	0.032	7.9	Hovering	Majority contact	Full contact
Pied kingfisher	0.09	6.4	Hovering	-	Full contact
Kestrel	0.216	7.6	Vertical climb or hovering	-	Partial contact
African goshawk	-	-	Take off	Majority contact	Full contact
Crowned hawk eagle	-	-	Take off	-	Partial contact
Hooded vulture	2.0	6.7	Take off	-	Within 0.5 cord
Turkey vulture	-	-	Take off	Within 0.5 cord	Full contact
Verreaux's eagle owl	-	-	Take off - Slow flight	-	Full contact
Black headed gull	0.251	10.1	Hovering	-	Partial contact

TABLE 7.2 continued

Species Name	Body Mass(kg)	Aspect Ratio	Type of Flight	Type of contact between feather tips	
				Primaries	Secondaries
Grey head gull	—	—	Take off	Within 0.5 cord	Full contact
Sacred ibis	—	—	Take off	-	Partial contact
Saddle bill stork	—	-	Take off	-	Partial contact
White necked cormorant	2.12	—	Take off	-	Partial contact
Chilean pelican	—	—	Take off	-	Partial contact
Mallard	1.1	8.7	Take off	-	Partial contact
Barnacle goose	1.15	—	Landing	-	Partial contact
Pigeon	0.34	7.2	Hovering Take off	Majority contact	Full contact

Figure 7.9

Examples of birds exhibiting the clap and fling.

i) Sacred ibis

ii) Barnacle goose

iii) Chilean pelican

iv) Verreaux's eagle owl

v) Saddle bill stork

vi) White necked cormorant

vii) Turkey vulture

viii) Kestrel

ix) African goshawk

Figure 7.9

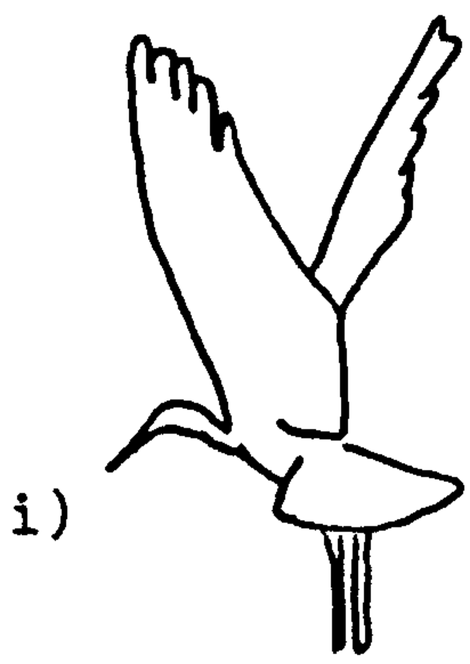

i)

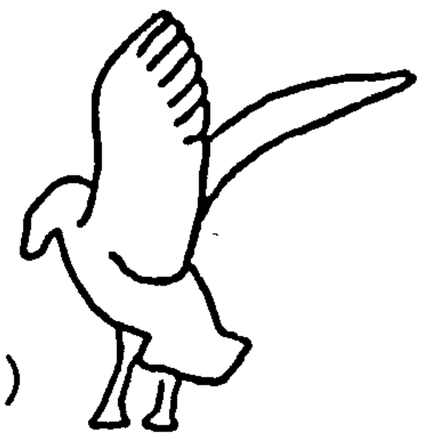

ii)

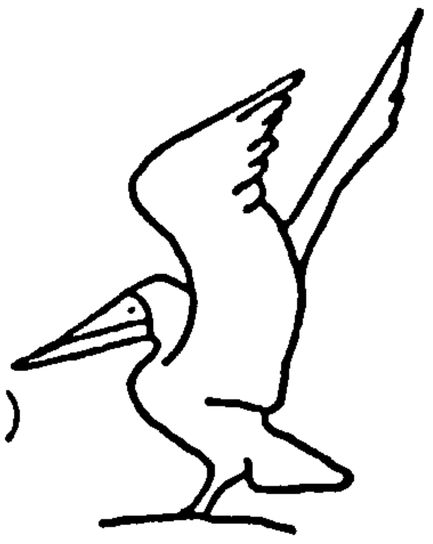

iii)

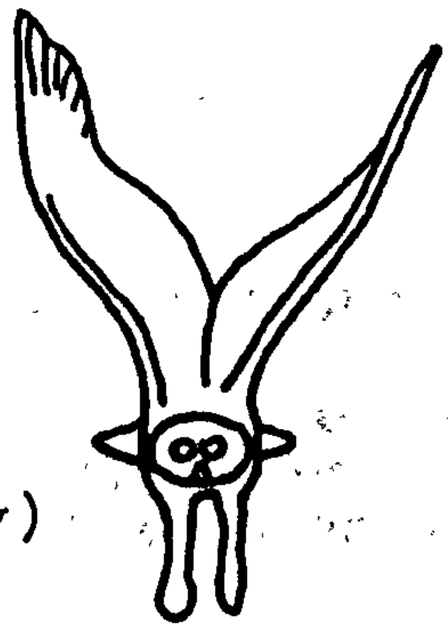

iv)

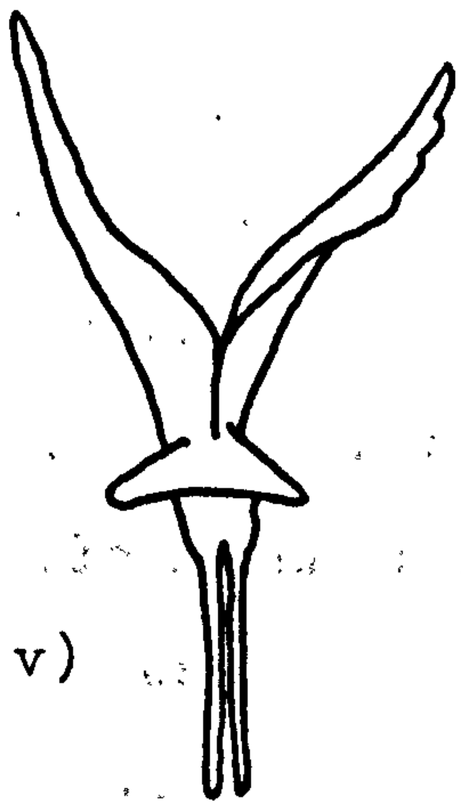

v)

vi)

vii)

viii)

ix)

7.6 Steady flight at speeds between hovering and cruise

7.6.1 Introduction

Steady flight at speeds less than cruise speed is practiced by many hunting birds when there is an ambient wind. Such birds can remain stationary relative to the ground by flying into the wind, balancing their forward speed with the wind speed. This form of flight is regularly termed hovering. It is not hovering in the true sense as many of the birds which hunt in this manner, such as the kestrel (Falco tinnunculus 0.20kg), the common buzzard (Buteo buteo 0.8kg) and the osprey (Pandion haliaetus 1.1kg) are all theoretically too large to hover for more than a few strokes (Rayner, 1979b) The hunting technique is usually carried out in an area of updraught, for example along a slope or above an obstacle such as a hedge or a line of trees, and it is only carried out over flat areas in strong winds greater than about 5m s^{-1}, by the kestrel.

7.6.2 Kinematics of the kestrel Falco tinnunculus in steady slow forward flight

The kestrel nearly always hunts in this manner when the wind is suitably strong and the terrain favourable. In calm conditions it hunts from a perch. Film was obtained of a male kestrel hunting into wind, and the stroke for head-on and side-on views is illustrated in Figure 7.10 . . The head-on wing tip trace is also given

Figure 7.10A

Male kestrel hunting into wind viewed from head on and side on. Every fifth frame is illustrated and the film speed is 200fps. The wing span is 0.73m.

Figure 7.10A Kestrel

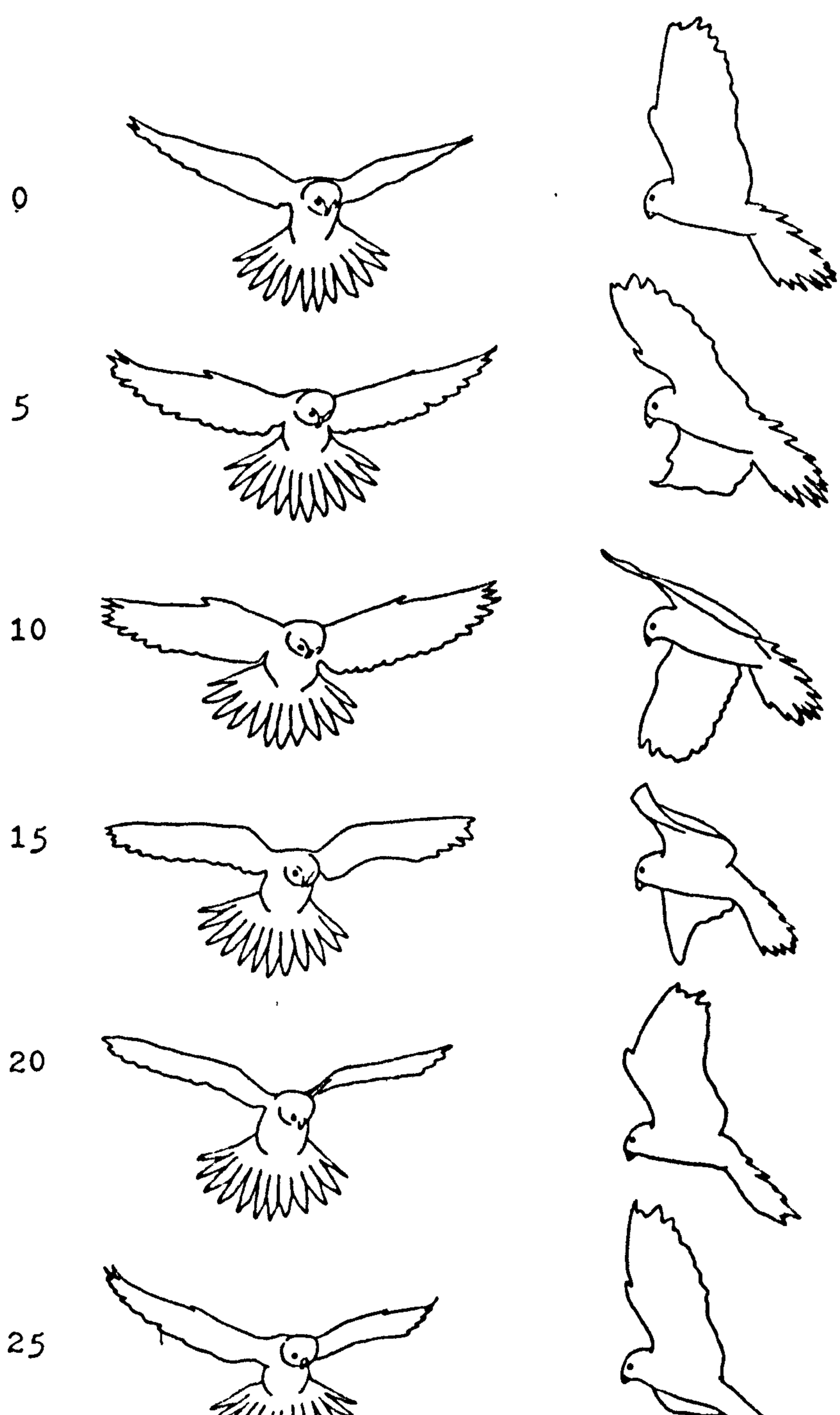

Figure 7.10B

Wing tip traces of a male kestrel hunting into wind in an updraught. The position of the wing tip is given by the solid circle for each frame and the film speed is 200fps. The wing span is 0.73m.

Figure 7.10C

Wing tip trace of a male kestrel in cruise flight flying directly away from the camera. The film speed is 200fps and the wing semi-span is 0.365m.

Figure 7.10B Kestrel head on slow forward flight into wind.

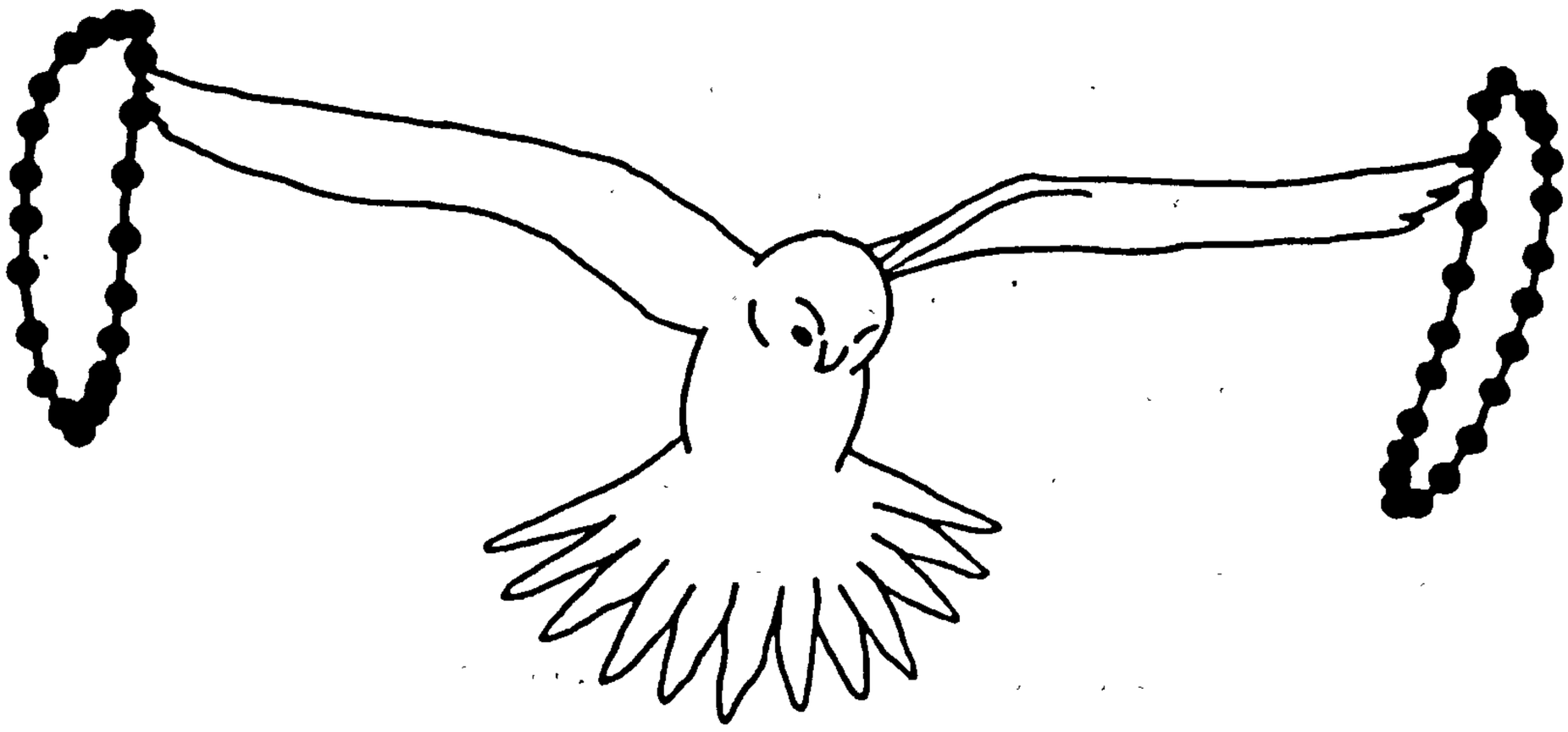

Figure 7.10C Kestrel tail on cruise flight.

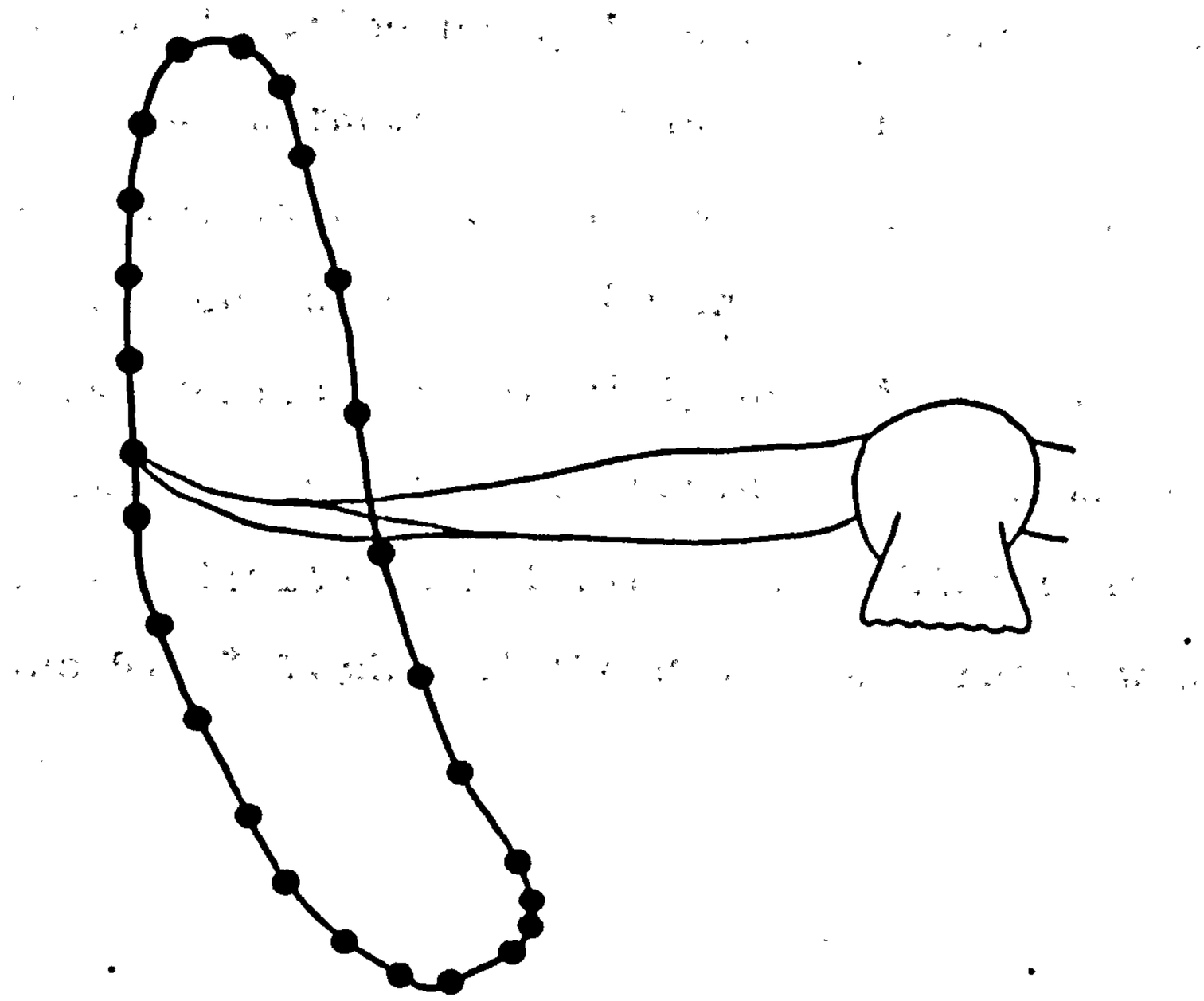

with a similar trace of a male kestrel in cruise flight for comparison. The downstroke begins with the wrist slightly flexed. It is extended during the first quarter of this period, and then the wing is pronated. The wing tips separate and bend at the tips, and the anula is raised. At the base of the downstroke the proximal wing is negatively rotated, supinated and raised, and the wrist is slightly flexed. During the upstroke the middle primary feathers are depressed at their trailing edge (side-on illustration, Figure 7.10) giving the distal wing trailing edge a U-shaped appearance. At the top of the upstroke the proximal wing is positively rotated and the next downstroke begins. The tail remains fully spread throughout the cycle.

The upstroke wing span is only reduced by 12% of the downstroke, compared to a 27% reduction in cruise flight. The amplitude varies greatly in the three sequences filmed, with up elevation being between 35^{o} and 28^{o}, and the down elevation between 0^{o} and 14^{o}. The downstroke period remains fairly constant at 55 ± 5 ms , while the upstroke period varies from 40 ms to 65 ms. Longer upstroke periods are possibly associated with larger wing amplitudes, but this could not be shown on the basis of the limited available film. Wing beat frequency was 9.2 ± 1.3Hz and the downstroke ratio was 0.5 ± 0.06 .

7.6.3 Discussion

The wing stroke of the kestrel when hunting into wind is of very high frequency, slightly higher than the value given for hovering. This may be an artificial difference; the bird filmed hovering was a female which is usually about 15% heavier than the male, and this could account for the frequency anomaly. The amplitude of this stroke, although it shows considerable variation, is far lower than for cruise or hovering flight. Field observations indicate that the stroke amplitude of the kestrel when hunting into wind decreases with increases in the strength of the updraught. In strong wind conditions they can remain stationary without flapping, the updraught balancing their rate of sink. In the filmed sequences, the combination of the high frequencies with low amplitudes results in downstroke peak wingtip velocities of 7 to 8m s^{-1}, similar to those in cruise flight.

The wing stroke is distinctly different from both hovering and cruise flight of the kestrel, having a combination of low amplitude, high frequency and a very small amount of wrist flexion and upstroke span reduction. The stroke is also not what would be expected for an intermediate between hovering and cruise; hence it is probably a specific stroke designed to enable the bird to fly with good control and stability for long periods, at slow speeds and at the lowest cost for the speed. The low amplitudes and small upstroke span reductions

are reminiscent of the cruise wing strokes of high aspect ratio birds (Chapter 6 Section 2), which were shown to use the upstroke for weight support. The kestrel wing stroke is probably gaining similar upstroke advantages. If it were not, a large amount of upstroke wrist and elbow flexion would be expected as in hovering and, to a lesser extent, in cruise flight. The continuously well-spread tail, not found in kestrel hovering, also indicates that lift is produced throughout the wing stroke. It is not clear how the primary feathers function in the upstroke, showing the curious bending at the trailing edge of the distal wing. The proximal wing appears to be suitably angled for lift production in both halves of the cycle. The stroke, therefore, probably produces forward thrust and weight support for the downstroke, and weight support and backward thrust on the upstroke. The horizontal forces must balance each other and the bird's drag so that it can remain stationary relative to the ground.

Very low amplitude wing movements are reported for Wilson's storm petrel (Oceanites oceanicus) by Withers (1979), which is a bird that 'hunts' in a similar manner to kestrels using the ambient wind. Withers claims that the Wilson's storm petrel 'hovering' stroke is unique, whereas it appears to be similar to that of the kestrel, judging by Withers' (1979) illsutrations. However, Withers' stroke description is almost impossible to interpret, since he claims that each frame of his

illustration represents 1/16 s and the stroke appears to consist of 10 frames, giving this 34g bird a wing beat frequency of 1.6Hz, which is considerably lower than that of an 8kg wandering albatross! The framing rate of the film Withers analysed was only 16Hz and this is approximately equivalent to the wing beat frequency expected for the bird's dimensions (Chapter 6). It seems that the petrel's wing beat frequency was slightly faster than that of the film framing rate, and so each frame exposed would be just more than a cycle after its predecessor. This means that the apparent stroke periods are completely dependent on the degree at which the bird's frequency and the camera framing rate are out of phase, and can bear no relationship to the bird's stroke period. Furthermore, rapid stages of the stroke may not be recorded at all by this 'stroboscopic' effect. This is a good example of how cine films at a framing rate which is far too low relative to the speed of the actions it is being used to analyse, can lead to completely misleading results.

7.7 The scaling of maximum power kinematics

The limited data on birds flying at maximum power is suitable for investigating the effects of body mass on maximum power kinematics, but not for investigating variations in wing span and area (as in Chapter 6 for cruise flight). Graphs of wing beat frequency, amplitude and downstroke ratio with body mass are given in Graphs 7.4A, 7.4B and 7.4C respectively, and the correlation equations and coefficients are given in Table 7.3 . The ——— line given on the graphs is that of the Reduced Major Axis (R.M.A.)

It can be seen that wing beat frequency decreased as $m^{-0.26}$ or approximately $m^{-\frac{1}{4}}$, the correlation coefficient being high at -0.91. Amplitude also decreases, scaling as $m^{-0.15}$. The general trend is slightly misleading, as maximum power amplitude remains very high for birds capable of hovering, (for example, the pigeon, with a body mass of 0.35kg, has an effective hovering amplitude of 180^{o}) and only decreases with birds whose maximum-power flying speed is higher than zero. Stroke plane angle has been shown to be independent of mass in hovering in Section 2.4, being determined by the type of hovering wing stroke which in turn is related to the wing's aspect ratio. The stroke plane angles of larger birds with forward air speed at take-off is also likely to be mass-independent, being determined by the take-off speed.

Downstroke ratio in maximum power flight, similar to cruise flight, shows little alteration from 0.5 for birds below approximately 2kg, and above this gradually increases to approximately 0.6 for birds between 7kg and 10kg.

The product of downstroke period, amplitude and wing span, the downstroke wing tip velocity, is plotted with mass on Graph 7.5A, and the measured downstroke peak velocity on Graph 7.5B. Correlation equations and coefficients are given in Table 7.3. Graph 7.5A has a low correlation coefficient of 0.45 with a low level of significance (10%) and the R.M.A. has a slope of 0.12. Measured downstroke peak velocity has a higher correlation coefficient of -0.67 (significant at the 1% level) although it is calculated from only six data points. The slope of the R.M.A. is -0.06.

GRAPH 7.4A

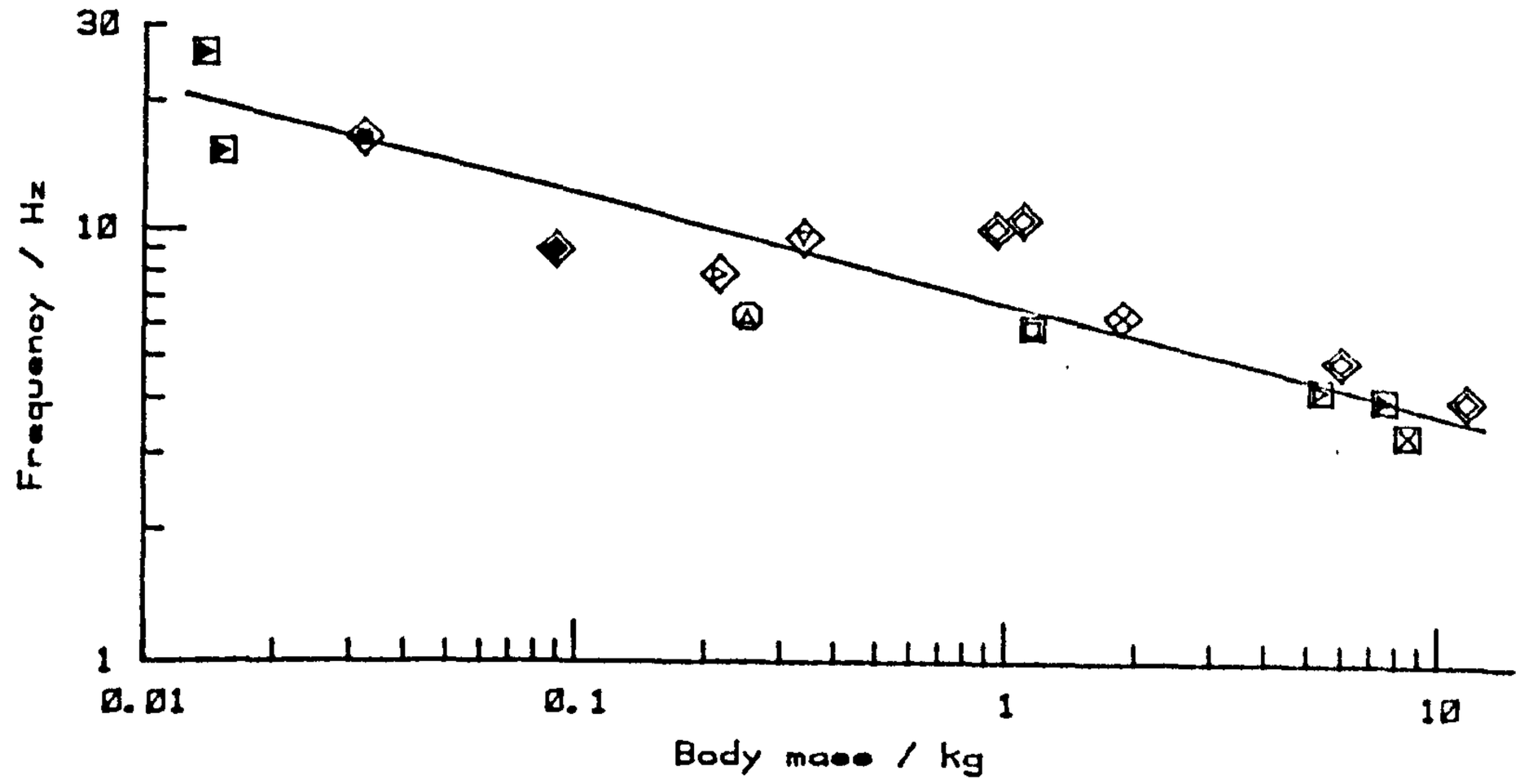

GRAPH 7.4B

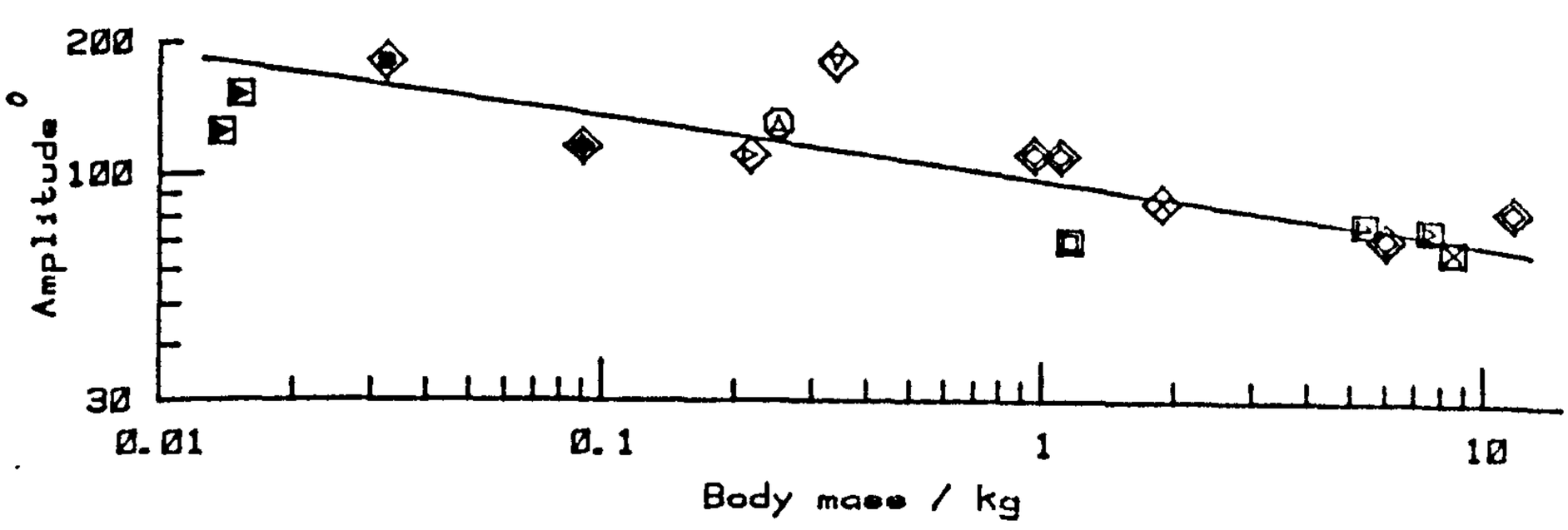

GRAPH 7.4C

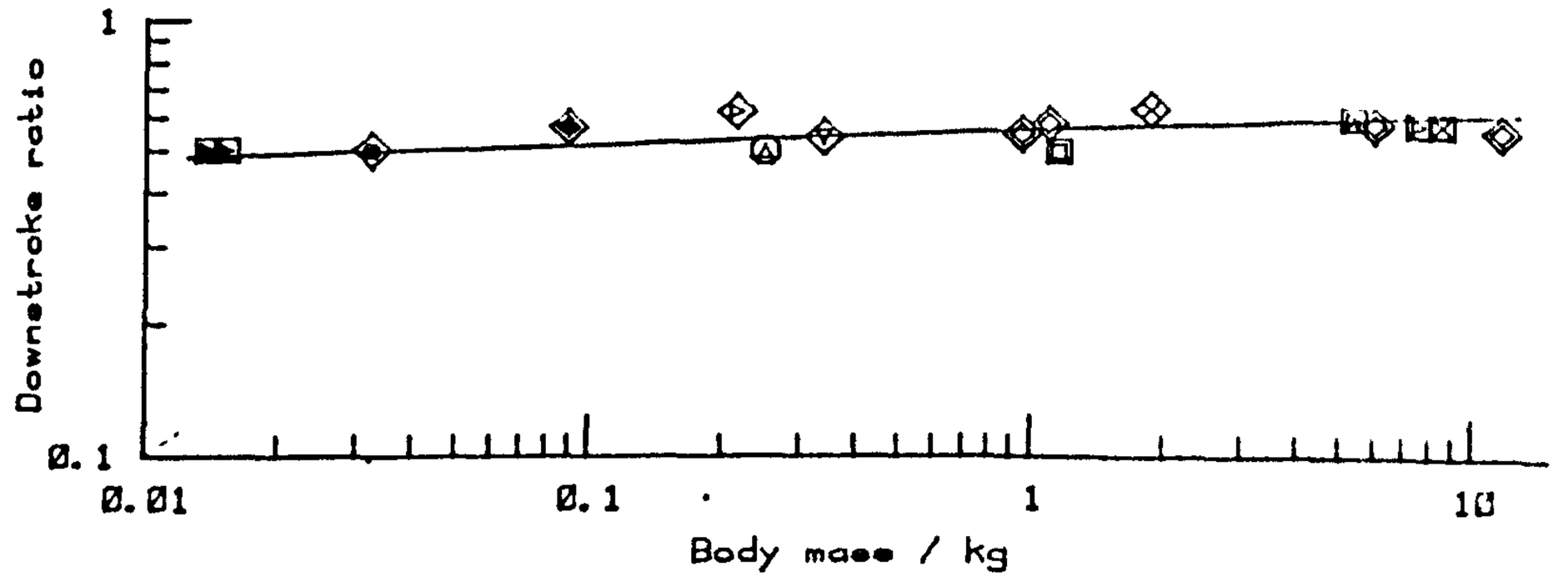

GRAPH 7.4A

Wing beat frequency f (Hz) and body mass m (kg).*

GRAPH 7.4B

Stroke amplitude Φ (degrees) and body mass m (kg).*

GRAPH 7.4C

Downstroke ratio ζ and body mass m (kg).*

* In each case the R.M.A. is shown, the symbols are as in Figure 6.1B and the equations are given in Table 7.3.

GRAPH 7.5A

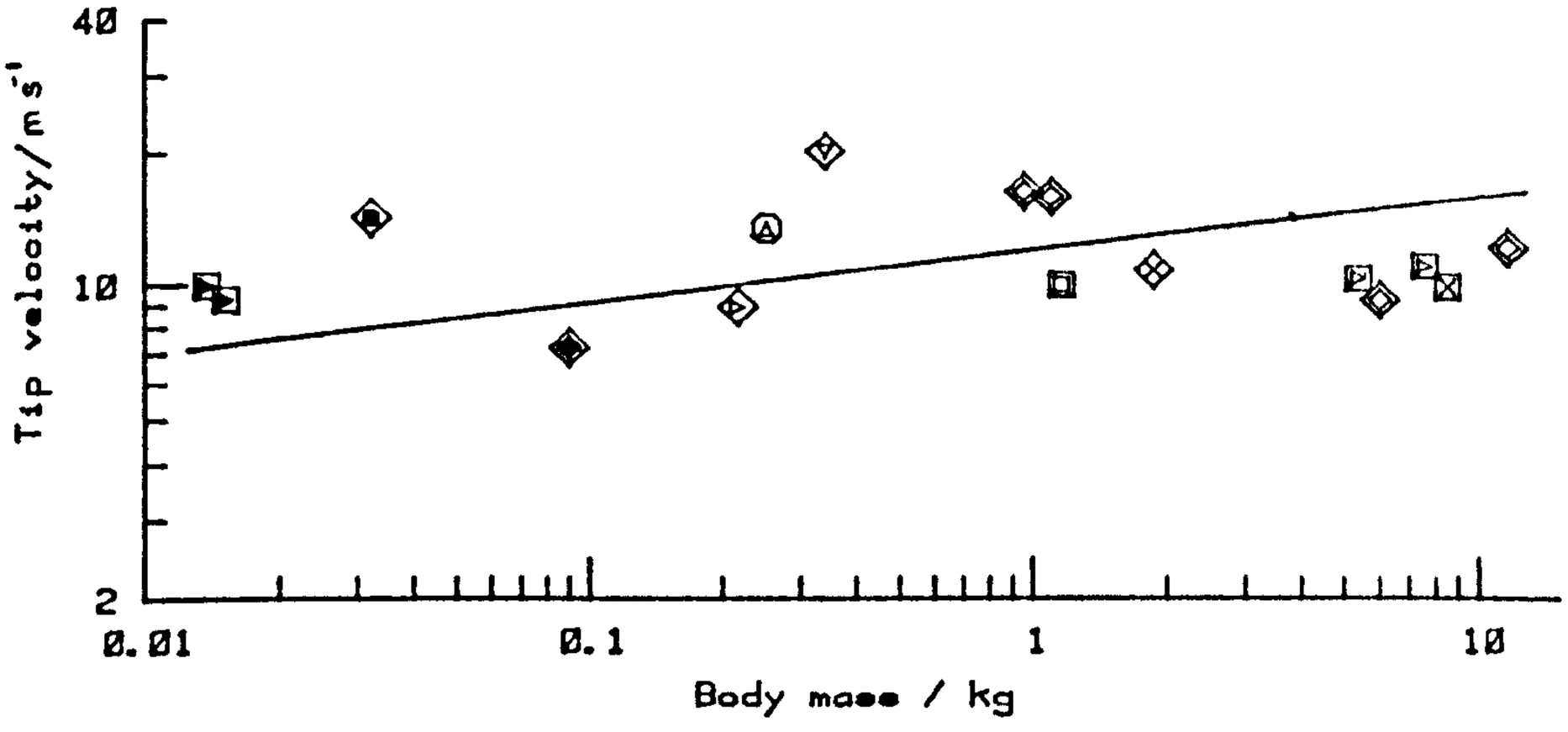

GRAPH 7.5B

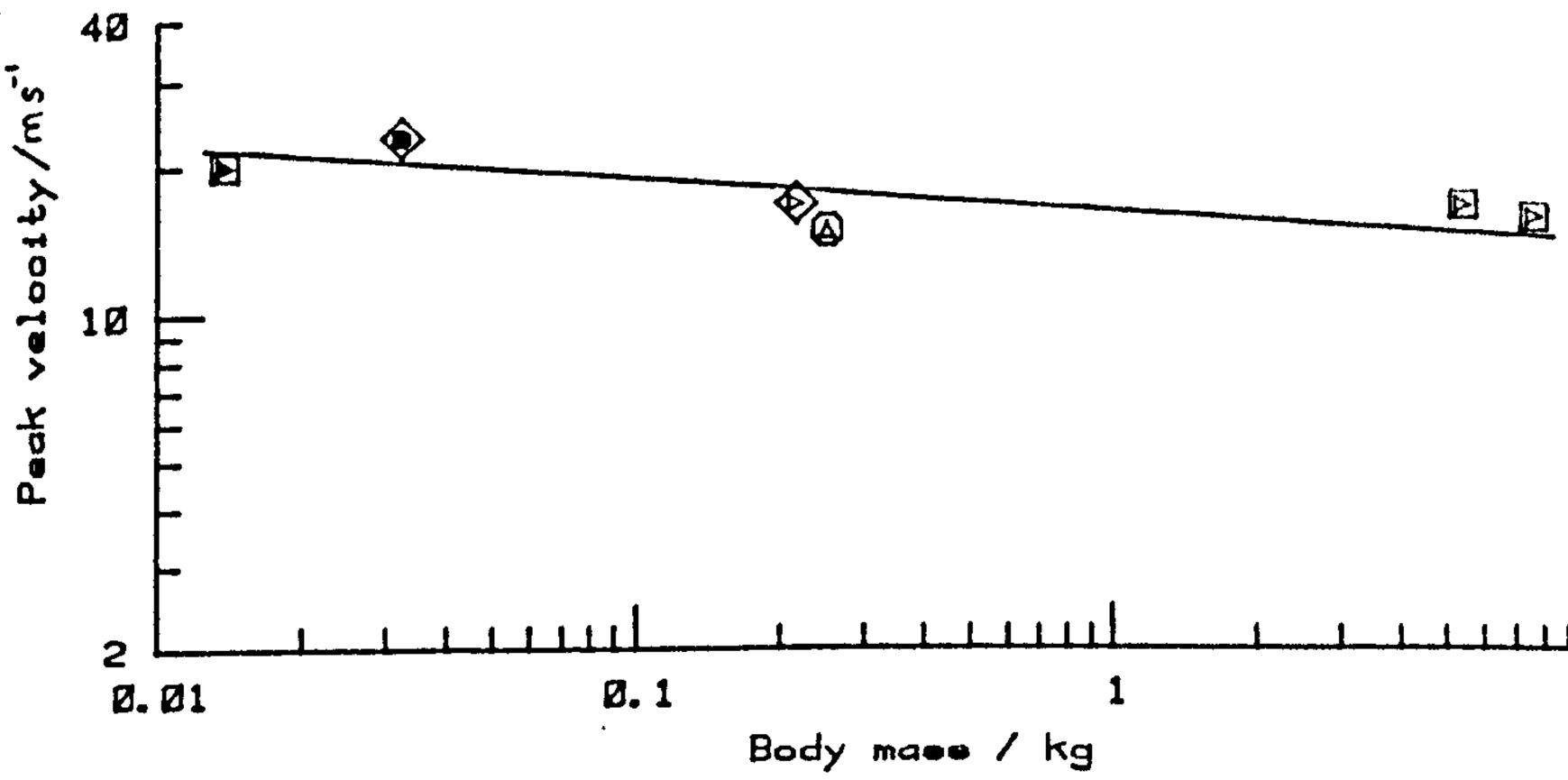

GRAPH 7.5A

Mean downstroke wingtip velocity ('tip velocity') ($m\ s^{-1}$) and body mass m (kg).*

GRAPH 7.5B

Measured peak downstroke wingtip velocity ('peak velocity') ($m\ s^{-1}$) and body mass m (kg).*

* In each case the R.M.A. is shown, the symbols are as in Figure 6.1B and the equations are given in Table 7.3.

TABLE 7.3 Equations for Graphs 7.4 and 7.5.

		n	r	F	α	β	$\alpha-$	$\alpha+$	$\beta-$	$\beta+$	Graph No.
FREQUENCY(Hz)	Y(X)	16	-0.908***	65.4	6.80	-0.233	5.92	7.80	-0.294	-0.171	7.4A
AND BODY MASS(Kg)	RMA				6.72	-0.256	5.84	7.74	-0.318	-0.195	
AMPLITUDE(Degrees)	Y(X)	16	-0.810***	26.8	97.9	-0.118	87.7	109	-0.167	-0.0692	7.4B
AND BODY MASS(Kg)	RMA				96.6	-0.146	86.1	108	-0.195	-0.0968	
DOWNSTROKE RATIO	Y(X)	16	0.602**	7.96	0.559	0.0216	0.539	0.580	5.16×10^{-3}	0.0380	7.4C
AND BODY MASS(Kg)	RMA				0.563	0.0358	0.541	0.587	0.0194	0.0522	
MEAN WING TIP VELOCITY($m\ s^{-1}$)	Y(X)	16	0.449*	0.0283	11.4	5.27×10^{-3}	9.77	13.2	-0.062	0.0762	7.5A
AND BODY MASS(Kg)	RMA				12.0	0.117	9.73	14.7	0.0501	0.185	
MEASURED PEAK WING TIP VELOCITY($m\ s^{-1}$)	Y(X)	6	-0.669***	3.25	17.0	-0.0409	14.4	20.0	-0.104	0.0221	7.5B
AND BODY MASS(Kg)	RMA				16.6	-0.0610	13.9	19.8	-0.124	1.91×10^{-3}	

7.8 General discussion of hovering and slow forward flight

The average wing tip velocity of the downstroke in maximum power flight is given as proportional to $m^{0.12}$. However, the correlation coefficient is low and only significant at the 10% level. The correlation coefficient for measured peak velocity is higher and more significant (1%)level) and its R.M.A. has a slope of -0.06 (See Table 7.3). Now, for dimensionally similar birds, if the angular velocity of the wing ω is limited by the strength of the bird's materials it should scale as $m^{-\frac{1}{3}}$ and consequently the wing tip velocity as m^0 (Hill, 1950; Pennycuick, 1975; Lighthill, 1977; Weis Fogh, 1977). As birds deviate slightly from dimensional similarity (Greenewalt, 1975) some variation from the predicted slope may be expected. However, this limited data gives a slope very similar to m^0, indicating that the maximum angular velocity may be limited by material strength.

It is interesting that the wing beat frequency at maximum power is proportional to $m^{-\frac{1}{4}}$ which is different from the estimate for the scaling of angular velocity. Angular velocity is approximately proportional to $m^{-\frac{1}{3}}$ if the wing tip velocity is proportional to m^0. Hence, as with cruise flight, it appears that it cannot be assumed that wing beat frequency and angular velocity scale similarly. The shallower scaling of f_{max} as $m^{-\frac{1}{4}}$ (rather than $m^{-\frac{1}{3}}$ if it were proportional to ω) may be

due to larger birds having to increase relatively their wing beat frequency to compensate for the reductions in stroke amplitude, stroke amplitude scaling as approximately $m^{-0.15}$. The reductions in amplitude may be caused by the dramatic increases in wing inertia with body size, moment of inertia crudely scaling as $m^{5/3}$. This tendency for larger birds to move their wings through a small amplitude but at a relatively higher frequency, may be represented in an extreme form by the landing wing stroke of the wandering albatross Diomedea exulans. Its wings, when landing, move through only about 15^{o} but at twice the wing beat frequency of cruise flight.

The scaling of the angular velocity of the upstroke was not estimated in this survey due to the complexity of the wing movements during the upstroke. However, the downstroke ratio of the wing beat $\simeq$ does give an indication as to how upstroke angular velocity is limited. It would be expected that birds with wings of moderately low aspect ratio, which probably do not use the upstroke to generate lift while hovering or taking off, would increase $\simeq$ as much as possible. Increases in $\simeq$ are observed for small birds, such as the pied kingfisher Ceryle rudis which uses a 'feathered' upstroke, its $\simeq$ being 0.5 in cruise flight but 0.57 when hovering. However, large birds with wings of moderately low aspect ratio, such as the Ruppell's griffon vulture Gyps ruppellii have similar values of $\simeq$ in take-off as in cruise flight. This indicates that the upstroke angular velocity is being limited, probably again due to

to the restrictions imposed by the bird's materials' strength. A maximum value of the angular velocity of the upstroke in turn must limit the maximum downstroke ratio. This restriction on $\geq_{max}$ has some interesting consequences for hypothetical giant birds, with low aspect ratio wings, which exceed the body mass limit of extant birds (Chapter 9).

The maximum angular velocity of the wing, if limited by material strength, can presumably be increased if the critical structural components, such as wing bones and tendons, are reinforced (Norberg,1979). This reinforcement may however be counterproductive in that the added mass required will increase the inertia of the wing and so too the power required to overcome this inertia. Extra reinforcement is therefore limited and so too is ω_{max}, and so slow flight performance can then only be improved by reducing the wing loading or increasing the effective lift coefficient of the wing. Hence, it is not surprising that most birds when taking off or hovering use some form of clap and fling to increase their effective lift coefficient.

CHAPTER 8

GENERAL DISCUSSION OF FLAPPING FLIGHT IN BIRDS

8.1 A comparison of the kinematics of cruise and slowest speed flight

By comparing the values of wing beat frequency and stroke amplitude for individual species, in fast forward 'cruise' (between V_{mp} and V_{mr}) flight with those required for their slowest possible flight speed (maximum aerodynamic power) an indication of the range of these two parameters can be found for each species. Graphs 8.1 and 8.2 show the ranges of frequency and amplitude respectively for the birds of this survey filmed flying at both speeds. In the two graphs the highest value of frequency and amplitude are those of the minimum flying speed and the lowest for 'cruise' flight. These ranges for each species are only estimates of the total range because, although the kinematics at the slowest flying speed probably represent the maximum possible, those of cruise flight do not necessarily represent the minimum required for horizontal flight, as the bird could be flying at or above its maximum range speed V_{mr}.

It can be seen that in both cases the range is generally largest for birds between 0.2 and 1.1kg and becomes reduced for larger birds. These data clearly show that frequency is not constant for individual species over a range of flying speeds; for example, the value of frequency for the black headed gull

GRAPH 8.1

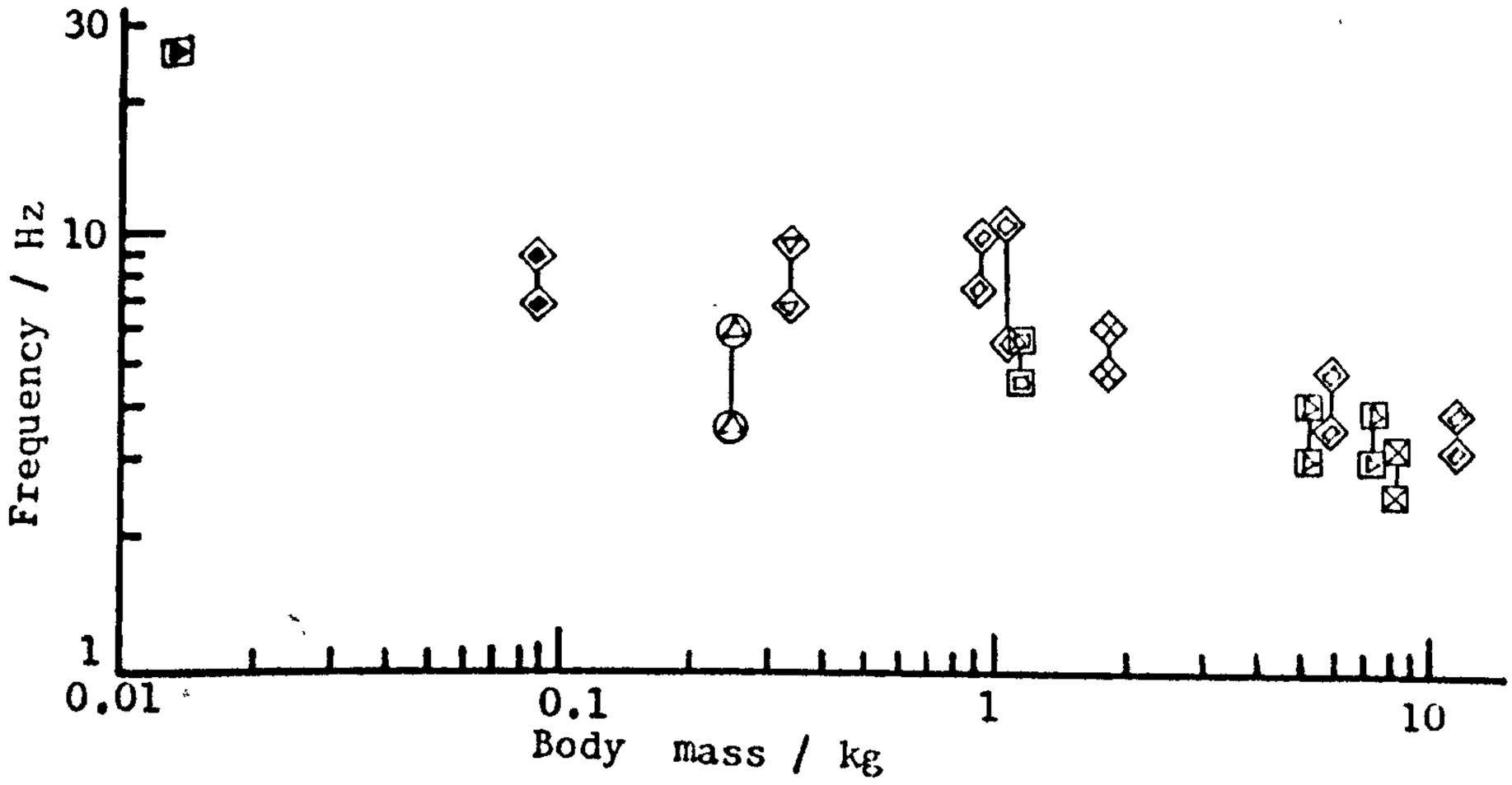

GRAPH 8.2

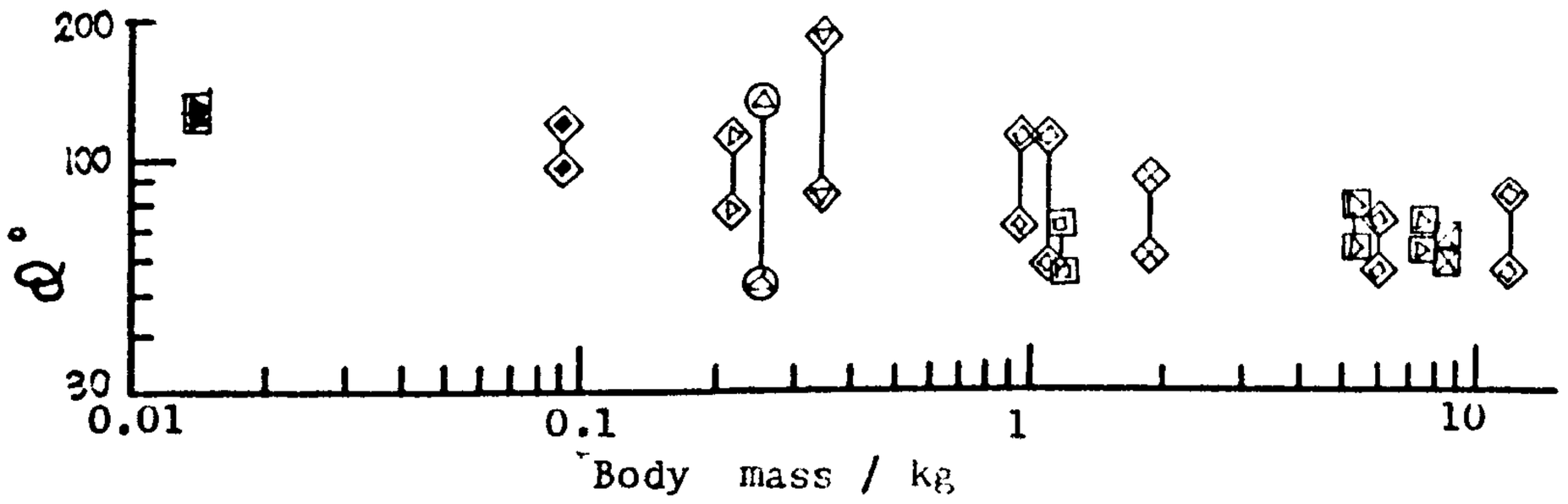

GRAPH 8.1

The ranges of wing beat frequency f (Hz) for birds over a range of body masses m (kg). Each individual of a species is represented by two points joined by a vertical line. The highest point is the value for flight at the minimum flying speed (presumed to be maximum power) while the lowest point is that for 'cruise' flight.

GRAPH 8.2

The ranges of wing stroke amplitude Θ (degrees) for birds over a range of body masses m (kg), as in graph 8.1.

Larus ridibundus when hovering is twice that of cruise flight. Pennycuick (1969) showed that frequency varied with flight speed in the pigeon Columba livia and Tucker (1972) observed similar variation for the laughing gull Larus atricilla. Clearly the hypothesis of Greenewalt (1960) that frequency remains constant for individual birds is unfounded.

The explanation for the reduction of the range of frequency and amplitude with an increase in size is directly related to the scaling of the angular velocity of the wing ω at these two extremes of required power. It was found in Chapter 6 that ω for cruise flight scales similarly to the theoretical aerodynamic rule of $m^{-\frac{1}{6}}$, whereby ω is just sufficient to provide weight support and overcome drag. In Chapter 7.7 ω for maximum power flight was found to be similar to $m^{-\frac{1}{3}}$, which is the predicted scaling rule if ω is limited by the strength of the bird's materials. Graph 8.3 is of the peak wing tip velocity against mass for cruise and maximum power (solid and broken lines respectively) and they have approximate slopes of $\frac{1}{6}$ and 0 respectively (equivalent to $-\frac{1}{6}$ and $-\frac{1}{3}$ if converted to angular velocities as explained in Chapter 6). It can be seen that the two lines converge and meet at a mass of approximately 40kg. Hence, as the angular velocity required for cruise flight becomes increasingly similar to that required for maximum power as birds become larger, and angular velocity is a product of frequency and amplitude, it follows that the ranges of frequency

GRAPH 8.3

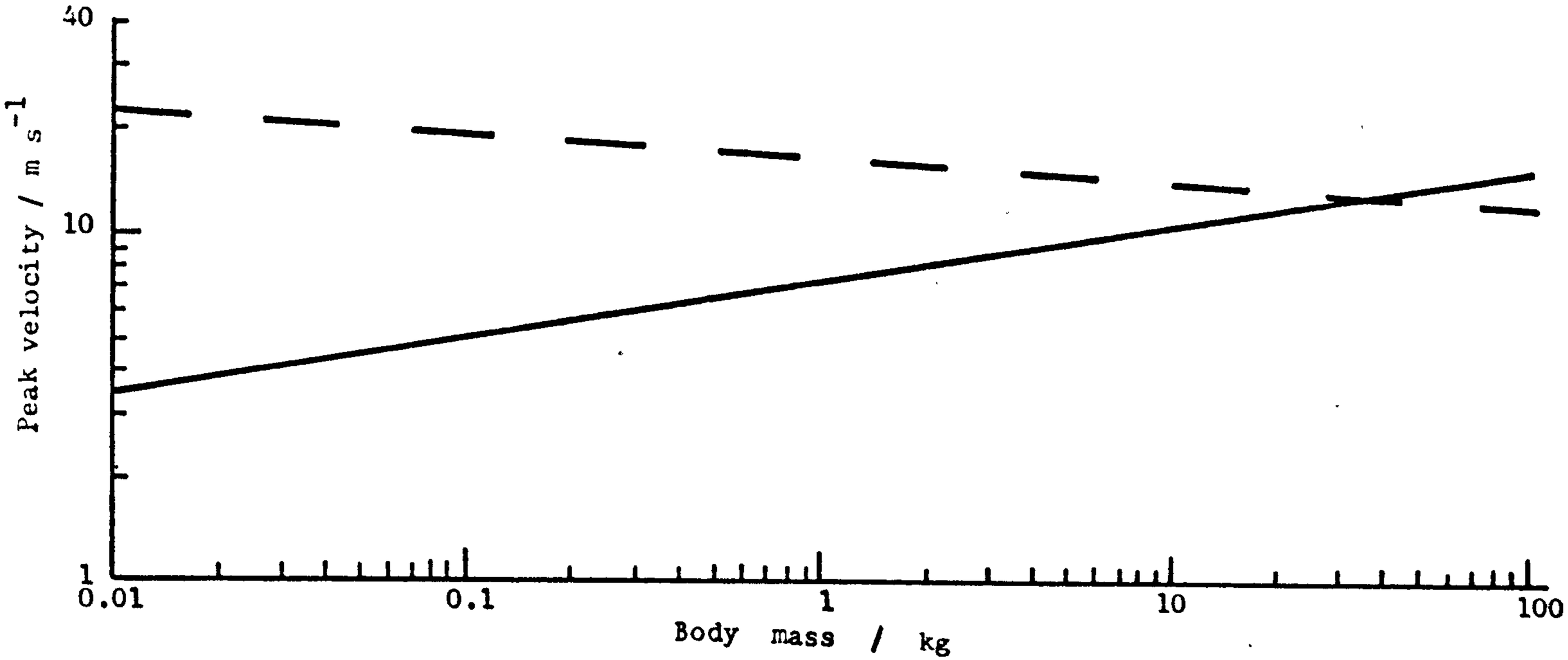

GRAPH 8.3

Peak downstroke wingtip velocity (' peak velocity') (m s^{-1}) and body mass m (kg). The solid line is the R.M.A. for the cruise flight data and the broken line that for the maximum power data, as in graphs 6.6 and 7.5B respectively.

and amplitude must also decrease with size increases.

Pennycuick (1975) suggested that the meeting of the two proportionalities of angular velocity should indicate an upper limit of size of birds capable of horizontal powered flight. The intercept in Graph 8.3 gives an unrealistically high maximum value of mass at about 40kg, considering that few known flying birds exceed 12kg. Small variations in either slope cause very large alterations in the mass which corresponds to the intercept of the lines and so this method, with such limited data is unsuitable for an absolute prediction of maximum size. Even if the lines had accurate slopes it is not necessarily true that the intercept would denote the maximum size. A small difference between the two values of ω_{max} and ω_{min} is probably essential for any 'practical' bird to enable take-off, a small amount of climbing, emergency manoeuvres and to permit the carrying of extra loads. Hence the maximum feasible size of a powered flight bird will be lower than the intercept mass. Although an exact maximum size cannot be found, Graph 8.3 is useful in demonstrating that the theoretical predictions of the scaling of ω_{max} and ω_{min}, and the consequences on limiting powered flight as size increases, are sound.

For birds smaller than 0.1kg it is unlikely that they require the maximum anaerobic metabolic power for hovering. This appears to be the case for the pied kingfisher Ceryle rudis (90g) which can sustain hovering for up to 10s and certainly for the zebra finch

Poephila guttata (13g) which 'bounds' when hovering (Chapter 7.7.2). The ranges of frequency and amplitude would therefore not be expected to continue to increase as size decreases below 0.1kg. This may explain the relatively narrow ranges of frequency and amplitude for the pied kingfisher in Graphs 8.1 and 8.2 .

However the situation of the zebra finch, where the kinematics in hovering and cruise flight are almost identical, demands a completely different explanation. In both cases the wing beat frequency is almost the same, the stroke plane angle relative to the body is similar, and it is only amplitude that exhibits slight differences in cruise and hovering (Chapter 6.3 and Chapter 7.2.2). It is only the period of the bound, when the wings are folded next to the body, that varies dramatically between cruise and hovering flight. Apparently, this set of kinematics is more than sufficient to maintain hovering flight, as the finch bounds even when it has no forward air speed, and as flight speed is increased the bounding period also increases (presumably up to the minimum power speed) to compensate for the reductions in the required aerodynamic power.

This strategy, flapping at what would appear to be maximum power, must have two distinct advantages of firstly reducing profile power in the forward flight bound and secondly having a limited frequency range over which the muscles operate (Rayner, 1977). As the wing amplitude also remains within a small range, the muscle strain rate need not be varied greatly and so

the muscle can be tuned to contract at its maximum efficiency. Having the kinematic parameters of the wing stroke so similar must make it possible for all the other structures involved in flapping to be finely tuned to that stroke and not to have to be a compromise for a number of stroke variations. Such a compromise is required of most larger birds like the pigeon. As other small bounding passerines have higher wing beat frequencies for their size than predicted by the frequency with body mass R.M.A. line for all birds (Graph 6.1A) it is likely that they all use a similar mechanism to that of the zebra finch.

In this survey maximum power flight has only been recorded for the particular birds at their slowest flying speeds. Obviously there are similar maximum power limits on the fastest flying speed of a bird. It would be valuable to investigate the kinematics involved in such flight for a range of birds and to see if this ω_{max} still scales as $m^{-\frac{1}{3}}$, or if maximum flying speed is limited by different factors. Profile power is the most likely limiting factor for maximum speed and Lighthill (1977) predicts that this should scale as $m^{-2/9}$. The filming of birds at such flight speeds can probably only be achieved if the bird is flying in a wind tunnel and is then forced to its maximum flying speed as was done for the pigeon by Pennycuick (1969).

8.2 Conditions for using the upstroke in flapping flight to generate lift

In both hovering and fast forward flight birds with wings of high aspect ratio apparently utilise the upstroke. In hovering an upstroke flick of the inverted primary feathers appears to generate lift. Whether or not a high aspect ratio wing is the best for hovering is not clear. The penalties of high wing inertia, caused by the relatively long wing span, must be great as it is not possible to utilise aerodynamic forces to a large extent to decelerate the wing. Hence birds specialised for hovering (other than humming birds) may opt for a low aspect ratio wing and use a feathered upstroke (even if the penalties of induced drag are higher) as have the pied kingfisher and sunbirds. However the high aspect ratio wing (approximately above AR 9) must be ideal for slow forward flight. This is because firstly the wing has low induced drag, ideal for slow flight where induced power is high, and secondly, as there is some forward air speed, aerodynamic forces can be used to decelerate the wings (Alexander and Goldspink, 1977) and so reduce the problems of their high inertia. Since high aspect ratio wings are suitable for upstroke gliding, this can be done in slow forward flight and it is possible to increase the relative period of the upstroke and so reduce the wing beat frequency and the overall metabolic costs of flapping. Prolonging the upstroke glide is probably analogoug to the flap glide used by many large

birds. This increasing of the upstroke glide period is done by terns (Sterninae) which are specialised to fly slowly into sea breezes, in order to hunt for small fish. For example, the little tern Sterna albifrons has a mean downstroke ratio of only 0.47 .

The use of the upstroke must cause retardation on forward flying speed. If so, for birds of the same wing loading, those with higher aspect ratio should have lower flying speeds in flapping flight. These reductions in flight speed are of little importance to slow forward flight specialists, such as terns, or to the majority of high aspect ratio sea birds which generally rely on soaring. These reductions may however be one important reason why birds that require rapid flight for hunting or travelling, such as the Falconidae and the Anseriformes respectively, have aspect ratios below 10.

A systematic study of the wake of a number of birds, of various aspect ratios, using the technique of Spedding (1981), coupled with obtaining accurate stroke kinematics and flight speed data, would enable the variations of the use of the upstroke by birds of different wing shapes, and the consequences, to be accurately quantified. This information could then be used to modify existing flight models.

8.3 An importance of rapid wing acceleration

It has been shown in Chapter 6.6.3 that the well tapered wing shape of Group B birds permits more rapid wing acceleration than those of Groups A and C. This being so it follows that the initial angle through which the wing must be swept to accelerate it can be less for Group B birds and so too the overall stroke amplitude. This difference in acceleration rates was not accounted for in the calculation of the average lift coefficient Γ_L for a wing stroke in Chapter 6.5 . The relatively low amplitudes of especially the Anseriformes of Group B may be another reason why their values of Γ_L in Graph 6.12 are higher than the overall regression line.

If superior wing acceleration rates do permit lower stroke amplitudes, this must improve flapping flight efficiency. This, combined with a moderate use of upstroke lift, to reduce the vertical body recoil and only cause a small degree of retardation of forward speed, must make the Group B wing design superior to both Group A and Group C birds as far as fast flapping forward flight is concerned.

8.4 Lift coefficient and steady state aerodynamics in cruise flight

The predicted scaling of the minimum angular velocity ω required of the flapping wing in horizontal flight (Pennycuick, 1975; Weis-Fogh, 1977; Lighthill, 1977) of ω_{min} proportional to $m^{-\frac{1}{6}}$ assumes that the lift coefficient of the wing remains constant for all sizes and that steady state aerodynamics pertain. Now, since it has been shown for steady state forward flight that wing tip velocity scales similarly to this prediction , this indicates that both these assumptions are valid. However this theory assumes that birds are dimensionally similar and it has been shown by Greenewalt (1975) that birds slightly depart from dimensional similarity as size increases. These departures are probably not great enough to dramatically alter the predicted proportionality, especially for the range of birds of this survey. The Pennycuick (1978) modification of this theory, based on the same assumptions, accounts for the dimensions of each bird, and so is more suitable for testing if constant lift coefficient and steady state aerodynamics apply. The modified version, which included all kinematic variation (6.5.2) when plotted to test the prediction (Graph 6.10) had an R.M.A. line whose slope was close to that predicted by Pennycuick's theory. Broadly therefore, in fast forward flight, it can be assumed that steady state aerodynamic theory is sufficient to model flapping flight and that the lift coefficient used remains similar, regardless of their size, for birds within the size range of this survey.

CHAPTER 9

CONCLUSIONS

It has been shown that the selective pressure to reduce cost of transport, and so increase foraging radius, is of paramount importance in the evolution of vertebrate powered flight. The evolution of flight induced by this selection pressure is feasible, and in certain cases inevitable, only for arboreal vertebrates.

Non-arboreal vertebrates, evolving under a selection pressure to increase their foraging range, can best achieve this by becoming larger. This is because basal metabolism scales as $M^{0.75}$ and so the period an animal can endure without food increases with its body size. Larger animals can therefore travel further from one feeding site to another. Both aquatic and cursorial vertebrates which migrate or have large home ranges tend to be big, elephants and whales being two extreme examples.

Arboreal vertebrates cannot dramatically increase their size, as it is limited by the strength of tree branches. With few exceptions, such as the orang utan Pongo hygmaeus, arboreal vertebrates do not exceed 50kg in mass. Those other than primates are generally smaller than 10kg. When selection pressure to increase foraging range acts on them, the evolution of flight allows them to increase their range without increasing their size . Flight can easily be evolved for a tree dweller, so long as aerial niches are available for it to occupy, by developing first gliding and then powered

flight.

The selection pressure to lower transport costs is greatest for arboreal animals who have fixed nest sites from which they forage daily. The primates, which can carry their young from birth, are not under such great pressure and so have never evolved gliding or flight. It is interesting that in South America, where primates occupy most of the arboreal rodent niches of the Old World, there are no gliding mammals.

A prime candidate for flight evolution is therefore an arboreal nest-building vertebrate where vacant gliding and powered flight niches exist in its environment. I think it very likely, therefore, that the ancestors of both birds and bats were such animals.

Each level of development of vertebrate flight is limited by design of wing shape and by body size. A progression from one level to another allows a change in these limits. First, in gliding and climbing vertebrates it is clear that, if the wing is attached to all the limbs, its shape is determined largely by limb length. The need to climb efficiently, which requires fore and hind limbs of similar size, dictates that the aspect ratio of the wing must be between 1 and 2. If the wings are not attached to the hind or any limbs the aspect ratio can be increased. High aspect ratio wings for an arboreal vertebrate may, however, be cumbersome, and this may be why those of Draco are only 2. Some arboreal lizards with wings supported by

ribs have, however, evolved higher aspect ratio wings, as with the extinct Icarosaurus (Colbert, 1970). This implies that this animal lived in more open terrain than Draco.

If climbing and gliding is used as a cheap form of locomotion, there is an upper size limit above which it does not produce energy savings over conventional running. This is because the power required to climb is approximately proportional to $m^{1.1}$, and gliding mammals are therefore not larger than about 2kg. If the tree must be climbed as part of foraging behaviour, as with Draco, this limit does not apply, and theoretically such animals could become larger than 2kg. It is probably the nature of their food source, small arthropods, which restricts their maximum size with trunk foraging for such prey being unsuitable for larger animals. For gliding mammals it is not the gliding adaptation which limits minimum size but probably those factors which limit the size of all quadrupedal mammals, such as the need to maintain homeothermy. The gliding mammal Acrobates (14g) is close to the size of the smallest quadrupedal mammals. The low wing loadings associated with small gliding mammals (Thorington and Lawrence, 1981) result in their having very low glide speeds, and so they are greatly affected by ambient air currents. This may restrict small gliding mammals from operating in open woodland, as suggested by Thorington and Lawrence (1981). Very low wing loadings may also pose similar problems for flying

lizards and possibly limit their minimum size.

The development of powered flight permits a far greater maximum size than that achieved by climbing and gliding vertebrates. The theoretical prediction of Pennycuick (1978) that the angular velocity of the wing required for cruise flight becomes increasingly closer to the maximum possible angular velocity as size increases, has been shown in this thesis to be broadly correct, and this must eventually restrict the maximum size where horizontal powered flight is possible. It was found that the maximum angular velocity scales as would be expected if it was limited by the strength of the animal's materials. It is realised that maximum metabolic power could also be of importance in limiting maximum power performance, but the investigation of this was beyond the scope of this thesis.

Relatively large size may be achieved by powered flying vertebrates in cruise flight, but only at the expense of slow forward flight performance. Minimum flight speed is crudely dependent on the dimensions of the animal, its maximum lift coefficient and the angular velocity of the wing. Lift coefficient can be increased by unsteady aerodynamic mechanisms, such as the clap and fling, which has been shown to be used to some extent by most birds. However, there must always be a maximum possible lift coefficient, and hence there is a certain angular velocity for the wing required for flight at a particular speed. As birds become larger, the angular velocity demanded for

hovering, instant take-off and cruise flight become increasingly difficult, and eventually impossible, of achievement.

For a given size of flying vertebrate there are upper and lower limits on the range of possible wing loading. High wing loading has the advantage of fast cruise speeds but at the expense of slow flight performance. Very high wing loadings are exhibited by auks (Alcidae), as they use their wings for propulsion underwater as well as in the air, and consequently require a long skitter run for take-off. The need to take off and land on cliffs during breeding probably limits the increase in wing loadings.

The limits to low wing loading, for a given size of bird, are probably determined by at least two factors. Firstly, although low wing loading allows good take-off performance, cruise flying speeds are slow. The inability to penetrate ambient air currents would undoubtedly impair cross-country performance. Second, a large wing area of high profile drag has been shown to involve long acceleration periods in flapping flight, and so is probably inefficient.

Wing span for a given size of flapping vertebrate also has lower and upper limits. Low span wings incur high induced drag, and this must impose minimum span limits. Maximum span is apparently limited by a number of factors in flapping flight. First, available space for flight must be of great importance: for example, woodland birds all have far lower aspect ratios

than marine birds. Secondly, any increase in span increases the moment of inertia of the wing, and this is of appreciable importance in very slow forward flight and especially in hovering, where aerodynamic forces can play only a small part in decelerating the wing. Vertebrates which take off by running or into wind can probably develop higher wing spans, since aerodynamic forces can then be used to help the deceleration of the downstroke and also the raising of the wing in the upstroke.

The maximum size limit of extant vertebrates is approximately 12kg (Pennycuick, 1975), with the mute swan Cygnus olor, the Andean and Californian condors Vultur, and the wandering albatross Diomedea exulans reaching about this size. The mute swan Cygnus olor is exceptional as it apparently relies totally on powered flight, whereas the other two are largely dependent on soaring. It is curious that the largest flying mammals, the fruit bats of the genus Pteropus, are only about 1.5kg in mass. The argument that being nocturnal restricts soaring, and this restricts the size of bats, is unfounded since there are non-soaring powered flight vertebrates eight times their size. The maximum size of the Megachiroptera may be limited by the fact that they forage for fruit and flowers at the tips of branches which will only carry a certain weight, and also because they need a certain amount of slow forward flight control and a correspondingly low wing loading to land amongst foliage. Such fruit bats must also be able to compensate for a considerable increase in their wing loading when

they produce offspring, since the young are carried by the parent in flight, and this may be of great importance in limiting their maximum size.

Good soaring conditions may permit size increases for birds above the limits for powered flight. It is interesting that the largest African vultures, the lappet-faced Torgos tracheliotus and the Ruppell's griffon Gyps ruppellii are only about 8 to 9kg compared to the Andean and Californian condors which can weight in the region of 12kg.

Prevalent mountain and sea breezes probably allow these condors to evolve this greater size. If conditions were even more constantly favourable for soaring, and so reduced the problems of powered take-off, it is possible that greater sizes could be achieved. If so, it is unlikely that such a giant bird would be able to have a low aspect ratio wing. If the kinematics and aerodynamics of low aspect ratio soaring birds, such as vultures, are extrapolated for hypothetically larger birds, it can be seen that flapping flight for such giants becomes very cumbersome, if not impossible. First, since little weight support is produced by the upstroke, the downstroke ratio must increase to reduce the period of this part of the wing cycle. It has been shown that the downstroke ratio for low and medium aspect ratio birds scales as $m^{0.065}$. Increases in downstroke ratio must be limited by the maximum velocity of the upstroke. Now an increase in size results in an increase in stroke period, and if the downstroke ratio is at a maximum then the

upstroke period must increase in proportion with the total period. This means that, as low aspect ratio birds are further enlarged, there is an increasingly long phase in the wing cycle where the body weight is largely unsupported, and so a dramatic increase in vertical body recoil. It is likely that a very large bird would require some flapping ability to gain extra thrust in emergencies, even if this thrust was insufficient to sustain horizontal flight. The giant bird with a low aspect ratio wing would probably be thrown into such large body oscillations when it flapped that the action would hamper rather than aid flight.

For this hypothetical giant bird, a high aspect ratio wing would be suitable for flapping flight. If an initial air speed existed over the wings, aerodynamic forces would support the body weight and raise the wing in the upstroke. So in flapping the giant bird would not have pronounced vertical recoil, and the problem of raising the very long span wings in the upstroke would be overcome by using aerodynamic forces. As this flapping relies on an initial air speed over the wings it could not be used for slow flight manoeuvres or probably for take-off in still conditions. Such an animal would have to take off by jumping off a precipice or by running into a strong wind.

The recording, for a number of birds of varying morphology, of:

1) the variation of wing stroke kinematics with flying speed

2) flight speeds in natural fast forward flight

3) the structure of the wake at various flying speeds

would greatly increase our understanding of flapping flight. An investigation of the change of flight kinematics with speed can probably only be done by flying birds in a wind tunnel. The birds using bounding flight would be especially interesting. Data of flight speeds in the field can be acquired by using radar techniques or a visual tracking device similar to that devised by Pennycuick (1982 a). The flow visualisation technique used by Spedding (1981) is ideal for the required wake analysis. Information from these three areas of research would enable the conformation or rejection of the majority of hypotheses and suggestions put forward in the sections of this thesis on bird flight. It would enable more accurate modelling of the energetics of bird flapping flight.

REFERENCES

Alexander, R. McN., Langman, V.A. & Jayes, A.S. (1977) Fast locomotion of some African ungulates. J. Zool., Lond. 183 : 291-300

Alexander, R. McN. & Goldspink, G. (1977) "Mechanics and energetics of animal locomotion". Chapman & Hall

Alcala, A.C. (1967) Population biology of the flying lizard, Draco volans, on Negros Island, Philippines. Nat. appl. Sci. Bull. Univ. Philipp. 20 : 335-372

Bartholomew, G.A., Leitner, P. & Nelson, J.E. (1964) Body temperature, oxygen consumption, and heart rate in three species of Australian flying foxes. Physiol. Zool. 37 : 179-198

Baudinette, R.V., and Schmidt-Nielsen, K. (1974). Energy cost of gliding flight in the herring gull. Nature, Lond. 248 : 83-84

Bilo, D. (1971) Flugbiophysik von Kleinvögeln. I. Kinematik und Aerodynamik des Flugelarschloages beim Haussperling (Passer domesticus). Z. bergl. Physiol. 71 : 382-454

Bilo, D. (1972) Flugbiophysik von Kleinbögeln. II. Kinematik und Aerodynamik des Flugelaufschlages beim Haussperling (Passer domesticus). Z. bergl. Physiol. 76 : 426-437.

Bock, W.J. (1965). The role of adaptive mechamisms in the origin of higher levels of organisation. Syst. Zool. 14 : 272-287.

Bock, W. J. (1979). The synthetic explanation of macroevolutionary change - a reductionistic approach. Bull. Carnegie Mus. Nat. Hist. 13 : 20-69

Borodulina, T. L. & Blagoskolonov, K. N. (1951). (On the biology of flying squirrels (Pteromys volans L.).) Bull. Soc. Nat. Mosc. 56 (6) : 18-24 (In Russian)

Boulenger (1885). Catalogue of the lizards in the British Museum (Nat. Hist.). 1. London

Bramwell, C. D. & Whitfield, G. R. (1974). Biomechanics of Pteranodon. Phil. Trans. R. Soc. (B) 267 : 503-592

Brown, F. G. (1955). Forest trees of Sarawak and Brunei and their products. Kuching, Sarawak : Gov. Print Office 369 : 1-47

Brown, R. H. J. (1948). The flight of birds : The flapping cycle of the pigeon. J. Exp. Biol. 25 : 322-333

Brown, R. H. J. (1961). The power requirements of birds in flight. Symp. Zool. Soc. London 5 : 95-99

Brown, R. H. J. (1963). The flight of birds. Biol. Rev. 38 : 490-589

Buchler, E. R. (1976). The use of echolocation by the wandering shrew Sorex vagrans. Anim. Behav. 24 : 858-873

Clark, B. D. (1977). Energetics of hovering flight and the origin of bats in "Major patterns in vertebrate evolution" 423-425. Hecht, M. K., Goody, P.C. & Hecht, B. M. (Eds.) New York : Plenum Press

Colbert, E. H. (1970). The Triassic gliding reptile Icarosaurus. Bull. Am. Mus. Nat. Hist. 143 : 85-142

Csicsaky, M. J. (1977). Body-gliding in the zebra finch. Fortschr. Zool. 24 : 275-286

Dathe, H. H. & Oehme, H. (1978). Typen des Ruttelfluges der Vögel. Biol. Zbl. 97 : 299-305

Davis, D. D. (1962). Mammals of the lowland rain-forest of North Borneo. Bull. Singapore. Nat. Mus. No.31 : 1-129

De Beer, G. (1954). Archaeopteryx lithographica: a study based upon the British Museum specimen. London : British Museum (Natural History)

Ellington, C. P. (1977). Vortices and hovering flight. In "Proceedings of the conference on unsteady effects of oscillating animal wings". Nachtigall, W. (Ed.). Saarbrucken, West Germany.

Feduccia, A. & Tordoff, H. B. (1979). Feathers of Archaeopteryx: assymetric vanes indicate aerodynamic function. Science, N.Y. 203 : 1021-1022

Fenton, M. B. (1974). The role of echolocation in the evolution of bats. Am. Nat. 108 No.961 : 386-388

Fleay, D. (1954). Australia's sugar gliders. Animal Kingdom 57 : 187-190

Gabrielli, G. & von Karman, Th. (1950). What price speed? Mechanical Engineering. October 1950 : 775-781

Gould, E., Negus, N., Novick, A. (1964). Evidence for echolocation in shrews. J. exp. zool. 156 : 19-38

Greenewalt, C. H. (1960). The wings of insects and birds as mechanical oscillators. Proc. Amer. Philos. Soc. 104 (6) : 605-611

Greenwalt, C. H. (1962). Dimensional relationships for flying animals. Smithson. misc. collns. 144 (2) : 1-46

Greenewalt, C. H. (1975). The flight of birds. Trans. Am. phil. Soc. 65 (4) : 1-67

Grzimek, B. (1967). "Four-legged Australians." Collins

Gruson, E. S. (1976). A checklist of the birds of the world. Collins. London

Guidi, G. (1938). A study of the wing-beats of pigeons in flight. J. R. Aero. Soc. 42 : 1104-1115

Hairston, N. G. (1957). Observations on the behaviour of Draco volans in the Philippines. Coneia. No.4 : 262-265

Harvey, P. H. & Mace, G. M. (1982). Comparisons between taxa and adaptive trends : problems of methodology. In "King's College Sociobiological Group : Current problems in Sociobiology." 343-361. Cambridge University Press.

Height, M. E., Goodman, M. & Prychodko, W. (1974). Immunological studies of the Sciuridae. Syst. Zool. 23 : 12-25

Hennig, W. (1936). Revision der Gattung Draco (Agamidae). Temminckia 1 : 153-220

Hertel, H. (1966). Structure, Form and Movement. Van Nostrand Reinhold Publishing Corporation, New York.

Herzog, K. (1968). Anatomie und Flugbiologie der Vögel. Stuttgart : Gustav Fischer Verlag

Hill, A. V. (1950). The dimensions of animals and their muscular dynamics. Sci. Progr. (London) 38 : 209-230

Hummel, D. (1980). Aerodynamics of wing tip slots in soaring birds. Proc. 17th Internat. Ornithol. Congr. Berlin. 391-396

Hurst, C. H. (1895). The structure and habits of Archaeopteryx. Stud. Biol. Dept. Owens Coll. Manchester 3 : 267-287

Jepson, G. L. (1970). Bat origins and evolution. In "Biology of Bats." 1 : 1-64 Wimsatt, W. A. (Ed.). Academic Press, New York

Kirsch, J. A. W. (1968). Prodromus of the comparative serology of Marsupialia. Nature, Lond. 217 : 418-420

Klingel, H. (1965). Uber das Flugverhalten von Draco volans (Agamidae) und verwandten Arten. Zool. Ang. 175 : 273-281

Kokshaysky, N. V. (1979). Tracing the wake of a flying bird. Nature, Lond. 279 : 146-148

Lighthill, M. J. (1973). On the Weis-Fogh mechanism of lift generation. J. Fluid Mech. 60 : 1-17

Lighthill, M. J. (1974). Aerodynamic aspects of animal flight. Bull. Inst. Maths. Appls. 10 : 369-393

Lighthill, M. J. (1977). Introduction to the scaling of aerial locomotion. In "Scale effects in animal locomotion." 365-404. Pedley, T. J. (ed.) London & New York : Academic Press

Lythgoe, J. N. (1979). The Ecology of Vision. Clarendon Press, Oxford

Mackinnon, K. S. (1978). Stratification and feeding differences among Malayan squirrels. Malay Nat. J. 30 (3/4) : 593-608

Marey, E. J. (1980). Physiologie du mouvement : Le vol des oiseaux. Paris : G. Masson et Cie

McGahan, J. (1973). Flapping flight of the Andean Condor in Nature. J. Exp. Biol. 58 : 239-253

Medway, Lord (1972). Phenology of a tropical rain forest in Malaya. Biol. J. Linnean Soc., Lond. 4 : 117-146

Mertens, R. (1960). Fallschirmspringer und Gleitflieger unter den Amphibien und Reptillien. In "Der Flug der Tierre." 135-144. Schmidt, H. (Ed.). Frankfurt am Main : Verlag Waldemar Kramer

Muybridge, E. (1899). "Animals in motion". New Edition (1957), New York : Dover Publications.

Nachtigall, W. (1979a). Gleitflug des Flugbeutlers Petaurus breviceps papuanus. II. Filmanalysen fur Einstellung von Gleitbahn und Rumnf sowie zur Steurung des Gleitfugs. J. Comp. Physiol. A. 133 : 89-95

Nachtigall, W., Grosch, R. & Schuttze-Westrum, T. (1974). Gleitflug des Flugbeutlers Petaurus breviceps papuanus (Thomas). Flugverhalten und Flugsteuerung. J. Comp. Physiol. A92 : 105-115

Norberg, U. M. (1975). Hovering flight in the pied flycatcher (Ficedula hypoleuca). In "Swimming and flying in Nature." 2 : 869-881. Wu, T. Y.-T., Brokaw, C. J. & Brennen, C. (Eds.). New York : Plenum Press

Norberg, U. M. (1979). Morphology of the wings, legs, and tail of three coniferous tits, the goldcrest and the tree creeper in relation to locomotor pattern and feeding station selection. Proc. Roy. Soc. Lond. 287(b) : 133-164

Norberg, U. M. (in press). Flying, gliding, and soaring.

Norberg, R. A, & Norberg, U. M. (1971). Take off, landing and flight speed during fishing flights of Gavia stellata Ornis. Scand. 2 : 55-67

Novick, A. (1958). Orientation in palaeotropical bats II : Megachiroptera. J. exp. zool. 137 : 443-462

Novick A. (1977). Acoustic orientation, in "Biology of bats." 3 : 73-287. Wimsatt, W. A. (Ed.). Academic Press, London

Novick, A. & Leen, N. (1969). The world of Bats. Holt, Rinehart & Winston, New York

Oehme, H. & Kitzler, U. (1974). Untersuchungen zur Flugbiophysik und Flugphysiologie der Vögel. I. Uber die kinematik des Flügelschlages heim unbeschleunigten Horizontalflug. Zool. Jb. Physiol. 78 : 461-512

Olson, S. L. & Feduccia, A. (1979). Flight capability and the pectoral girdle of Archaeopteryx. Nature, Lond. 278 : 247-248

Ostrom, J. H. (1974). Archaeopteryx and the origin of flight. Q. Rev. Biol. 49 : 27-47

Ostrom, J. H. (1975). The origin of Birds. In vol 3 "Annual Review of Earth and Planetary Sciences." Donatn, F. A. (Ed.). 55-57. Palo, Alto : Annual Rev. Inc.

Ostrom, J. H. (1979). Bird Flight : how did it begin? Am. Scient. 67 : 46-56

Pennycuick, C. J. (1968). Power requirements for horizontal flight in the pigeon Columba livia. J. exp. Biol. 49 : 527-555

Pennycuick, C. J. (1971). Gliding flight of the dog-faced bat Rousettus aegyptiacus observed in a wind tunnel. J. exp. Biol. 55 : 833-845

Pennycuick, C. J. (1972a). Animal Flight. Arnold, London

Pennycuick, C. J. (1972b). Soaring behaviour and performance of some East. African birds, observed from a motor glider. Ibis 114 : 178-218

Pennycuick, C. J. (1975). Mechanics of flight. Avian Biol. 5 : 1-73

Pennycuick, C. J. (1978). Fifteen testable predictions about bird flight. Oikos 30 : 165-176

Pennycuick, C. J. (1979). Energy costs of locomotion and the concept of foraging radius. In "Serengeti, dynamics of an ecosystem". 164-184. Sinclair, A. R. E. & Norton-Griffiths, M (Eds.). Chicago. University of Chicago Press

Pennycuick, C. J. (1982a). The ornithodolite : an instrument for collecting large samples of bird speed measurements. Phil. Trans. R. Soc. Lond. (B) 300 : 61-73

Pennycuick, C. J. (1982b). The flight of Petrels and Albatrosses (Procellariiformes) observed in South Georgia and its vicinity. Phil. Trans. R. Soc. Lond. (B) 300 : 75-106

Pennycuick, C. J. & Lock, A. (1976). Elastic energy storage in primary feather shafts. J. exp. Biol. 64 : 677-689

Pirlot, P. (1977). Wing design and the origin of bats. In "Major patterns in vertebrate evolution." 375-410. Hecht, M. K., Goody, P. C. & Hecht, B. M. (Eds.). New York, Plenum Press

Prandtl, L. & Tietjens, O. G. (1957). Applied Hydro and Aerodynamics. Dover Publications. New York

Rayner, J. M. V. (1977). The intermittent flight of birds. In "Scale effects in animal locomotion." 437-443. Pedley, T. J. (Ed.). London & New York, Academic Press

Rayner, J. M. V. (1978). The mechanics of animal flight. PhD thesis. Queen's College, Cambridge University

Rayner, J. M. V. (1979a). A vortex theory of animal flight. Part 1. The vortex wake of a hovering animal. J. Fluid Mech. 91 : 697-730

Rayner, J. M. V. (1979b). A vortex theory of animal flight. Part 2. The forward flight of birds. J. Fluid Mech. 91 : 731-763

Rayner, J. M. V. (1979c). A new approach to animal flight mechanics. J. exp. Biol. 80 : 17-54

Rayner, J. M. V. (1981). Flight adaptations in vertebrates. Symp. zool. soc. Lond. 48 : 137-172

Rayner, J. M. V. (in prep. a). Techniques for the analysis of high-speed film of flapping bird flight

Rayner, J. M. V. (in prep. b). Form and function in avian flight.

Reyes, A. Y. (1968). The food habits of Draco volans (L) Silliman J. 17 : 67-72

Ruppell, G. (1972a) Chlorostilbon melanorhynchus (Trochilidae), Flug auf der Stelle. Begleittext zum Film E 1617. Encyclopaedia cinematographica. Göttingen.

Ruppell, G. (1972b). Pheonicurus phoenicurus (Turdidae) Flugmanöver. Begleitlext zum Film E 1844. Encyclopaedia cinematographica. Göttingen.

Schlichting, H. (1968). Boundary-layer theory. McGraw-Hill, 6th Edition

Schmidt-Nielsen, K. (1972). Locomotion: energy cost of swimming, flying and running. Science 177 : 222-228

Shestakova, G. S. (1956). On the mechanics of bird flight. Zoologicheskii zhurnal XXXV 7 : 1043-1050

Smith, J. D. (1977). Comments on flight and the evolution of bats. In "Major patterns in vertebrate evolution." 427-437. Hecht, M. K., Goody, P. C. & Hecht, B. M. (Eds.) New York. Plenum Press

Smythies, B. E. (1960). The Birds of Borneo. Oliver & Boyd. Edinburgh & London

Sokal, R. R. & Rohlf, F. J. (1981). Biometry: The principles and practice of statistics in biological research. W. H. Freeman and company. San Francisco

Sollberger, D. E. (1943). Notes on the breeding habits of the eastern flying squirrel (Glaucomys volans volans) J. Mammal. 24 : 163-173

Spedding, G. R. (1981). The vortex wake of flying birds: an experimental investigation. PhD Thesis. Department of zoology, Bristol University.

Stolpe, M. & Zimmer, K. (1939). Der Schwirrflug des Kolibri im Zeitlupenfilm. J. orn. 87 : 136-155

Storer, J. H. (1948). The flight of birds. Bull.Carnegie Inst. Tech. 28

Taylor, C. R., Caldwell, S. L. & Rowntree, V. J. (1972). Running up and down hills : Some consequences of size. Science 178 : 1096-1097

Taylor, C. R. (1977). Locomotion and body size in vertebrates. In "Scale effects in animal locomotion." Pedley, T. J. (Ed.). Academic Press. London

Thomas, S. P. (1975). Metabolism during flight in two species of bats, Phylostomus nostatus and Pteropus gouldii. J. exp. Biol. 63 : 273-293

Thorington R. W. & Lawrence R. H. (1981). Body proportions and gliding adaptations of flying squirrels (Petauristinae). J. Mam. 62 No1 : 101-114

Tucker, V. A. (1972). Metabolism during flight in the laughing gull Larus atricilla. Am. J. Physiol. 222 237-245

Tucker, V. A. (1973). Bird metabolism during flight: evolution of a theory. J. exp. Biol. 58 : 689-709

Walker, E. P. (1964). "Mammals of the World." 1 and 2. Baltimore. John Hopkins Press

Weiss-Fogh, T. (1972). Energetics of hovering flight in hummingbirds and in Drosophila. J. exp. Biol. 59 : 169-230

Weiss-Fogh, T. (1973). Quick estimates of flight fitness in hovering animals, including novel mechanisms for lift production. J. exp. Biol. 59 : 169-230

Weiss-Fogh, T. (1977). Dimensional analysis of hovering flight. In "Scale effects in animal locomotion." 405-420. Pedley, T. J. (Ed.). London & New York. Academic Press

Wilson, D. E. (1973). Bat faunas: a tropic comparison. Systematic Zool. 22 (1) : 14-29

Withers, P. C. (1979). Aerodynamics and hydrodynamics of "hovering" flight of Wilson's storm petrel. J. exp. Biol. 80 : 83-91

Wolda, H. (1978). Seasonal fluctuations in rainfall, food and abundance of tropical insects. J. anima. ecol. 47 (2) : 369-381

Young, J. Z. (1962). "The life of vertebrates." Oxford University Press. New York & Oxford

Zimmer, K. (1943). Der Flug des Nektarvogels (Cinnyris). J. orn. 91 : 371-387

Zimmerman, C.-H. (1932). Characteristics of clark Y aerofoils of small aspect ratios. Natl. Advisory Com. Aeronautics 431 : 1-12

Appendix by J.M.V.Rayner

Estimation of frequency from morphology

The relation between morphology and kinematics is intricate, being complicated by the many factors involved and the difficulties of adequately describing the wing beat. Pennycuick (1975, III.A.2 and 1978, 7) gives a simple theory for the relationship between frequency and wing morphology. The purpose of this note is to present a general derivation of Pennycuick's formula, and to extend the method to other cases.

a) Notation and assumptions

Assume that a bird of weight W has square wings of span b and area S, aspect ratio $A = b^2/S$, and that the wings beat in a vertical stroke plane through amplitude 2ϕ, with frequency f and downstroke ratio z. Assume also that during both downstroke and upstroke angular velocity is constant, that is

$$\text{downstroke} \quad \omega_d = 2\phi f/z \tag{A1}$$

$$\text{and upstroke} \quad \omega_u = 2\phi f/(1-z) \tag{A2}$$

The bird is flying on a level path at a steady velocity V, which is μ times the stalling speed $V_s = (2W/\rho S C_{L_0})^{1/2}$

where ρ is the air density and C_{L_o} the maximum lift coefficient in steady gliding.

We also assume that the magnitude of the aerodynamic lift force is adequate to describe the force balance throughout the wing stroke - the direction of the force is effectively irrelevent - and that profile and induced drag forces are unimportant. Adequate corrections for these factors complicate the theory beyond the levels of simple algebra, but without them it can only have limited validity. However, treating force as a scalar quantity may be quite serious.

On these assumptions, the magnitude of the lift force from both wings during the downstroke is

$$L_d = \rho S C_{L_d} \left(\tfrac{1}{24} \omega_d^2 b^2 + \tfrac{1}{2} V^2 \right), \qquad (A3)$$

and during the upstroke

$$L_u = \rho S C_{L_u} \left(\tfrac{1}{24} \omega_u^2 b^2 + \tfrac{1}{2} V^2 \right), \qquad (A4)$$

after Pennycuick (1975, equation 48). Since it is assumed that angular velocity is constant, the lift force is also constant in each phase of the stroke. If values can be assigned to the lift coefficient and the force developed then it is possible to calculate angular velocity; if the stroke amplitude Φ and downstroke ratio z are also known then frequency f can be calculated.

Pennycuick (1978) assumes that weight is supported

steadily throughout the entire wing stroke, but that the force to overcome parasite drag is provided only by the downstroke, and therefore

$$L_d = \left(W^2 + \left(\frac{D}{2}\right)^2\right)^{1/2} , \qquad (A5)$$

and

$$L_u = W . \qquad (A6)$$

On substituting from (A5) and (A1) into (A3) we obtain

$$f^2 = \frac{6z^2}{Q^2}\left[\frac{\left(W^2+\left(\frac{D}{2}\right)^2\right)^{1/2} - \frac{1}{2}\rho V^2 S C_{L_d}}{\rho C_{L_d} S^2 \Lambda}\right] , \qquad (A7)$$

and can further simplify this in the form

$$f^2 = \frac{6z^2 W}{Q^2 \rho S^2 \Lambda}\left[\frac{1}{C_{L_d}}\left(1 + \left\{\frac{A}{S}\frac{\phi^2}{\pi C_{L_0}}\right\}^2\right)^{1/2} - \frac{\phi^2}{C_{L_0}}\right] , \qquad (A8)$$

which is the general form of eqn. 17 in Pennycuick (1978). With the values $z=\frac{2}{3}$, $Q=\frac{1}{4}$, $C_{L_0}=1.6$, $\phi=1.8$ as suggested by Pennycuick this becomes

$$f^2 = \frac{4.323\,W}{\rho S^2 \Lambda}\left[\frac{1}{C_{L_d}}\left(1 + 9.23\,\frac{A^2}{S^2}\right)^{1/2} - 2.025\right] . \qquad (A9)$$

For most birds the parsite drag term is negligible, contributing at most a factor of 1.01 to the $1/C_{Ld}$ term. If C_{Ld} = 0.48 then the term in brackets becomes 0.058, suggesting that very little extra lift is contributed from flapping the wings as opposed to gliding and that very low frequencies are all that is needed. The values of the two terms in the brackets are so similar that Pennycuick's rounding to 2s.f. introduces a 5% reduction in estimated f compared with the 3s.f. used here. While this problem casts doubt on the assumptions behind the model in this form, it also indicates clearly the need for accurate estimation of the parameters involved, and in particular of the lift coefficients C_{Lo} and C_{Ld}. At present these have not been determined at all reliably, but every indication is that mean lift coefficients in flapping flight are rather higher than 0.48, in the region of 0.65-1.2 (Rayner, unpublished), and on this theory would result in more lift than is required to support the weight.

This theory does not use the equivalent equation to A8 for the upstroke, derived from A2, A4 and A6, which would produce a secondary constraint on f, within the limit of this approach. Presumably this can be satisfied by setting the value of C_{Lu}, which is otherwise undetermined.

An alternative approach is to combine force generation in upstroke and downstroke according to the need to support weight, so that the mean scalar lift force balances

the bird's weight. Equations A5 and A6 are replaced by the less strict condition

$$\frac{\tau}{\ell} L_d + \frac{(1-\tau)}{\ell} L_u = \frac{1}{\ell} W . \qquad \text{(A10)}$$

Parasite drag is now neglected; since profile and parasite drags have broadly the same magnitude it is unreasonable to include one and not the other, and the errors introduced by considering lift as a scalar quantity do not justify the extra algebra arising from a more accurate treatment of drag. By substituting in A10 from A1-A4 we derive

$$\ell^2 = \frac{6W}{\rho Q^2 S^2 \Lambda} \frac{\left[1 - \frac{\mu^2}{C_{L_0}}\left\{\tau C_{L_d} + (1-\tau) C_{L_u}\right\}\right]}{\left[\frac{C_{L_d}}{\tau} + \frac{C_{L_u}}{1-\tau}\right]} . \qquad \text{(A11)}$$

This confirms the major trend that $\ell \propto (W/S^2\Lambda)^{1/2}$ if other kinematic quantities are scale-independent.

There are two extreme cases at this stage: first that all force is generated by the downstroke and none by the upstroke ($C_{Lu}=0$), and second that lift coefficient is constant throughout ($C_{Ld}=C_{Lu}$).
In the first instance we derive

$$\ell^2 = \frac{6W}{\rho S^2 \Lambda} \frac{\tau}{Q^2}\left[\frac{1}{C_{L_d}} - \frac{\mu^2 \tau}{C_{L_0}}\right] , \qquad \text{(A12)}$$

which with Pennycuick's suggested values becomes

$$f^2 = 6.485 \frac{W}{\rho S^2 v} \left[\frac{1}{C_L} - 1.350\right] . \qquad (A13)$$

with constant lift coefficient C_L we find

$$f^2 = \frac{6\,W}{\rho S^2 v} \frac{z(1-z)}{Q^2} \left[\frac{1}{C_L} - \frac{\varphi^2}{C_{L_0}}\right] \qquad (A14)$$

which evaluates as

$$f^2 = 2.162 \frac{W}{\rho S^2 v} \left[\frac{1}{C_L} - \frac{\varphi^2}{C_{L_0}}\right] . \qquad (A15)$$

With C_L taken to be 0.48 the three equations A9, A13 A15 result in three different estimates of the frequency needed to sustain level flight, namely

$$f^2 = 0.2522 \frac{W}{\rho S^2 v} \qquad (A16)$$

$$f^2 = 4.756 \frac{W}{\rho S^2 v} \qquad (A17)$$

$$f^2 = 0.1261 \frac{W}{\rho S^2 v} \qquad (A18)$$

The apparent difference in f by a factor of about 6 between A17 and A18 is of course extreme, but illustrates the care with which the assumptions underlying any

theoretical model of a subject as complex as bird flight must be considered. The wide variation between apparent expected frequency in birds not using the upstroke (A17) and birds using it as much as in the downstroke (A18) will be explained by compensation in kinematics, wing shape, flight speed and lift coefficient (perhaps by differences in wing camber profiles). These factors can be incorporated in the theory where values for the appropriate quantities are known, but failure to reconcile measured and predicted values of frequency does not necessarily imply any breakdown of the theory, as much as its misapplication.

Allowance can be made for the shape of the wings and for the time course of the wingstroke by a simple correction factor for f; these features determine the coefficient of $\omega^2 b^2$ in equations A3 and A4, and changing them will produce a multiplicature factor for the final f^2 estimate. The theory is derived for a square wing with constant angular velocity. A triangular wing should flap at frequency $\sqrt{2}\,f$ (n.b. not 2f as given by Pennycuick), while a more realistic tapering wing should flap at about 1.18f. If the wing beat is sinusoidal rather than constant then the 1/24 factor in A3 and A4 becomes $\pi^2/192$, with ω still given by A1 and A2 as mean angular velocity; f should be scaled by 0.900 to correct. These two corrections together cannot account for all of the difference between frequencies estimated from A12 and A14 (birds not using, and using, downstroke),

and the majority will be the result of kinematic changes. If birds using the downstroke alone have long, large amplitude downstrokes compared with those using the upstroke (i.e. larger z, Φ), then the predicted values of f will be more likely to coincide. Broadly speaking this is what is observed.

As is evident from the above, the one-dimensional description of scalar wing force is inadequate for many birds. I have used a three-dimensional approach to this problem elsewhere (Rayner, 1979, 5(57); a simplified version of this methods has been used to derive the forward flight lift coefficients referred to above, and is currently in preparation.

Jeremy Rayner

January 1982

ACKNOWLEDGEMENTS

I would first like to offer my thanks to the three people I have worked with throughout this project. Dr. Pennycuick, my supervisor, has given much academic, practical and personal assistance. In particular, during his visit to South Georgia, he filmed a variety of Procellariiformes. This film proved to be of great importance to this research. Dr. Pennycuick also organised and supplied a large proportion of the funds from his own income for the fieldwork in Peru, for which I am most indebted. Dr. Jeremy Rayner created a series of computor programmes for the complex film analysis and supplied a large set of data of bird morphology, both of which were invaluable. I very much appreciate the many hours of discussion with him where he patiently educated my 'biological mind' in aerodynamics, mathematics and statistics, and I am also grateful to him for reading and criticising this thesis. Some of the later analysis of the bird flight kinematics would not have been possible without the use of Dr. Rayner's 'power model' which he modified to be suitable for the requirements of this project's analysis. His assistance and company during United Kingdom and Kenya fieldwork were appreciated. Dr. Geoff Spedding provided assistance in many laboratory experiments and also during the first Brunei field trip. I am especially indebted to him for the many useful discussions we had and for keeping me laughing through some of the humourless periods of this project.

A number of people within the Zoology Department of Bristol University assisted in this research. Of these, I am especially grateful to Professor Brian Follett who, regardless of his numerous other commitments, provided important assistance and advice especially when he supervised my research in the absence of Dr. Pennycuick. I would also like to thank Dr. John Lythgoe for the many useful discussions about vertebrate sensory systems which were ofgreat help in developing some of the theory of bat evolution. Neil Prior kindly allowed me to analyse his film of Whooper Swans. Dr. Steven Harris, with the help of his many local contacts and especially the R.S.P.C.A., provided numerous dead birds which were useful in increasing the data of bird dimensions. Many thanks are also due to Dr. James Kirkwood at Langford for providing a tame kestrel and advice on training techniques. He also sacrificed many hours of his free time to fly his kestrels so that they could be filmed.

For assistance in fieldwork in the United Kingdom I would like to thank the Wildfowl Trust at Slimbridge, the Nature Conservance Council in Pembrokeshire and the Hawk Conservancy in Wiltshire. I would particularly like to thank Reg Smith, who owns this Conservancy, for flying many of his birds of prey purely for my benefit.

The fieldwork in Brunei would not have been possible if my parents had not supplied two return air fares, accomodation and transport within Brunei. I would also like to thank them, Dick Beales, Ian Scholey

and Caroline Selkirk for their assistance in Brunei. I am also grateful for the enthusiastic help of the Brunei Museum during all my visits, and particularly Mohamed Jaya.

The Kenya fieldwork was kindly permitted by the Kenya Government through the office of the President. I would also like to thank the Department of Wildlife Conservation and Management and the Wardens of Lake Nakuru, Lake Naivasha and Masai Mara National Parks for allowing and helping my Eastern African fieldwork. Thanks are also due to Dr. Sean Avery and his wife Carol for providing accomodation in Nairobi and logistic assistance during fieldwork. I am also grateful to Alan Root for the invaluable advice he gave on contacts and filming locations. I wish to thank Peter Davey for flying his Bateleur eagle for filming, providing the best and cheapest accomodation in the Masai Mara, and for his useful advice. I am also grateful to Simon Thomset for allowing me to film his birds of prey in flight.

Thanks are due to Felipe Benavides for providing the luxurious accomodation at the Instituto Oceanografic in Paracus, Peru.

The BBC Natural History Unit were of great help in supplying film for analysis and advice about filming . locations and techniques. I would especially like to thank Richard Brock for his advice and assistance which included introducing me to some of the people mentioned above.

I am grateful to Deborah Taylor for reading this thesis, pointing out some of my numerous lapses from correct English, and for typing the final draft.

Finally, little of this research would have been possible if the Science Research Council had not generously supplied the funds for myself, and for the equipment and fieldwork. For this I am extremely grateful.